THE INFLUENCE OF THERMAL HISTORY ON THE HOT DUCTILITY OF Ti CONTAINING, C-Mn-AL AND C-Mn-Nb-Al STEELS

By

Charles SPRADBERY

A dissertation submitted to:

City University

In fulfillment of the requirement for the degree of:

Doctor of Philosophy

Department of Mechanical Engineering and Aeronautics

City University
London
November 2002

To Almighty God,
With Whom nothing is impossible.

ACKNOWLEDGEMENTS

I would like to express my sincerest thanks to Prof. Barrie Mintz for his outstanding scientific support and help throughout this work program. Also to Mr. Jim Hooker and Mr. Tom Rose for their assistance with laboratory facilities. Thanks also to Dr. Rouckaya Abushosha for her help in the laboratories.

My gratitude is also extended to CORUS and the EPSRC for providing the funding and resources to enable me to carry out this research under CASE award number 98590041.

Finally to Carla, my Wife, for her endless support all the way through this project.

`

TABLE OF CONTENTS

LIST OF FIGURES

LIST OF TABLES

Declaration

I grant powers of discretion to the university librarian to allow this thesis to be copied in whole or in part without further reference to me. This permission covers only single copies made for study purposes, subject to normal conditions of acknowledgment.

ABSTRACT

THE INFLUENCE OF THERMAL HISTORY ON THE HOT DUCTILITY OF Ti CONTAINING, C-Mn-AL AND C-Mn-Nb-Al STEELS

A series of C-Mn-Al and C-Mn-Al-Nb steels having nominal composition 0.1%C, 1.4%Mn, 0.3% Si and 0.005%N with Ti additions from 0 to 0.013% have had their hot ductility determined over the temperature range 700-1100°C. Tensile specimens were cast (melted) in situ and cooled at a rate of 100°C/min to the test temperature. They were subsequently strained to failure using a strain rate of 3×10^{-3} s^{-1}. The influence of the addition of a 100°C undercooling step into the test cycle with a subsequent re-heat to the test temperature (at 500°C/min) was investigated.

It has been shown that Ti additions, both to C-Mn-Al and C-Mn-Nb-Al steels impair hot ductility. Also, Nb containing steels give worse hot ductility with or without Ti additions for the steels examined.

Thermal history was seen to have a small but significant effect on the hot ductility of steel. The addition of a 100°C undercooling step generally resulting in worse ductility due to additional precipitation of AlN and in the case of Nb containing steels probably both AlN and NbCN.

TiN precipitation has been shown to have a more significant detrimental effect on hot ductility than AlN precipitation when one thermal cycle is introduced.

Two regression equations have been obtained which may show that P is beneficial to ductility in Nb, Ti containing steels but detrimental to ductility in C-Mn-Al-Ti steels.

Results have shown that increasing the test temperature (which will encourage coarser particles) generally leads to an increase in the dimple size and to better ductility. Interestingly, adding Ti to steels causes a larger dimple size to occur even though ductility deteriorates as the formation of TiN removes small AlN particles from solution. Thus the dimple size increases as it relates more and more to the presence of the larger MnS inclusions.

The addition of an undercooling step in the test cycle reduces the dimple size in accordance with more precipitation taking place, most likely from AlN.

During the work program it was discovered that there was potential for Ti to be lost should tensile samples be melted within silica tubes. Re-testing with an alumina based sheath ensured no Ti loss could occur.

List of Symbols

α	Ferrite phase
γ	Austenite phase
δ	Delta phase
D_0	Grain size
D_I, D_f	Initial, final diameter
L	Liquid phase
[ ]x[ ]	Product of solubility
p or p_s	Particle size
n_i	Number of precipitates considered in the "i" range of size
s_i	Size precipitates in the "i" range
CR	Cooling rate
ε	Strain
ε_t	Total strain
ε_g	Strain due to grain boundary sliding
HDH	High ductility, high temperature region of the hot ductility diagram
HDL	High ductility, low temperature region of the hot ductility diagram
HSLA	High strength low alloy steels
HAZ	Heat affected zone in welding
Ar_3	Temperature which the ferrite formation starts on cooling out of equilibrium
Ae_3	Temperature which ferrite starts on cooling on equilibrium
w	Wedge crack
r	Rounded crack
PFZ	Precipitate free zone
σ	Stress
D	Depth of void
H	Height of void
L	Length of void
CP	Cooling pattern
Ac_3	Temperature at which austenite starts forming on heating, out of equilibrium
R of A	Reduction of Area
$\dot{\varepsilon}$	Strain rate
t	Thickness of the slab
V	Casting velocity
R	Bending radius
L	Gauge length
SEM	Scanning electronic microscope
TEM	Transmission electronic microscope
EDAX	Energy dispersive X ray analysis

CHAPTER 1 - INTRODUCTION

1 INTRODUCTION

Steel first became widely available following the industrial revolution in the late 1800s. It is one of the most versatile engineering materials available; being used for an enormous range of products from life saving medical equipment to weapons, cars and ships. It is a remarkable material with property changes easily produced by simple heat treatment processes and extremely small changes in composition. Steel is easily welded and worked, being inexpensive to produce and readily available.

Commercial steel casting originated in 1743[1] when Benjamin Huntsman, a clock maker from Doncaster, began Crucible steel making, although there is limited information about his work. Better known is Henry Bessemer who applied for a patent for direct strip casting in 1857. His sketch of the process is shown in Figure 1-1 below:

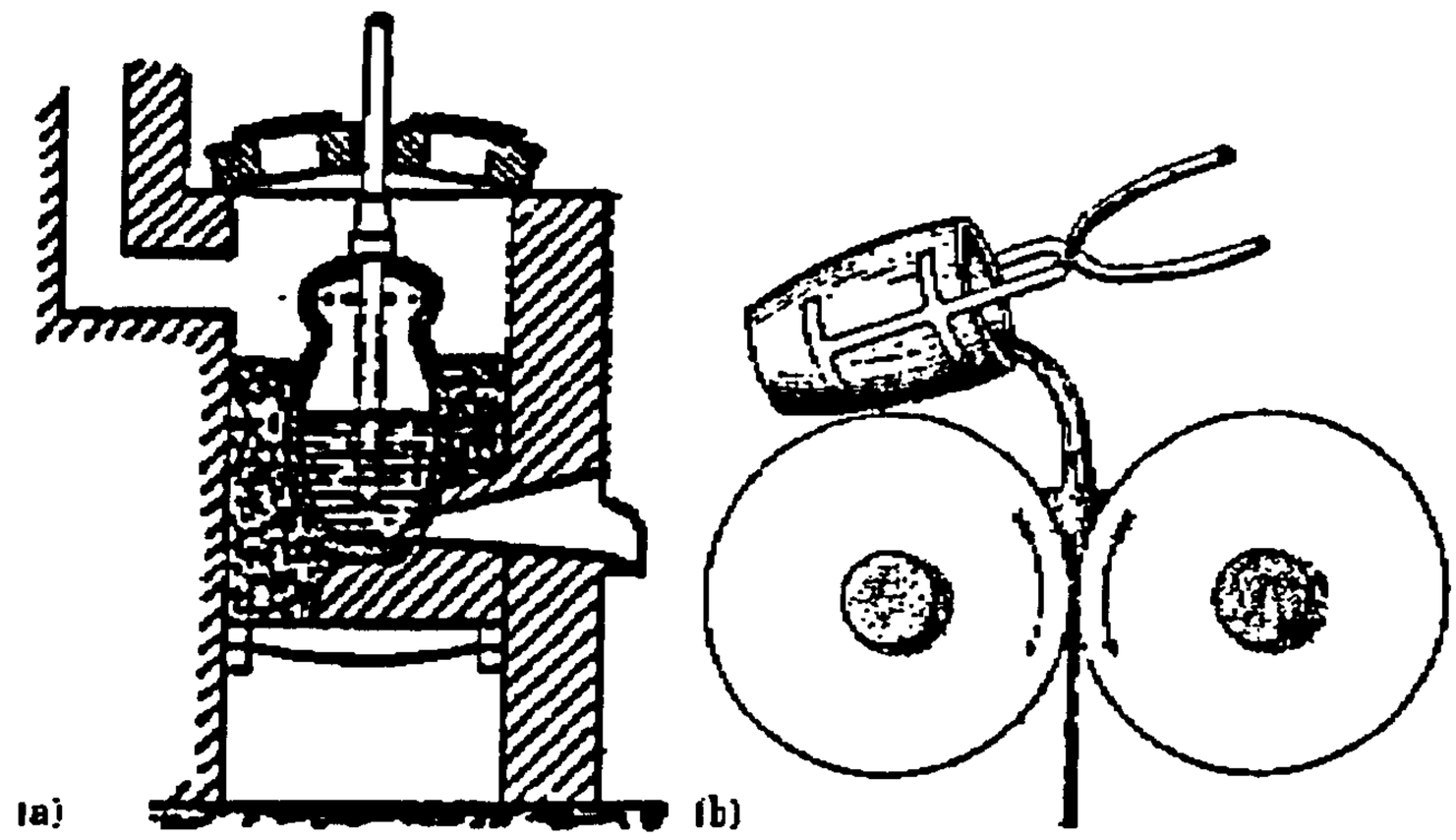

Figure 1-1 – Bessemer's sketch of pneumatic steel making and direct strip casting

However, it was not until 1920 when John T. Rowley designed and operated the first fully continuous caster. This was used to cast billet sections which were forged into horseshoes. Since then there have been many developments in continuous casting technology and a greater understanding of process control and microalloying elements has been obtained.

The objective of this work is to investigate the effect of thermal history on steels with varying titanium levels in order to gain a greater understanding of how temperature changes within the continuous casting process may effect the hot ductility of HSLA (High Strength Low Alloy) Steels.

CHAPTER 2 - LITERATURE SURVEY

2 LITERATURE SURVEY

2.1 Continuous Casting

Continuous casting of steel was introduced commercially in the 1960's. The process involves molten steel being poured from a ladle via a tundish into an oscillating water-cooled copper mould[2]. This mould is often curved so that the strand can be transferred from the vertical to the horizontal plane. The mould oscillates to prevent sticking and this causes transverse ripples on the surface of the strand. Under certain conditions cracks may occur along these ripples (or oscillation marks). These cracks then propagate when the strand is straightened and the top surface is put under a tensile load. The process is shown schematically in Figure 2-1 below.

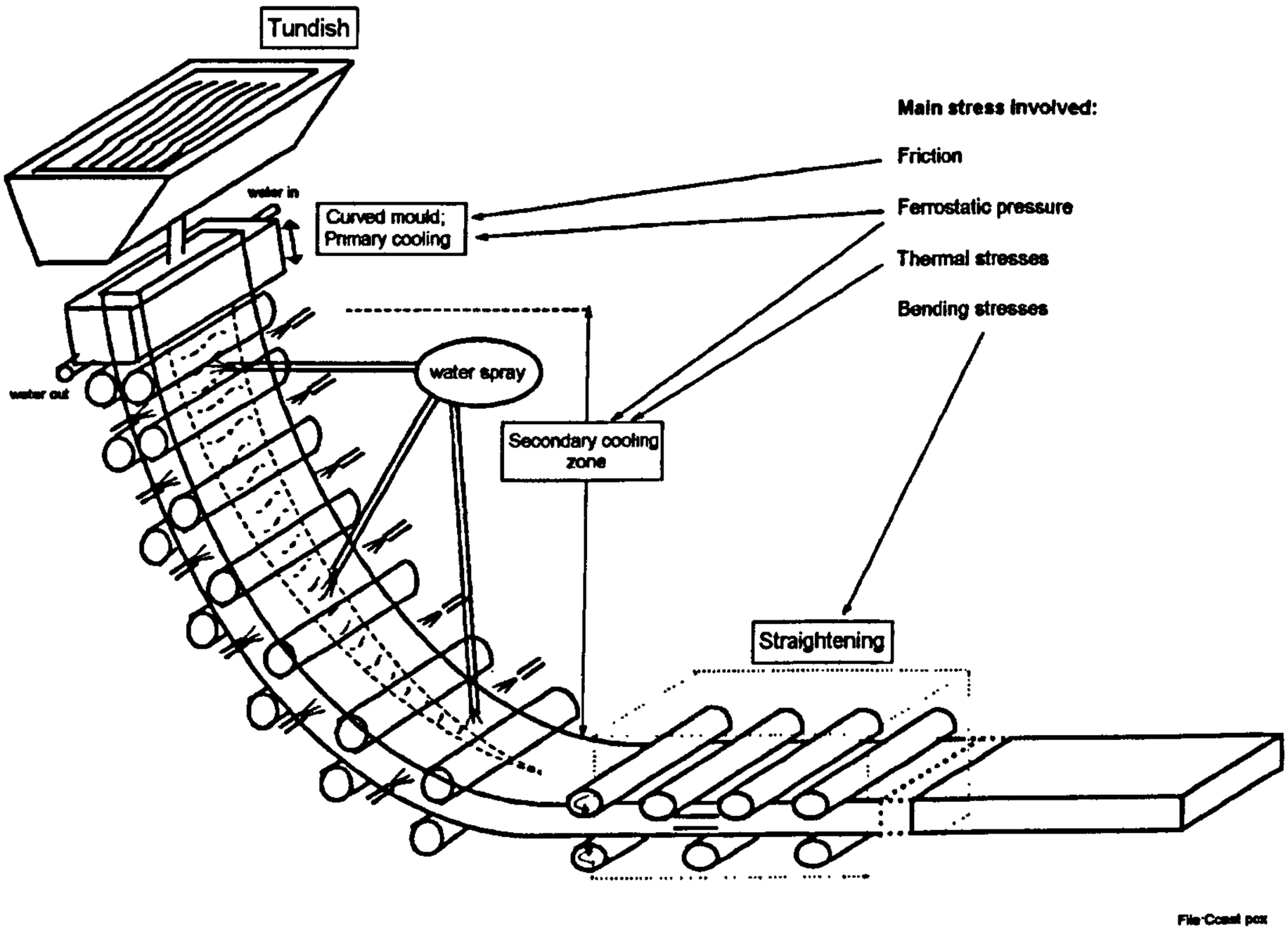

Figure 2-1 - Continuous Casting Schematic[2]

The unbending operation occurs in the temperature range of 1000-700 °C which coincides with the interval in which steel exhibits a trough in ductility.

2.2 Stresses and Strains Produced by Continuous Casting

The stresses developed in the cast sections are extremely complex combinations of thermal and mechanical stresses. Each point along the caster will have a different thermal history and thermal gradients with their associated property gradients will be present throughout the material.

Starting at the top of the process, the mould oscillates in order to prevent the cast material sticking to it and resulting in a tear in the solidifying skin. However, even with the oscillations and mould powder lubrication some friction still occurs and leads to stresses in the skin, as well as leaving transverse ripples on the surface. As the cast progresses down the mould an upward friction force acts on the skin surface. The magnitude of this force depends on the mould roughness, the mould material, the type of lubrication and the ferrostatic force[3]. This friction in turn causes an axial tensile force in the material and an axial tensile stress in the skin. Axial stresses on the skin are also caused by the weight of the casting. Additional stresses occur as the frictional force on the surface is eccentric to the axial force thus causing a bending moment in the skin. The bending stresses will be tensile at the surface and compressive at the solidification front. Figure 2-2 below shows these more clearly.

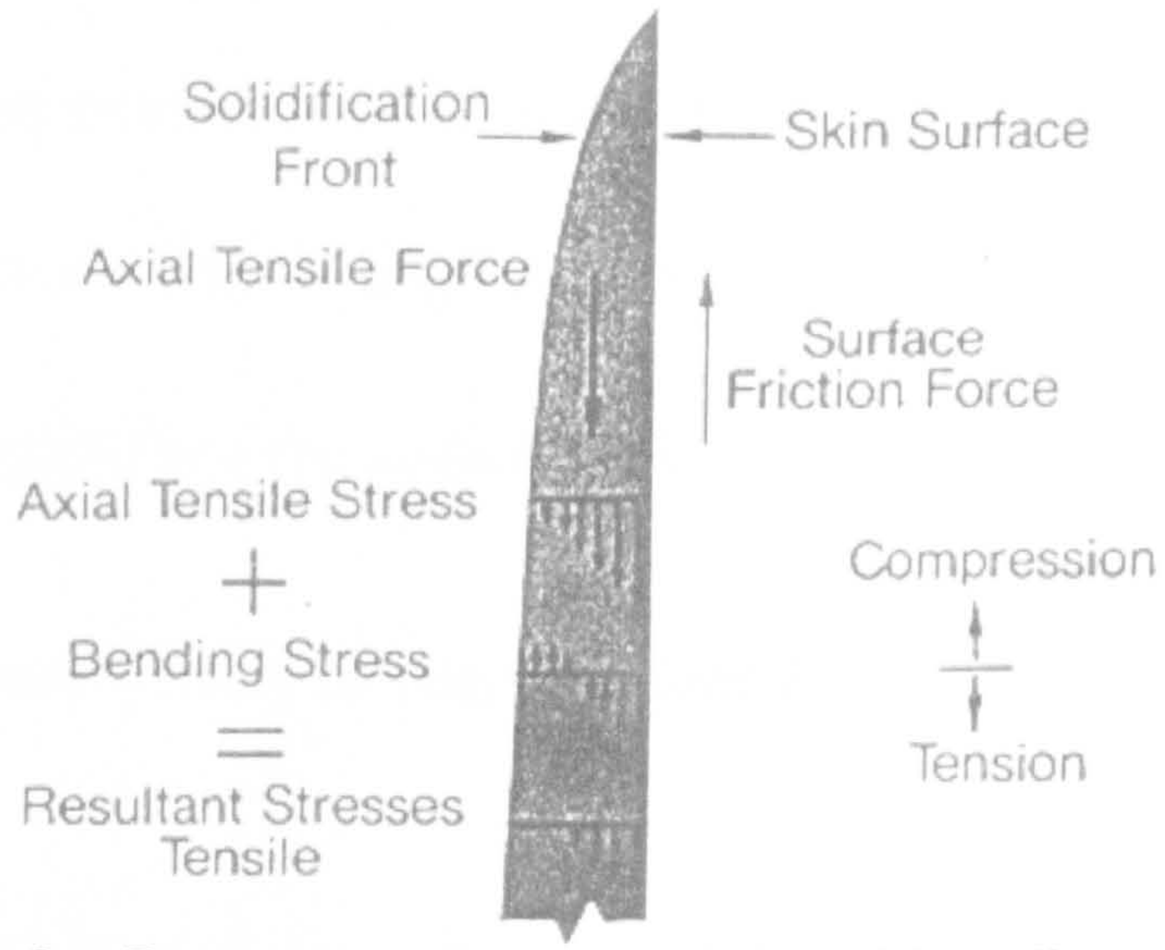

Figure 2-2 - Representation of axial and bending stresses in the solidifying skin in the mould[3]

Thermal stresses will occur throughout the caster due to thermal gradients which will exist along the axis of the casting as well as through the thickness of the solidifying skin. Generally speaking, tensile stresses will occur in the cooler regions caused by the contraction restraint from the adjacent hotter regions. Conversely, compressive stresses will occur in the hotter regions. Importantly, when a horizontal cross section of the skin is taken, the axial temperature gradient along with the through thickness gradient will cause an axial tensile stress at the skin surface and an axial compressive stress near the solidification front. However, should the surface temperature not decrease but rebound to a higher value than previously existed in the casting, the stress distribution will be altered so the stress near the solidification front becomes tensile . Thus the nature of the actual temperature gradients can markedly alter the stress distribution.

The greatest strains to which the cast is subject occur during the straightening process. Lankford[3] gives the surface strain as being equal to $\frac{1}{2r}$ where r is the bending radius, with surface stress as the velocity of the cast multiplied by the surface strain divided by the gauge length:

Surface Stress = (Cast Velocity x Surface Strain)/Gauge Length

2.3 The Hot Ductility Trough

The hot ductility trough, shown in Figure 2-3 below, is a well documented phenomenon which generally occurs in steel in the temperature range of 600-900 °C.

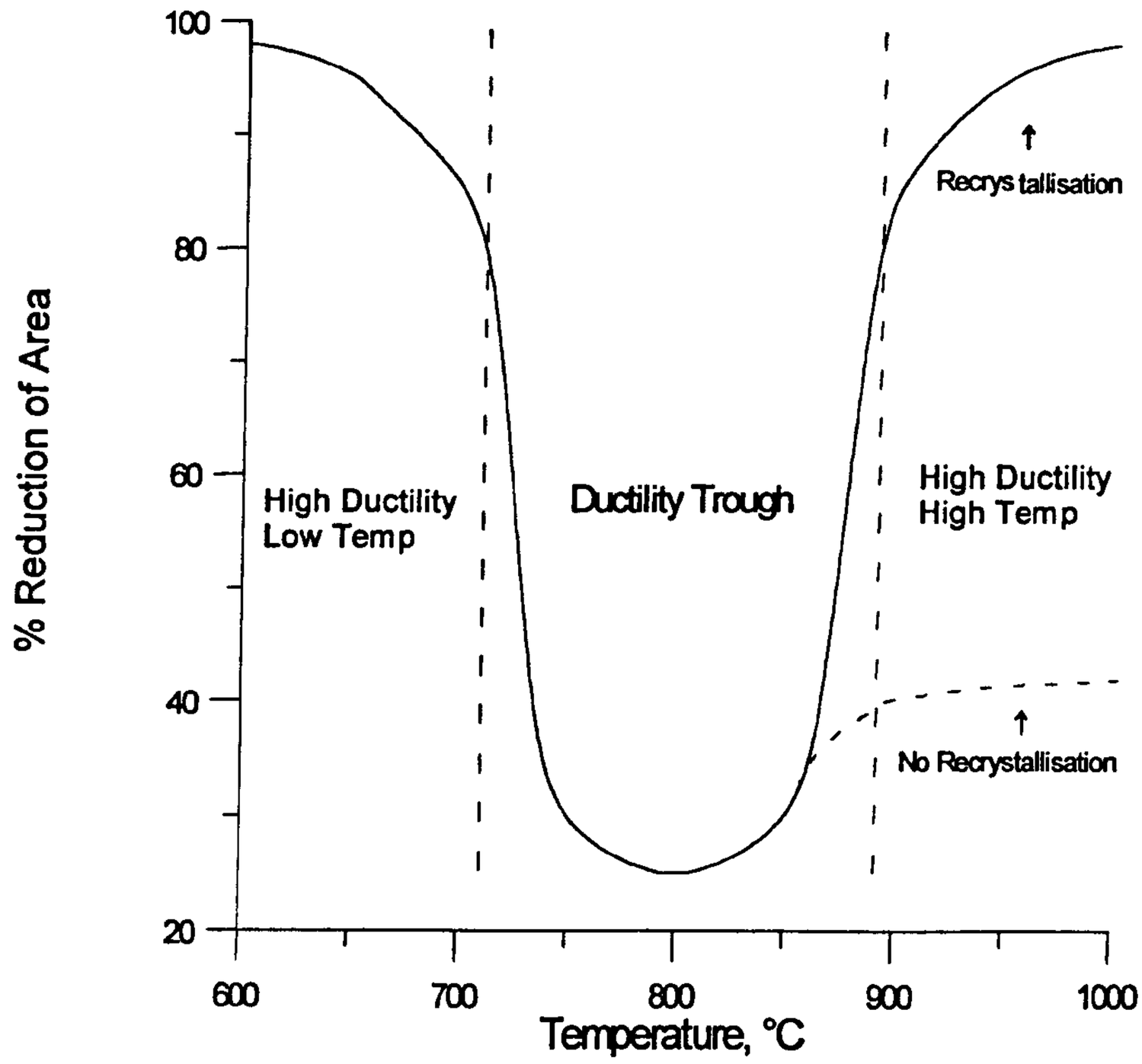

Figure 2-3 The Hot Ductility Trough

To gain a proper understanding of the mechanisms controlling the shape of the trough it is necessary to split it into three distinct regions.

- The Trough
- The High Ductility Low Temperature Region (HDL)
- The High Ductility High Temperature Region (HDH)

2.4 The Trough

An understanding of the fracture mechanisms present in this region is essential if deductions are to be made regarding the depth and width of the trough. Mintz et al (1991)[2] have noted that the poor ductility in the trough is always related to intergranular failure at the (austenite) γ grain boundaries. There are two distinct mechanisms that can cause cracks to form along the grain boundaries: grain boundary sliding in the austenite and /or transformation controlled intergranular failure. Grain boundary sliding is very much encouraged by the presence of particles at the boundaries[4] and further encouraged by the presence of a fine matrix precipitation such as in Nb containing steels[5]. Fine matrix precipitation will often be accompanied by precipitate free zones thus helping to further concentrate the strain onto the grain boundary. When grain boundary sliding is the dominant form of failure, the fracture surfaces are very flat and often show ripples on the surface caused by the grain boundary sliding.

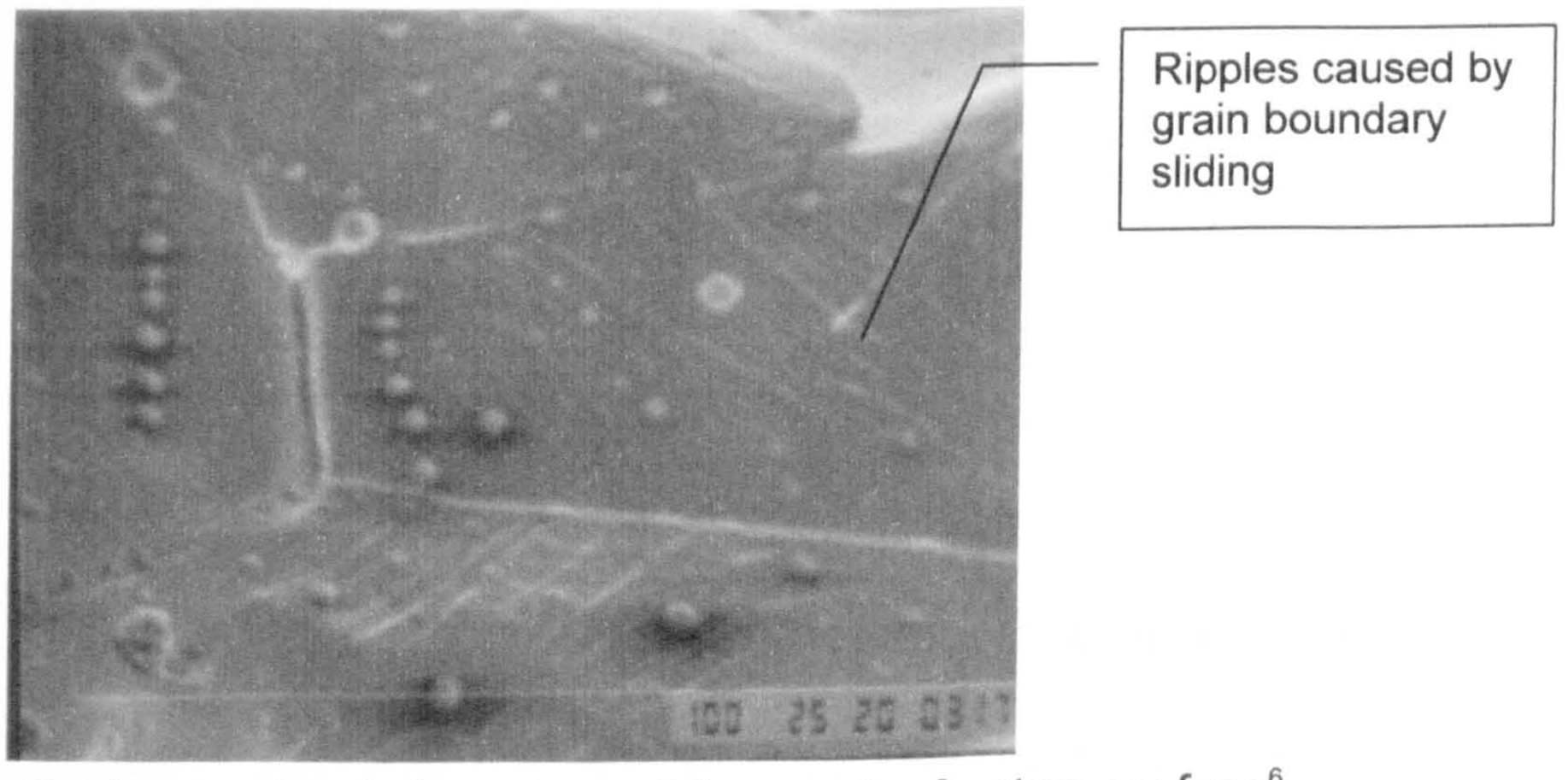

Figure 2-4 - Evidence of grain boundary sliding on the fracture surface[6]

Transformation controlled intergranular failure is due to thin films of ferrite (~5-20μm) forming around the austenite grains[7]. This layer may be deformation induced[8] or the growth of the layer can be accelerated by deformation. Since ferrite is softer than austenite in the temperature range of interest, the strain is concentrated in these films. The strain concentrated in the ferrite films is often an order of magnitude higher than the global strain[9]. This encourages voiding around MnS inclusions situated at the grain boundaries. These voids eventually link up to give failure[10]. See Figure 2-5 below. A major feature of these fractures is that the fracture surface is covered with fine dimples or micro-voids[11] suggesting that the fracture has occurred at the sulphides situated along the grain boundaries.

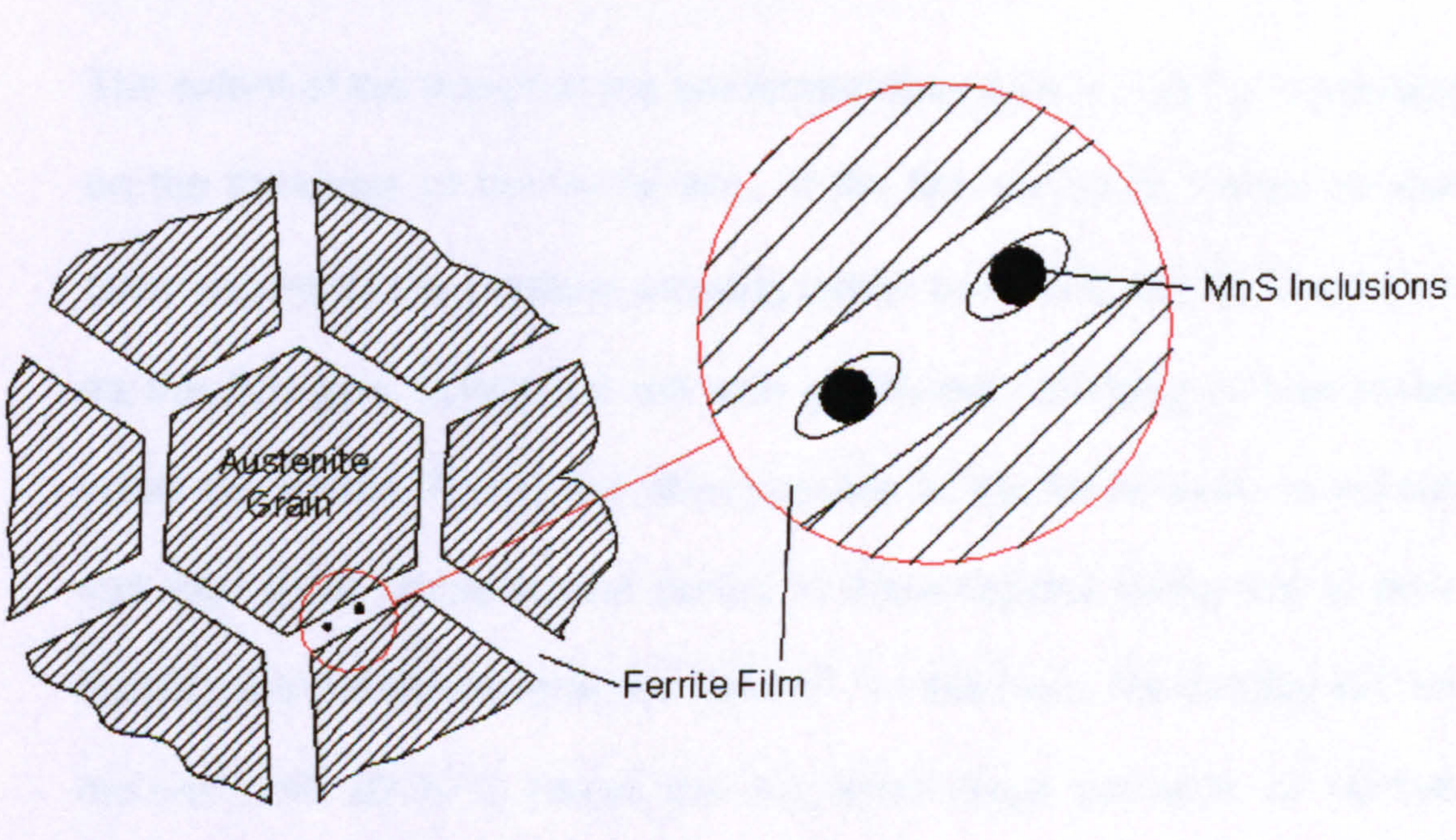

Figure 2-5 Voiding around MnS Inclusions

Ductility is therefore improved by having small amounts of MnS or other inclusions present. It has been shown[12] that the ratio of Mn:S is also

influential on the hot ductility, when the ratio is very low grain boundaries are weakened by sulphur or other sulphur compounds[13,14] such as FeS.

As the temperature decreases, ductility will recover as greater amounts of ferrite are formed either prior to or during the deformation. This is due to the more even distribution of strain over the greater percentage of ferrite present, ferrite having excellent ductility in itself. Generally 30-40% ferrite is required for ductility to be good i.e. 40-50% reduction of area values[9,15,16].

Besides intergranular failure, it has been found[17] that interdendritic fracture is a brittle fracture mode which may also be responsible for low hot ductility.

The extent of the trough at the low temperature side is entirely dependent on the thickness of the ferrite film. If the film can work harden so that other regions of the γ deform allowing further transformation to ferrite then as the film gets stronger it will also get thicker, bringing in new areas within the γ grain. This is not often possible as the ferrite tends to remain soft thus strain concentration occurs in these regions giving rise to poor ductility and ductile intergranular failure[18]. In this case, the ductility will not recover until 20-30°C below the Ar_3 when large amounts of normal transformation ferrite are present.

2.5 The Hot Tensile Test

The hot tensile test has been widely used as tool to assess the hot ductility behaviour of a steel in order to determine its susceptibility to cracking during the continuous casting process.

There are several types of hot tensile test with varying degrees of complexity; the simplest test is to reheat the sample to a temperature around 1350°C in order to redissolve all the microalloying elements and create a coarse grain size that is reminiscent of that produced by casting. The sample is then cooled at a similar average cooling rate to that undergone close to the surface of the strand and then strained at a rate similar to that used in the straightening operation. The reduction of area (R of A) of the sample is taken as the measure of the hot ductility. Mintz[5] suggests that a R of A value of 40% is required to ensure cracking does not occur.

This style of test has been found[18,25,44] to be adequate in assessing the likelihood that steel will develop cracks during the straightening operation in continuous casting. There are however, several problems with this simple test as the solution treatment may not allow all the microalloying and grain refining elements to fully redissolve and may also not create a large enough grain size to be reminiscent of the continuous casting process.

The grain structure in the melted samples is normally equiaxed whereas a dendritic columnar grain structure is more common in continuous casting. This columnar structure has been shown to favour crack propagation over the equiaxed grain structure.

A more accurate representation of the commercial process is to re-melt the samples (or cast them) in-situ. A notch type as-cast sample has been recently developed by Reveaux[19] et al which results in a columnar grain structure which is more reminiscent of the structure that occurs at the slab surface during the continuous casting process. Further refinements still can be made with the improved accuracy of computer-controlled furnaces by trying to simulate more closely the commercial cooling profile as opposed to using an averaged value for the bulk cooling of the plate.

Carpenter et al[20] found that for a Nb-Ti steel, casting in-situ caused a wider and deeper ductility trough to occur when compared with solution treated samples again showing the need for casting in situ, in order to more accurately simulate commercial continuous casting conditions.

2.6 Grain Boundary Pinning

Grain boundary pinning occurs when particles are situated on the boundaries between the grains, thus decreasing the grain boundary area and the overall grain boundary energy. It has been well documented that the smaller the pinning particles, the more effectively the grain boundaries will be pinned. Thus precipitates which form at lower temperatures, in the

solid state, will be more effective than the larger precipitates which may form in the liquid state or during solidification.

2.7 The Effect of Cooling Rate and Thermal History

Hater et al[21] found that it was not necessary to have bending forces present in order to form transverse cracks. In fact, they report that defects are induced by local temperature differences in the strand shell.

Figure 2-6 below shows the differences between the surface temperature and at two levels below the surface, as a strand passes through a water spray nozzle. It can be seen that the surface temperature rapidly drops about 500°C and is connected to a shrinkage of about 1%. From this, stresses can be calculated which are considerably above the hot yield strength.

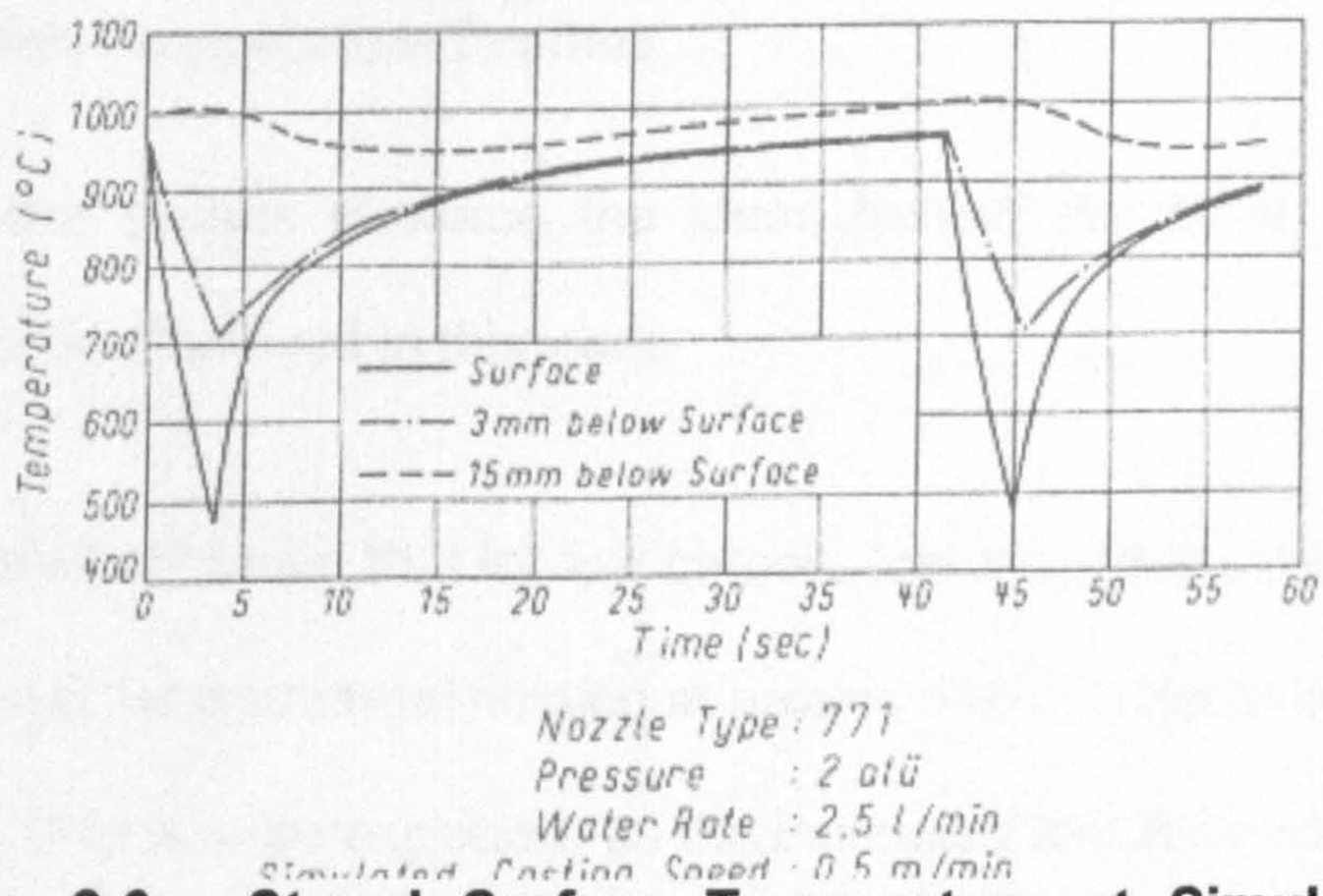

Figure 2-6 - Strand Surface Temperature at Simulated Spray Cooling[21]

Similar differences between the surface temperature and the bulk temperature can be seen in Figure 2-7 below[22] (taken from data supplied by the Scunthorpe works of CORUS).

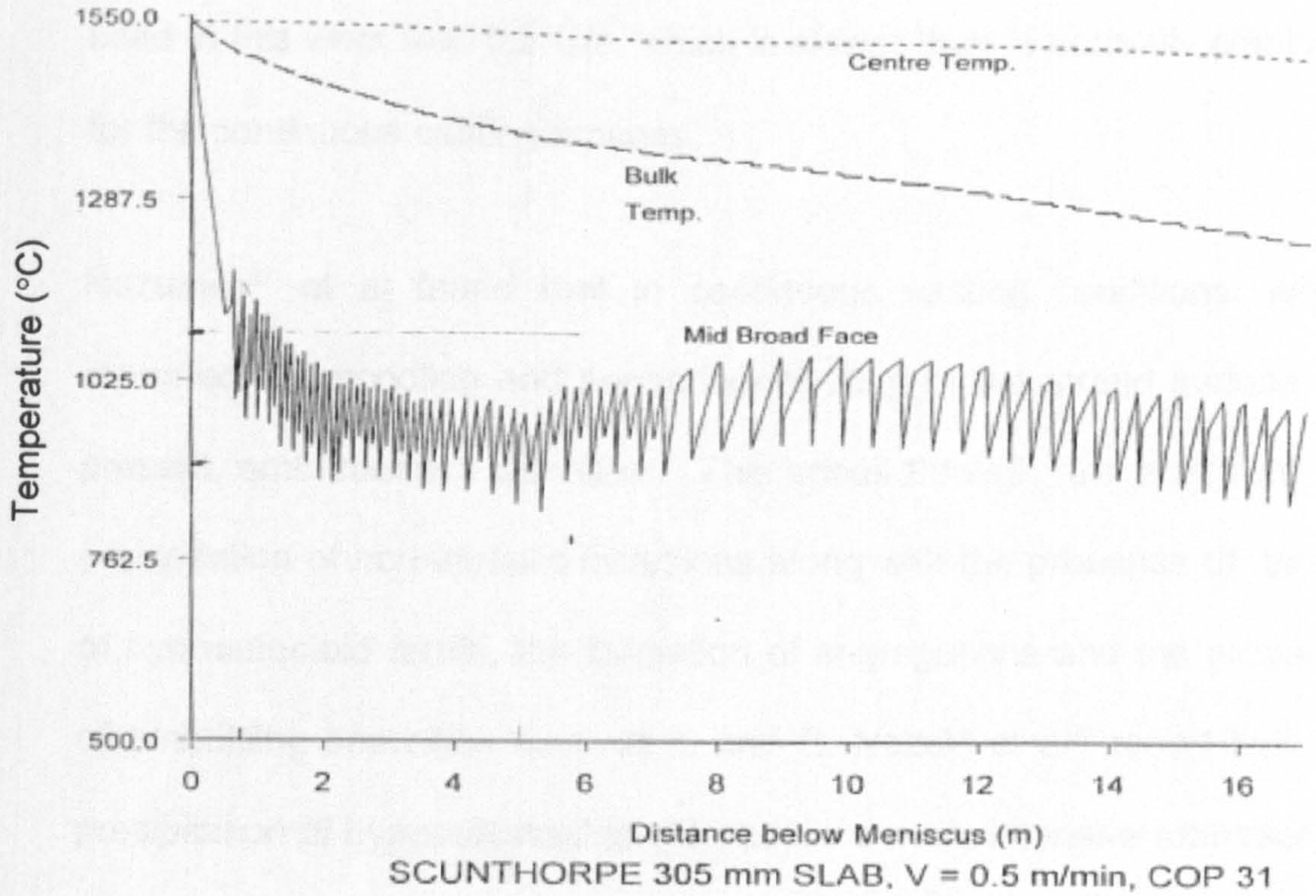

Figure 2-7 - Scunthorpe Works Continuous Caster Bulk and Surface Temperature Profiles

The above graphs reinforce the ideas behind the more complex hot tensile tests employed in this work.

Maehara et al[23] found that for low carbon, low alloy steels decreasing the cooling rate (or isothermal holding at around 1100°C) led to increased hot ductility. This is to be expected, as the increased test time would allow for particulate growth, thus reducing the effects of the precipitates on the grain boundaries, hence allowing better ductility. Several other authors[24,25] have also found that decreasing the cooling rate leads to better ductility.

Maehara et al also found[26] that an improvement in ductility occurs during slow cooling due to the depletion of carbon and nitrogen atoms which in turn are due to precipitate growth. However, the average cooling rate used in this work was 0.5°C/s, which is slower than is normally employed for the continuous casting process.

Razumov[27] et al found that in continuous casting conditions, where repeated supercooling and secondary heating of the strand surface are present, embrittlement will occur. This arises through the action of the precipitation of non-metallic inclusions along with the presence of bands of hypoeutectoid ferrite, the formation of segregations and the presence of embrittling impurities such as S and B. Nozaki et al[28] report that the precipitation of hypoeutectoid ferrite causes a more intensive formation of aluminium nitrides. With the repeated heating of the bands, the quantity of AlN at the boundaries will increase thus reducing ductility.

Mintz et al[29] report that temperature cycles on a C-Mn-Nb-Al steel produce both a wider and a deeper trough to that obtained by direct cooling. It was found that the greater the amplitude of the oscillation, the wider the trough became. It is thought that the widening of the trough is due to enhanced NbCN precipitation causing a delay in the onset of dynamic recrystallisation. They[29] have also shown that introducing a thermal cycle to a C-Mn-Al steel causes a widening of the trough.

It has also been found[30] that temperature cycles have no effect on a Ti containing steel. It is suggested that this is because in the Ti free steel more AlN is precipitated out on cycling whereas with the Ti containing steel, as all the N was combined as TiN, cycling produced no more precipitation. Gao[31] and Sorimachi carried out some hot tensile tests on (although they were re-heated and not re-cast) on a Ti containing interstitial free steel and similarly found that temperature cycles on the Ti containing steel had no effect. Their tests showed that temperature cycles did affect the Ti free steels, actually improving the ductility. It is thought that the improvement in ductility was due to increased time (due to the addition of the temperature cycles into the cooling program) being available for the MnS precipitates to coarsen. They also found that the ductility of the Ti containing steel could not be improved by isothermal holding as it could for the Ti free steels.

It is suggested that when enhanced precipitation occurs as at the lower end of the oscillation, sufficient time is given to allow greater amounts of NbCN to precipitate out before tensile testing at a higher temperature. This lower temperature precipitation (pre-precipitation) will result in a larger quantity and a finer precipitate than would be present from simply cooling directly to the test temperature.

Nozaki et al[32] have observed that temperature oscillations above and below the transformation temperature lead to enhanced precipitation of AlN.

Darsouni et al[33] have performed some work on a Ti containing steel using undercooling with long hold times (i.e. the samples are held for an hour at a temperature lower than the test temperature) as well as short time holds of 4 minutes at temperatures above the final testing temperature. As expected, the results showed that longer time holds below the testing temperature produced a wider and a deeper ductility trough due to the increased amount of time allowing greater and finer precipitation to occur. Interestingly, they found that in the shorter time programme the precipitates were mainly mixed TiN and MnS precipitates but for the undercooling programme they tended to be MnS with some trace of Al.

Deprez et al[34] have compared results for a C-Nb-V Steel cast in situ and then cooled directly to the test temperature and strained to failure with results for the same steel cast in situ, cooled to room temperature and then re-heated to the test temperature. They found that the re-heating tests resulted in a finer grain size than the plain cast in situ tests. It therefore follows that the samples that underwent the plain tests had a smaller specific grain boundary area (due to the coarser grain size) and as such a higher precipitate density on the grain boundaries (i.e. the same volume fraction of precipitates were present in a smaller area). They also found that the effect of temperature history was affected by the strain rate used; for instance at the lowest strain rate used ($10^{-3}s^{-1}$) the re-heated samples gave better reduction of area values, however at the highest strain rate ($0.5s^{-1}$) the effect was reversed. This was probably related to the increased time available at the slower strain rate for the precipitates to grow.

2.8 Strain Rate Effects

Generally[35], in the temperature range of the ductility trough, the lower the strain rate employed, the worse the ductility becomes. It is thought that this is partly due to the fact that at higher strain rates a larger energy is stored in the material consequently producing a larger driving force which could in turn be enough for the grain boundaries to surmount the drag effect and more rapidly begin dynamic recrystallisation. More generally, at high strain rates grain boundary sliding is less important, voids created at particles have less time to grow and fewer elements have time to segregate to the grain boundaries. Also at low rates of strain[36] dynamic precipitation of carbonitrides is enhanced. Low strain rates also allow sufficient time for the ferrite to recover and remain soft during deformation[37]. Although at higher strain rates deformation induced ferrite forms at a later stage, it is able to work harden so that the strength differential between the austenite and the ferrite is reduced. Thus strain concentration does not occur and hence premature failure is avoided. This ability to accommodate higher rates of strain often encourages the formation of more deformation induced ferrite which in turn helps the ductility as the strain is then spread more uniformly throughout the structure.

2.9 Titanium in Steels

2.9.1 General

Titanium is often added to steel in order to improve the surface quality of the finished product. It has other uses as an addition to steel, mainly due to its formation of extremely stable compounds with other elements. For instance, Titanium Nitride (TiN), which is extremely stable, is formed with nitrogen being stabilised thus reducing the total amount of nitrogen present[38]. This occurs as TiN crystallises out of the liquid steel and can rise out due to its low specific gravity. However, the TiN also precipitates out in the solid state[27] and remains in the austenite grain.

Ti can also be used as a deoxidiser (although it is not as strong as aluminium) and as grain refining agent (although again it is not as strong an agent as aluminium). It has been reported[39] that Ti does not cause grain refinement in continuously cast steels. A probable cause of this is the nature of the Ti precipitates formed; large cuboidal precipitates are formed in the liquid which have no effect on inhibiting grain growth[40]. These large cuboidal precipitates have no effect due to their size (>0.5μm) which is five times higher than the 0.1μm shown to be required by Gondoh et al[41]. It is thought that the occurrence of these precipitates could be reduced by decreasing the concentrations of Ti and N in the liquid. The precipitate size could also be reduced by using a fast cooling rate during solidification.

Refining the austenite grain size has been shown to improve the hot ductility[42] by decreasing the crack aspect ratio and thus reducing the stress concentration at the crack tip. There will also be an increased surface grain boundary area which reduces the precipitate density at the boundaries for a given volume fraction of precipitate. Furthermore, the reduction in critical strain for dynamic recrystallisation of the finer grains will encourage recrystallisation to occur causing boundaries to move away from cracks, thus limiting their growth.

It has also been found[23] that the addition of a small amount of Ti in Al killed steels can improve ductility by trapping the N atoms as coarse TiN precipitates prior to deformation which has the effect of suppressing the dynamic precipitation of carbonitrides during the final straining. Also the TiN forms at higher temperatures than the AlN which if the cooling is very slow may result in a coarser less detrimental precipitate.

Luo et al[43] report that precipitates in Ti-bearing steels are mainly $Ti_4C_2S_2$ and Ti(C,N). The former usually precipitating along the grain boundaries with a size of >50nm. The latter was found to be dispersed extensively throughout the matrix and had a size of less than 50nm. Thus the effect of excess Ti on ductility depends on which of the precipitates comes out more easily. The fine precipitation of Ti(C,N) deteriorated ductility and caused a wider trough, however, the coarser $Ti_4C_2S_2$ had either no effect or in fact led to a slight improvement in the ductility

It is thought that this improvement is because precipitates of $Ti_4C_2S_2$ are coarse and more stable than MnS thus removing S from the matrix and the grain boundaries. However, it has also been reported[31] that the formation of $Ti_4C_2S_2$ causes a deterioration in the hot ductility when compared to Ti free steels.

Generally it is the Ti(C,N) precipitates which are the most likely to precipitate out in a fine form thus causing a deterioration in ductility. TiN will precipitate out at higher temperatures and if there is enough Ti then TiC will form at lower temperatures.

2.9.2 The Ti:N ratio

The stoichiometric Ti:N ratio is 3.4:1

In contrast to the work by Maehara et al[23] (which was based on re-heated steels) it has been found by the author and others[44] that the addition of Ti to as cast C-Mn-Al steel causes ductility to deteriorate. This deterioration continues until the stoichiometric ratio is reached. Further increases in the amount of Ti added was found to cause an improvement in ductility, but the ductility values never recovered to those given by the Ti free steel.

Keijan and Baker[45] have shown that a hyperstoichiometric Ti:N ratio can suppress the precipitation of AlN producing many large and complex Ti – Nb carbonitrides in Ti and Nb containing steels.

2.9.3 *Titanium Nitride (TiN)*

As already mentioned, Ti is a very strong Nitride former. It also has very low solubility in Austenite. In fact Figure 2-8 below shows TiN to have the lowest solubility of all the conventional microalloying elements[46].

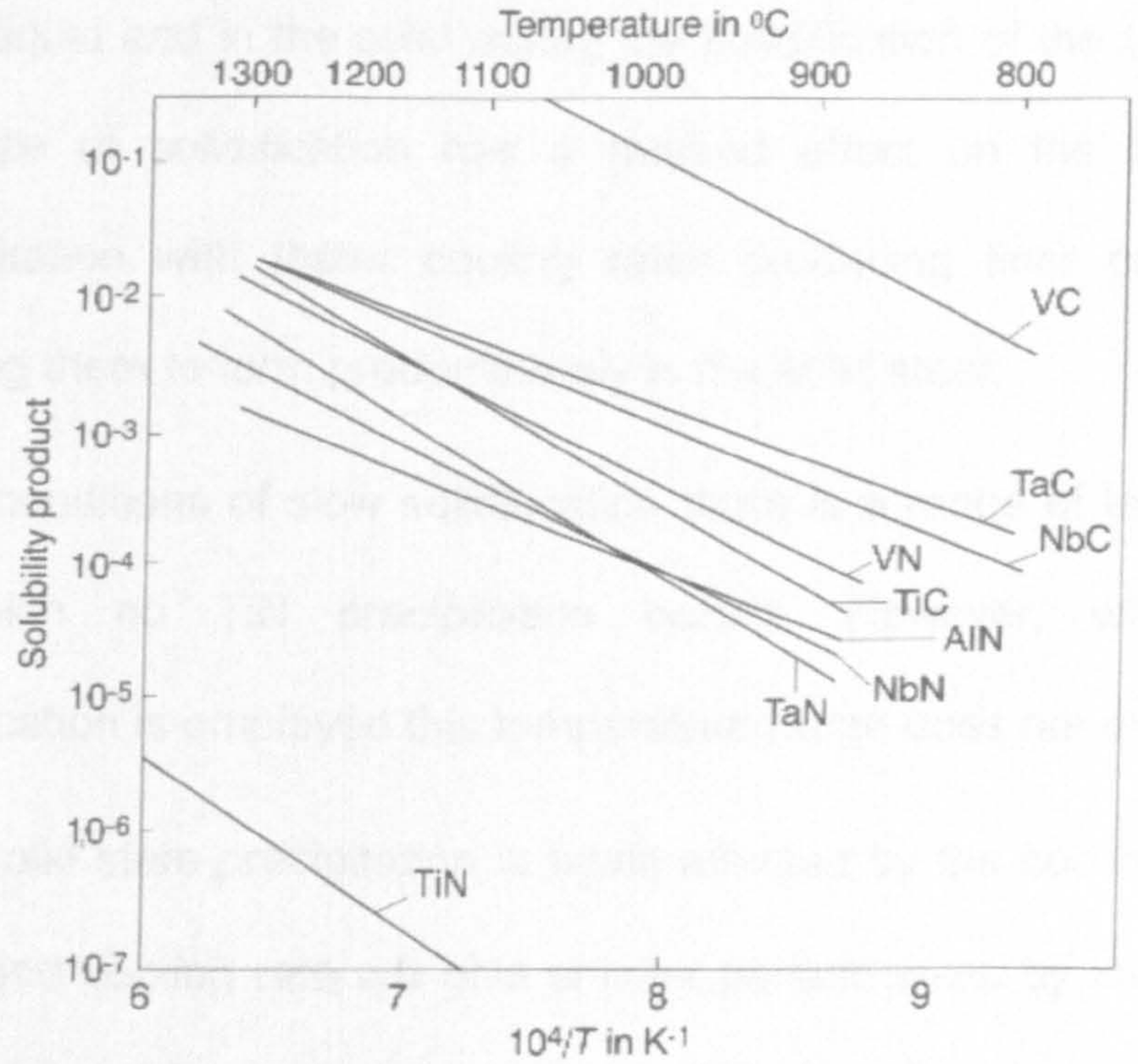

Figure 2-8 - Solubilities of microalloyed carbides and nitrides in austenite[46]

Due to its low solubility in austenite, TiN may precipitate from the liquid steel prior to and during solidification. Because TiN has low solubility and hence a slow particle coarsening rate, it is often used as a grain refining precipitate most notably as and addition to aid grain refinement in the heat affected zone (HAZ) after welding has taken place.

As stated earlier, for a given volume fraction, the smaller the precipitate the more effective it will be at grain boundary pinning. Thus the lower the

temperature at which TiN is precipitated the greater will be its effect on the grain size. Pickering[46] suggests the following 4 regimes in which TiN can form:

1. In the liquid steel. This results in large particles which are not very effective for grain boundary pinning. The size of these particles is not greatly affected by the rate of cooling of the liquid steel.

2. In the liquid and in the solid during the solidification of the steel. Here the rate of solidification has a marked effect on the process of precipitation with faster cooling rates producing finer particles by causing them to form predominately in the solid steel.

3. Under conditions of slow solidification there is a range of temperature in which no TiN precipitation occurs. However, when rapid solidification is employed this temperature range does not exist.

4. In the solid state precipitation is again affected by the cooling rate, an increased cooling rate will give smaller particle sizes by lowering the precipitation temperature.

It has been found that[47] nucleation of TiN is possible if the concentration product [%Ti][%N] exceeds the solubility product L_{TiN} by more than a factor of 10. Similarly[48] nucleation of TiN is possible if the supersaturation (η) exceeds 10 where $\eta = [\%Ti][\%N]/ L_{TiN}$.

2.9.4 Titanium Carbide

Ti is also a strong carbide former with the solubility of TiC being similar to that of NbC shown in Figure 2-8. TiC may be precipitated either in the

austenite or during the austenite to ferrite transformation as well as in the ferrite phase.

2.10 Precipitation Time Temperature Curves

The precipitation time temperature curves[49] for Ti (C,N) are shown in Figure 2-9 below. Where steel Ti-a has a Ti:N ratio of 2:1 and Ti-b has a Ti:N ratio of 6.5:1. Steels Ti-a and b were heated to 1460°C before being strained at between 0.3 and $1s^{-1}$ whereas in the other curves (Medina et al[50] and Liu and Jonas[51]) a much lower strain rate of around $0.05s^{-1}$ was used. It is likely that the top curves refer to TiN whilst the lower ones are for TiC.

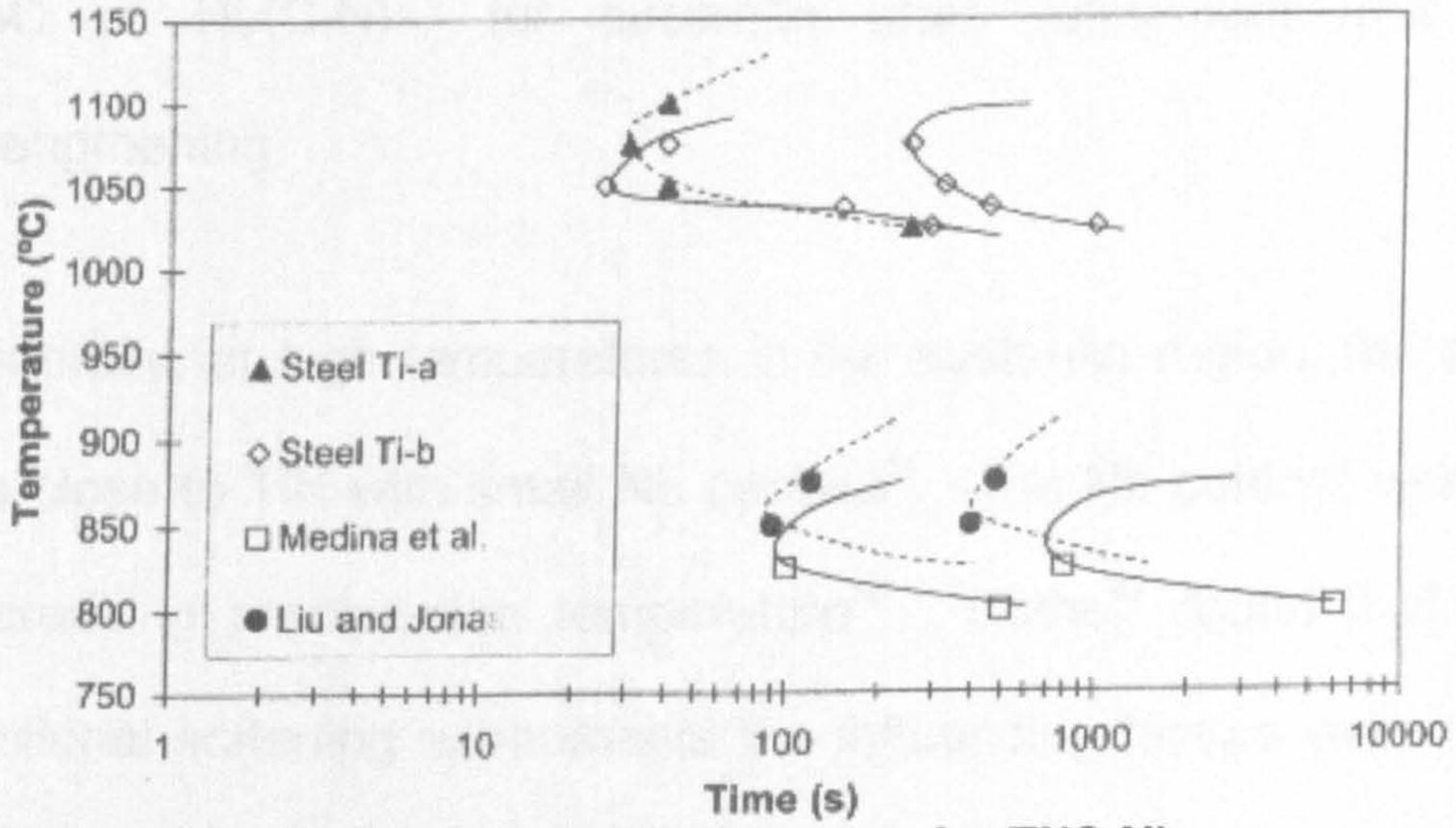

Figure 2-9 - Comparison of PTT curves for Ti(C,N)

It can be seen that the curves for Ti-a and Ti-b are similar in their temperature range, with Ti-a having a slightly lower "nose" at about 1050°C with Ti-b at around 1075°C. The lower temperature curves again occupy similar temperature ranges however with "noses" at around 840°C

2.11 Ti – Nb Steels

When Ti and Nb are both present as additions in steels the combined influence of Ti and Nb has been found[52] to improve ductility as the complex coarser Ti-Nb carbonitrides that are formed are less detrimental to ductility than the fine Nb(CN) precipitates.

It has been shown[53,54] that Ti additions to Nb-containing High Strength Low Alloy (HSLA) steels lead to the formation of complex Ti-Nb carbonitrides with various chemistries and morphologies. These nitrides and carbides are mutually soluble[55] and are strongly influenced by the steel composition, the processing route and the Ti/N ratio. Substantial amounts of Nb combine with TiN thus reducing the potential amount of NbC or Nb(C,N) for austenite grain refinement and dispersion strengthening.

Generally, at high temperatures in the austenite region, the precipitates are close to TiN with small Nb content[56]. The Nb content increases with decreasing precipitation temperature[55]. Kothe[47] found that during his fractional softening experiments the influencing factors were (in order of decreasing significance) T_{def} (Temperature of deformation), [Ti], [Nb], [Ti]·[Nb]. Where the [Ti]·[Nb] term vanished below 1000°C this points to a separate nucleation of Nb(C,N) precipitates below 1000°C.

Subramanian and Weatherly[57] show that mixed carbides enriched in Nb appear to grow epitaxially on nitrides enriched in Ti. This will raise the recrystallisation temperature as the growth of the Nb-rich carbides on the

already present Ti-rich nitrides will increase the Zener drag force on the boundary mobility.

Zhou and Presitner[58] et al found that they were getting (Ti,Nb) N precipitates with particle sizes of >100nm in all alloys where there was more than 0.012% Ti present if the samples were quenched at any temperature up to 1408°C. For samples with less than 0.012%Ti, particles were only detected when ingots were slowly cooled to 1000°C and quenched.

2.12 Nb containing steels

Niobium, like titanium, has been found to have a very powerful strength enhancing effect on steels at alloying levels of only a few hundredths of a percent. Recently there has been a great deal of work done on Nb containing steels and many papers published.

Nb is often added to steels because of its grain-refining effect and precipitate hardening during hot rolling. It seems to work in several ways, Lee et al[59] suggest that Nb atoms segregate to the austenite/ferrite interfaces. This has the effect of causing reduced grain growth velocity due to solute drag effects. It has also been suggested[60] that the Nb carbonitride precipitates either work as nucleation sites for ferrite formation or have a pinning effect on the grains.

Kop et al[61] report that the pinning effect of precipitates on the development of the austenite microstructure is much stronger than the solid drag effect of the Nb in solution. Others[62,26,63,64] propose that it is

matrix strengthening due to the dynamic precipitation of carbonitrides accompanied by the formation of comparatively soft precipitate free zones that controls the ductility in the austenite region. This occurs in a similar fashion to the mechanism encountered when thin films of soft ferrite occur round the stronger austenite grains. Strain becomes concentrated in the softer regions (in this case the precipitate free zones {PFZ}). It was found that coarse NbC particles tended to precipitate out on the grain boundaries and very fine NbC particles (brought out by dynamic precipitation) were dispersed within the matrix. The PFZ's tend to occur in the vicinity of the grain boundaries.

An investigation by Wang and Akben[65] suggests that a 0.1% Nb addition will result in a strength increase of 76%. This is in contrast to a 0.1%Al addition, which produces a 5% increase. In each case the strength increase is due to solid solution strengthening. The relative difference in the strength increases caused by each alloying element is mainly due to the greater electronic difference between iron and niobium as compared to that between iron and aluminium. Although strengthening differences have been attributed to the relative atomic size difference between the addition and the base[66,67] the relative size differences of Al and Nb with iron are 0.12 and 0.15 respectively which is not considered to be significant enough to cause the marked difference in strengthening between the elements.

Thillou et al[68] propose the following schematic diagram (Figure 2-10) for the different roles of Nb during thermomechanical processing.

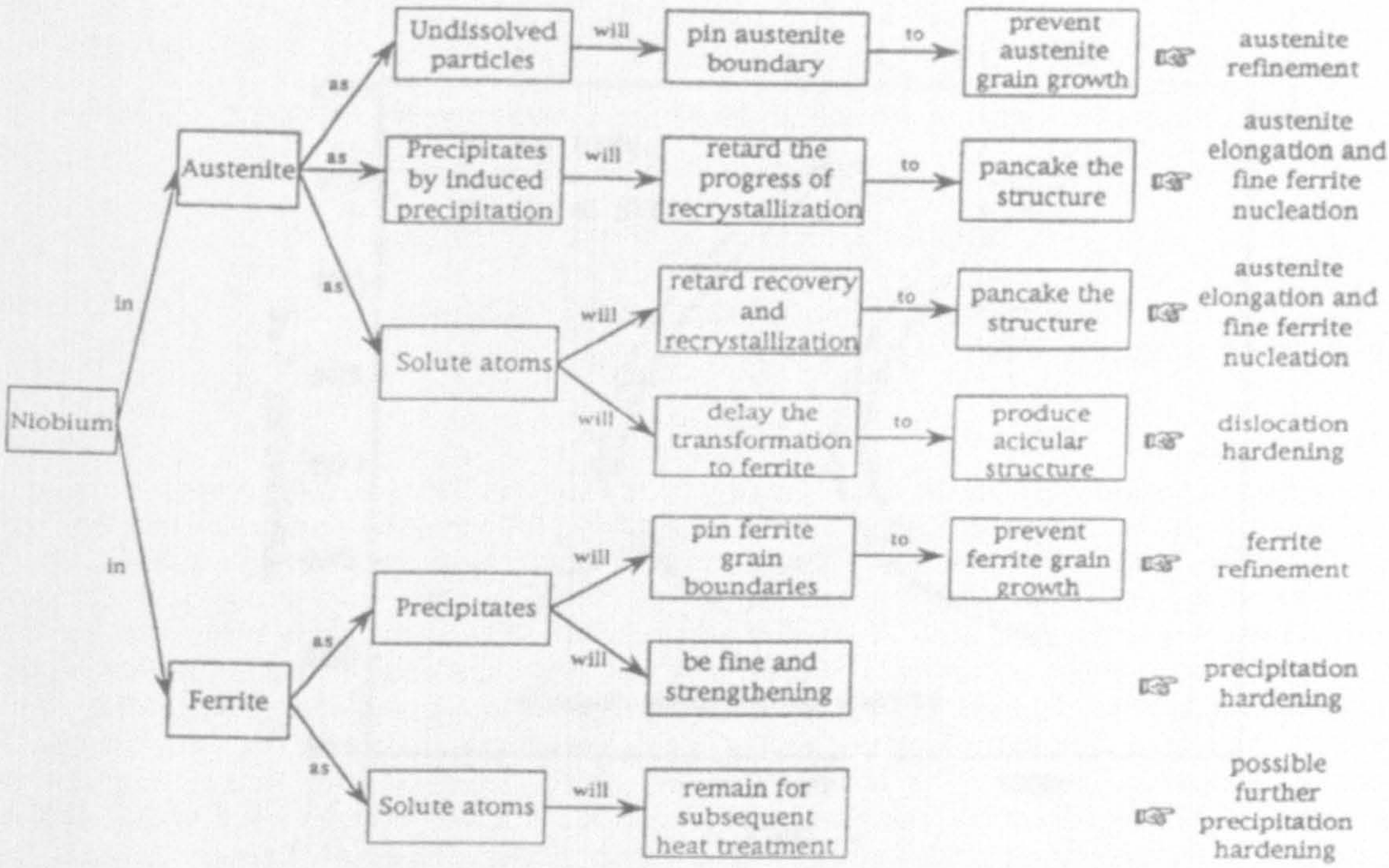

Figure 2-10 - Schematic of the different roles of Nb

The PTT (precipitation, time, temperature) curves for Nb[65] are shown below, where Ps relates to the onset of dynamic precipitation and Pf to the finish. The curves show that precipitation for Nb(C,N) starts at about 10 s and finishes at about 240 s at the nose temperature of 900 °C. The curves also show that when Al is added to a Nb containing steel that there is a small retardation in the onset of precipitation. The above study also showed that the addition of Al to an Nb steel will enhance the austenite to ferrite transformation.

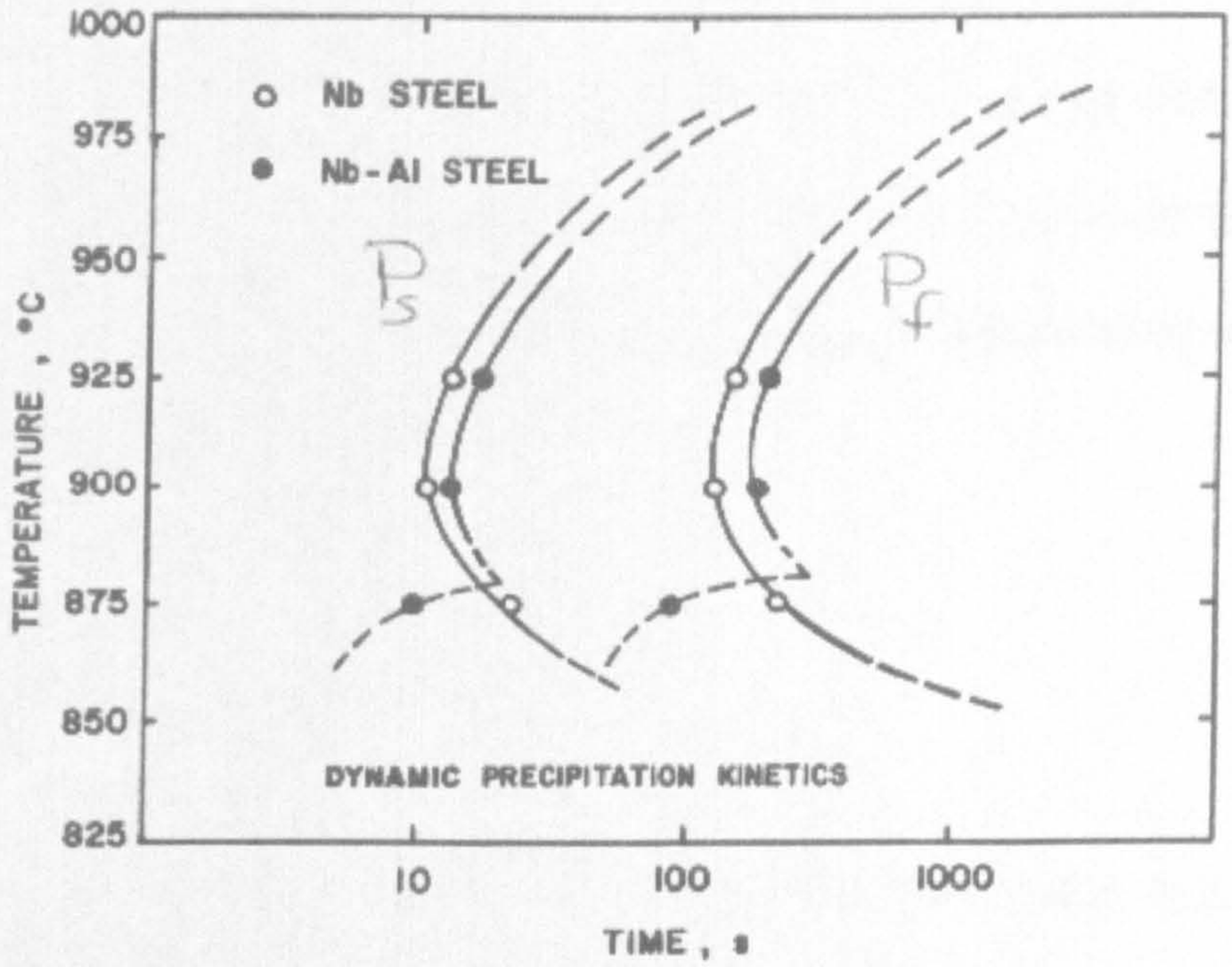

Figure 2-11 - PTT Curves for Nb

The above curves are in good agreement with the model for Nb precipitation proposed by Banks et al[69] and also with work done by Akben et al[70].

2.13 Steels containing Nb and Al

The addition of Al to a Nb containing steel has been shown[65] to delay the start and finish of precipitation in the austenite. There is some speculation about the order in which the precipitation occurs. Some authors[65,71] state that the AlN will precipitate earlier and at higher temperatures followed by NbN and NbC. However, it has been proposed more recently[72] that the order is in fact reversed with NbC precipitating earlier (although only slightly) than NbN and then followed by AlN. The "nose" temperatures (i.e. those giving the maximum rate of precipitation) proposed by Michel et al[81] seem to agree with this with Nb(CN) at 900°C and AlN at 885°C.

It has been found that the combined influence of Al and Nb on strength is stronger than the sum of their respective strengthening effects. Wang attributes this to a synergistic effect when the two microalloying elements are added. Darsouni[33] also suggests a synergistic effect when more than one microalloying element is added.

2.14 Steels containing Al

Aluminium is often added to steel as a de-oxidising agent. It is common practice for the steel maker to add more aluminium than is necessary to remove all the oxygen this is generally termed "free" or "soluble" aluminium. This soluble aluminium tends to combine with nitrogen to form aluminium nitride which then acts as a grain refining agent during subsequent processing.[73]

As a result of the above, aluminium is usually present in steels in excess of the stoichiometric ratio of 2:1, thus aluminium is often present in solid solution in the ferrite. Al additions have been found to be detrimental to the surface quality of the finished slab.

Al has also been found to be detrimental to the hot ductility of the steel[27,44,64,74,75] although the reduction in ductility is not related directly to the Al level but in fact to the AlxN product as expressed by Leslie's solubility law:

$$\text{Log (AlxN)} = -6770/T + 1.033 \quad \ldots..^{76}$$

The ductility is not only influenced by the volume fraction of AlN but also by the particle size[77], the smaller the particles, the greater the grain boundary pinning effect and as such the poorer the ductility. Conversely where larger particles are formed which allow relatively easy grain boundary migration the ductility drop is not as great. Funnel and Davies[7577] as well as Woodfine and Quarrell[78] suggest that the AlN precipitates are more detrimental to ductility than Ti precipitates and in fact advocate using Ti to tie up N in order to inhibit AlN formation.

AlN can precipitate out in two ways, within the austenite grains, and with Ti containing steels is frequently associated with Ti(C,N) precipitates, or at the austenite grain boundaries. Wilcox[63] suggests that the precipitates nucleate out at the grain boundaries as it is easier for them to form in these areas. Turkdogan[79] calculates that segregation of Al to the grain boundaries during solidification will increase the concentration of Al in these areas by a factor of 6. This segregation combined with strain accounts for the marked intergranular precipitation that has been observed by Maehara[26] and Mintz et al.[18]

Heritier et al[80] have however shown that AlN has no effect on ductility when present in an ultra high purity steel. It only has an effect when there are other elements (such as sulphur) present. They suggest that the AlN allows the sulphur to segregate by pinning the austenite grain boundaries hence embrittling the metal. These steels are very different to the normal commercial steels which have sufficient Mn present to reduce the sulphur

in solution to very low levels. Michel et al[81] show the maximum rate of precipitation for AlN to be at 885°C.

2.15 Nitrogen in Steels

It has been established for some time now that soluble N levels have no effect on the hot ductility of plain C-Mn steels.[82] However, it has been shown recently[83] that increased N content in as cast C-V and C-V-Nb steels deepens the ductility trough due to the greater volume fraction of precipitates though it does not influence the temperature at which the deterioration of the ductility begins.

Hannerz[84] has shown that although N is very influential in encouraging transverse cracking, he has also shown that it is only when N is present with Al that that ductility deteriorates. Thus it is the influence that N has on precipitation processes that affects ductility.

Wilcox and Honeycombe[64] have shown that increased N levels encourage precipitation of carbonitrides to occur at higher temperatures due to the decreasing solubility as nitrogen replaces carbon. Higher temperature precipitates tend to be coarser than those formed at lower temperatures and hence have less effect on hot ductility.

2.16 Strength of steel

2.16.1 At room temperature

The Hall Petch Relationship relates grain size to yield strength and is given by the following equation:

$$\sigma_y = \sigma_o + kd^{-\frac{1}{2}}$$

Where:

σ_y = yield stress

σ_o and K are material specific constants

d = average grain diameter

This equation has been found very satisfactory in relating the yield strength to the grain size of the steel at room temperature.

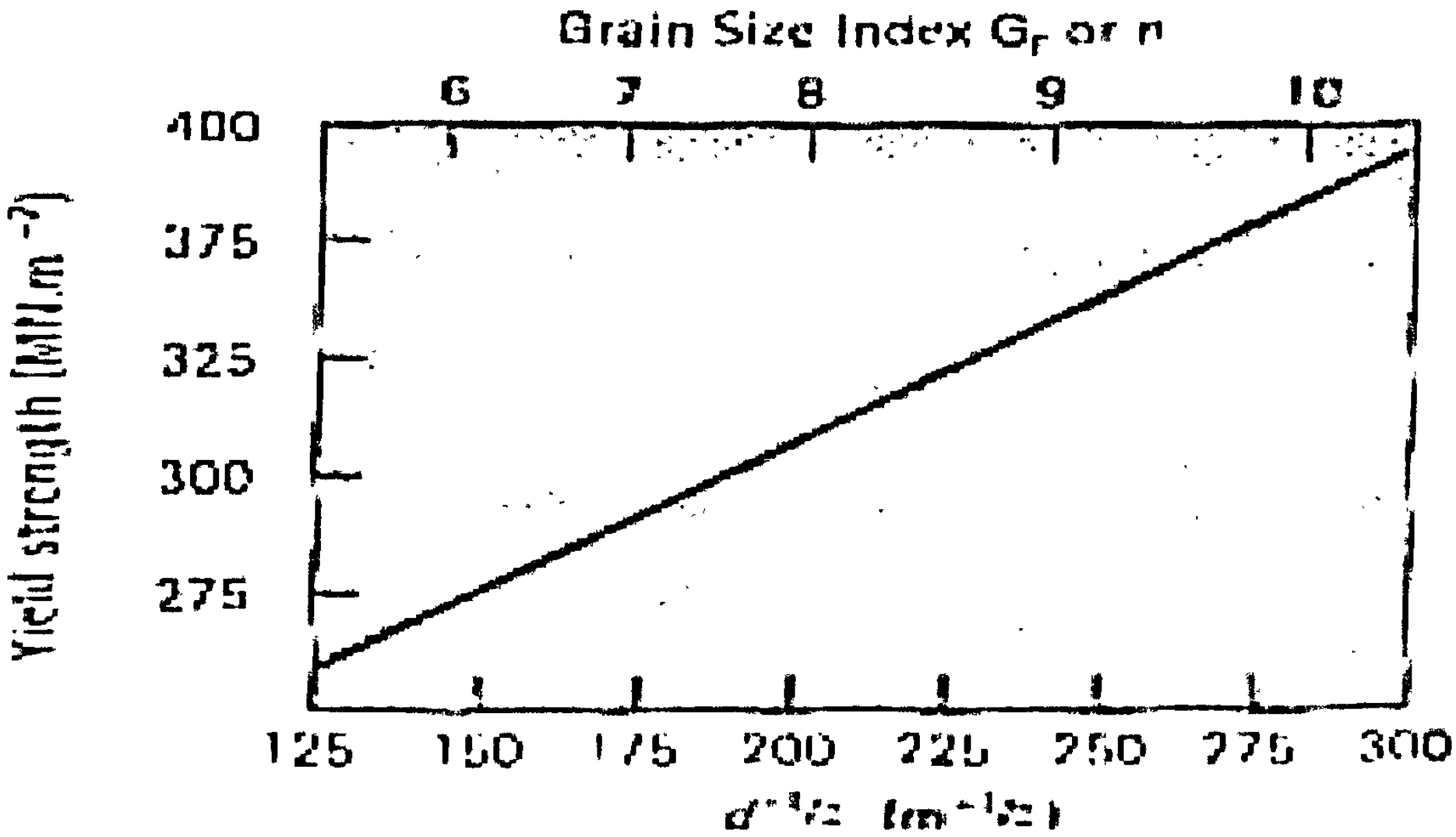

Figure 2-12 - The Relationship Between Yield Stress and Grain size

Askeland[85] publishes the above graph showing the relationship between yield stress and grain size.

2.16.2 At elevated temperatures

At elevated temperatures, the strength of austenite is more controlled by the temperature and strain rate rather than the grain size. The maximum stress at a given temperature and strain rate is dependant on when dynamic recrystallisation occurs. This occurs more readily in fine grained materials and at slower strain rates.

Work has also been produced by Maki et al[86] that shows that hot ductility is also influenced by grain size. Namely that the ductility in the austenite ferrite two phase region decreased with increasing austenite grain size. This is partly due to coarser grain size increasing the crack aspect ratio. However, they also found that the ferrite formed in different patterns depending on the grain size; in large grain size samples (350μm) the ferrite formed as detrimental thin films around the grains. However, in the smaller grained material (100μm) the ferrite formed in a globular manner leading to more uniform strain concentration.

2.17 Deformation induced Ferrite

The production of ferrite from austenite on cooling through the transformation is diffusion controlled. As such, the temperature that the transformation occurs at is dependant on the cooling rate, the faster the

cooling rate, the lower the temperature. Under equilibrium conditions the temperature that the transformation occurs is termed the Ae_3. With faster cooling rates the temperature is lower and is denoted by Ar_3. Deformation, by creating more rapid paths for diffusion, speeds up the transformation and the Ar_3 can then often approach the Ae_3.

Ferrite when it first forms from the austenite is generally in the form of films surrounding the prior austenite grain boundaries. In this form it can be very detrimental to ductility as although ferrite is very ductile, when both austenite and ferrite are present, because ferrite is the softer phase almost all the strain concentrates in this region leading to low ductility, ductile intergranular failures.

Once this band thickens ductility improves as the strain is taken by a larger volume fraction of the material. There will always be a trough in steels but the width of the trough will depend on how easy it is to thicken up the ferrite film.

The film is deformation induced and generally forms just below the Ae_3. As it often doesn't thicken up significantly until the temperature falls below the Ar_3 these troughs can be very wide > 100°C.

However, under suitable conditions this deformation induced ferrite can form large quantities just below the Ae_3 and the trough is very narrow. It is not entirely clear what conditions are required to achieve this, although recent work suggests that a high Ae_3 (i.e. low C and Mn) is beneficial as it

speeds up the austenite-ferrite deformation induced transformation. Rapid work hardening (i.e. high strain rates) may also be beneficial as by raising the strength of the ferrite more deformation can be transferred to the austenite in the boundary region possibly causing it to transform to ferrite.

THIS PAGE INTENTIONALLY LEFT BLANK

CHAPTER 3 – EXPERIMENTAL ARRANGEMENTS

3 EXPERIMENTAL ARRANGEMENTS

3.1 Test Pieces

Each of the samples tested had been machined from a 50Kg Vacuum melt cast hot rolled to 15mm gauge at the CORUS Swinden Laboratories site.

Following casting, the slabs were rolled and then the tensile samples were machined from them in the longitudinal direction. The samples were 110mm in length and 7.94mm in diameter. Each end of the samples was threaded with a 5/16 BSF thread which enabled them to be screwed in to the grips of the test machine. They also had a 2mm diameter hole drilled in the centre that ran up to the mid point in the length of the sample in order to allow access for a thermocouple into the melt zone.

A schematic diagram of the samples is shown in Figure 3-1 below

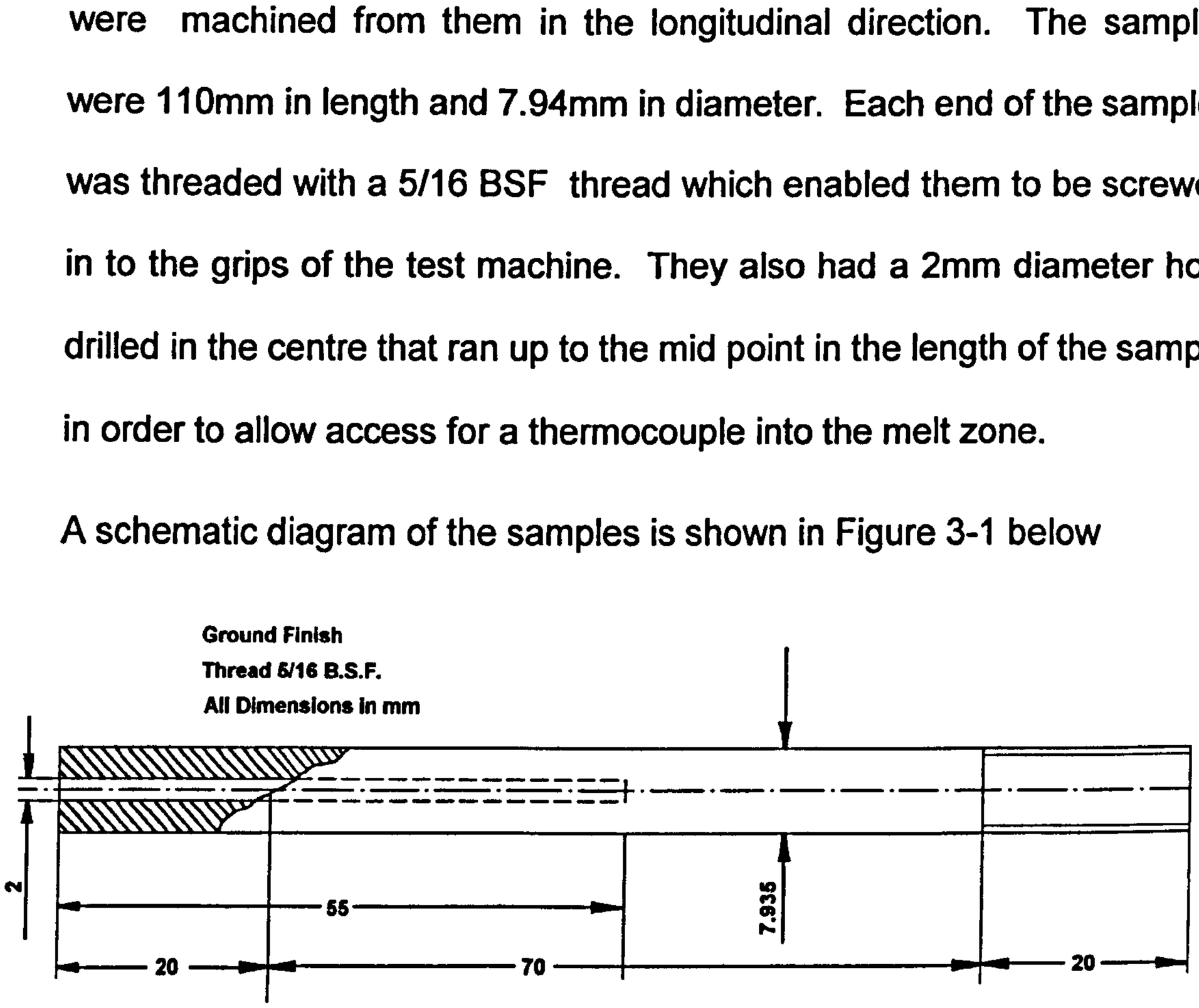

Figure 3-1 - Induction test piece

3.2 Test Equipment

The melt zone was approximately 22mm long (11mm either side of the mid point of the sample). The molten steel was contained in a silica tube that had 0.2mm diametrical clearance of the sample. Protection from oxidation was achieved by surrounding the sample with a larger glass tube through which argon was passed.

This is shown schematically in Figure 2 below.

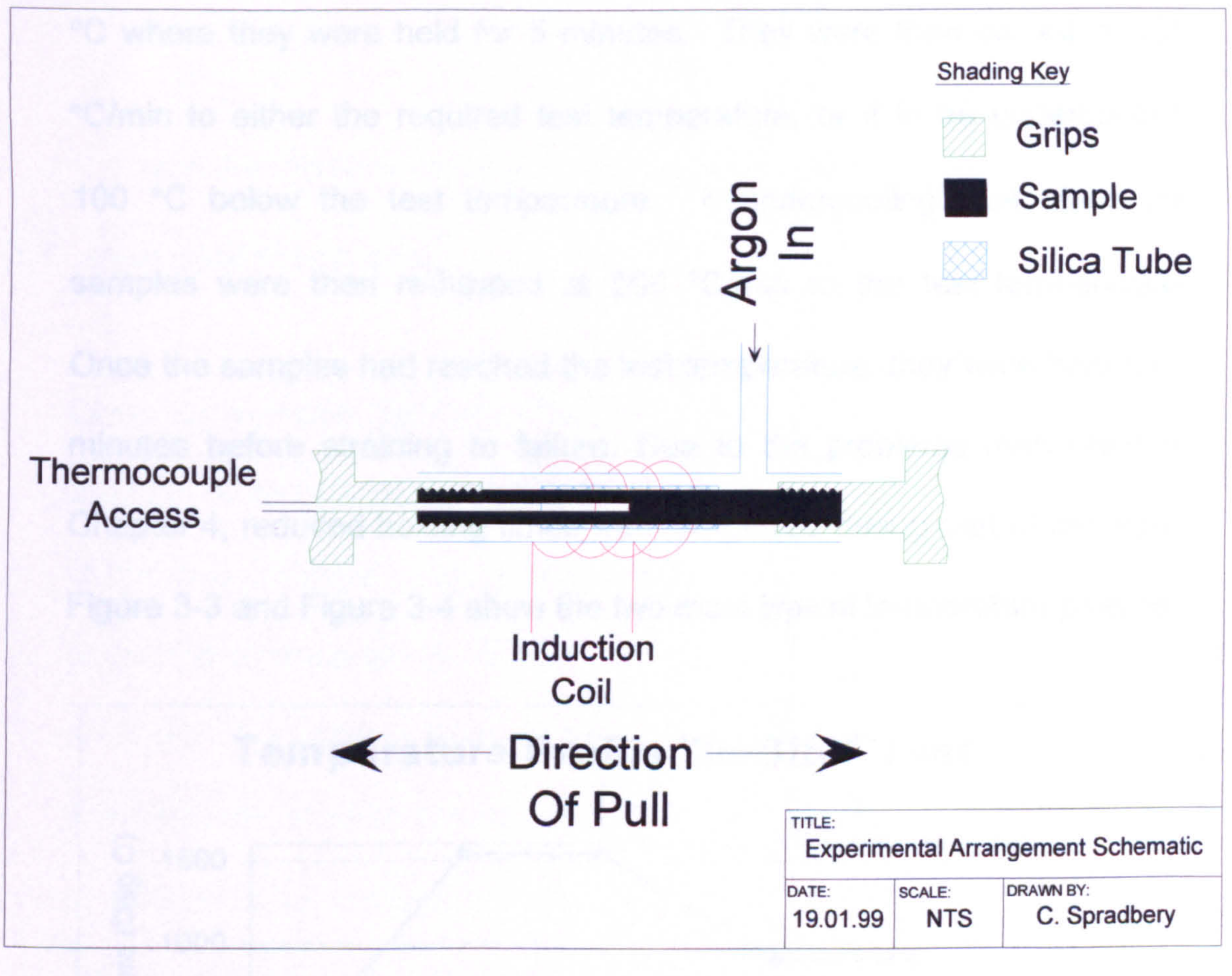

Figure 3-2 - Experimental Arrangements Schematic

The test machine housed in the City University Laboratories was a converted Hounsfield tensometer to which an induction heating device had been fitted. The induction heater was controlled by a Eurotherm

device that in turn was programmed and monitored by a PC. This enabled temperature accuracy of ±5°C to be obtained.

Temperature measurements were taken using a R type thermocouple (platinum/platinum 13% Rhodium).

3.3 Test Profiles

The samples were initially heated at 200 °C/min until they reached 1520 °C where they were held for 5 minutes. They were then cooled at 100 °C/min to either the required test temperature, or if to be undercooled, 100 °C below the test temperature. If undercooling took place the samples were then re-heated at 500 °C/min to the test temperature. Once the samples had reached the test temperature, they were held for 5 minutes before straining to failure. Due to the problems mentioned in Chapter 4, reduced holding times were employed during part of the work. Figure 3-3 and Figure 3-4 show the two most typical temperature profiles.

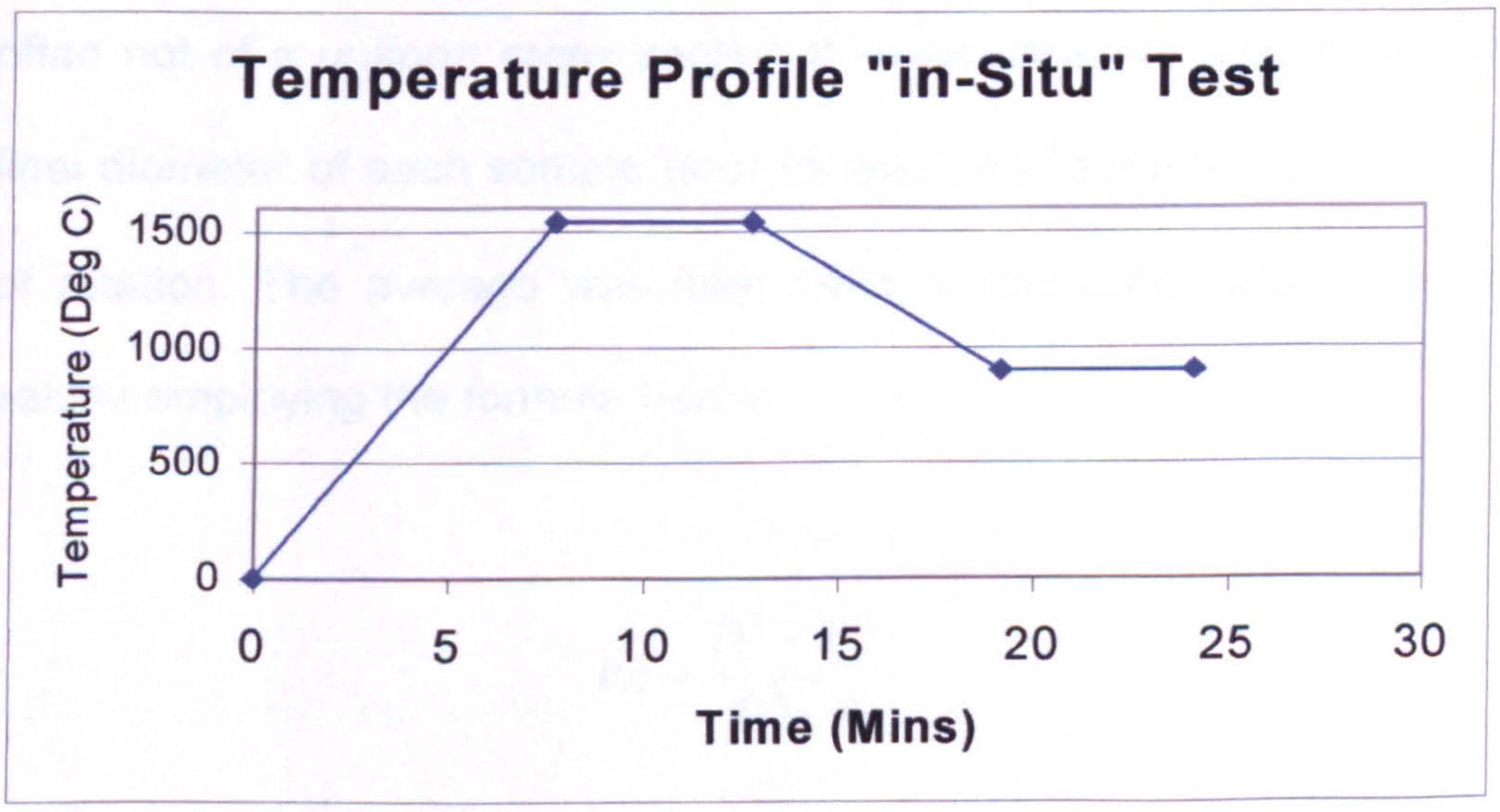

Figure 3-3 - Typical Test Profile

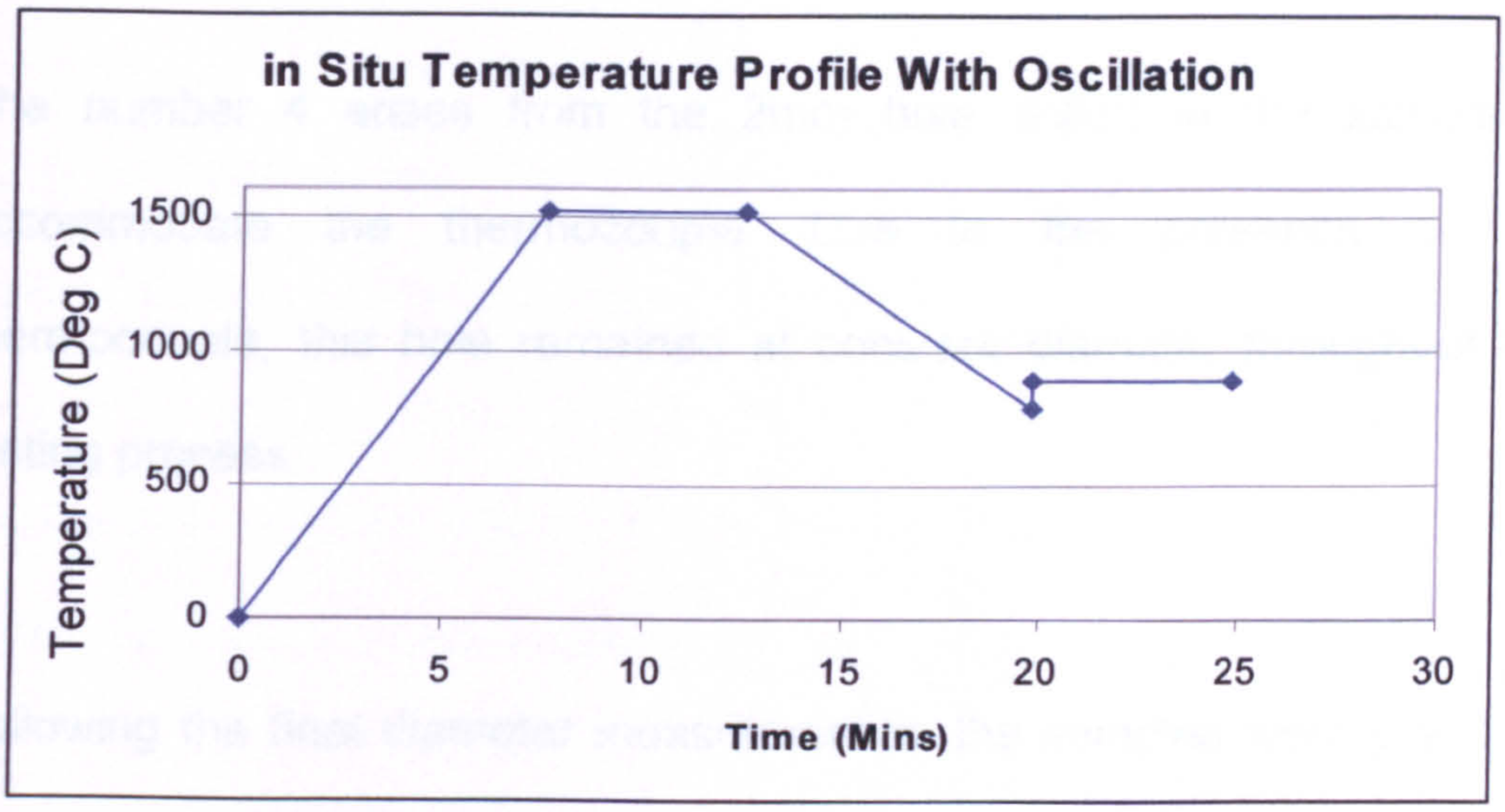

Figure 3-4 - Typical Test Profile with Undercooling

3.4 Post Test Processing

Once the samples had failed they were immediately gas quenched with argon in order to preserve the grain structure and fracture surface present at the time of failure. The samples were then measured under a Vickers projection microscope at 16 times magnification. As the samples were often not of a uniform cross section 8 measurements were taken of the final diameter of each sample (four for each half sample) at 45° intervals of rotation. The average was then used to calculate reduction of area values employing the formula below:

$$RA = \frac{D_i^2 - D_f^2}{D_i^2 - 4}$$

Where:

D_i = Initial Diamteter

D_f = Final Diameter

The number 4 arises from the 2mm hole drilled in the sample to accommodate the thermocouple. Due to the presence of the thermocouple, this hole remained at constant diameter throughout the testing process.

Following the final diameter measurements, the samples were prepared for optical and/or SEM (Scanning Electron Microscope) examination.

3.5 Grain size measurement

Grain size measurements were taken from the samples using the intercept method. The actual grain size was measured using a grain counting microscope. This is an optical microscope that has the capability to project a "light marker" on to the samples and is also fitted with a screw gauge micrometer. The light marker is moved over the sample and the number of grain boundaries encountered is recorded. The distance covered by the light marker was measured using the micrometer. In order to gain an accurate result between 30 and 40 grains were measured. The size was then determined using the following formula:

Grain size = Number of boundaries crossed/Distance traversed

3.6 Carbon Replicas

Carbon replicas were also prepared from the samples. This is a technique to copy the topography of a body on to a thin film of carbon in order to study it under an electron microscope. In order to obtain the carbon replica, specimens were mounted in the longitudinal direction in a clear plastic. They were subsequently ground down until the centre of the sample was reached and polished with increasingly fine materials until a final polish with 1 micron diamond paste.

The samples were then etched with a 2% Nital (Nitric acid and ethanol) solution. Following this, the samples were washed and then coated with a layer of carbon approximately 1 micron thick by arc evaporation of a carbon rod in a vacuum chamber.

The deposited carbon layer was then removed by immersing the sample in a 10% Nital solution. The resulting carbon film was placed onto small copper grids and examined under transmission electron microscope (at CORUS Swinden Laboratories). Some samples were also sent to the University of Pretoria, S.A. for replica examination.

The fracture surfaces of the samples were also examined using a scanning electron microscope in order to determine the fracture mechanism. Measurements were made of the dimple size to see if there was any relationship between this measurement and the reduction of area values Photographs were taken at salient points in this process.

3.7 Reliability of Results measurements

The temperature gradient along the melt zone was measured by gradually moving the thermocouple out from the centre of the sample. The results are shown in Figure 3-5 below. Figure 3-6 shows temperature gradient measurements for a further 20mm along the sample. It can be seen that the temperature remains relatively stable over the first 5mm from the centre of the melt zone but then begins to drop off significantly. The reliability of the temperature measurement is therefore inversely proportional to the distance between the fracture surface and the tip of the thermocouple. Only samples in which the fracture was within 5mm of the centre of the sample have been used in the results.

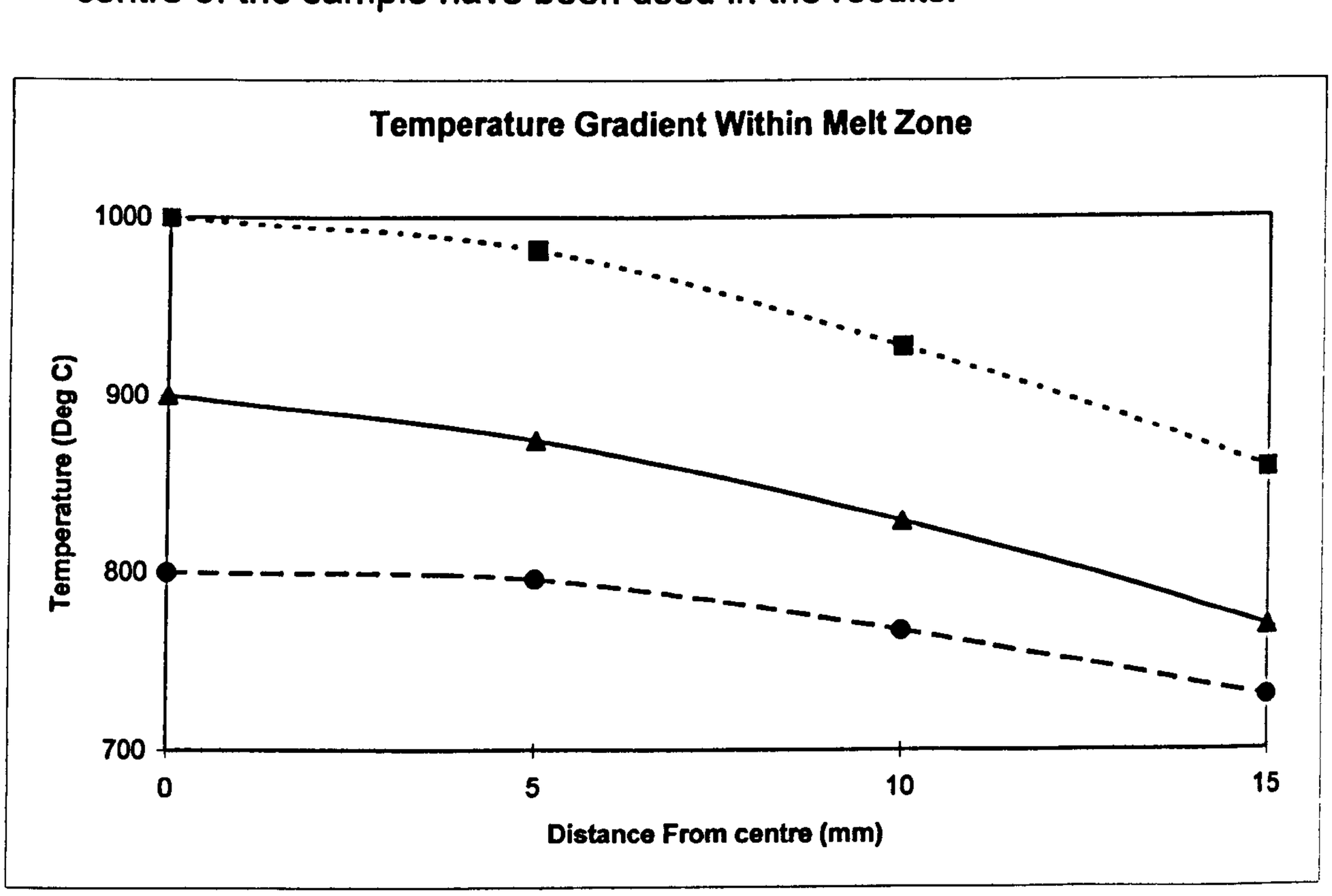

Figure 3-5 - Temperature Gradient Along the Melt Zone

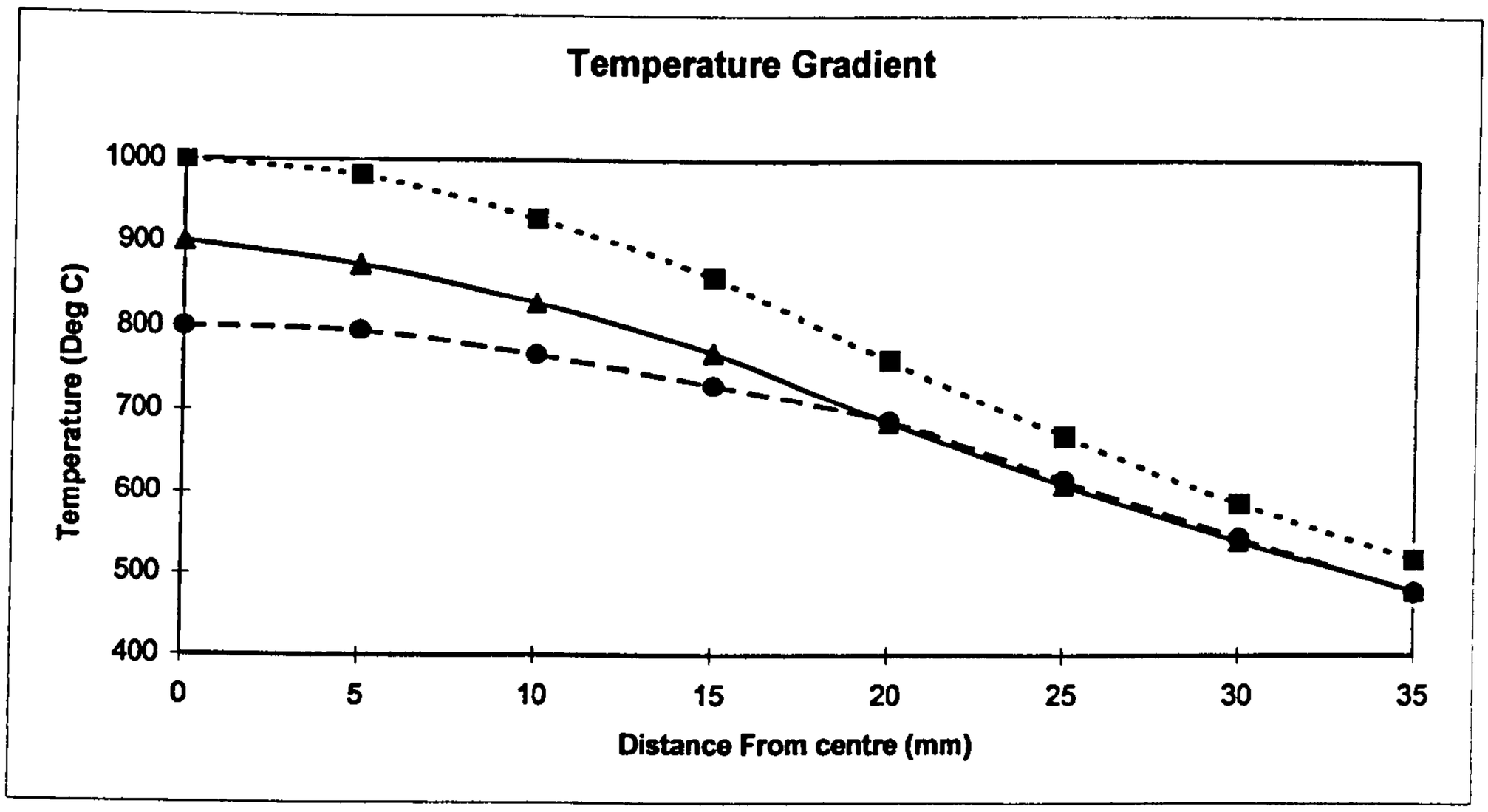

Figure 3-6 – Temperature Gradient Along The Test Piece

A number of results were repeated throughout the testing process in order to gain an idea of the reliability of the results produced. The repeat tests were all found to be within five percentage points of the original tests. Also any unusual results not fitting the general shape of the curve were repeated.

CHAPTER 4 – PROBLEMS ENCOUNTERED WITH EXPERIMENTAL ARRANGEMENTS

4 PROBLEMS ENCOUNTERED WITH THE EXPERIMENTAL ARRANGEMENTS

During the post-experimental analysis of the tested samples it was noted that many of the samples contained less Ti than in the pre-tested state. This was confirmed when the carbon replicas produced minimal TiN precipitates suggesting that some of the samples may be oxidising during the testing procedure and in particular Ti was being removed (see Alison Tulings Report contained in Appendix A).

Oxidation would explain the reduction in the post test Ti values as Ti could easily form oxides which would remove it from the solution. However, the tested samples did not exhibit any of the generally accepted signs of oxidation; they remained clean and shiny and the fracture surface remained clean under the SEM. Spark analysis will not of course differentiate between Ti in solution, TiN or TiO and gives only the total Ti content. Therefore it was difficult to ascertain where the Ti had gone. Furthermore, using very similar conditions, no problems with loss of Ti had been encountered in the previous five years of research work on Ti containing steels.

When the samples are re-melted the heating, cooling and testing is carried out in an argon atmosphere with the molten steel contained within a silica glass tube. The flow rate of argon around the silica tube is around

0.5 L/min which should be easily sufficient to prevent oxidation of the 22mm melt zone from occurring.

The argon employed in the testing procedure is the purest commercially available argon, being certified as 99.99% pure. The tubes that supply the argon to the test bed were leak tested and found to be sound (also should a leak occur the tendency would be for the pressurised argon to seep out rather than the surrounding air to seep in).

However, work carried out by Köthe[87] on an ESC programme on Ti containing steels ran into a similar problem in 1997 when it was suggested that Ti loss to the silica tube surrounding the molten metal was occurring. An analysis of the melted and unmelted region as a function of melting time is shown in Table 1 below for two of Köthe's samples. It can be seen that as the melting time increases from zero to 1 minute that the Ti level falls from 0.014/0.013 to 0.003/0.004.The City University Hot ductility Research group were notified of this problem in 1997 (see Appendix 3) and checks were made at that time to ensure Ti loss was not occurring in our samples, but no significant losses were experienced even with as long a holding time of 5 minutes at the melting temperature.

Holding Time (s)	Mn	Si	Al	Nb	Ti
0	1.31	0.37	0.022	-	0.014
10	1.33	0.33	0.019	-	0.013
60	1.04	0.45	0.002	-	0.003
0	1.31	0.33	0.02	0.021	0.013
10	1.18	0.39	0.007	0.021	0.009
60	0.95	0.46	0.003	0.020	0.004

Table 1 – Composition Change with increasing hold time

Checks and relevant analyses were carried out on molten sections of the City University Ti Steels by Köthe at IFW and also at CORUS (at that time British Steel). No Ti loss was found suggesting that our experimental techniques were acceptable. The present crisis therefore came completely by surprise. Obviously once we were aware of the problem, investigations were undertaken to identify the source. Comparison with earlier work showed that the results of the initial work on this project i.e. steels P8H27 and P8H28 (steels containing no Ti) along with P8H31 and P8H32 (the earliest steels to be tested) could be relied upon. Particularly as subsequent analysis on these steels showed no loss of Ti for all conditions.

One possible cause could be the change in glass supplier that occurred at a date which corresponds approximately to the onset of the problems.

This change was required as the original supplier became unable to manufacture the tubes to the correct tolerances. To establish whether this was the cause, samples of the silica tubes from the old and the new supplier have been sent for comparative analysis and the results are shown in Table 2 below.

	Original Supplier	New Supplier	Original Glass supplier (2 years later)
Fe_2O_3	0.54	0.53	0.66
CaO	1.71	0.54	0.11
SiO_2	94.36	97.22	97.7
MgO	0.73	0.47	0.14
Al_2O_3	0.52	0.36	0.22
P_2O_5	0.007	0.007	0.007
MnO	0.005	0.001	0.005
K_2O	0.007	0.008	0.013
V_2O_5	0.002	0.001	0.003
TiO_2	0.099	0.032	0.017
Na_2O	0.082	0.065	0.130
Cr_2O3	0.071	0.064	0.56
Ignition Loss	1.78	0.49	0.50

Table 2 – Silica Glass Analysis

It can be seen that there is little difference in the composition of the two silica tubes (original and new in the above table) however, it should be noted that the original glass does contain less Si oxide and more of the aggressive oxide formers Ca, Ti and Na. The wall thicknesses of the glasses were also very different, the newer glass being much thicker. It is possible that the heat loss through the thicker walled glass was lower producing a higher temperature and increasing reaction rates. The coil had also been replaced during the research program with the new coil

being slightly longer. This change only occurred within the last three months of testing making this again an unlikely explanation.

The only other possible source of oxygen in the apparatus could occur if one of the argon bottles used to shield the samples during testing (each argon cylinder will contain sufficient for approximately 80 tests to be carried out) had become contaminated.

As the cause of the presence of oxygen within the test apparatus could not be exclusively isolated it was decided to continue testing with the use of a sacrificial reactant and shorter test times. Fe/Ti filings were placed within the argon atmosphere, although just outside the silica tube. The argon cylinder was also replaced with a new one and testing was performed using a small supply of the original silica tubes. Ti loss was much reduced, however, some loss still occurred.

Because of this problem, a considerable amount of re-testing and subsequent re-writing has had to be carried out causing a significant delay in the production of the thesis.

Recently, it has been possible to obtain a full analysis of the melted and unmelted regions on samples tested after the change in glass composition/manufacturer occurred (originally only a Ti analysis was possible from these small samples but the CORUS laboratories at

Teeside have now managed to obtain a full analysis). When these (Table 3 and Table 4) are compared to those obtained by Köthe (Table 1) it can be seen that the analysis is very similar. Not only is there a loss of Ti with increased melting time but the Si level increases and the Mn content decreases as with Kothe's work. This proves beyond doubt that the problems encountered are due to the silica glass tube reacting with the Ti in the sample. The Ti combines with the oxygen in the silica replacing the silicon which then enters the sample. Again, reducing the melting time from 5 minutes (Table 3) to 30 seconds as in Table 4 results in a much reduced loss of Ti.

The silicon content of the melted region can be seen in Table 3to be on average ~40% greater than the original content. In contrast, analysis of melted samples when tested using an alumina tube instead of silica gives no loss in the Ti level as shown in Table 5. It should be noted that there are also no losses or gains in the other elements.

Cast	C	Si	Mn	P	S	Al	Ti	Ti:N
P8H31 (unmelted)	0.110	0.3	1.41	0.009	0.002	0.028	0.013	2.6
P8H31 (5 min hold melted)	0.12	0.452	0.929	0.011	0.002	0.002	0.002	
P8H33 (unmelted)	0.100	0.3	1.40	0.01	0.002	0.028	0.022	4.4
P8H33 (5 min hold melted)	0.097	0.483	0.976	0.013	0.003	0.022	0.005	

Table 3 - Analysis of melted and unmelted regions with a 5 minute holding time and a silica tube

Cast	C	Si	Mn	P	S	Al	Ti	Ti:N
P8H29 Cast Composition	0.100	0.3	1.40	0.01	0.002	0.027	0.008	1.6
Analysis Results								
P8H29 (unmelted)	0.11	0.31	1.36	0.008	0.002	-	0.008	
P8H29 (1/2 min hold melted)	0.1	0.283	1.38	0.014	0.001	-	0.009	
P8H29 (unmelted)	0.10	0.29	1.4	0.006	0.002	-	0.1	
P8H29 (1/2 min hold melted)	0.11	0.353	1.24	0.006	0.005	-	0.005	

Table 4 - Analysis of melted and unmelted regions with a 1/2 minute holding time and a silica tube

Cast	C	Si	Mn	P	S	Al	Ti	Ti:N
P8H30 Cast Composition	0.100	0.3	1.40	0.01	0.002	0.025	0.008	1.6
Analysis Results								
P8H30 (unmelted)	0.09	0.303	1.36	0.004	0.006	-	0.009	"
P8H30 (1 min hold melted)	0.09	0.298	1.38	0.003	0.006	-	0.009	"

Table 5 - Analysis of melted and unmelted regions with a 1 minute holding time and an alumina tube

In order to verify the above, further testing was carried out using alumina tubes on a steel with a similar base composition although a higher N level (0.1%C, 0.35%Si, 1.41%Mn, 0.007%P, <0.005%S, 0.017%Al, 0.009%N, 0.028%Nb, 0.026%Ti). A hold time of 5 minutes was used for this sequence of tests. 4 of the samples tested were sent to CORUS Teeside laboratories for analysis. The results of which are shown in the following table.

No.	Cast	C	S	Si	Mn	P	Al	Ti
1	P0H32 (unmelted)	0.100	0.002	0.35	1.41	0.008	0.019	0.026
1	P0H32 (melted)	0.099	0.002	0.34	1.41	0.009	0.04	0.026
2	P0H32 (unmelted)	0.106	0.002	0.33	1.37	0.010	0.015	0.024
2	P0H32 (melted)	0.108	0.003	0.33	1.40	0.010	0.09	0.024
3	P0H32 (unmelted)	0.103	0.003	0.31	1.36	0.007	0.015	0.023
3	P0H32 (melted)	0.098	0.002	0.33	1.39	0.009	0.036	0.027
4	P0H32 (unmelted)	0.100	0.002	0.34	1.41	0.012	0.025	0.025
4	P0H32 (melted)	0.113	0.002	0.34	1.43	0.009	0.084	0.028

Table 6 - Analysis of melted and unmelted regions with a 5 minute holding time and an alumina tube

It can be seen from Table 6 that, when the alumina tube is employed, there is no loss of Ti even when a holding time of five minutes is used. All subsequent re-tests were therefore carried out using alumina as opposed to silica tubes. The high Al levels found in the melted tensiles are most likely due to contamination from the thermocouple sheath, parts of which invariably break off into the thermocouple hole on fracture.

However, this does not explain why no problems were encountered when using the original silica glass tubing. Although differences in composition were small, the original glass did have a lower silica level and more of the stabler oxides like Mg and Ca. Subsequent tests using tubes supplied by the original glass supplier still failed to solve the problem with large Ti losses being encountered.

However, analysis of the present silica tubes being supplied by the original manufacturer shows the composition to be very different from the tubes supplied at the beginning of this project (Table 2). A high Si level (98%) was found with none of the very stable oxides present. It is apparent that the original glass supplier has changed the composition of his tubing without notifying us (the manufacturer has also reduced the wall thickness). It is presumed that high silica glass is cheaper to manufacture and the compositional differences will not affect many customers. Some loss of Ti does occur with the better quality silica glass (~10-15% loss) and the most recent work has replaced the silica glass with alumina sheathing and no subsequent loss in Ti has occurred.

The results discussed in the thesis are given for samples which have been tested using silica sheaths. Some of the curves were obtained using the original silica tubes that had low silica levels and greater amounts of stable oxides in their composition. The curves for P8H27 and P8H31 were carried out using these tubes.

Subsequently, when it was discovered that Ti loss was occurring, melting times were shortened from 5 minutes to 1 minute and then to 30 seconds. This generally resulted in a small loss of Ti (~10-20%). This method of testing forms the basis for the remaining curves. It is likely that even with the original silica tubes some small loss of Ti took place.

The problem of Ti loss has now been solved using alumina tubes and no loss now takes place (see Table 6). Unfortunately Very few samples remained that could be tested using these tubes. The results from these samples are given in Figure 4-1.

Figure 4-1 shows the results of a series of tests carried out on P8H30, a 0.008%Ti, 0.03 % Nb steel. The original results, which were obtained using a silica sheath, are plotted against a more recently obtained set, obtained by melting the sample within an alumina sheath. It can be seen from the graph that ductility is approximately 10% worse when using the alumina tubes which is to be expected as there is now no loss of Ti. The undercooling cycle leads to a small deterioration in ductility in accord with further precipitation occurring.

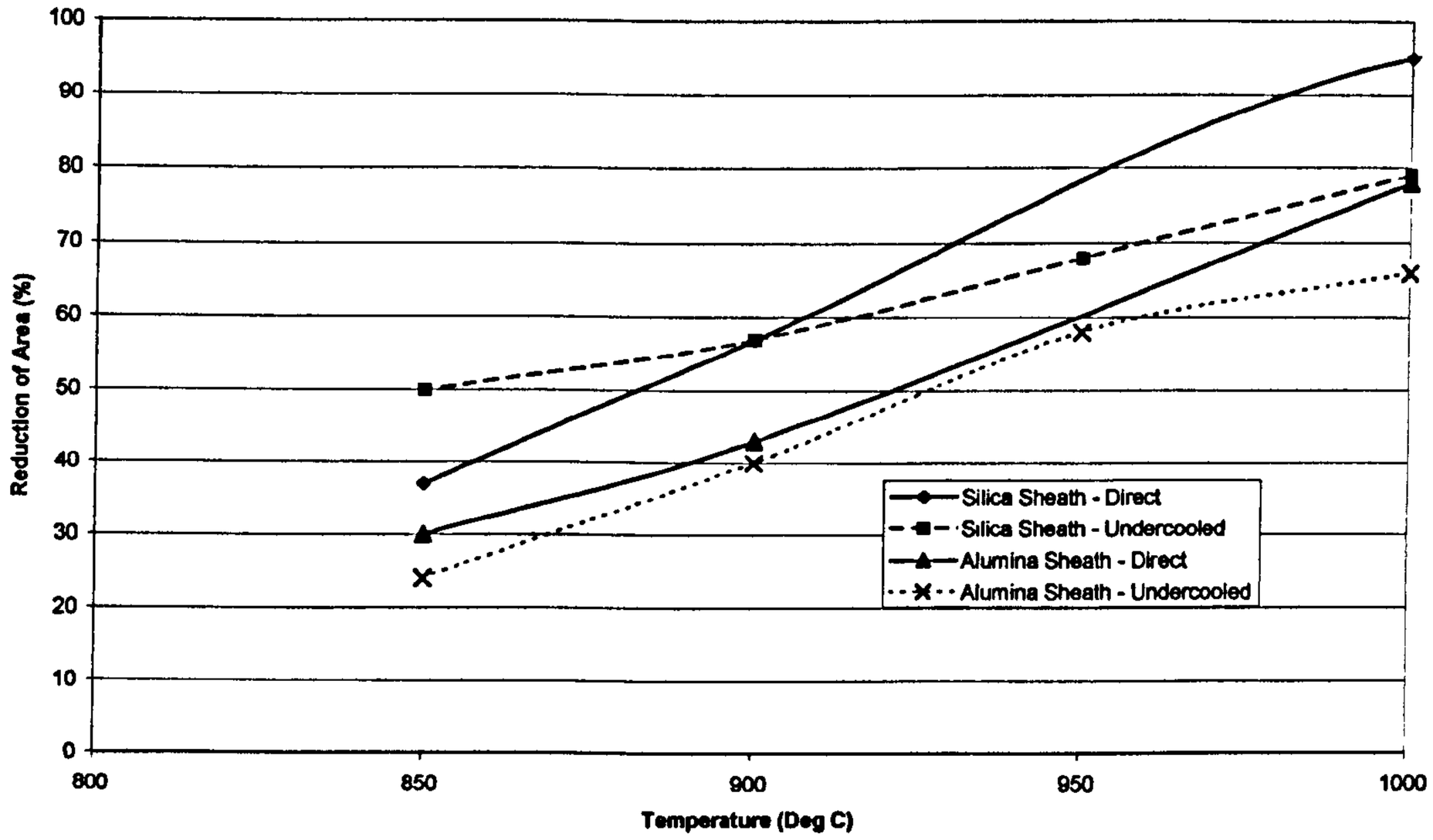

Figure 4-1 – Comparison of P8H30 Results using Alumina and Silica Sheath Materials

CHAPTER 5 - RESULTS

5 RESULTS

Because of oxidation problems during the experimental work many of the original results had to be repeated (please refer to Chapter 4). However, stringent checks indicated that some of the earlier work was satisfactory. The results thought to be satisfactory are shown in this chapter. This chapter also contains the results of all re-tests and additional testing performed in order to verify the original results. The original (potentially erroneous) results are shown in Appendix 2.

5.1 Steel compositions

The compositions of the steels tested (by weight per cent) are as follows:

Cast	C	Si	Mn	P	S	Al	N	Nb	Ti	Ti:N
P8H27	0.091	0.3	1.38	0.01	0.002	0.031	0.005	<0.005	<0.005	0
P8H28	0.091	0.3	1.38	0.01	0.002	0.029	0.005	0.029	<0.005	0
P8H29	0.100	0.3	1.40	0.01	0.002	0.027	0.005	<0.005	0.008	1.6
P8H30	0.100	0.3	1.40	0.01	0.002	0.025	0.005	0.03	0.008	1.6
P8H31	0.110	0.3	1.41	0.009	0.002	0.028	0.006	<0.005	0.013	2.2
P8H32	0.110	0.3	1.40	0.01	0.002	0.026	0.005	0.031	0.013	2.6

Table 7 - Steel compositions

Steels were C-Mn-Al and C-Mn-Nb-Al having Ti additions from zero to 0.013 covering the Ti:N ratio range from 0 to 2.6:1.

The first part of the work consisted of examining the influence of Ti on the hot ductility of C-Mn-Al and C-Mn-Nb-Al steels using the standard

temperature profile (i.e. without undercooling) shown in the experimental arrangements section. This was followed by the tests involving undercooling and also by some analysis of the dimple sizes present in the failed samples.

5.2 Ae_3 Temperatures

The Ae_3 temperatures for the steels were calculated using Andrews formula. The results are shown in Table 8 below. Not surprisingly the calculated Ae_3 temperatures are in a very narrow band 839-852°C

Steel	Ae_3 (° C)
P8H27	852
P8H28	852
P8H29	846
P8H30	846
P8H31	839
P8H32	839
P8H33	839
P8H34	843

Table 8 - Ae_3 Temperatures

5.3 The Influence of Ti on Al containing steels

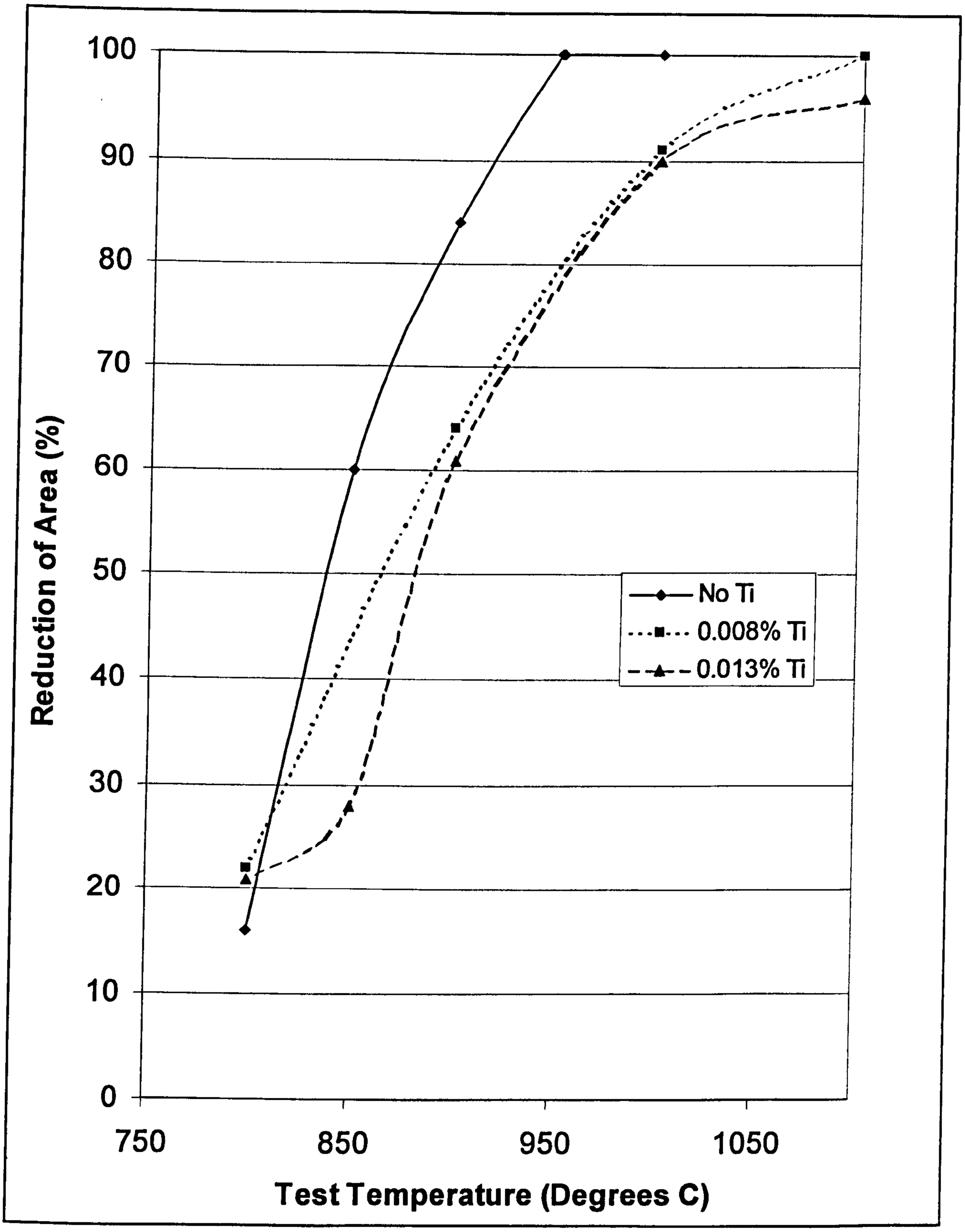

Figure 5-1 - The influence of Ti on Al Containing Steels - without undercooling

The above figure clearly shows that the addition of 0.008% Ti to a plain C-Mn-Al steel causes the ductility of the steel to deteriorate. A slightly greater deterioration in ductility is experienced with the addition of 0.013% Ti to the steel.

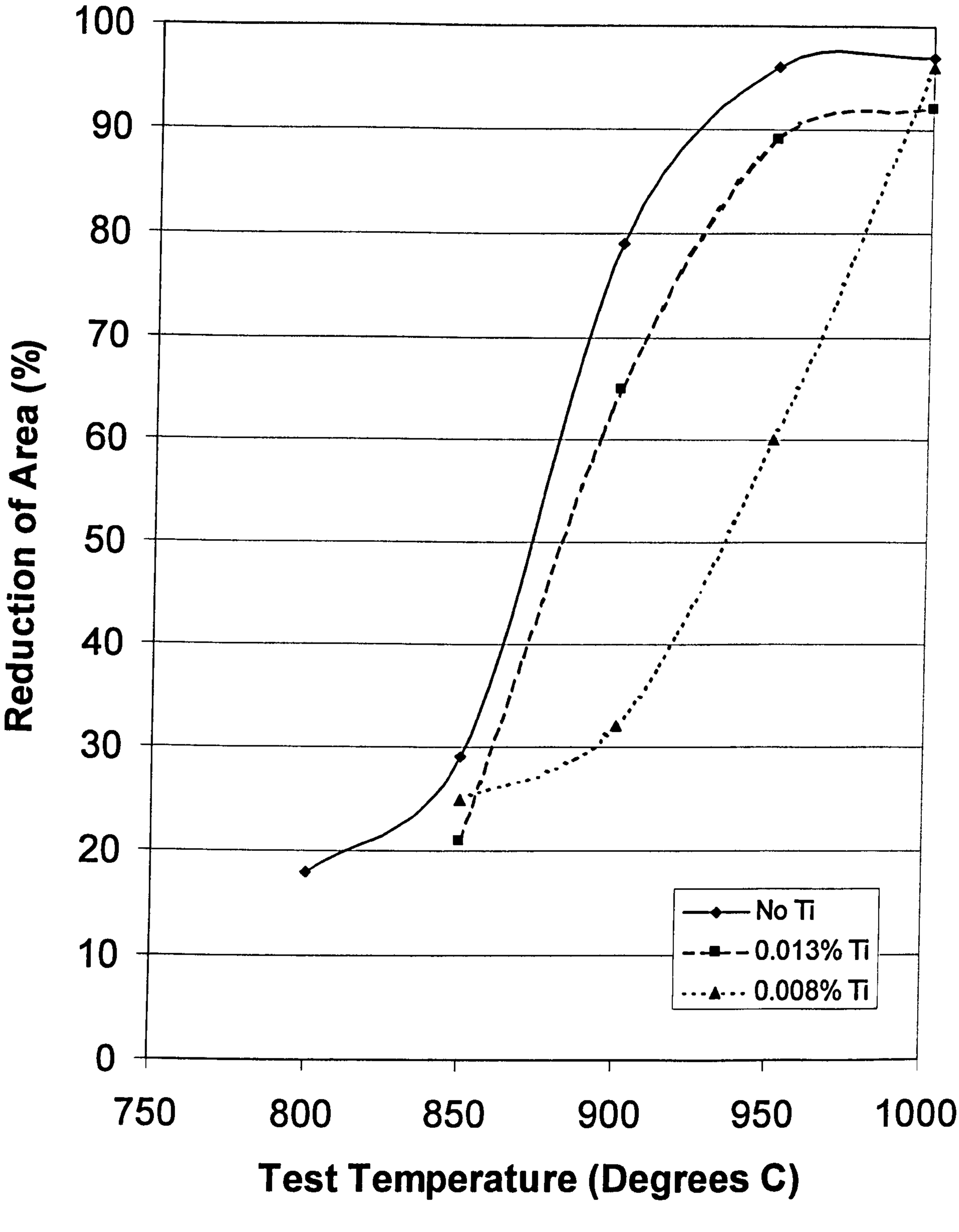

Figure 5-2 - The influence of Ti on Al containing steels with Undercooling

Figure 5-2 above shows the influence of the addition of Ti on Al containing steels which have undergone a 100 °C undercooling step before being reheated to the test temperature. It can be seen that adding Ti to the steel in this instance causes the ductility to deteriorate however some improvement in ductility apparently occurs on raising the Ti level from 0.008% to 0.013%.

5.4 The Influence of Nb

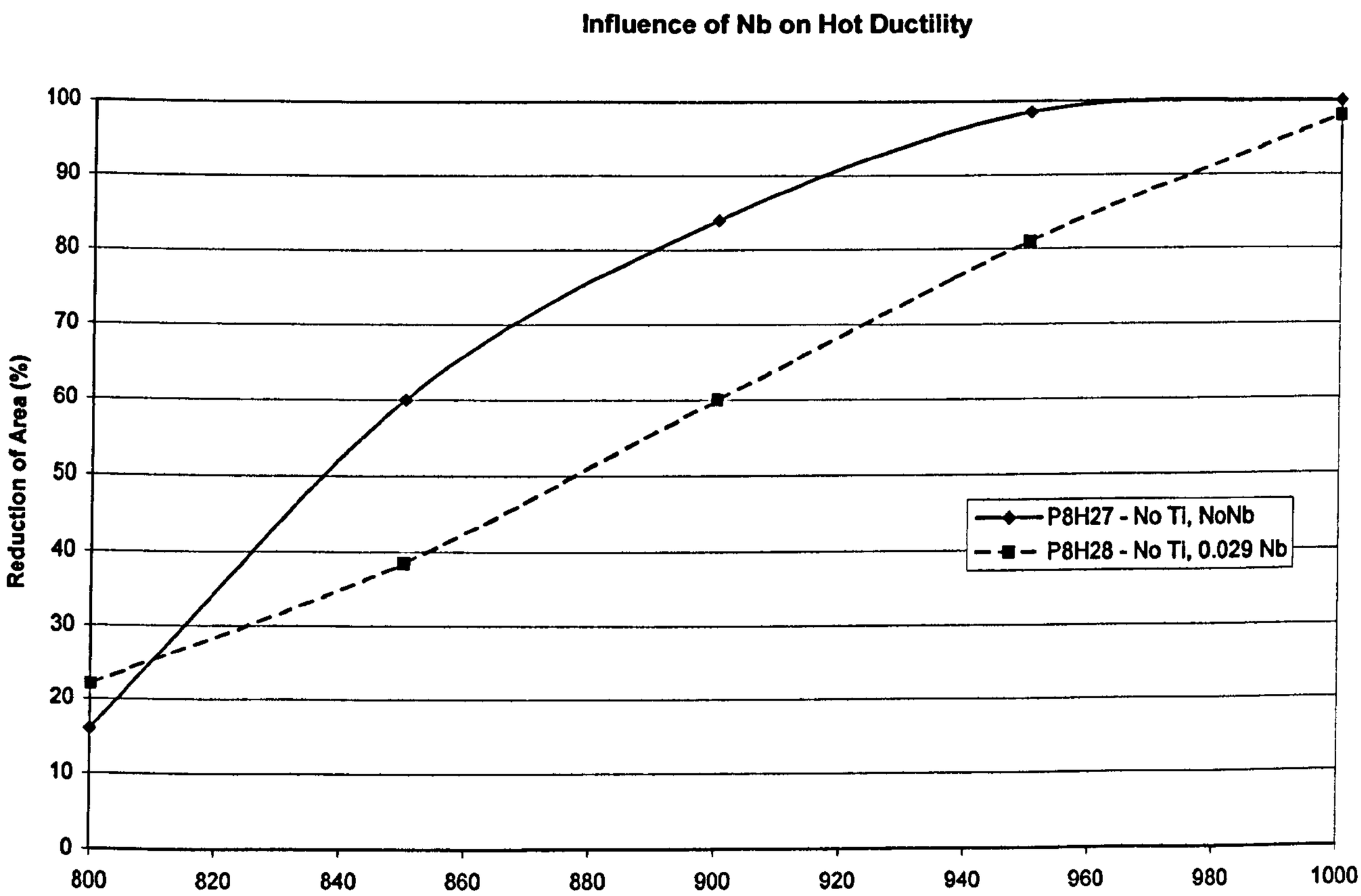

Figure 5-3 - The influence of Nb on hot ductility of a Ti free steel with ~0.005% N – No undercooling

The above figure shows that the addition of 0.03% Nb to a plain C-Mn steel under simple cooling conditions causes a deterioration in the hot ductility. This is in line with previous work[5].

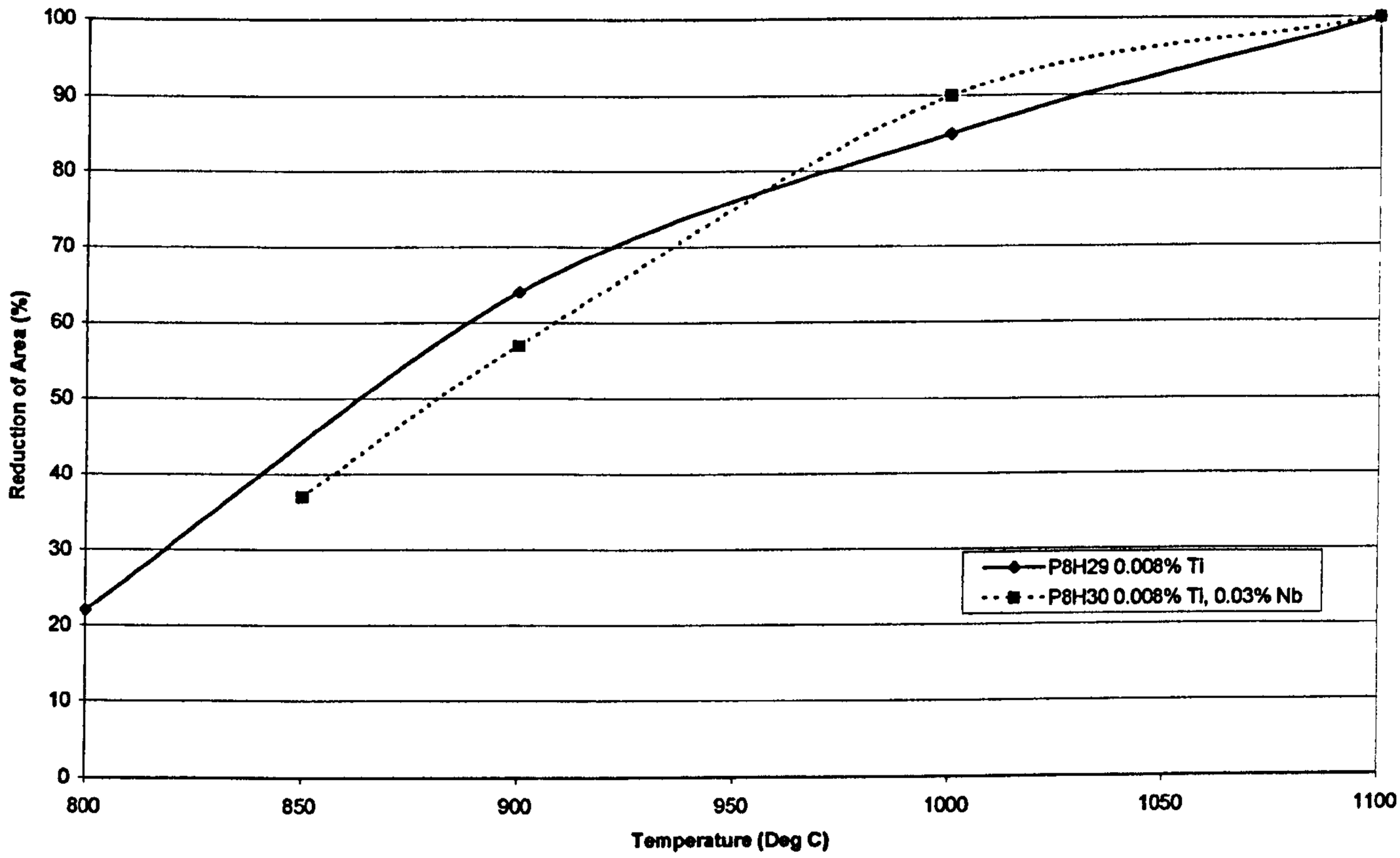

Figure 5-4 - The addition of Nb to 0.008%Ti Steel – No undercooling

Figure 5-4 shows the effect of the addition of Nb to a steel containing 0.008% Ti. It can be seen that a small deterioration in the ductility of the Ti containing steel occurs below 950°C with the addition of Nb when no undercooling is present.

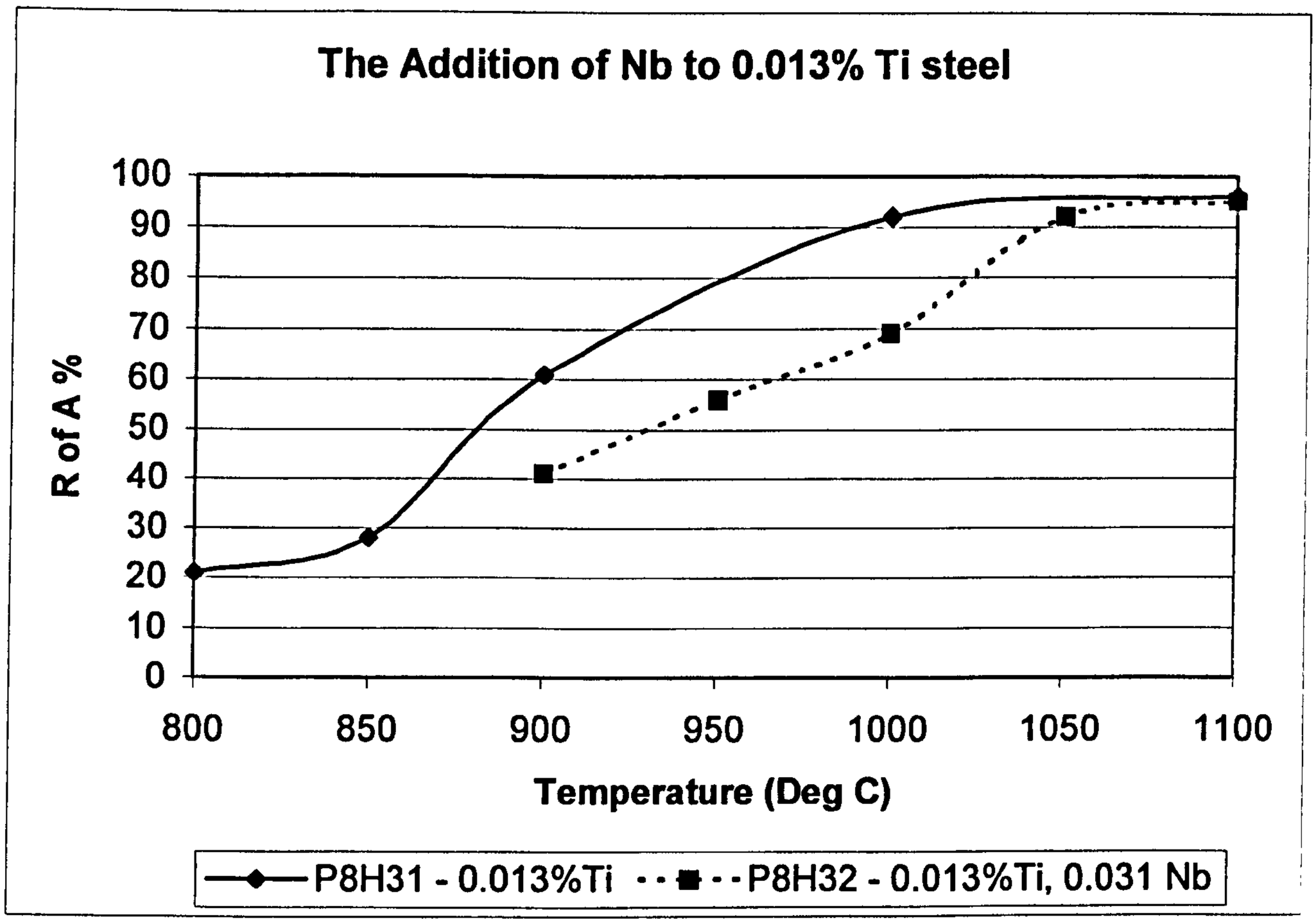

Figure 5-5- The Addition of Nb to a 0.013% Ti Steel – No Undercooling

A more marked deterioration is noted in Figure 5-5 which shows the addition of 0.031 Nb to a steel containing 0.013% Ti. This addition has a detrimental effect on the hot ductility, significantly increasing the width of the trough.

5.5 The influence of Ti on Nb containing steels

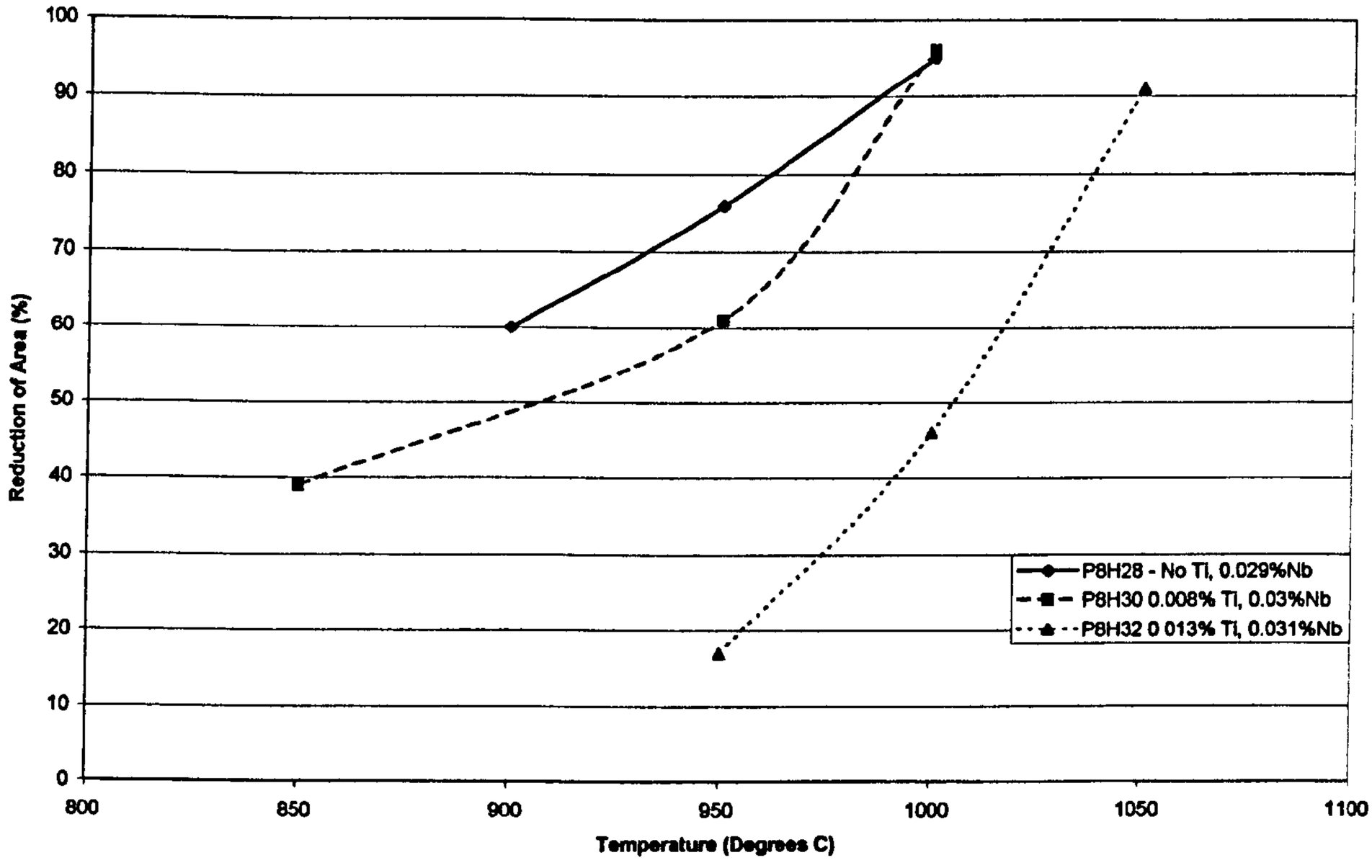

Figure 5-6 - The influence of Ti on Nb containing Steels - No undercooling

The above figure clearly shows that, under normal cooling conditions, as the Ti level of the Nb containing steels is increased, the ductility deteriorates.

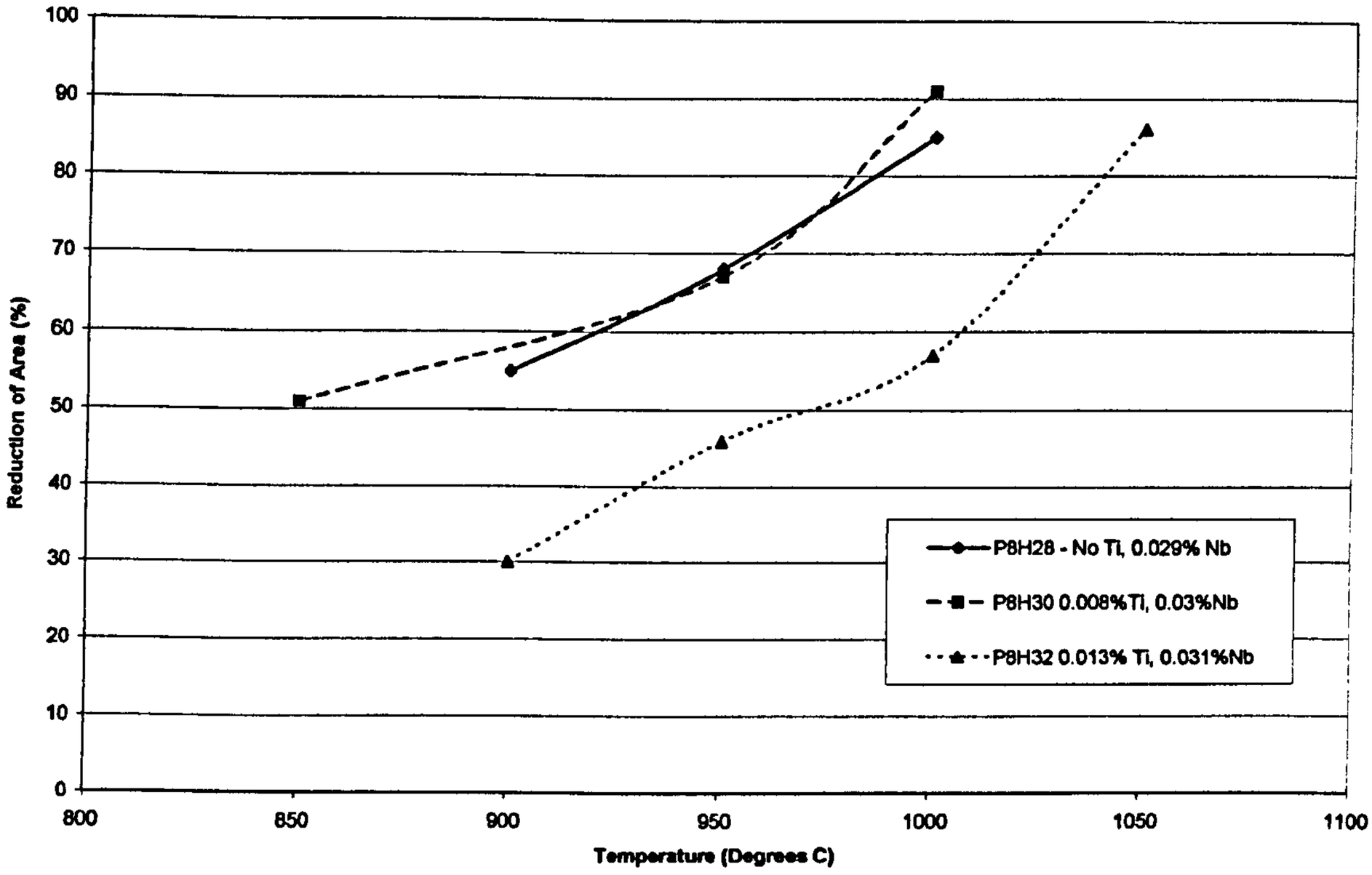

Figure 5-7 - Influence of Ti on Nb containing Steels - With undercooling

This is also noted when undercooling is introduced but the effect of Ti is less marked (Figure 5-7) particularly at the very low Ti level of 0.008% Ti.

5.6 The effects of undercooling

The following set of Figures show the results of the undercooling tests on each of the individual steels. Generally undercooling results in ductility deteriorating but there are a few exceptions.

5.6.1 Undercooling of Ti free steels

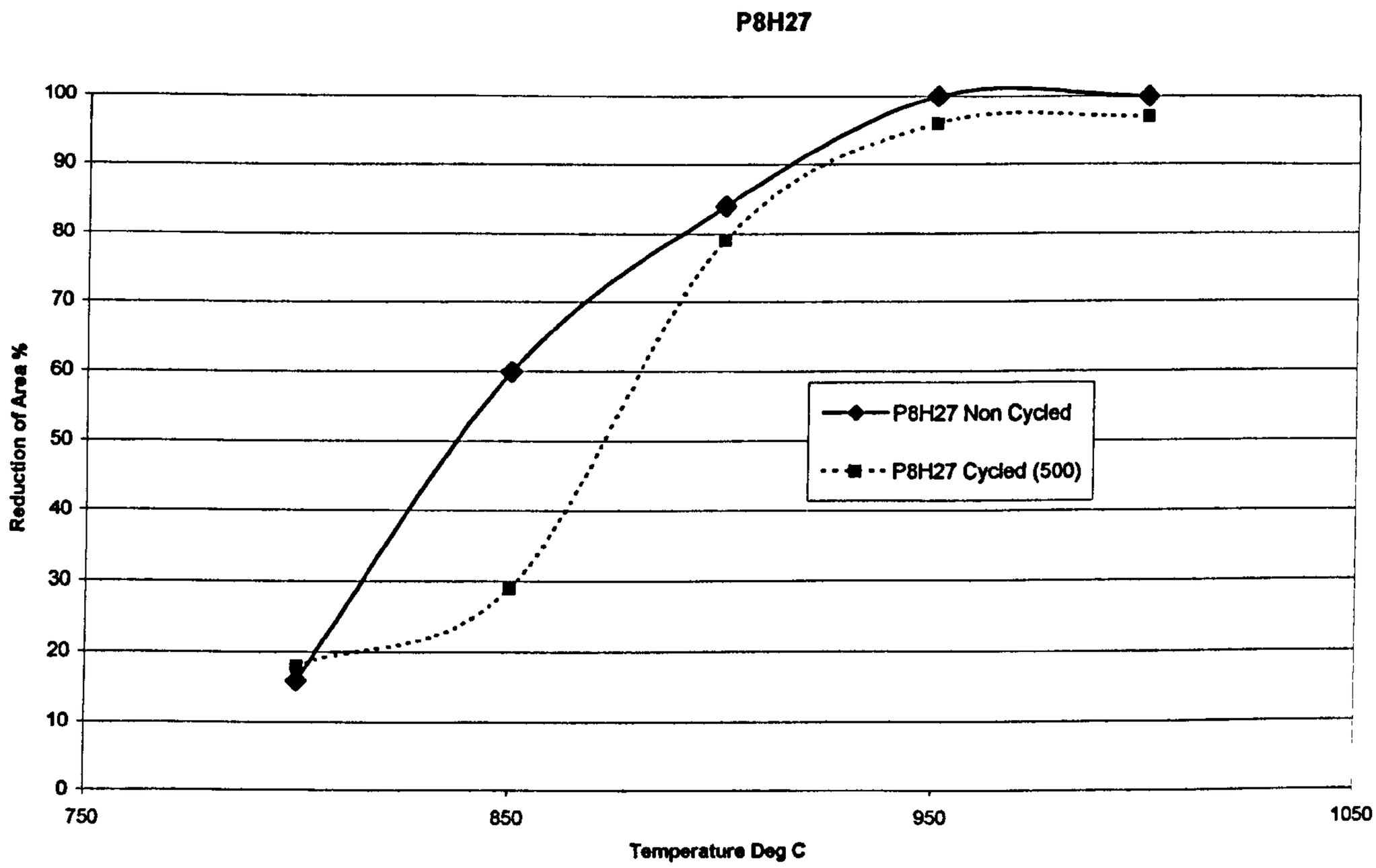

Figure 5-8- The effect of undercooling on simple C-Mn steel

Figure 5-8 above clearly shows that the 100°C undercooling step with the subsequent re-heat at 500°C/min has a marked effect in deteriorating the

ductility of the steel. It can be seen that the effect gets more pronounced as the test temperature is reduced.

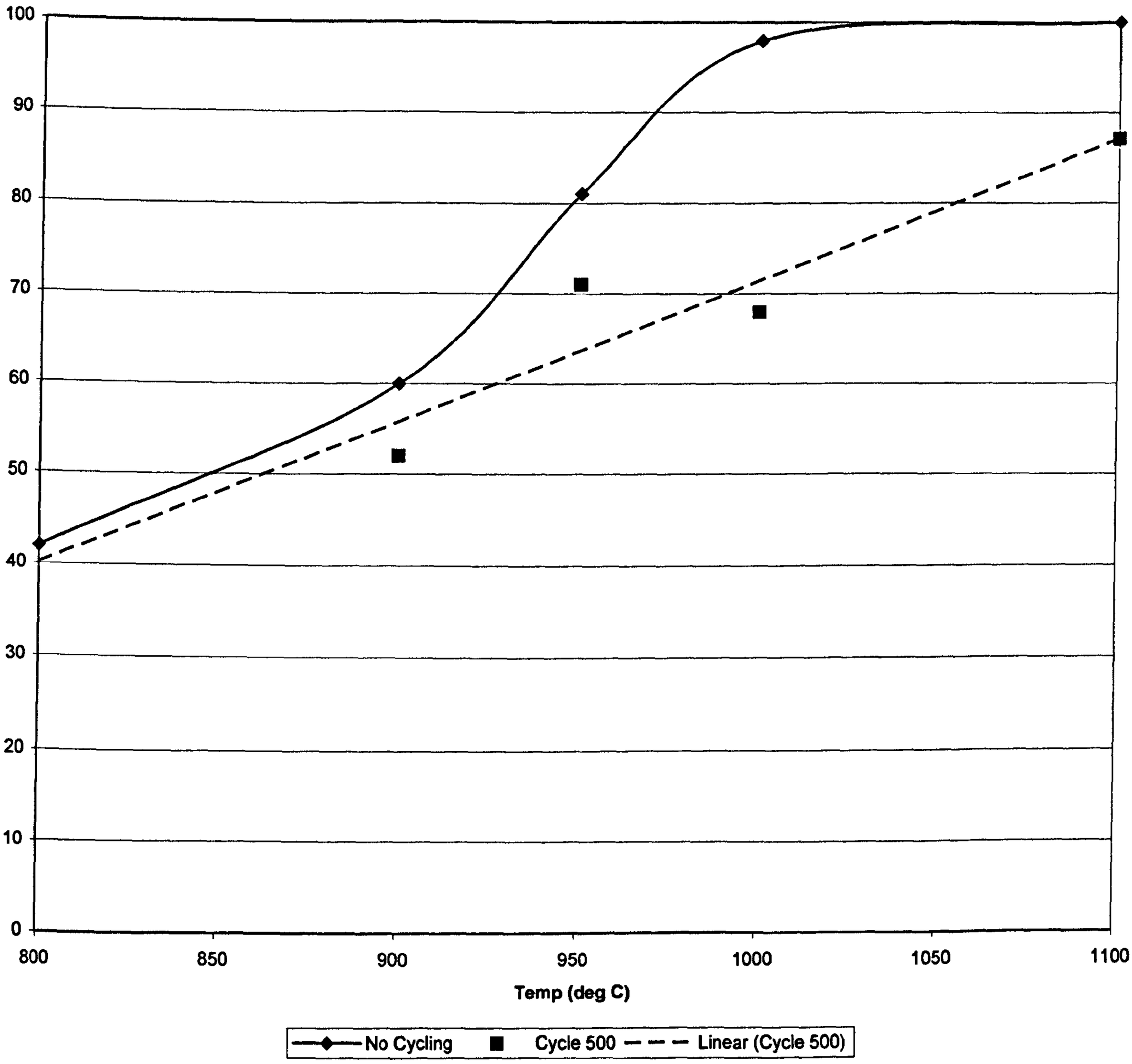

Figure 5-9 - the effect of undercooling on a Ti free steel containing 0.029 Nb

The above Figure again shows that the undercooling has a detrimental effect on the hot ductility of a Ti free Nb containing steel.

5.6.2 Influence of undercooling on Ti containing steels

When the undercooling cycle is applied to Ti containing steels the general effect is a resulting decrease in ductility. However, in some cases ductility is hardly affected (Figure 5-10) and occasionally with the Nb containing steels there is a small improvement in ductility. All the undercooling curves are compared with their straight counterparts in Figures 5-11and

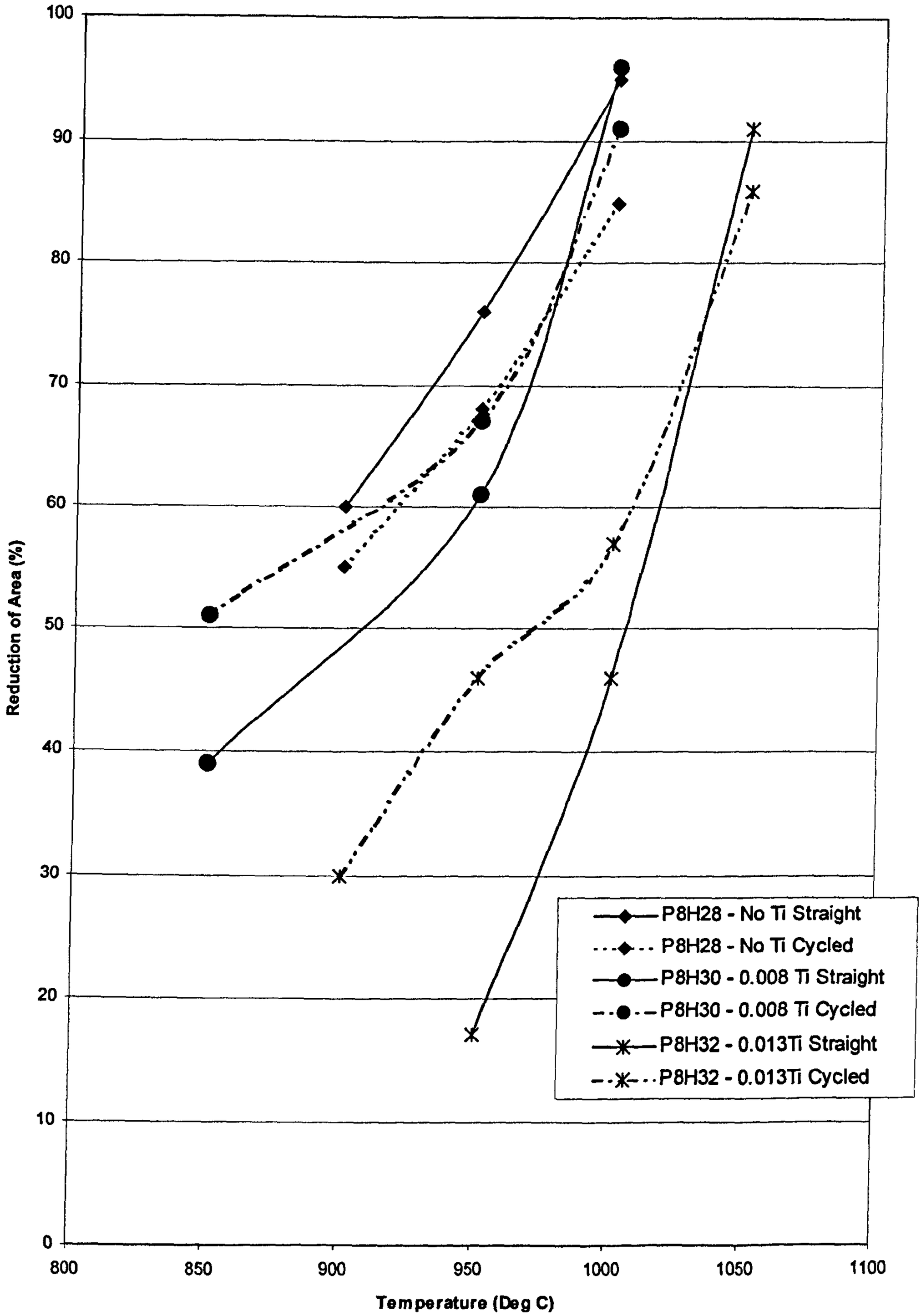

Figure 5-12 for the C-Mn-Al and C-Mn-Nb-Al steels respectively.

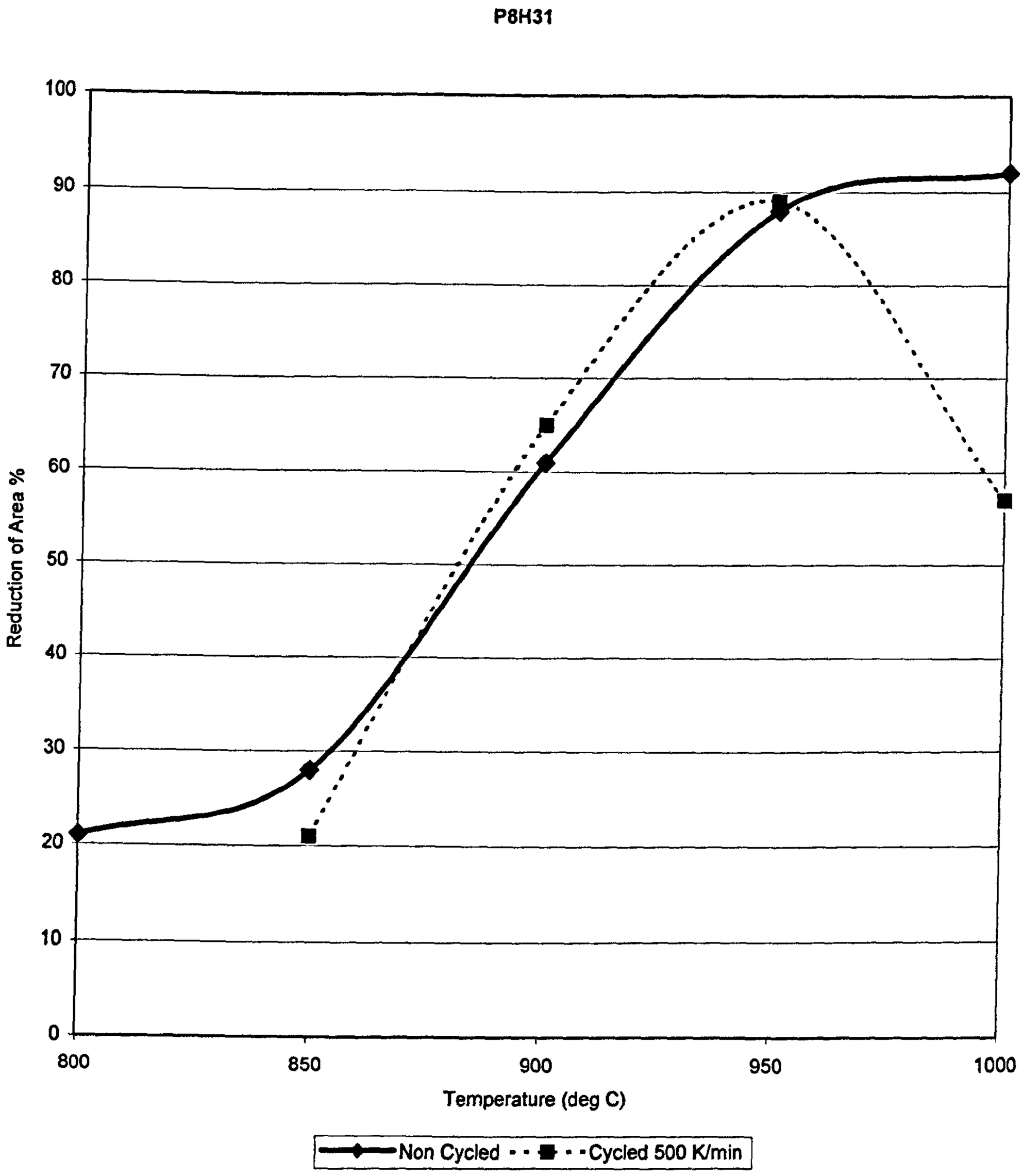

Figure 5-10- The effect of undercooling on a Nb free steel with 0.013% Ti

The above Figure shows that the effects of undercooling are limited on this steel (0.013% Ti) which has a Ti:N ratio of 2.3. A small improvement may occur at the upper temperature ranges.

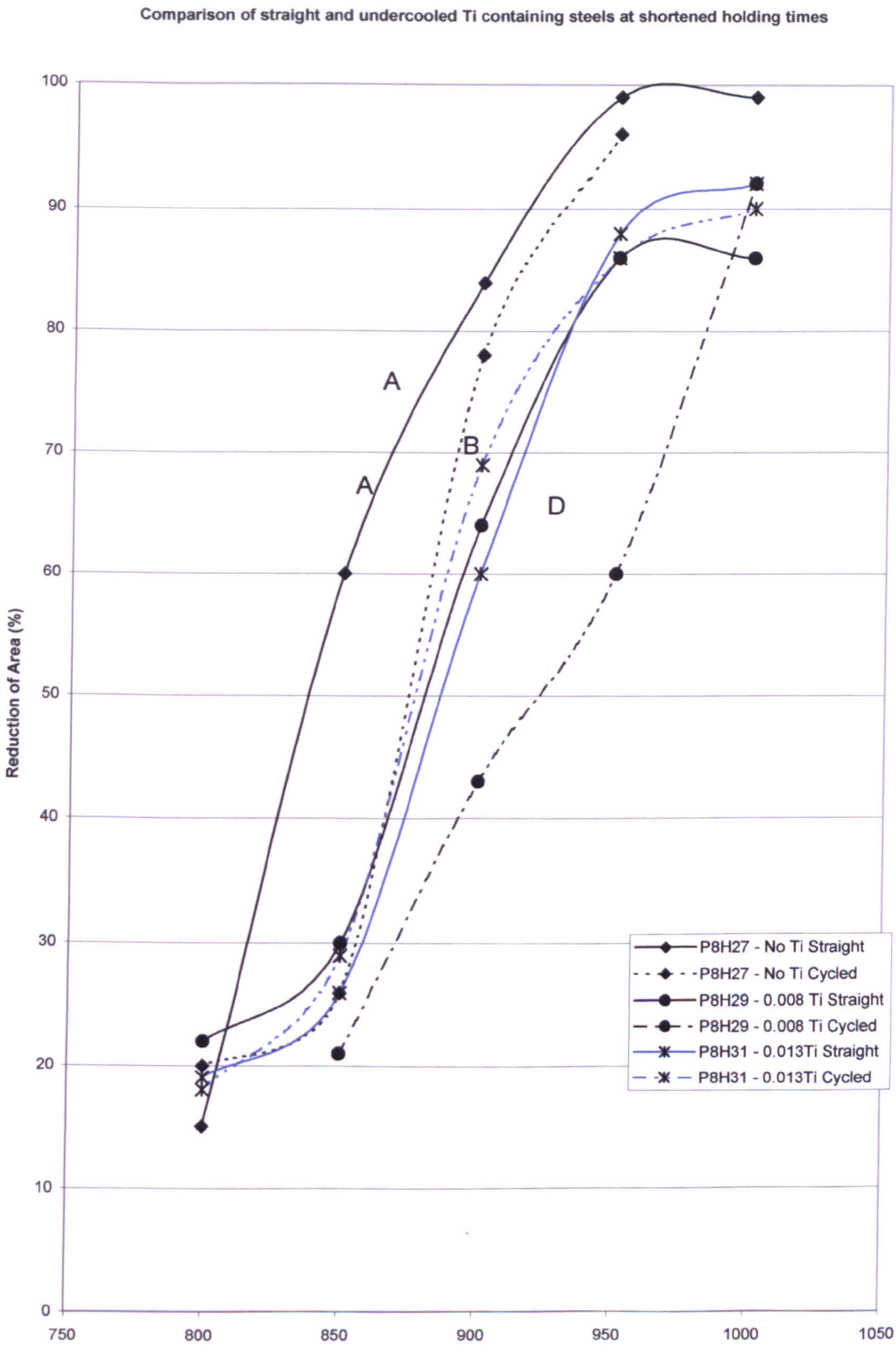

Figure 5-11 The effect of Ti on C-Mn-Al Containing Steels at a reduced holding time of 2 minutes.

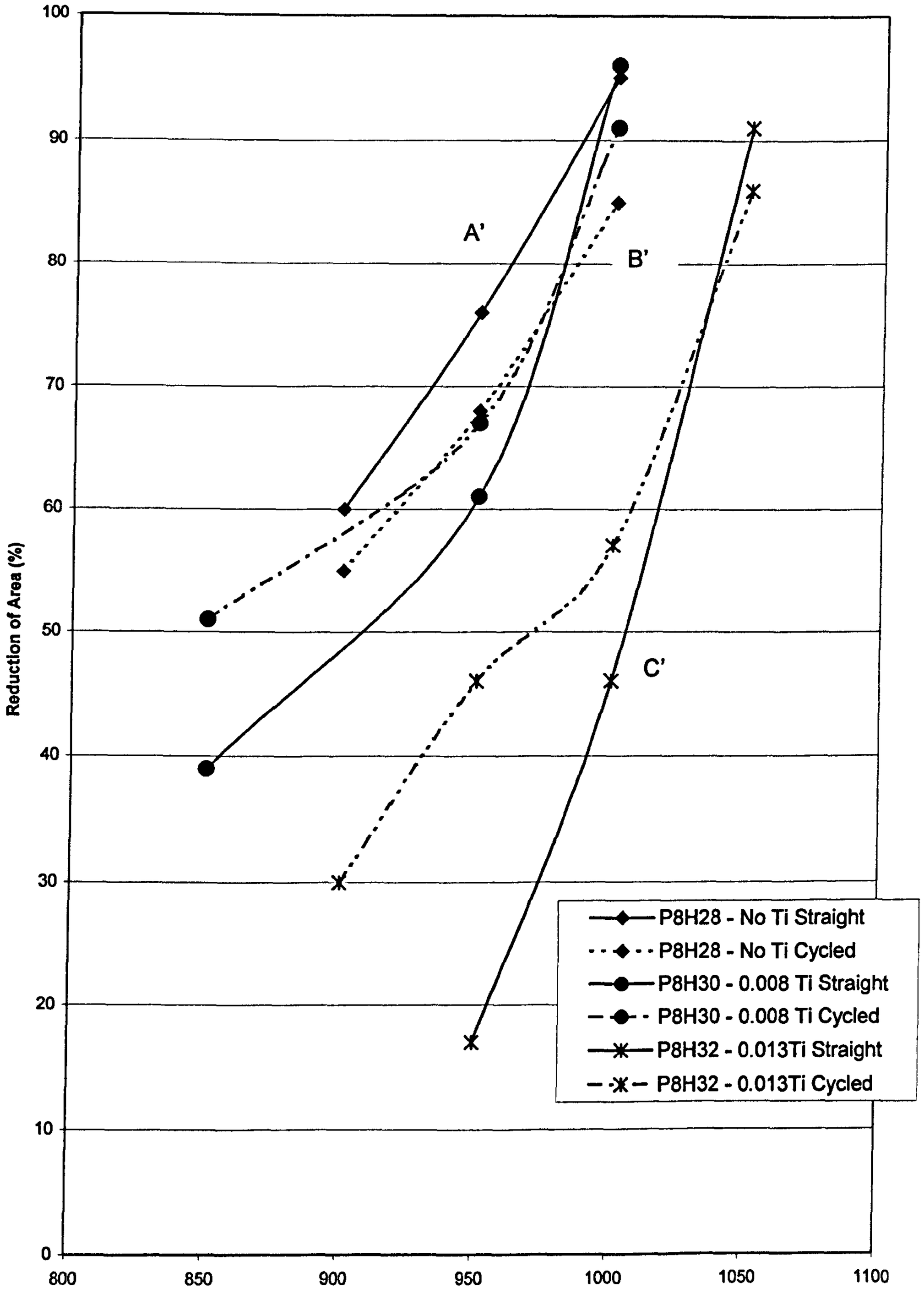

Figure 5-12 Effect of Ti on Nb containing steels at a reduced holding time of 2 minutes

5.7 Solubility Products

The soluble Ti and N levels at equilibrium were calculated for the Nb free Ti containing steels using the following equation[46]:

$$\text{Log Ks} = -\frac{8000}{T} + 0.322$$

Where Ks = [Ti][N]

The results are shown in the following set of Figures. All the steels contained 0.005% Total N.

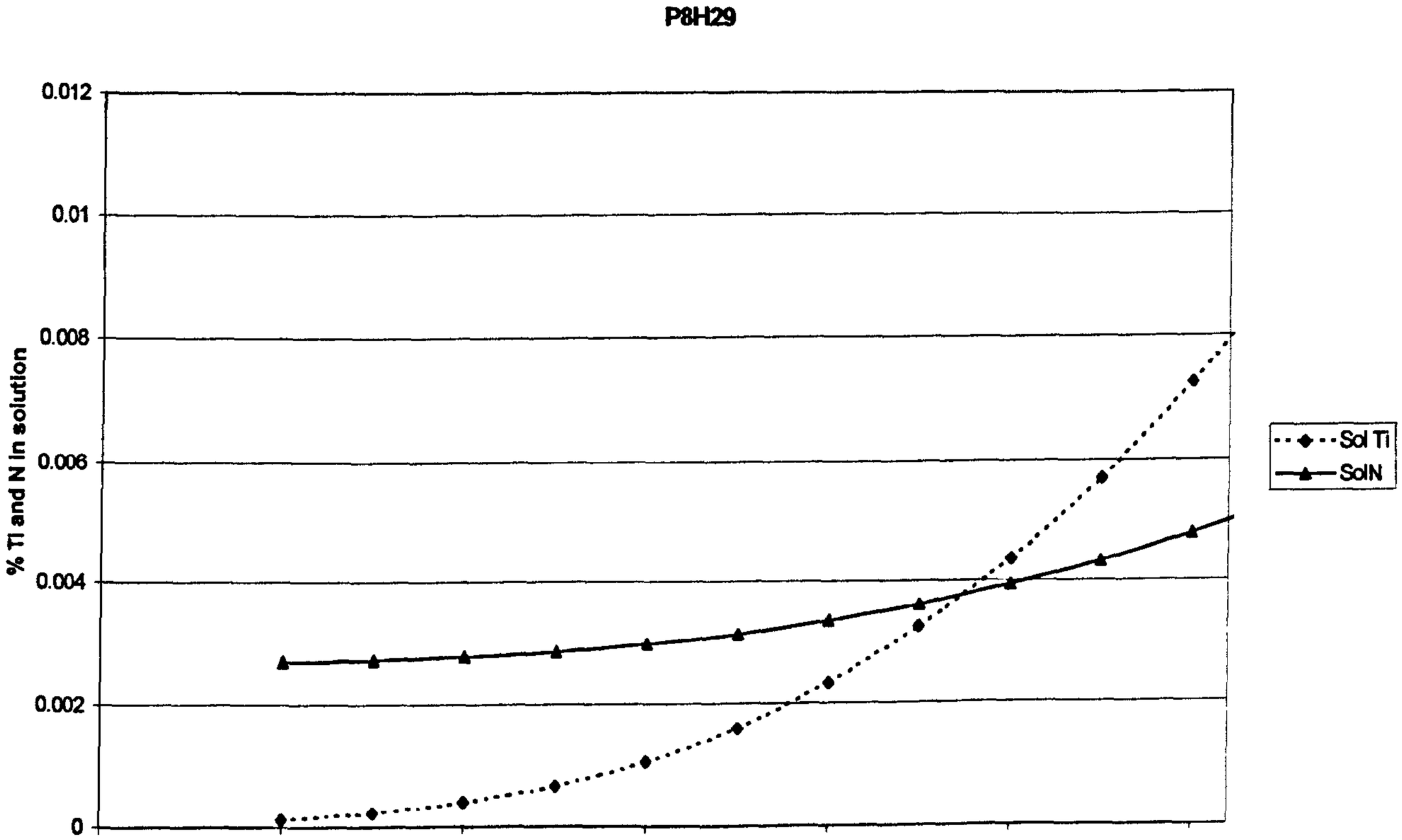

Figure 5-13- Soluble Ti an N levels on a Nb free 0.008% Ti steel

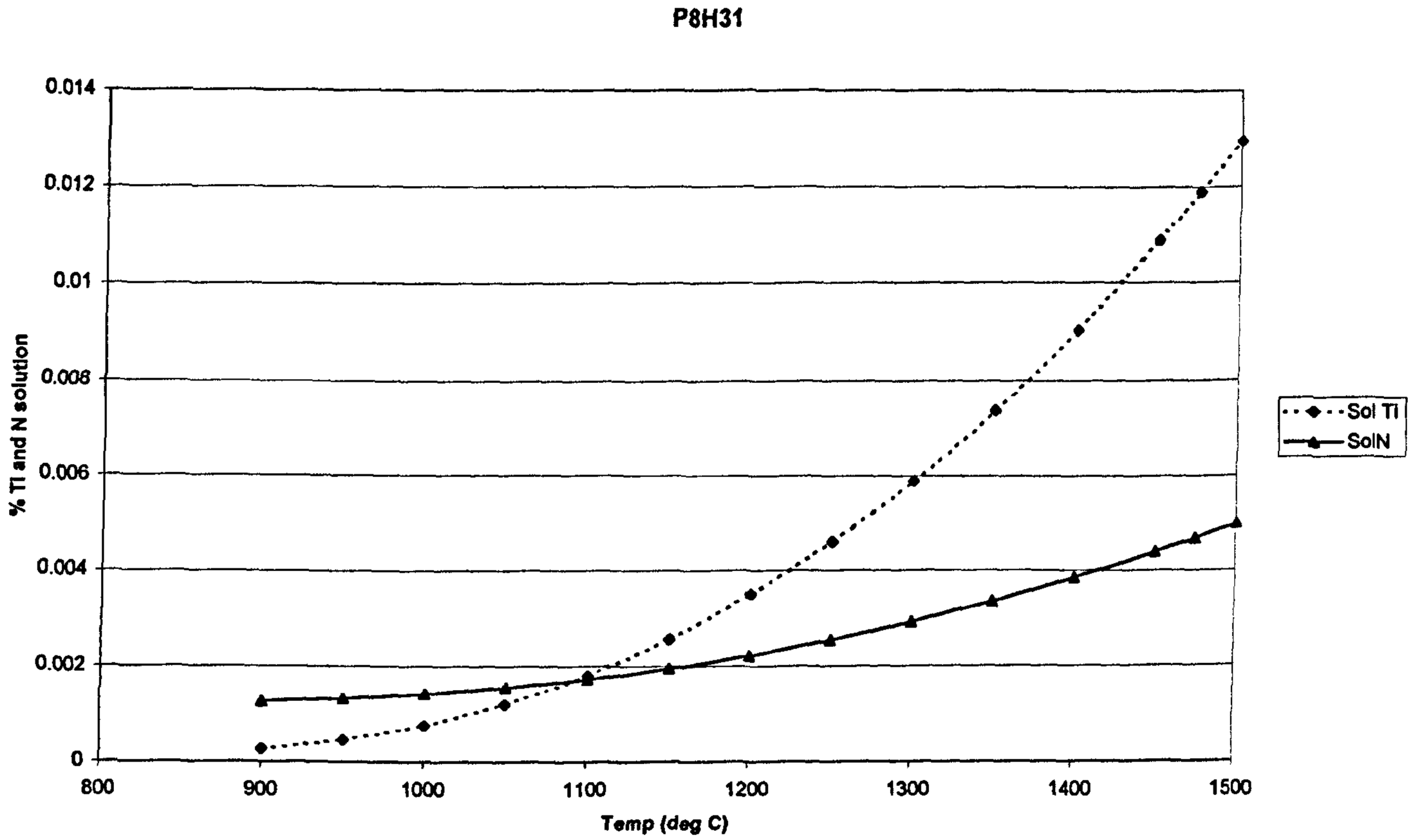

Figure 5-14- Soluble Ti and N levels of Nb free steel containing 0.013%Ti

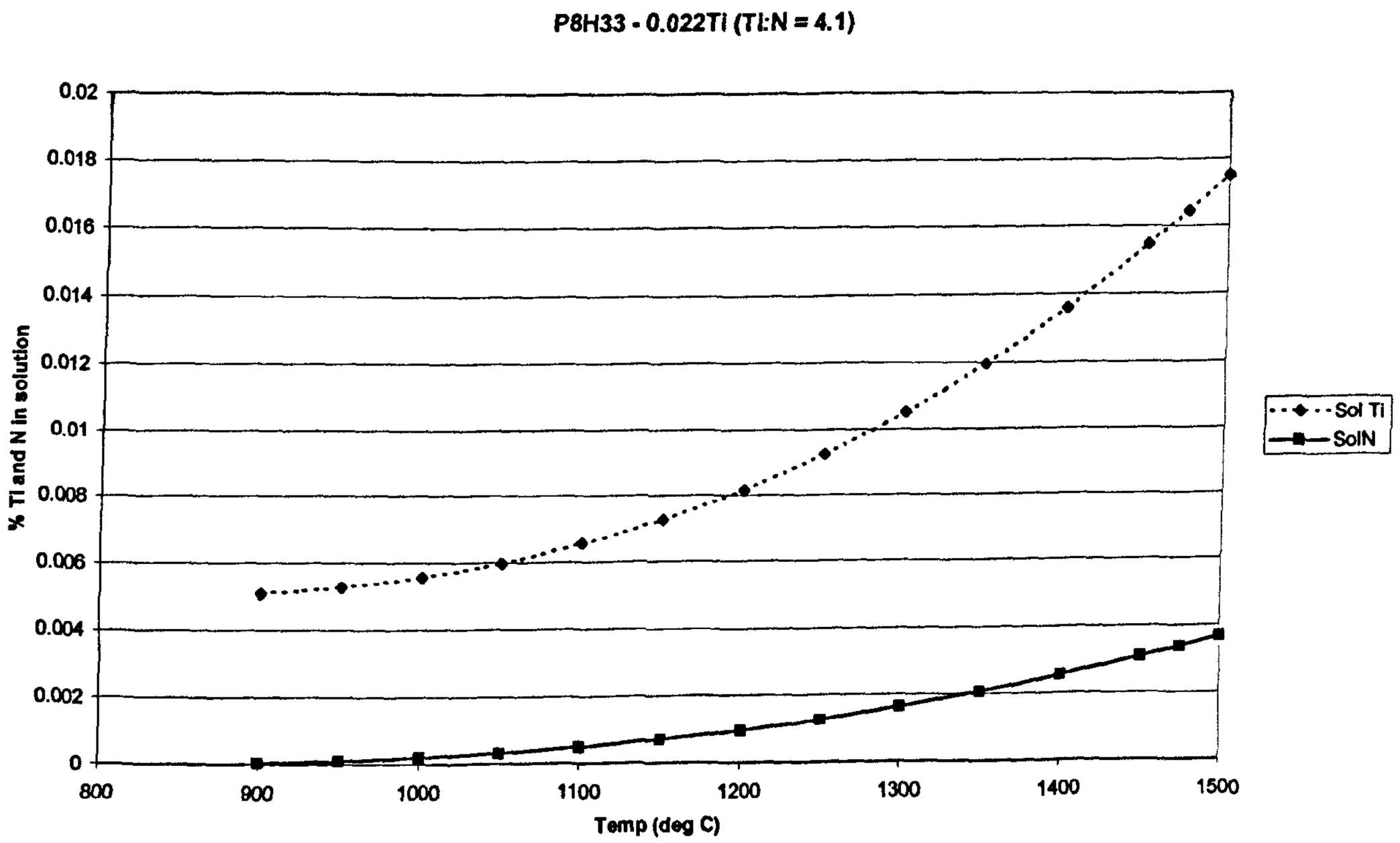

Figure 5-15- Soluble Ti and N levels on Nb free steel with 0.022%Ti

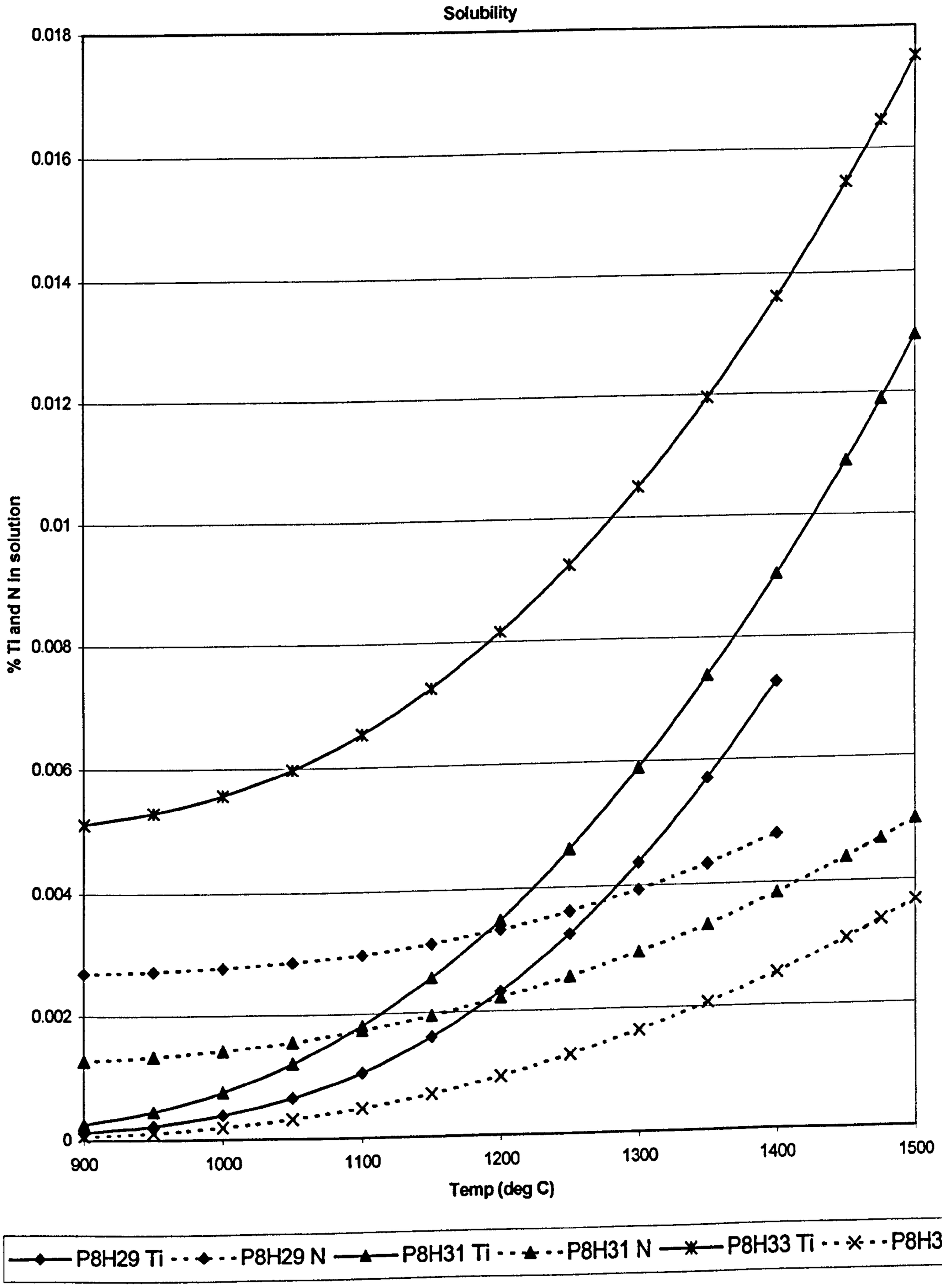

Figure 5-16 Summary of solubility results

It can be seen from the curves shown in Figure 5-16 that for the Nb free steels containing 0.005%N, the temperature at which all the Ti is dissolved is 1420 -1500°C and the melting point of the steel (~1520°C) for steels with 0.008, 0.013 and 0.022% Ti respectively (Figure 5-13 to Figure 5-15). This indicates that very high temperatures are required to dissolve all the Ti for steels with 0.005%N and for Ti levels in excess of 0.015% it is necessary to melt the samples. "Solution Treating" at 1330°C as has been used by many research workers[5] will result in the presence of TiN particles which will refine the grain size and give better hot ductility than in the as-cast coarse grained condition, and the results from such work are therefore invalid.

5.8 Metallography

5.8.1 C-Mn-Al Steels

The Ae_3 temperature for these steels varied approximately from 840-850°C. In the case of the C-Mn-Al, Ti free steel (Figure 5-11) ductility can be seen to start falling at 950°C but really low values (<30%) do not occur until the temperature range 850-800°C. Examination of this steel at a test temperature of 800°C shows the normal thin bands of the softer ferrite surrounding the austenite grains. This can be seen in Figure 5-17.

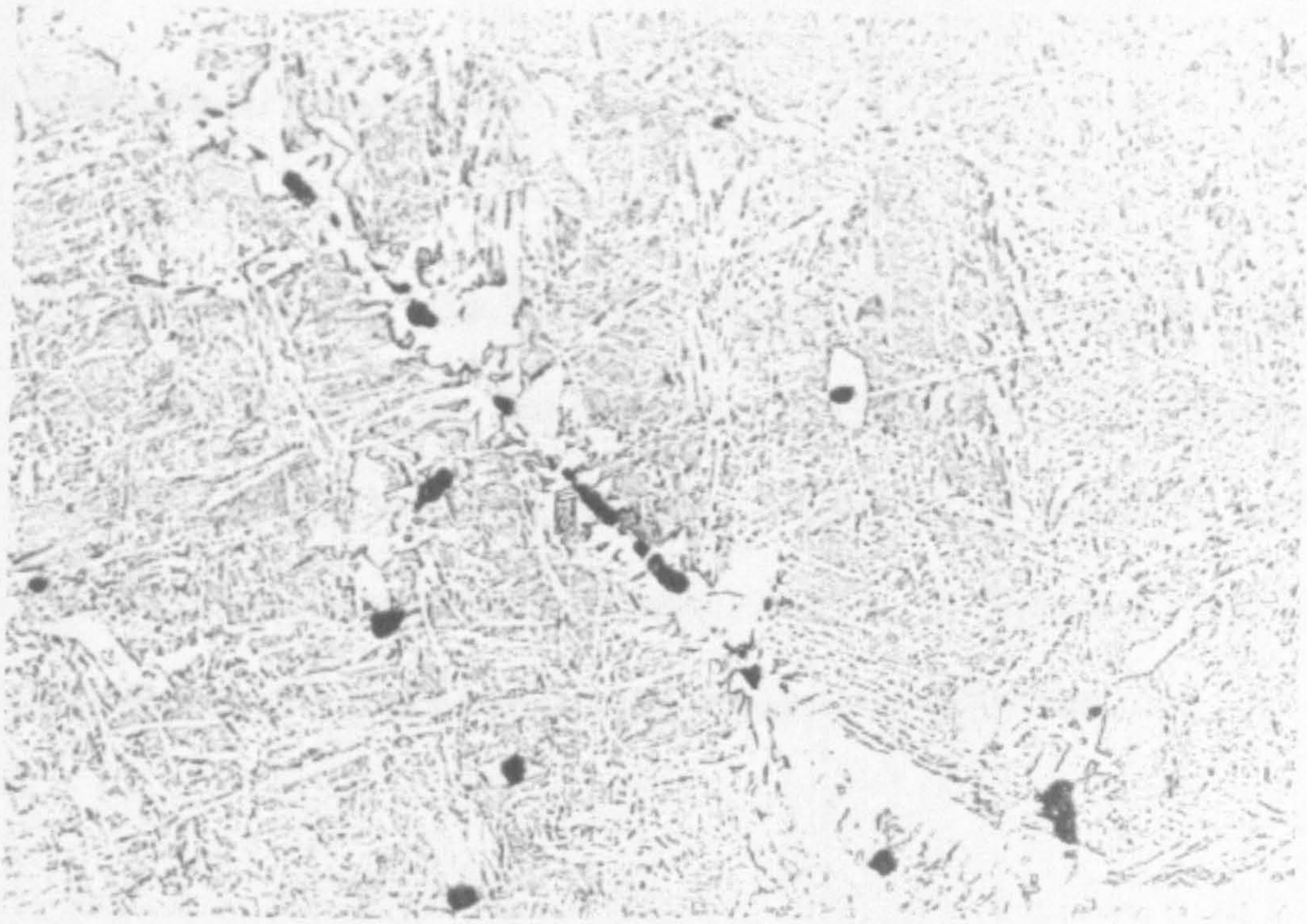

Figure 5-17 Inclusion controlled cavitation at grain boundaries (x 170) for a sample tested at 800°C

Inclusion controlled cavitation at the boundaries can be clearly seen in Figure 5-17 showing how the cracks are starting along these bands leading to low ductility intergranular failure. In the present instance it would appear that deformation has caused these ferrite bands to form well above the expected Ar_3 temperature (which from previous work[15] would be 730°C) and close to the Ae_3 temperature

Ti containing steels were generally similar and intergranular ductile failure was the main mode of fracture.

Because of the problems discussed in Chapter 4 it has not been possible to do more than SEM and metallographic examinations (i.e. no TEM work was peformed).

5.8.2 C-Mn-Nb-Al Steels

For these steels, the ductility trough was extended to higher temperatures and for the highest Ti containing steel examined 0.013%Ti ductility was poor at as high a temperature as 950°C. In this case failure was by grain boundary sliding in the austenite. The Ae_3 temperatures for these steels were between 840 and 850°C.

5.9 Dimple Size

One of the objectives of the present work was to see whether the dimple size on samples showing intergranular failure could be related to the reduction of area values. Typical fracture surfaces for steels tested in the ductility trough are shown in Figure 5-18 and Figure 5-19. Two steels were examined, P8H27 (Ti and Nb Free) and P8H31(0.013% Ti, Nb Free).

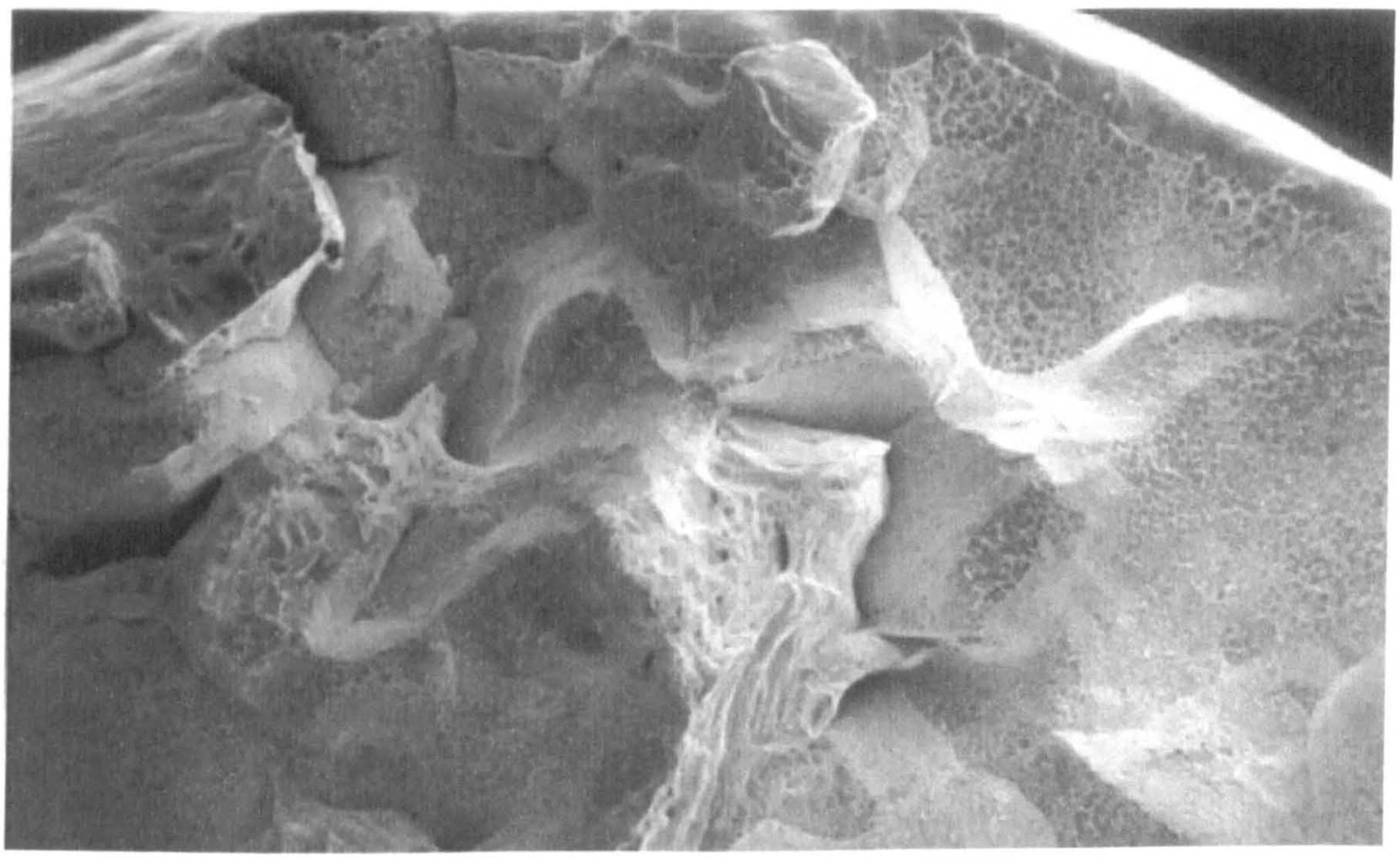

Figure 5-18 - Typical Fracture Surface of C-Mn-Al steel containing 0.013%Ti tested at 800°C

It can be seen from the figures overleaf (Figure 5-20 to Figure 5-21) that increasing the temperature of testing increases the size of the dimples as well as the R of A values. This would be in accord with a coarsening of the particles at higher test temperatures. Surprisingly the dimple size of

the Ti containing steel is shown to be significantly greater than that of the Ti free steel as shown in Figure 5-20.

The effect of introducing the undercooling cycle to both the Ti free and Ti containing steels is given in Figure 5-21. It can be seen from Figure 5-22 that introducing undercooling reduces the dimple size, particularly at higher testing temperatures. For example, for the 0.013% Ti containing steel (P8H31) tested at 850°C, the dimple size is 32μm and 18μm for the direct cooled and undercooled tests respectively. For the Ti free steel (P8H27) tested at 900°C, the dimple size is 30μm with no undercooling and 16μm with undercooling. Such behaviour could be caused by the occurrence of increased precipitation.

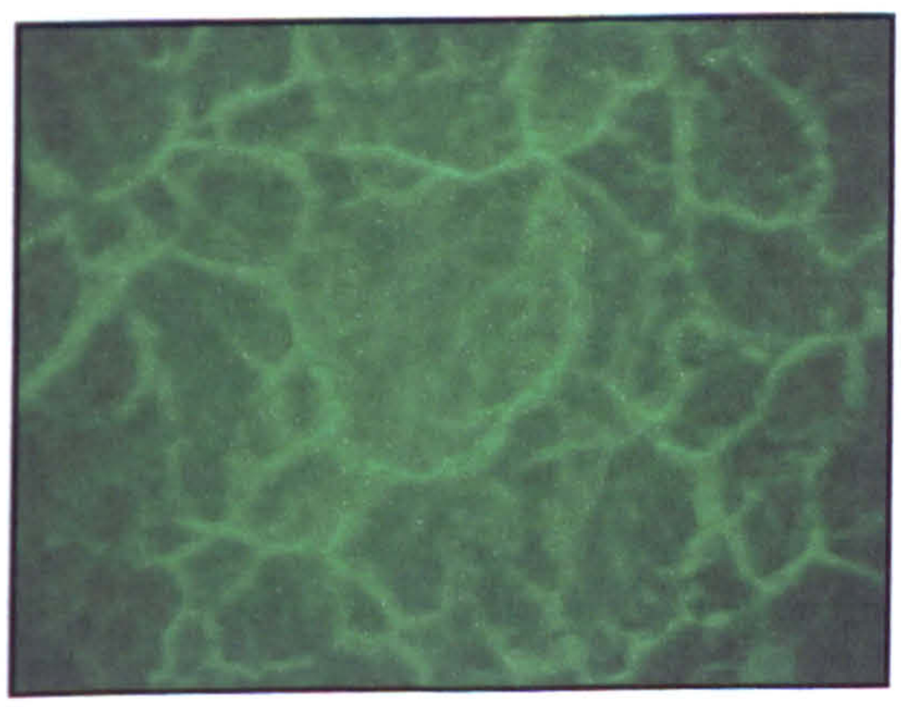

Figure 5-19 Dimples x1500 (P8H27, cycled, 700-800°C, 17% R of A – No Ti)

Figure 5-19 above shows the dimples formed in a Ti free, Nb free steel which has been undercooled by 100°C to 700°C and then reheated to the test temperature of 800°C.

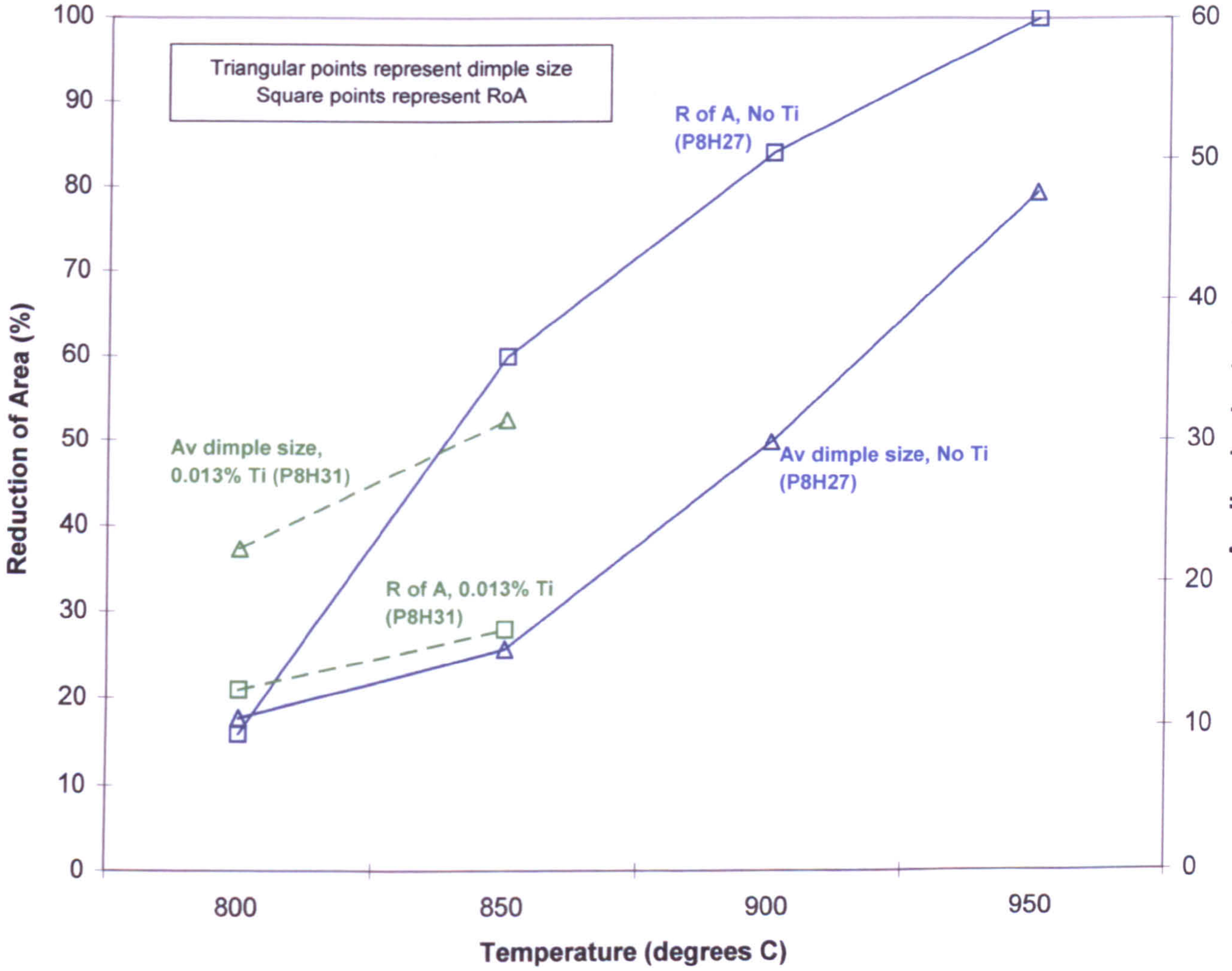

Figure 5-20- Summary of Non cycled Dimple size and R of A results

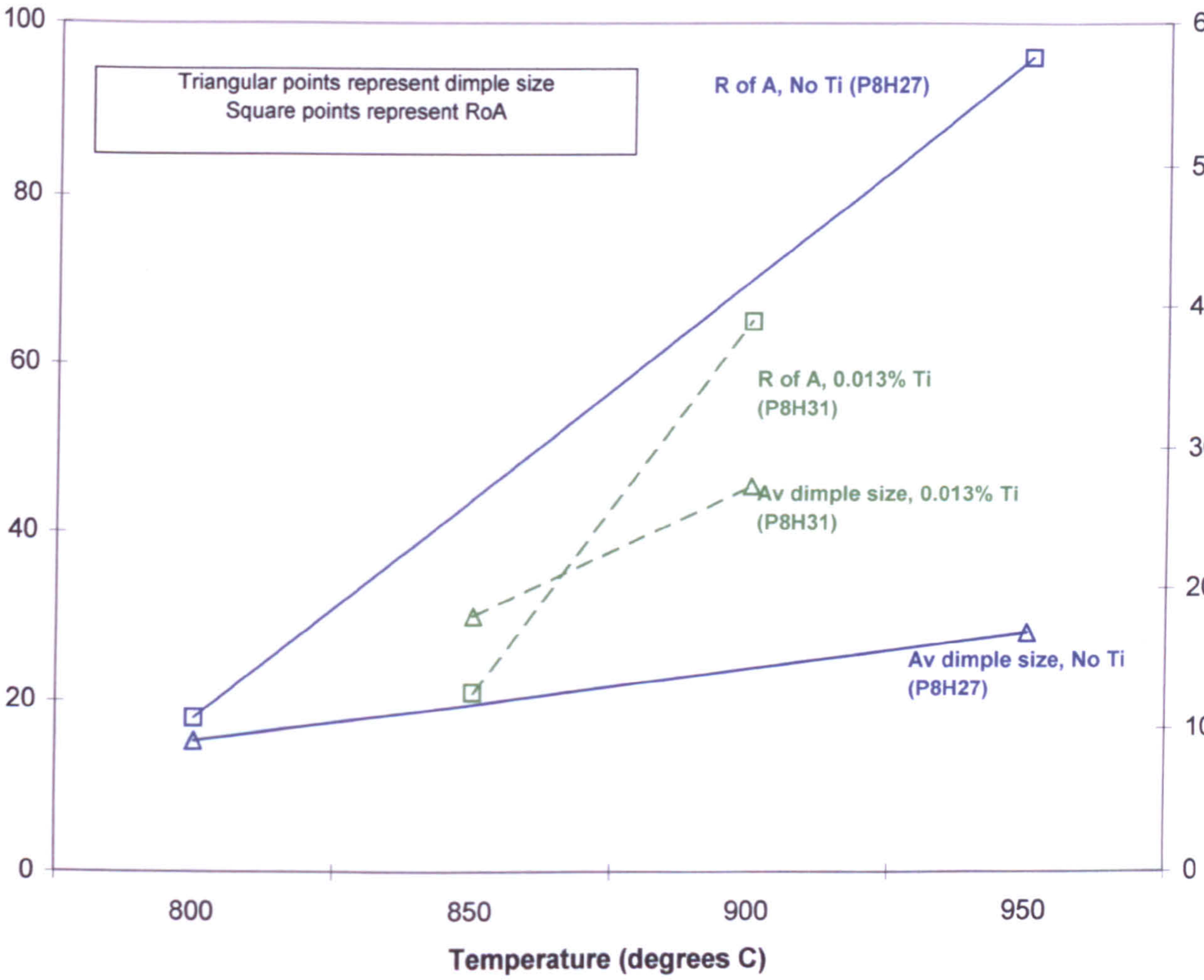

Figure 5-21- Summary of Results for Dimple size and R of A when re-heated at 500 °C/min

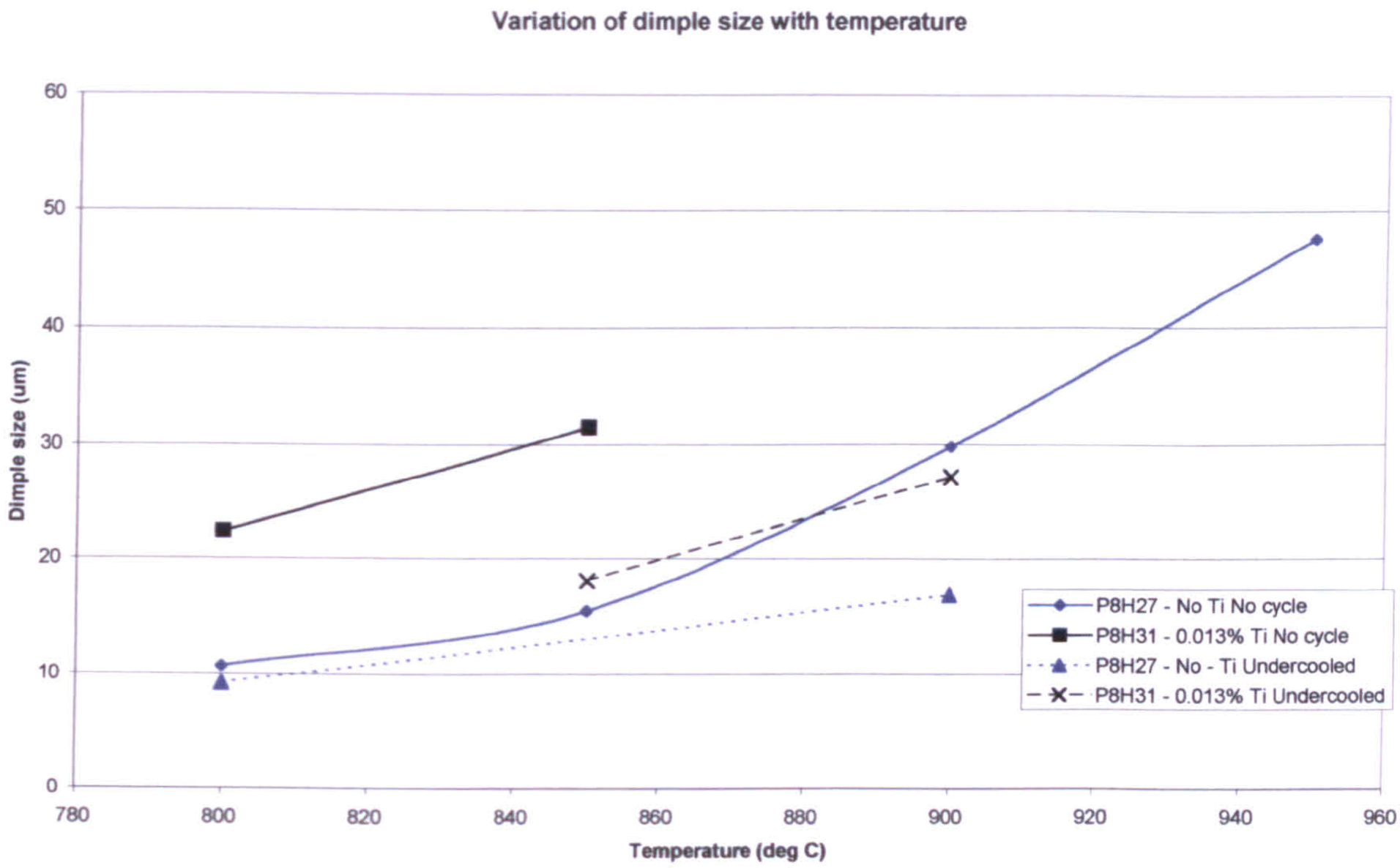

Figure 5-22– Effects of undercooling on dimple size.

5.10 Grain Size

Grain size measurements were made by the intercept technique. However, because the grains were very coarse, the number of grains present in the sample was limited. The limited number of grains present in the samples introduces a significant possibility of error into the grain size calculation. Therefore the results of the individual sample grain sizes have not been reproduced within the thesis. However, it was established that the grain size was always very coarse and was generally in the range 0.8 to 2 mm.

CHAPTER 6 - DISCUSSION

6 DISCUSSION

6.1 Comparison with prior work

In order to draw conclusions from the work undertaken in this study it is necessary to ensure the reliability of the data by comparing it with similar already published work. Abushosha et al[88] published the following regression equation for predicting the behaviour of C-Mn-Al-Ti steels given normal cooling, i.e. without any undercooling:

$$\%R \text{ of } A = 44.1 - 0.169CR + 16.3p^{1/3} - 0.935 \times 10^{5}[Ti][N] - 119.2([Al][Ns])^{1/4} \quad \ldots\ldots(1)$$

A further regression equation was published by Comineli et al[89] which takes into account the effect of Nb additions

$$\%R \text{ of } A = 15.1 + 19p^{1/3} - 0.560[Ti][N] \times 10^{5} - 0.065CR + 2326Ns \quad \ldots\ldots(2)$$

and also a combined equation taken from both sets of data.

$$\%R \text{ of } A = 26.3 + 16.3p^{1/3} - 0.118CR - 0.439[Ti][N] \times 10^{5} \quad \ldots\ldots(3)$$

Where CR is the cooling rate in K min^{-1}, p is the particle size in nm and Ns in the amount of N available to combine with Al (assuming there is insufficient Ti to combine with all the N). It can be seen from these

formulae that the reduction of area values are related to a large number of variables and that small changes in particle size p and volume fraction of precipitations given by the terms [Ti][N] and [Al][Ns] can lead to a marked change in the reduction of area (R of A) values. In the present instance only a limited amount of replica work was carried out and the approximate particle size measurements have been taken from the particle size against Ti:N ratio curves derived by Abushosha et al[88] (shown below). The experimental arrangements and testing procedures in Abushosha's work were very similar to those employed in this program of work.

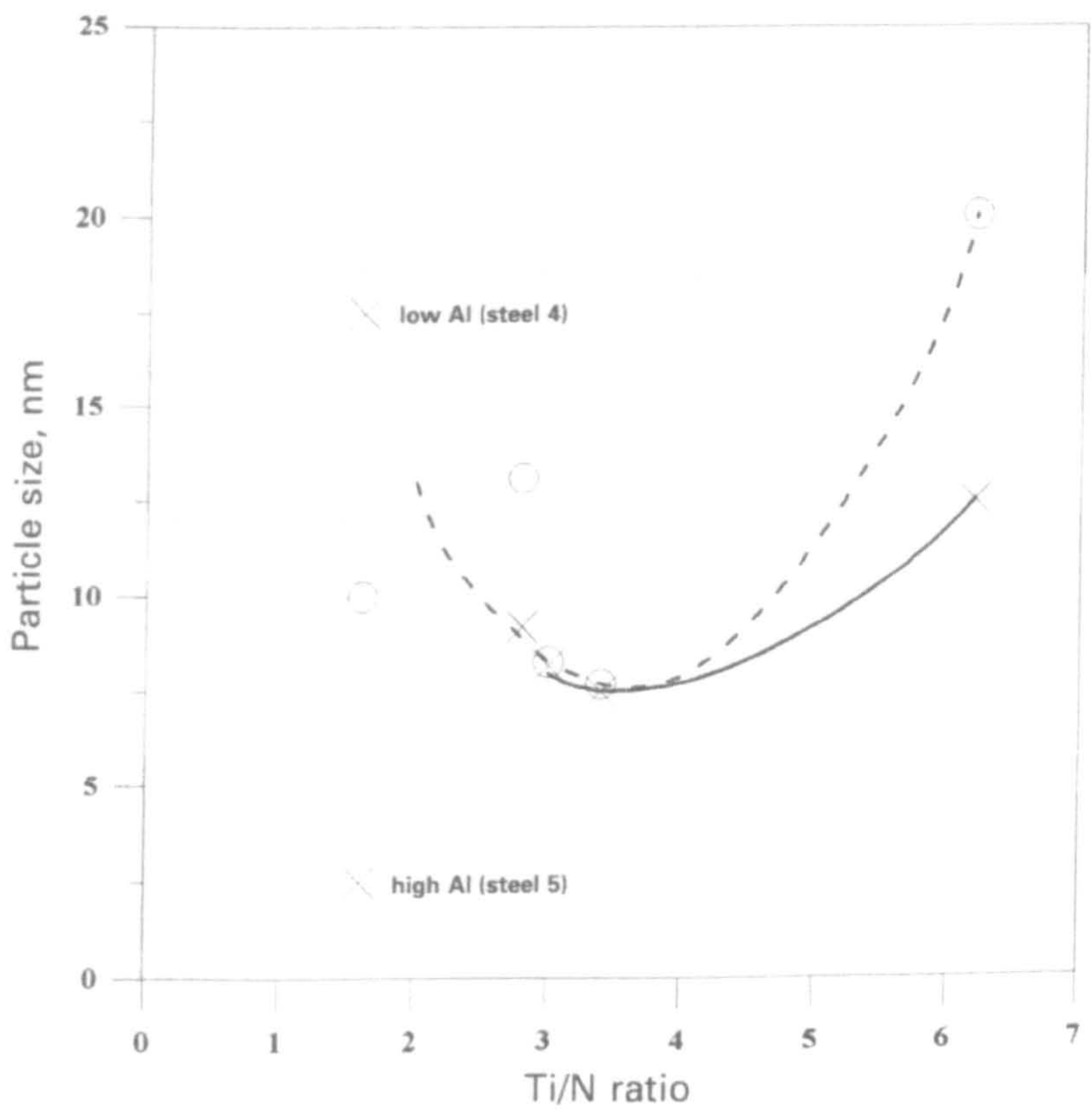

Figure 6-1 - Average particle size plotted against Ti:N ratio for steels tested at 950 °C Cooled at 25K/min (- - -) and 100-200K/min (___)

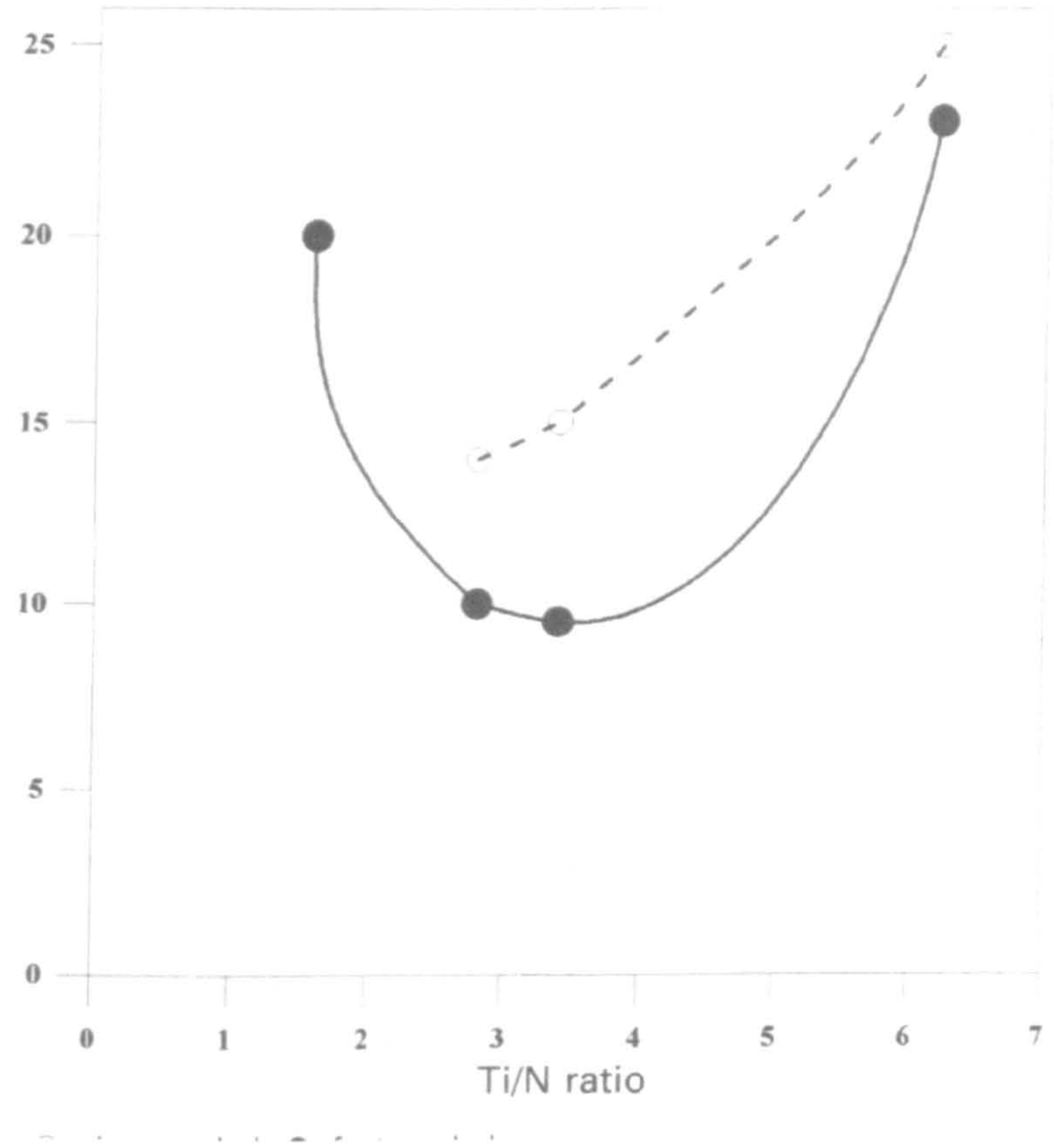

Figure 6-2 - Average particle size plotted against Ti:N ratio for steels tested at 1000 °C Cooled at 25K/min (- - -) and 100- 200 K/min (___)

The particle sizes chosen for use in the comparison work are detailed in Table 9 below:

Temperature (°C)	Cast No. (P8H)	Particle Size (nm)	Ti:N Ratio
950	29	12.5	1.6
	30	10	1.6
	31	10	2.2
	32	10	2.6
1000	29	20	1.6
	31	12	2.2

Table 9 – Particle sizes derived from previous work

In order to obtain the Ns level (the amount of N remaining after the TiN has formed at a given temperature) it was assumed that the Ti was always able to preferentially combine with the N and the equilibrium solubility product of TiN could be used. The latter was calculated using the following equation[46].

$$\text{Log}\,[Ti][N] = -8000/T + 0.322 \qquad \ldots\ldots(4)$$

Where T is the temperature in K.

The results of these calculations are shown in

Table 10 below.

Temp	P8H29		P8H31		P8H33	
°C	Ti	N	Ti	N	Ti	N
900	0.000118	0.002696	0.000249	0.001273	0.005106	6.22E-05
950	0.000221	0.002726	0.000453	0.001333	0.005284	0.000114
1000	0.000393	0.002777	0.000766	0.001424	0.005564	0.000196
1050	0.00066	0.002855	0.001212	0.001555	0.005972	0.000315
1100	0.001053	0.00297	0.001809	0.001729	0.006532	0.000479
1150	0.001602	0.00313	0.002569	0.001951	0.007256	0.000691
1200	0.002328	0.003342	0.003499	0.002223	0.008156	0.000954
1250	0.003248	0.003611	0.004605	0.002546	0.009237	0.00127
1300	0.004372	0.00394	0.005893	0.002923	0.010504	0.00164
1350	0.005707	0.00433	0.007368	0.003354	0.011961	0.002066
1400	0.007254	0.004782	0.009032	0.00384	0.013612	0.002548
1450			0.010892	0.004384	0.01546	0.003088
1475			0.011895	0.004677	0.016458	0.00338
1500			0.012948	0.004985	0.017507	0.003687

Table 10 - Results of solubility calculations

Table 11 and Table 12 below show the reduction of area values obtained from the linear regression equations (1),(2) and (3) compared with the actual results for samples cooled normally i.e. no undercooling. The steels that only contained Ti were evaluated against equation (1). The Ti/Nb steels were evaluated against equations (2) and (3).

R of A %	0.008% Ti	0.013% Ti
Calculated	50	46
Actual	72	87

Table 11 - Comparison of actual and calculated values for Ti containing steels at 950 °C using Equation 1 for non-cycled steels

R of A %	0.03%Nb 0.008%Ti	0.031%Nb 0.013%Ti
Calculated Equation (2)	53	49
Calculated Equation (3)	48	47
Actual	80	56

Table 12 - Comparison of actual and calculated values for Ti/Nb steels at 950 °C – normal cooling conditions

It is clear that the levels of agreement between the calculated and actual values are much better in Table 12 (the Ti and Nb containing steels) than in Table 11 (the Ti only steels).

It is thought that a possible reason for the difference between the high R of A values exhibited experimentally and the lower calculated values is

the lack of a sulphur term in the regression equations. Sulphur or more correctly MnS is known to have a major influence in dictating the reduction of area values for ductile failure. The authors of these regression equations note this lack of relationship in their case is probably due to the fact that all the steels tested had similar S contents. The steels used in their work had S levels of around 0.01, where as the steels in the current study have an S level of 0.002.

It has been shown by several authors[90,91,92] that increased S levels lead to increased cracking and worse hot ductility.

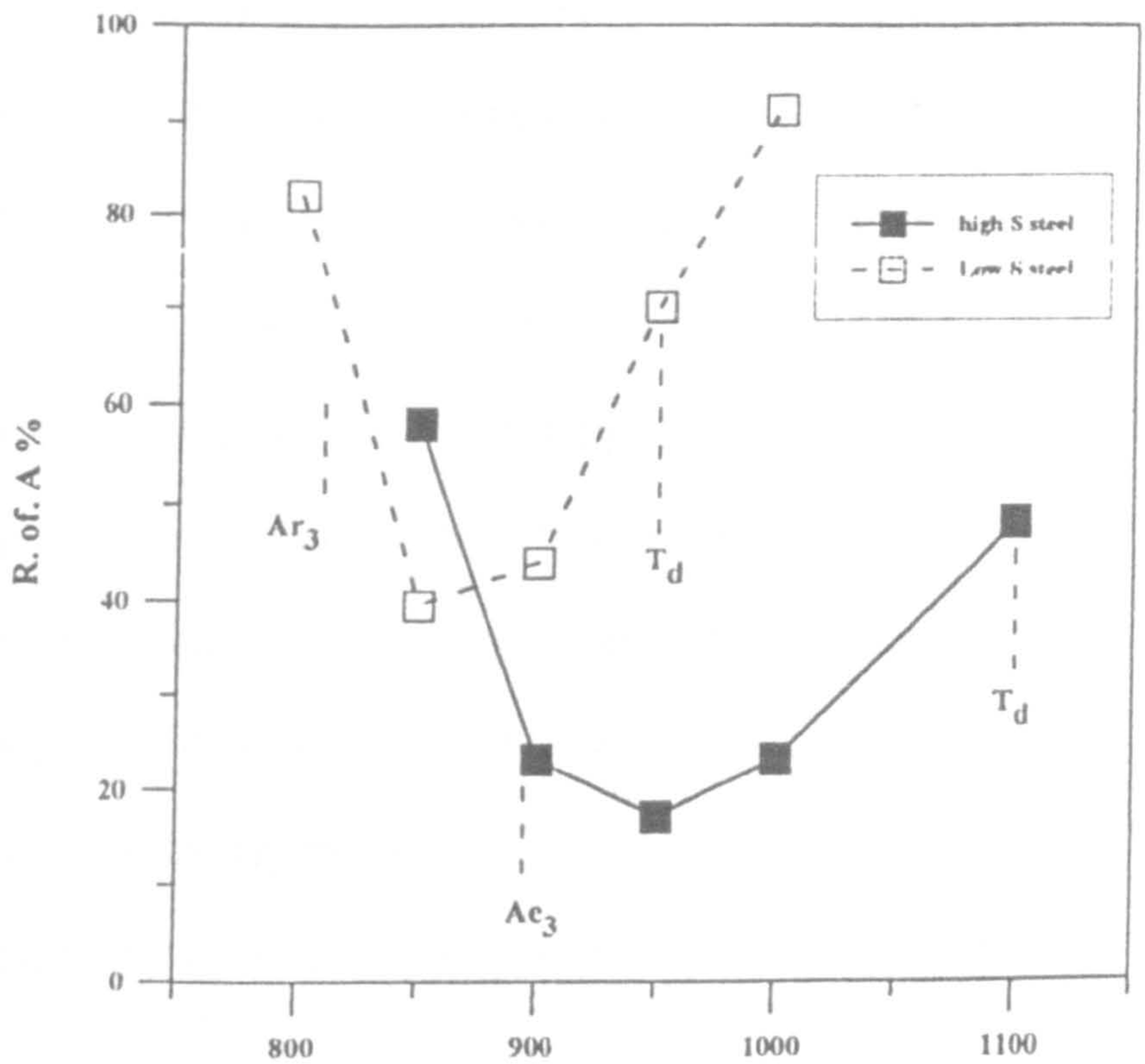

Fig. 1 Hot ductility curves for the high and low S, C-Mn-Al steels.

Figure 6-3 – Hot ductility Curves for high and Low S (C-Mn-Al) Steels

Mintz et al[93] published the above curves for C-Mn-Al steels showing the difference in ductility between a 0.032% and 0.003% S steel indicating the poor ductility at the higher S level.

It is thought that the reason why there is better agreement between the calculated and experimental figures for the Nb containing steels is that the Nb is so detrimental to ductility that the S levels become less significant.

Nevertheless, when the present data (without undercooling) is included with the previous data the following highly significant regression equations (equations 5 and 6) are obtained in which no influence of S is noted. Thus, the present data would appear to fit in very well with previous work. The new equations again show that the particle size (p) is very important, the finer the particles are, the lower the reduction of area values. Increasing the cooling (CR) leads to worse ductility as before but the factor is variable being 0.063 for the Nb steels and 0.216 for the Nb free steels. It should be noted that P, in contrast with S, does seem to have a major influence. High P levels seem to give an improvement in the ductility of C-Mn-Al-Nb steels (equation 5) . Conversely, the addition of P to Ti-Al containing steels has a detrimental effect on the hot ductility (equation 6). There is also a strong co-relation of P and S.

$$\% R \text{ of } A = 47.2 - 0.0632CR + 16.8\, p^{1/3} - 1521Nb - 3274[N] + 3452[Ns] + 2844P \quad \text{.....(5)}$$

The "t ratios" for the variables in equation 5, along with "p" (the probability of the variable being incorrect) are shown in Table 13 below.

Variable	"t" ratio	"p"
CR	-2.88	0.009
$p^{1/3}$	5.92	0.000
Nb	-1.55	0.137
N	-3.47	0.002
Ns	3.82	0.001
P	2.12	0.046

Table 13 - Statistical data for Equation 5

Equation 5 is suitable for use with Ti and Nb containing steels and has an R value of 88% and standard deviation of ± 7.235%. It can be seen that the two N terms in this equation are interlinked; higher total N levels will result in more TiN, AlN and NbCN being precipitated out giving worse ductility. In contrast the greater amount of N present in solution the less will be precipitated and therefore the better the ductility.

For Ti, Al steels the following equation was obtained:

$$\%\ R\ of\ A = 92.5 - 0.216CR + 16.8\ p^{1/3} - 0.596[Ti][N] - 3419P \qquad .....(6)$$

This equation has an R value of 84% and a standard deviation of ± 7.380%.

The "t ratios" for the variables in equation 6, along with "p" (the probability of the variable being incorrect) are shown in Table 14 below.

Variable	"t" ratio	"p"
CR	-5.88	0.000
$p^{1/3}$	3.05	0.009
[Ti][N]	-2.11	0.054
P	-5.32	0.000

Table 14 - Statistical data for Equation 6

In this case, without the presence of Nb, P does seem to be detrimental to ductility. The lack of any term for S in the Nb free steels may be because of the high correlation of S and P contents i.e. steels with higher P levels also had higher S levels and vice-versa. In contrast, for the Nb containing steels, P can be seen to be beneficial. This agrees with previous work[94] that shows P to be beneficial in C-Mn-Al-Nb steels, possibly as it segregates to the boundaries and vacant sites preventing the more detrimental fine NbCN precipitation from taking place. However, this is not the case in the Nb free steels where the P segregating to the grain boundaries may impair the ductility of the steel possibly by weakening the

grain boundaries[95]. Alternatively it is possible that without Nb the negative P term in the C-Mn-Al-Ti steel equation (6) may reflect the detrimental influence of S on ductility.

6.2 Explanation of current results

6.2.1 Simple Cooling

The results of the curves produced by simple cooling show that although their behaviour is complex, the addition of Ti (Figure 5-1 and Figure 5-6) and/or Nb (

Figure 5-3 to Figure 5-5) cause the hot ductility to deteriorate. The results indicate that as the amount of Ti added to the steel is increased so the ductility decreases. As Ti is a very reactive element it will tend to utilise all the N present to form precipitates. Previous work[5] has shown that without undercooling it is difficult to precipitate out the more detrimental AlN precipitation. Thus, with simple cooling, the amount of TiN precipitated will increase as the Ti level is increased giving rise to worse ductility until the stoichiometric ratio is reached.

In the present instance the maximum Ti level examined, 0.013%, is below that of the stoichiometric composition so ductility would be expected to continuously deteriorate with Ti additions. {Note: Although higher Ti steels had been proposed in the original programme, because of the problems outlined no results are available for these steels}

Ti levels greater than the stoichiometric have been shown to cause slight coarsening of the TiN particles to occur and hence to improve the ductility of the samples. This is because the growth of TiN particles depends on the amount of Ti in solution, this species being the slower and hence the

rate controlling element. This was not shown in the previous results for the Ti-Al steel (possibly due to the formation of TiC above the stoichiometric ratio which leads to the retardation of recrystallisation) but was seen in the Ti-Al-Nb steel, since Nb in the presence of Ti has been shown to aid coarsening[96].

It has been found[97,98] that the TiN precipitates out in two distinct ways within the steel. Firstly as very large (~800nm) coarse precipitates which tend to migrate to the edge of the melt zone and are so large as to in fact have no effect on the ductility. Secondly as an extremely fine matrix precipitation which is detrimental to ductility as they strengthen the matrix so increasing the shear stresses at the boundaries.

The addition of Nb to the steel tends also to have a detrimental effect on the ductility. This is because although Ti will preferentially combine with the nitrogen present, forming TiN, niobium carbonitride is mainly a carbide precipitate hence the fine Nb (C,N) precipitates can still form within the matrix but also at the grain boundaries. Often the region around the boundaries is devoid of precipitates allowing strain concentration to occur in these soft regions. Two factors are important in controlling the hot ductility. One is the size of the particles at the boundaries, the finer they are for a given volume fraction the smaller the interparticle spacing and the easier it becomes for the boundary to "unzip". The other factor is the

volume fraction; a higher volume fraction of particles again leads to a smaller interparticle spacing hence easier crack propagation.

6.2.2 *Influence of the re-heating rate after undercooling*

Prior to recognising that the samples were losing Ti, after undercooling, two reheating rates to the test temperature had been employed, 1000°C/min and 500°C/min; the fastest rate of 1000 °C/min consistently producing the worst ductility. The faster reheat will produce greater thermal stresses in the sample in turn possibly producing greater levels of precipitation. The faster re-heat will also allow less time for any precipitates to coarsen than the slower reheat rate of 500 °C/min.

However, the worse ductility at the faster heating rate may also be a consequence of a more dendritic structure in the centre of the sample. It was noticeable that whereas samples given the simple cooling direct to the test temperatures gave virtually no dendrites on the fracture surface. In contrast, the undercooling followed by rapid re-heating led to dendrites being exposed and this exposure increased with the heating rate (analysis of some re-heated samples showed dendritic coverage around 50% of the fracture surface for the faster reheating rate and 5-10% for the slower). Dendrites of course should not be present as this indicates some porosity in the samples.

It is possible that the direct cooling to the test temperature followed by the 5 min hold prior to testing allows the dendrites to knit together and reduce segregation effects which might cause weakening of the dendritic boundaries. The rapid heating up after undercooling may cause the dendrites to break open and this would be accentuated at the higher heating rate. As dendrites were only occasionally present when the slower re-heating rate was employed, only the results for the 500 °C/min heating rate have been included in this thesis.

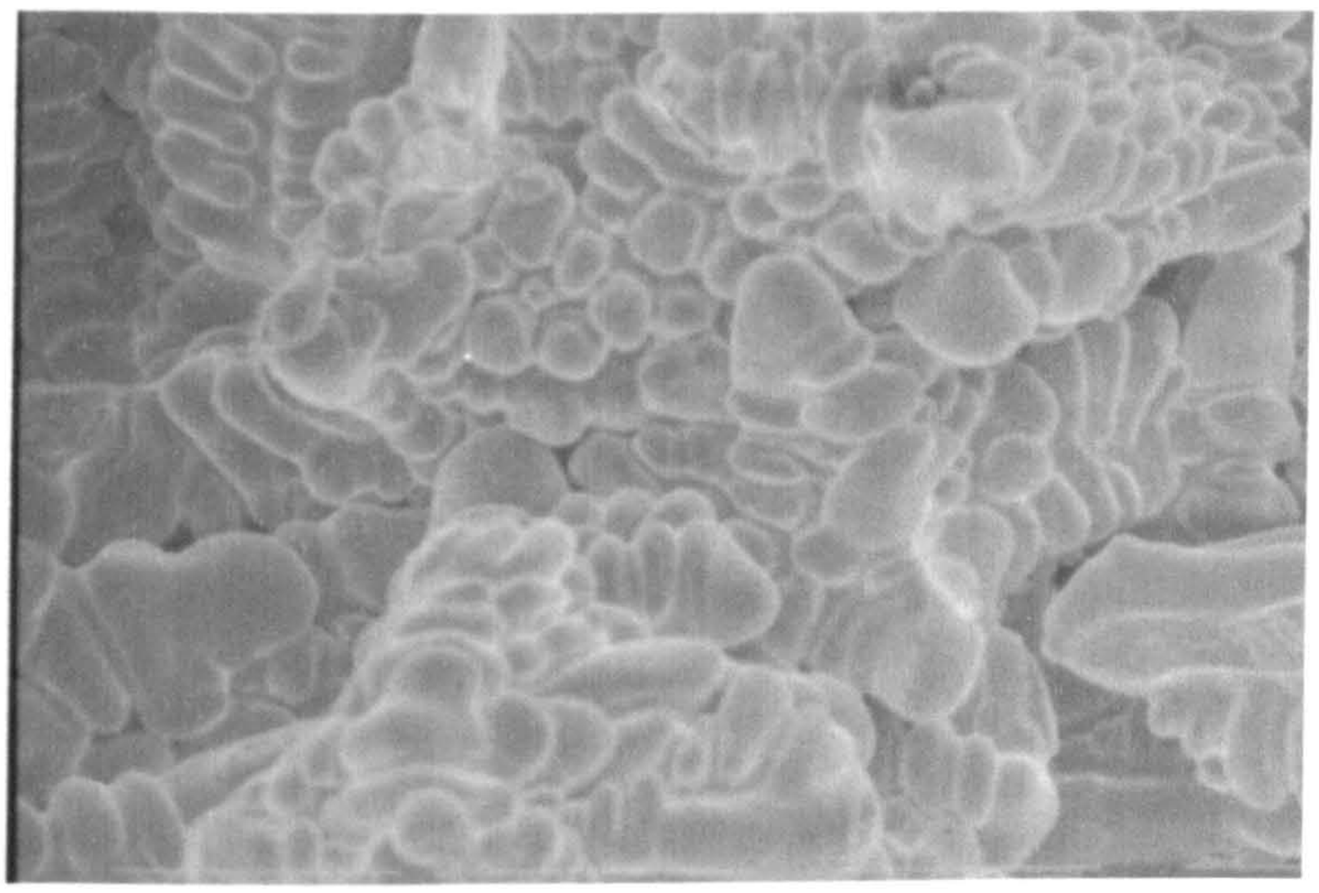

Figure 6-4 - Dendrites x 200

Kothe[99] has produced a table showing how holding times prior to deformation effect the size of TiN particles in pure Fe. His results for 900 and 1000°C are reproduced below: Whereas at 1000 °C there appears to be little influence of holding times up to 30 seconds, at 900 °C quite substantial growth seems to occur within this very short time interval.

Temperature	Holding Time	Particle Size
1000°C	15s	11-15nm
	30s	10-13nm
900°C	5s	9-13nm
	15s	7-16nm
	30s	15-23nm

Table 15- The effect of holding time on the size of TiN particles in pure Fe

This indicates that the nose temperature for TiN precipitation must be close to 900°C. Although the time spent, 12 seconds (500°C/min), in raising the temperature 100°C from the undercooling temperature to the test temperature might produce some growth it is likely to be small and can probably be ignored.

6.2.3 Explanation of undercooling results

For both kinds of steel, ductility generally becomes worse when an undercooling step is added into the test cycle. As already mentioned, without undercooling, AlN has difficulty in precipitating out and the addition of Ti merely serves to increase the amount of fine TiN precipitates which simply worsens ductility. Nb aggravates the loss in

ductility as Nb(CN) precipitation occurs and as this is mainly carbon based an increased volume fraction of precipitates will be present.

The process of undercooling the samples to a temperature 100°C below the test temperature and then heating them back to the test temperature at 500 °C min^{-1} produced some interesting results.

6.2.4 Undercooling of Nb free steels

In the plain C-Mn-Al steel (i.e. Ti free), the undercooling caused the ductility to deteriorate. This is probably due to the greater amount of precipitates that will be produced by cooling the sample to a temperature lower than the test temperature and then re-heating to the test temperature. These precipitates are also likely be finer than those produced at the test temperature without undercooling. Therefore, the undercooled sample will have a greater number of the detrimental fine precipitates present than the simply cooled sample, thus making ductility worse. In particular, the undercooling will help force out some of the AlN, which, as mentioned previously, has problems in precipitating under normal cooling conditions. The work of Cardoso et al[100] indicates that with undercooling the trough is moved to higher temperatures as more AlN is encouraged to precipitate out by this treatment.

For Nb free steels with zero Ti addition, ductility deteriorates severely with cycling due probably to large amounts of AlN being precipitated. From previous work[100] it is improbable that all the AlN comes out in one cycle,

and the detrimental influence of Al is likely to be more pronounced if more cycles are used.

With the 0.008%Ti addition (Figure 5-2) only a small fraction of the nitrogen will combine as TiN and most of the N will be free to combine with the Al to form AlN. This means on undercooling that there will now be considerable quantities of AlN precipitated out along with the small amount of TiN. This again results in worsening ductility on undercooling.

With the addition of 0.013%Ti, (Figure 5-2) ductility is little influenced by cycling as nearly all the nitrogen is taken up by the Ti, leaving little if any, available for AlN precipitation. From previous work, once the stoichiometric ratio is exceeded, all the N is combined with the Ti and further additions of Ti are likely to result in a coarser particle distribution, due to Ti in solution being the rate controlling element for the growth of TiN particles.

Surprisingly, ductility is somewhat better at the 0.013%Ti level both for the undercooled and normally cooled steel compared with the ductility behaviour shown by the 0.008%Ti steel in Figure 5-11 suggesting that TiN precipitation may be less deleterious that AlN. However, detailed analysis of the results suggests that the presence of N as TiN rather than AlN would appear to make ductility worse when only one undercooling cycle is used. For example, the effect of removing AlN can be estimated

by comparing curves A and B (Figure 5-11). At 900°C curve A for the C-Mn-Al Ti free steel gives a reduction of area value of 84% for uncycled and this is reduced to 77% reduction of area due to AlN precipitation. The effect of removing Ti as TiN is shown by comparing curves A and D (no undercooling) assuming the 0.013%Ti curve D will combine with all the N as TiN. At 900°C curve A for the uncycled C-Mn-Al Ti free steel the reduction of area is 84% but this is reduced to 60% when all the Ti is combined with all the N. It can be seen that the deterioration in ductility is slightly worse when the N is removed by the Ti.

Summarising

When the undercooling is applied to the Ti containing steels the lower temperature introduced into the test allows greater amounts of AlN to form than in the simply cooled tests (as in the C-Mn-Al steel) as evidenced in other work by Abushosha[88]. However as the Ti:N ratio is increased the amount of TiN formed increases and as a result there is less N available for AlN to form until, once the stoichiometric ratio is exceeded, all the N is tied up in TiN and no AlN can form.

TiN seems to be more detrimental to hot ductility than AlN. However, only one undercooling cycle has been performed and commercially when more cycles are introduced, more AlN may be produced.

6.2.5 Undercooling of Nb containing steels

When no Ti is present undercooling caused the ductility of the Nb containing steels to deteriorate markedly (Figure 5.12). This is because the undercooling allows the AlN to precipitate out and also finer Nb(CN) precipitation occurs (due to the lower temperature achieved with the undercooling step).

The addition of Nb to the undercooled steels results in worse ductility than found in the Ti-Al steels. This is due to a greater volume fraction of precipitates being present in the steels. In addition to the TiN, MnS and AlN will be present in the Nb free steels. The Nb containing steels will also have in addition Nb(CN) and possibly NbC. The greater volume fraction of precipitates will more effectively pin the grain boundaries and also help encourage crack propagation. Previous work[89] has however shown that the presence of Nb generally results in coarser Ti rich particles and this to some degree offsets the deleterious influence on hot ductility from the increased volume fraction of precipitation.

In contrast to the Nb free steels, when Ti is present in Nb containing steels, undercooling seems to improve the hot ductility. The improvement is relatively small both for the 0.008% and the 0.013% Ti steels. Undercooling will increase the amount of AlN present in the steels with a Ti:N ratio less than the stoichiometric and therefore might be expected to cause a deterioration in ductility as has been noted for the Nb free steel.

A possible explanation to account for the undercooling behaviour is that the undercooling favours NbC rather than Nb(CN) precipitation. NbC has a lower rate of precipitation than Nb(CN) thus reducing the number of precipitates and has been shown to result in better ductility than the higher temperature Nb(CN) precipitation.

It should be noted that TiN precipitation again seems to be worse than AlN on the basis of one undercooling cycle. If one compares curves A' and B' in Figure 5.12 where the deterioration in ductility is mainly due to AlN, with curves A' and C' in which precipitation is mainly due to TiN then the action of TiN can be seen to be very much worse.

6.3 Precipitation under equilibrium conditions

The following curves have been obtained from thermodynamic calculations for the compositions of the steels examined.

Figure 6-5[101] below shows a precipitation plot for the plain C-Mn-Al steel (P8H27) from this it can be seen that under equilibrium cooling conditions AlN precipitation does not start until around 990°C. However it should be noted that under non-equilibrium conditions that the "nose" of the PTT curves for AlN can be as low as 815°C.

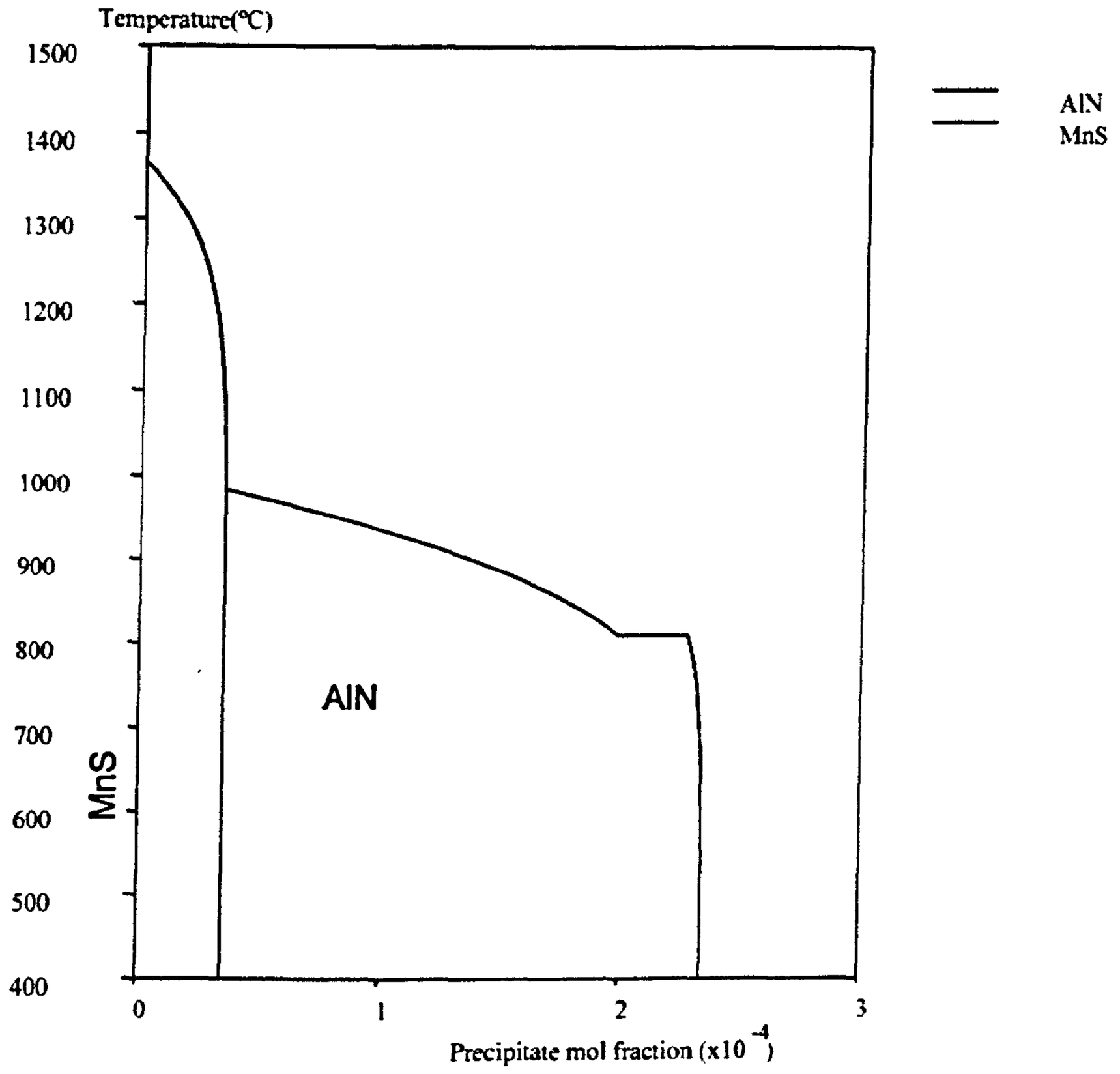

Figure 6-5 - Ti Free steel Precipitation plot (P8H27)

The above curve shows that MnS starts to precipitate out at 1370°C and precipitation is virtually complete at 1100°C. In contrast AlN starts to precipitate out at lower temps close to 1000°C and precipitation is complete by 800°C.

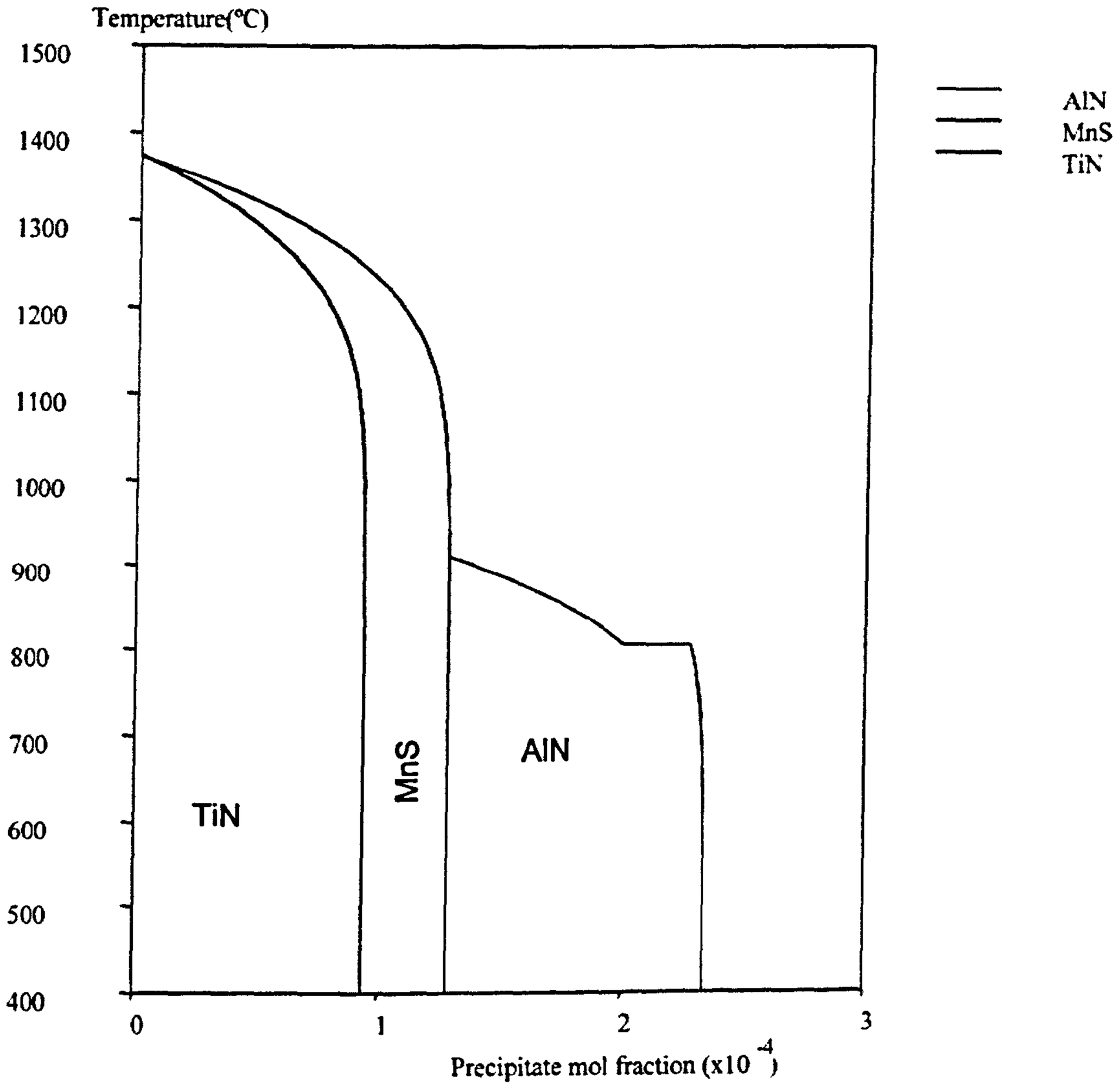

Figure 6-6 - 0.008% Ti Precipitation Plot (P8H29)

It can be seen from the above figure that both TiN and MnS precipitate out early on at high temperatures (1370°C) precipitation being virtually complete in both cases at 1100°C. In the case of Al because of the reduced N level due to TiN precipitation precipitation now starts at a lower temperature (900°C) and is completed again at 800°C.

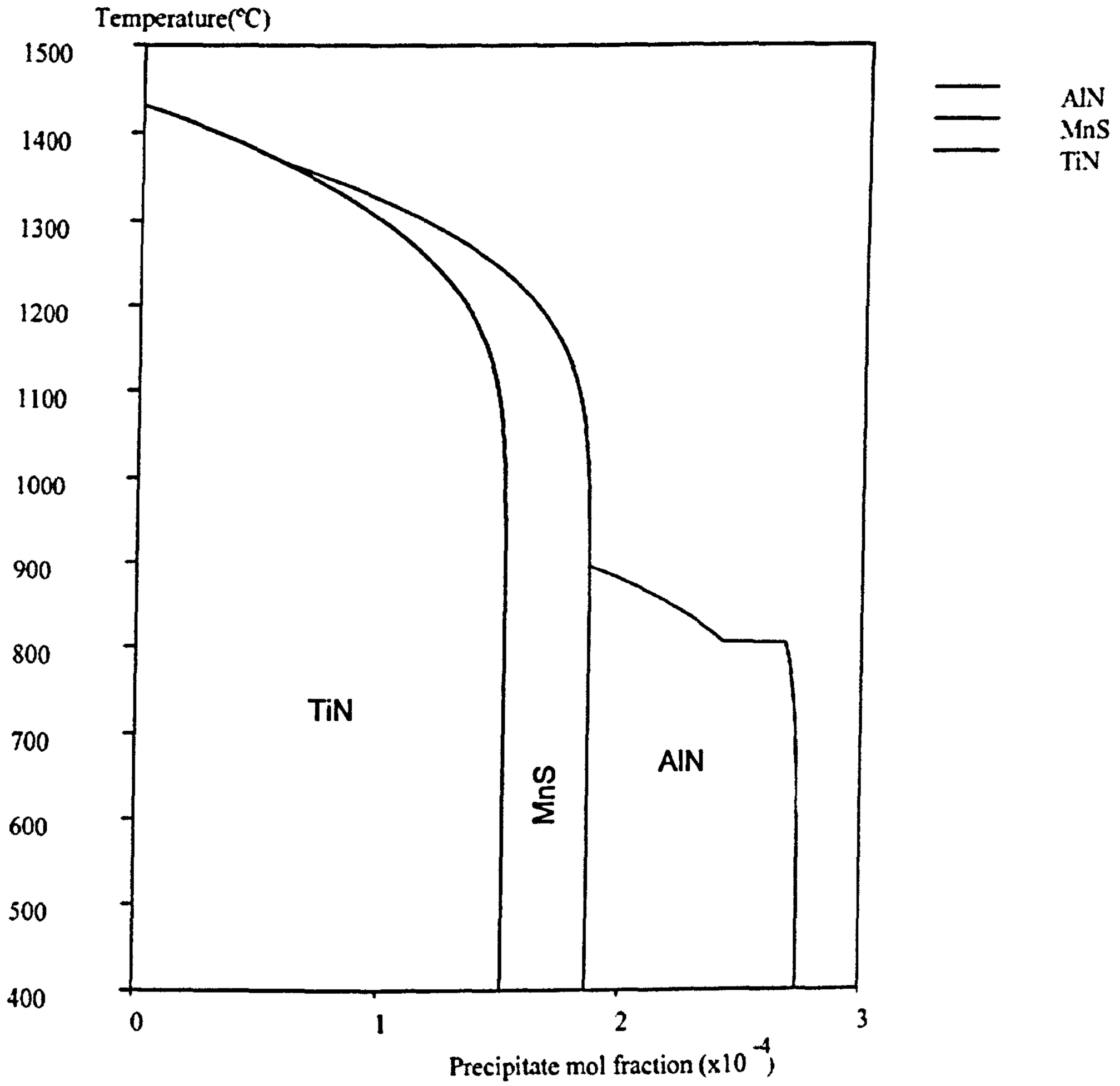

Figure 6-7 - 0.013%Ti Precipitation Plot (P8H31)

Further increases in Ti lead to more TiN being precipitated and less AlN until at the highest Ti level (0.022%) all the N is combined with the Ti and there is no nitrogen available for AlN precipitation. Raising the Ti level also ensures that the temperature at which it can first precipitate out on cooling is increased to close to the melting point. With Ti levels greater than the stoichiometric, the excess Ti is now able to combine with C to produce TiC, this precipitates out at 870°C with precipitation being

complete at ~ 800°C in a similar manner to AlN. However, TiC like TiN precipitates out randomly within the grains whereas AlN precipitation is more detrimental to hot ductility as it favours the austenite grain boundaries.

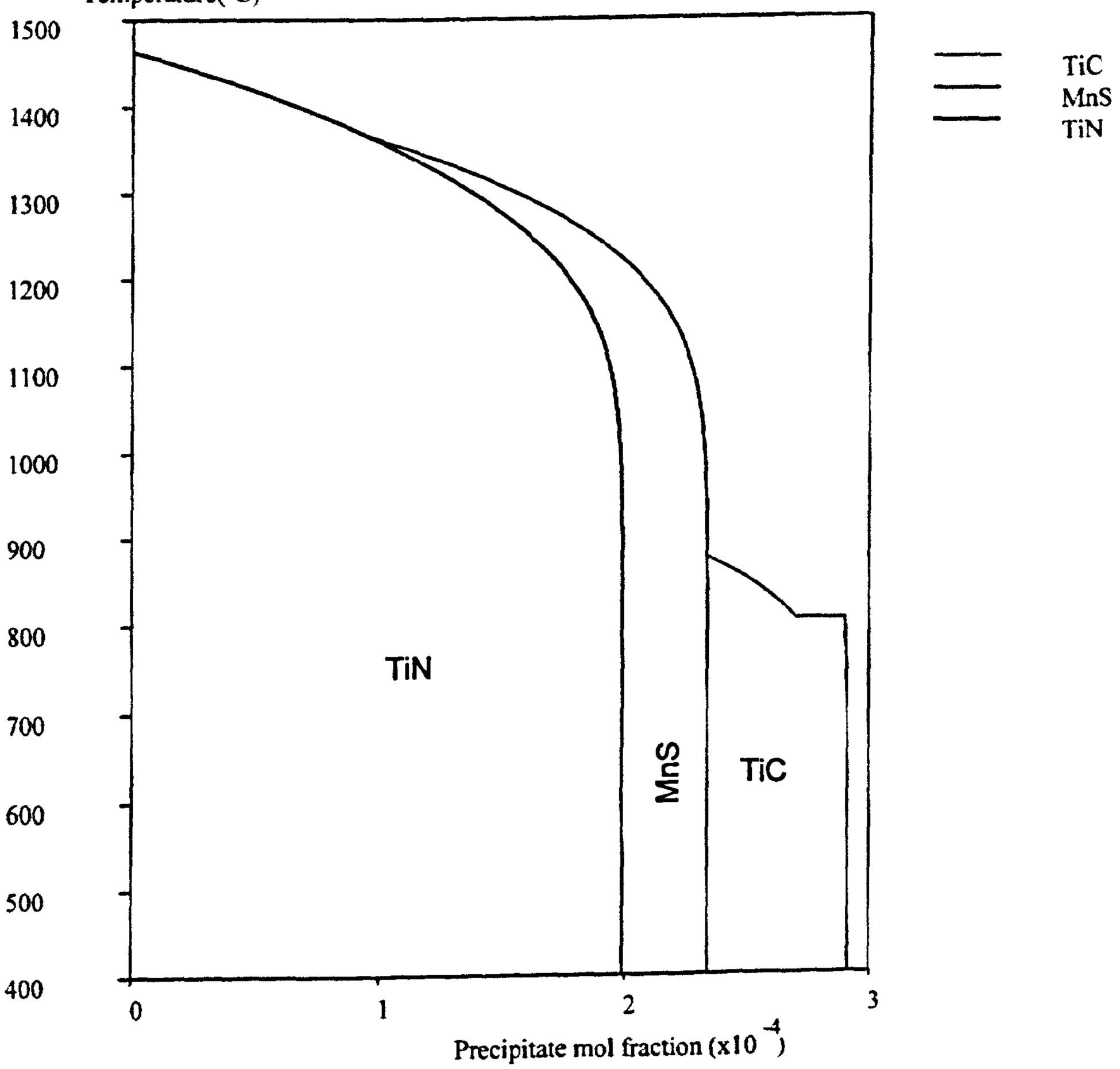

Figure 6-8 - 0.022%Ti Precipitation Plot (P8H33)

The above figures show that the TiN precipitates out at much higher temperatures, beginning at around 1420°C and finishing at around

1200°C, than the AlN which tends to begin precipitating out at just over 900°C.

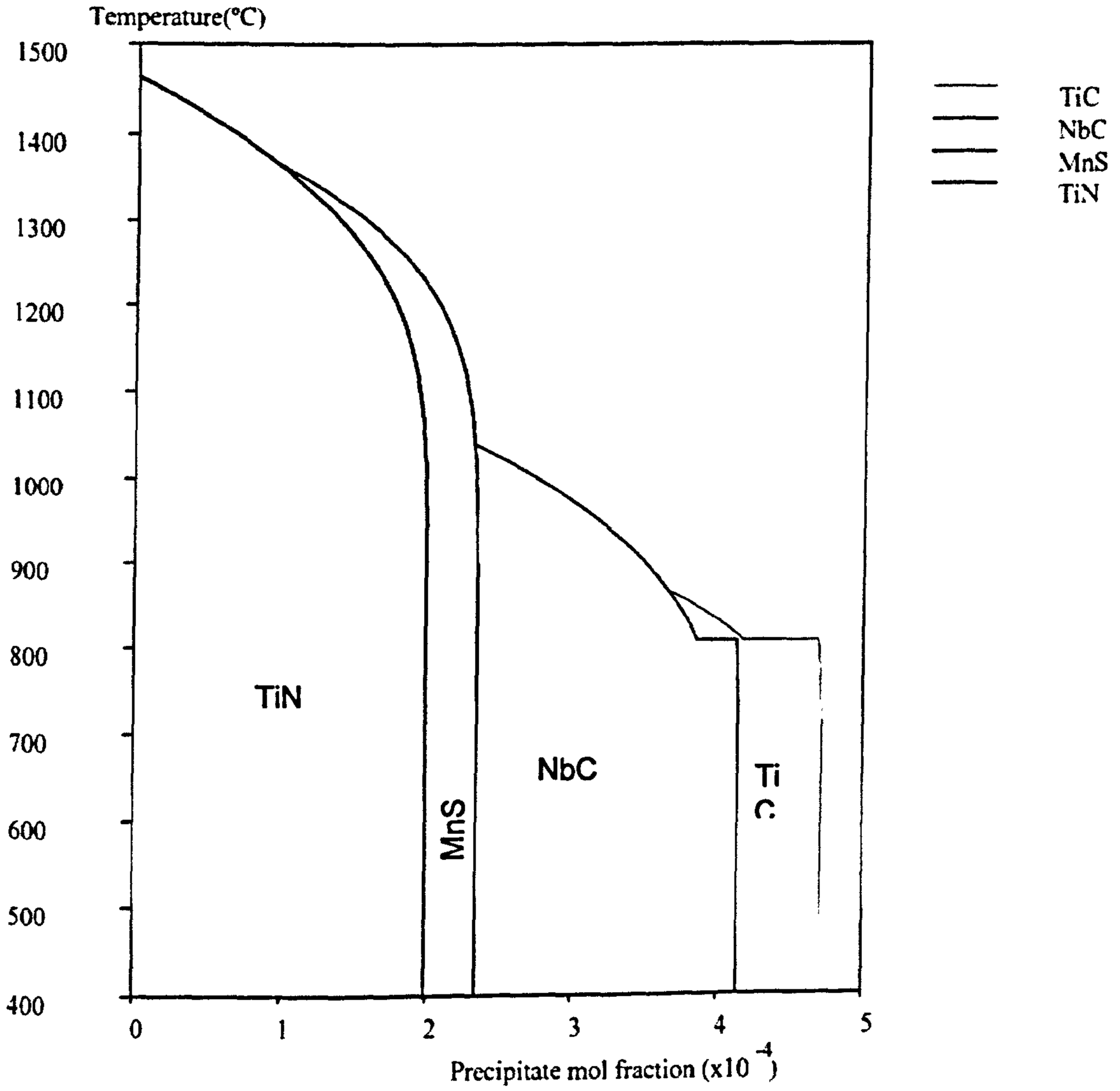

Figure 6-9 - 0.022%Ti, 0.03%Nb Precipitation Plot (P8H34)

The above curves have been thermodynamically derived and apply to equilibrium conditions. In the present instance cooling rates are far from equilibrium and deformation is also being applied. In this respect the PTT diagrams in which deformation is being applied at the temperature are of more use.

It should be noted that deformation speeds up the precipitation process by providing a large number of dislocation sites for nucleation. Often as in the case of Nb this is enough to completely precipitate out Nb(C,N) in short tensile testing times.

6.4 The Influence Of Dimple Size

It is well accepted that at room temperature the R of A values in a tensile test are dependent on the volume fraction of inclusions, their size and shape. The second phase particles cause voiding to occur around the particles and the greater their size and number and the more angular their shape the easier it is for voiding to occur and for fracture to take place.

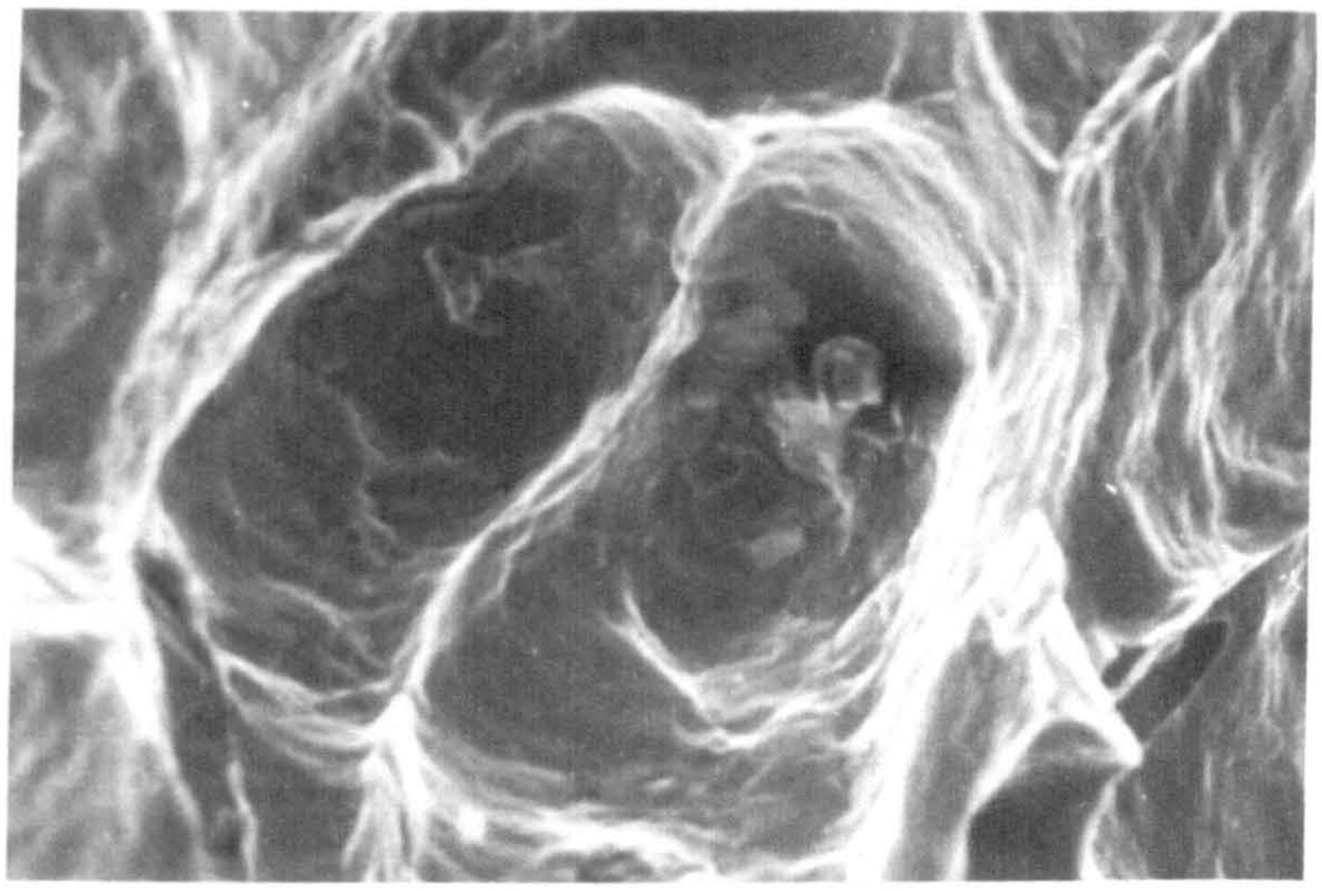

Figure 6-10 - Dimple with inclusion x 750 (P8H33)

When ductile failure occurs dimples are formed around the inclusions at the fracture surface. The coarser the particles the bigger are the associated dimples. Similar reasoning may be expected to apply for high temperature ductile failure but voiding at particles in this case is also influenced by grain boundary sliding and void formation is time and temperature dependent. Furthermore, the coarser the particles for a given volume fraction the better is the ductility. The greatest difference, however, is that whereas failure at room temperature is transgranular,

failure at high temperatures in the trough is intergranular and therefore it is the second phase particles that are at the boundaries that are of major importance.

The present work was undertaken to examine whether there was any relationship of the ductile dimple size to the R of A values.

It can be seen from Figure 5-20 that increasing the temperature, which will encourage coarser particles, leads to an increase in the dimple size and to better ductility. However, in contrast, for a given temperature it can be seen that the addition of Ti to the steels, although leading to decreased ductility, also causes a coarser dimple size. The probable explanation for this is as follows:

As mentioned earlier, failures are intergranular and it is therefore the particles at the austenite boundaries which are responsible for the dimples. These particles are mainly sulphides as can be seen from Figure 6-11. The sulphide inclusions at the boundaries have been shown to have a size range of 200-700nm[93]. AlN also precipitates at the boundaries preferentially and would therefore be expected to contribute to the formation of ductile dimples even though their size is generally finer 100-300nm[102]. TiN in contrast precipitates out randomly and has a much smaller size range ~2-15nm and so would be expected to have only a minor influence[103], if any, on the overall dimple size. For the Ti free steels, the dimples will therefore consist of a mixture of large dimples from the

MnS and smaller dimples from the AlN. Ti nitrides are so small that they will not give rise to dimples. As Ti is added the smaller dimples from the AlN particles are removed by the formation of TiN and the average dimple size in consequence increases as it relates more and more to the coarse MnS inclusions.

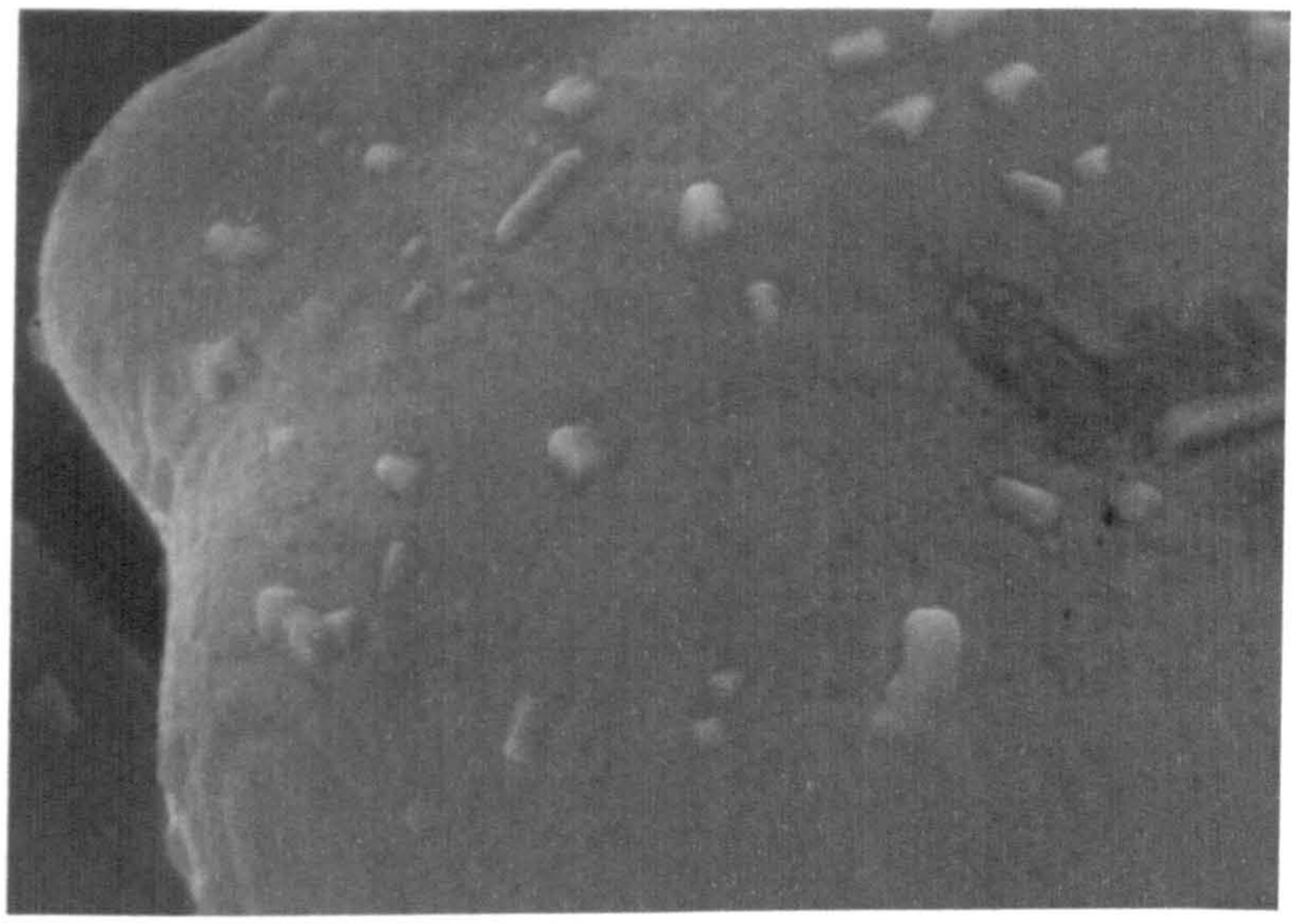

Figure 6-11 - Inclusions on dendrite x 35 Showing intergranular fracture with sulphides on the fracture surface.

Undercooling will encourage greater amounts of AlN to precipitate and hence will result in a finer overall dimple size. Thus, although there is some relationship between the R of A value and dimple size, the factors that influence dimple size are not always the same as those that influence the R of A.

The change in dimple size on undercooling does however indicate that further precipitation has occurred and that this precipitation will be mainly AlN.

CHAPTER 7 - CONCLUSIONS

7 CONCLUSIONS

This program of work was devised to investigate the effect of thermal history on steels with varying Ti levels in order to gain a greater understanding of how the continuous casting process may effect the hot ductility of HSLA Steels.

A series of samples with varying compositions were cast and machined by CORUS at their Swinden Laboratory. The samples were subsequently tested at the hot ductility research group facilities at City University. Two distinct groups of tests were carried out on the samples, a simple cooling test and subsequent tests containing a 100°C undercooling step.

Post test analysis of the samples showed that many of the samples originally tested had lost large amounts and in some cases all the Ti originally present. This resulted in a considerable amount of retesting being undertaken. Significant amounts of analysis were undertaken and the problem was traced to the composition of the silica tubes that are used to maintain the molten shape of the samples. Subsequent limited re-tests were carried out with the silica tube replaced by an alumina sheath. Re-tests were limited due to the long delay before the problem of Ti loss was discovered and the length of time required to completely solve the problem. This used up the majority of the samples allocated for the program. Post test analysis of samples tested in this way showed that no Ti loss was occurring.

The program produced the following results of note:

1. It has been shown that Ti additions (from 0 to 0.013%) both to C-Mn-Al and C-Mn-Nb-Al steels impair hot ductility.

2. Nb containing steels give worse hot ductility with or without Ti additions for the steels examined.

3. Thermal history was seen to have a small but significant effect on the hot ductility of steel. The addition of a 100°C undercooling step to C-Mn-Al-Ti steels generally resulted in worse ductility due to additional precipitation of AlN. In the case of Nb containing steels the undercooling step generally resulted in worse ductility for the Ti free steels however a slight improvement was noted for the Ti/Nb steels.

4. TiN precipitation is likely to have a more significant detrimental effect on hot ductility than AlN precipitation when one thermal cycle is introduced. However, whereas increasing the number of thermal cycles is unlikely to have any influence on TiN precipitation, further precipitation will occur for AlN and Nb(CN) thus causing further deterioration in the hot ductility.

5. The following regression equations have been obtained for calculating the reduction of area values at 950°C without undercooling.

$$\%\ R\ of\ A = 47.2 - 0.0632CR + 16.8\ p^{1/3} - 1521Nb - 3274[N] + 3452\ [Ns] + 2844P$$

$$\%\ R\ of\ A = 92.5 - 0.216CR + 16.8\ p^{1/3} - 0.596[Ti][N] - 3419P$$

Where CR is the cooling rate in K min^{-1}, p is the particle size in nm and Ns in the amount of N available to combine with Al. Equation (5) is suitable for use with Ti Nb containing steels and Equation (6) for Ti Al steels.

The regression equations produced from the results indicate that P is beneficial to ductility in Nb, Ti containing steels but detrimental to ductility in C-Mn-Al-Ti steels.

6. The results have shown that increasing the test temperature (which will encourage coarser particles) leads to an increase in the dimple size and to better ductility.

7. Adding Ti to steels will also cause a larger dimple size to occur as the formation of TiN removes small AlN particles from solution. Thus the dimple size increases as it relates more and more to the presence of the larger MnS inclusions

8. Undercooling reduces the dimple size in accordance with more precipitation taking place, most likely from AlN.

9. In all future work it is essential that the tensile specimens are melted in alumina tubes.

CHAPTER 8 – FUTURE WORK

8 FUTURE WORK

Some important results concerning the roles of thermal history, composition and dimple size have been presented within the present work. However, as with any scientific work, many other questions have also arisen encouraging a further and deeper scientific investigation.

Proposed future work is as follows:

1. Investigation of a different range of Ti:N ratios, so far only low N steels have been examined. An investigation of hyperstoichiometric Ti levels would also be beneficial.
2. Investigation of a complimentary set of casts with differing Al levels in order to more fully assess the relative effects of AlN and TiN precipitation.
3. Further progression towards the investigation of the influence of the commercial continuous cooling pattern used by CORUS. This is to be achieved by investigating increasing numbers of undercooling and re-heating cycles until the effect of additional cycles becomes negligible.
4. To ensure that no Al pickup is occurring from the alumina sheath a series of tests should be made using magnesium based sheaths.
5. Once a large data bank is established a computer based application could be written using variations of the proposed reduction of area calculations that would predict the hot ductility of a proposed HSLA steel from input data pertaining to thermal processing and composition.

[1] M.M. Wolf *Steel World* **4** No.1 (1999) p 7-13

[2] B.Mintz S.Yue and J.J. Jonas *Int Mat Reviews* **36** No. 5 (1991) p 187

[3] W.T. Lankford *Metall. Trans* **3** (1972) p1331-1338

[4] I Servi and N.J. Grant *Trans AIME* **191** (1951) p 917

[5] B. Mintz. *ISIJ International* **39** No. 9 (1999) p 833-855

[6] C. Spradbery Unpublished Work (2000)

[7] H.G. Suzuki, S. Nishimura and S. Yagamuchi *Trans ISIJ* **22** (1982) p48

[8] M.A. Hodgson, W.G. Ferguson NZ conf. of postgrad Eng and tech students Massey Uni, Aug 18-19 , (1994) p10-16

[9] C.M. Chimani and K. Morwald *ISIJ International* **39** No.11 (1999) p1194-1197

[10] M.A.Hodgson and W.G. Ferguson *Thermec 97 Conf. Proc* Ed T.Chandra and T.Sakai The Minerals Metals and Materials Society (1997) p531-585

[11] M.A.Hodgson and W.G. Ferguson 5th NZ materials Symp, Gracefield research Centre Dec 2-3 1992 p 11-15

[12] W. Jaeger, C. Klinkenberg, H. Pircher *Thermec 2000 Int. Conf. on processing and manufacture of advanced materials. Las Vegas USA De* Dec 6th-9th.*2000.* CD ROM section A1 Vol 117/3 "Special Issue Journal of Materials Processing Technology" Ed T.Chandra, K. Higashi, C. Suranaroyona and C. Toma. Elsevier Science, UK (Oct 2001).

[13] R.A.Hubert, C. Standaert, *Thermec 97 Conf. Proc* Ed T.Chandra and T.Sakai The Minerals Metals and Materials Society (1997).p 459-465

[14] Y.Maehara, T.Nagamichi *Mat Sci Technol* **7** (1991) p 915-921

[15] B.Mintz *Mat Sci Technol* **12** (1996) p132-138

[16] G.I.S.L. Cardoso and S. Yue. *In 31st mechanical working and steel processing conf.* Warrendale, PA ISS-AIME **29** (1989) p585-593.

[17] Z.Hongato, L. Zhen and W.Baorong *Thermec 97 Conf. Proc* Ed T.Chandra and T.Sakai The Minerals Metals and Materials Society **1** (1997) p 571-578.

[18] B.Mintz & J.M. Arrowsmith, *Met.Technology* **6** (1979) p24

[19] T.Revaux, J.P. Bricout and J Oudin J Mat. Eng and Performance **5** (1996) p260-268

[20] K.R. Carpenter, P.A. Manohar, B.A. Parker, C.R. Killmore *Thermec 2000 Int. Conf. on processing and manufacture of advanced materials. Las Vegas USA De* Dec 6th-9th.*2000*. CD ROM section A1 Vol 117/3 "Special Issue Journal of Materials Processing Technology" Ed T.Chandra, K. Higashi, C. Suranaroyona and C. Toma. Elsevier Science, UK (Oct 2001).

[21] M. Hater, R Klages, B. Rendez and K Taffner *Open hearth proc* AIME Warrendale (1973) p 202-217

[22] D. Crowther CORUS Swinden Laboratories – Private Communication (1999)

[23] Y. Maehara, K. Yasumoto, H. Tomono, Y. Ohmori *ISIJ* **27** (1987) p 222-228

[24] B.Mintz and R Abushosha *Hot working of Steels and composites* Ed H.J. McQueen et al. Pub The Canadian institute of mining metallurgy and petroleum (1996) p399-410

[25] R.Abushosha, S.Ayyad and B.Mintz *Mat Sci Technol.* **14** (1998) p 227

[26] Y. Maehara and Y. Ohmori *Mat Sci Technol* Eng. **62** (1984) p109-119

[27] S.D. Razumov, V.V. Sabilskii, V.I. Umanets, V.I. Lebedev and V.A. Obukhov *Steel USSR* **16** (1986) p225-228

[28] T. Nozaki et al *Trans ISIJ* **18** p330-338

[29] B. Mintz, J.M. Stewart and D.N. Crowther *Trans ISIJ* **27** (1987) p959

[30] B.Mintz, R. Abushosha, S.Ayyad and G.I.S.L. Cardoso *Proc HSLA Conf.* Beijing China Science and Technology Press (1996) p 342-345

[31] Y.Gao and K. Sorimachi *ISIJ International* **35** No. 7 (1995) p 914-919

[32] T.Nozaki J.Matsuno, K. Murata, H. Ooi and M.Kodama *Trans ISIJ* **18** (1978) p 330

[33] A.Darsouni B. Bouzabata and F. Montheillet *Journal De Physique* **IV** (1993) C7-347

[34] P. Deprez, J.P. Bricout and J. Oudin *Mat Sci and Eng.* **A168** (1993) p17-22

[35] L.E. Cepeda, J.M. Rodriguez Ibabe and J.J. Urcola *ISIJ* **32** (1993) p 799-806

[36] Y. Maehara H. Tomono and Y. Ohmori *Trans ISIJ* **27** (1987) p 499-505

[37] B.Mintz and J.J. Jonas *Mat Sci Technol* **10** (1994) p 721

[38] T.A. Towers J.H. Woodhead. *Ti Technology conf.* IOM Publications Sheffield Dec (1994) p 1-9

[39] R. Abushosha, R. Vipond and B.Mintz *Mat Sci Technol*, **7** (1991) p613

[40] Z. Chen, M.H. Loretto and R.C. Cochrane *Mat Sci Technol.* **3** (1987) p 836-844

[41] H. Gondoh, H. Nakasagi, H Matsuda, H. Tamehiro, and H. Chino, *Nippon Steel Tech* **14** (1979) p 55-65

[42] B. Mintz S. Yue and J.J. Jonas *Int. Mat Rev* **3** (1991) p 187

[43] H. Luo, and P. Zhao - As yet unpublished

[44] R. Abushosha, O. Comineli and B. Mintz *Mat Sci Technol.* **15** (1999) p 278

[45]He Kejian and T.N. Baker *Mat Sci. and Eng.* **A169** (1993) p53-65

[46] F.B.Pickering. *Ti Technology conf.* IOM Publications Sheffield Dec (1994). p10-43

[47] A.Kothe, J.Kunze G. Backman and C.Mickel *Mat Sci. Forum* **Vol 284-286** (1998) p493-500

[48] B.Engl and C. Klinkenberg *Mat Sci Forum* **Vols 284-286** (1998) p 501-508

[49] P.Uranga, A.I. Fernadez, B. Lopez and J.M. Rodriguez-Ibabe *Conf. Proc. Thermomechanical processing of steels.* (2000) p 204-213

[50] S.F. Medina and J.E. Mancilla *Acta Metall. Mater.* **42**, (1994) 3945

[51] W.J. Lui and J.J. Jonas *Conf. Proc Modelliing of metal rolling processes* (1993) p 39

[52] A.M. Guillet Ph.D Thesis McGill University Canada (1989)

[53] He Kejian and T.N. Baker Complex Carbonitrides in HSLA steels *Ti Technology conf.* IOM Publications Sheffield Dec (1994) p 115-132

[54] D.C. Houghton, G.C. Weatherly, J.D. Embury *Conf.Proc on Advances in physical metallurgy and applications of steels* Pub Metals Soc (1981) p135-146

[55] S.V. Subramnian, S. Shima, G. Ocampo, T. Castillo, J.D. Embury, G.R. Purdy Conf. Proc Beijing (1985) p151-161

[56] P.H. Li, A.K. Ibraheem and R. Priestner *Mat Sci Forum* **Vol 284-286** (1998) p 517-524

[57] S.V. Subramanian and G.C. Weatherly *Ti Technology conf.* IOM Publications Sheffield Dec (1994) p 133-149

[58] C. Zhou and R. Priestner *ISIJ* **36** (1996) p 397

[59] K. J. Lee, K.B. Kang, J. K. Lee, O. Kwon and R.W. Chang, *Proc. Int. Conf. On Math Modelling of Hot Rolling of Steel* Ed. S.Yue, Pub Hamilton (1990) p 435

[60] V.K. Heikkinnen, Scand .J. *Met* **3** (1974) p 41

[61] Th.A.Kop PGW Remijn J. Sietsma and S. van der Zwaag *Mat Sci* **Vol 284-286** (1998) p 193-200

[62] Y.Ohmori and Y. Maehhara *Trans. Japan Inst. Metals.* **25** No. 3 (1984) p 160-167

[63] J.R. Wilcox and R.W.K. Honeycombe *Mat Sci Tech* **3** (1987) p 849-854

[64] J.R. Wilcox and R.W.K. Honeycombe *Metals Tech.* **11** (1984) p 217-225

[65] G. Wang, and M. Akben *Proc. Int. Conf. HSLA Beijing* ASM, Metals, Park Oh, 4-8Nov (1985) p163-171

[66] M. Abken, and J.J. Jonas *HSLA Steels Technology And Application.* ASM metals park Oh, 1984, p149

[67] M.Akben, T. Chandra, P.Plaissard and J. Jonas *Acta Met.* **32** 1984 p 591

[68] V. Thillou, M. Hua, C.I. Garcia, C. Perdix and A.J. DeArdo Mat Sci Forum **Vol 284-286** (1998) p 311-318

[69] K.M. Banks, A.P. Bentley, and A. Koursaris *Thermec 2000 Int. Conf. on processing and manufacture of advanced materials. Las Vegas USA De* Dec 6th-9th.*2000.* CD ROM section A1 Vol 117/3 "Special Issue Journal of Materials Processing Technology" Ed T.Chandra, K. Higashi, C. Suranaroyona and C. Toma. Elsevier Science, UK (Oct 2001).

[70] M.G.Akben, B. Barcoix and J.J. Jonas *Acta Metallurgica* **31** (1983) p161-174

[71] K.J. Irvine, F.B. Pickering and T. Gladman, JISI **205** (1967) p.161

[72] S.V. Subrumanian Private communication 2000

[73] M.F. Eldridge and R.C. Cochrane *Mat Sci Forum* **Vol 284-286** (1998) p 217 – 224

[74] B. Charmont P. Chemelle and H. Biausser *Proc Conf. On Physical Simulation Techniques for Welding, Hot Forming and Continuous Casting* MTL 92-43TR, CANMET Ottowa II (1988) p 48-52

[75] G.D. Funnel R.J. Davies *Met. Technol* **5** (1978) p 150-153

[76] W.C. Leslie R.L. Ricket, C.L. Dotson and C.S. Walton *Trans. ASM* **46** (1954) p 1470

[78] B.C. Woodfine and A.G.Quarrell *ISIJ* (1960) p195-409

[79] E.T. Turkdogan *AIME Steelmaking Conf.Proc.* **70** (1987) p 399

[80] P. Heritier A. Fourdeux A.kobylanski *Scripta Metallurgica* **15** (1981) p753-755

[81] J.P. Michel, M. Akben, and J.J. Jonas *Rev Mat CIT* (1981) p111-120

[82] K.J. Irving and F.B. Pickering *Iron Steel* **30** (1957) p219

[83] K.Banks, A.. Koursaris, F.Verdoom, and A. Tuling *Thermec 2000 Int. Conf. on processing and manufacture of advanced materials. Las Vegas USA De* Dec 6th-9th.*2000.* CD ROM section A1 Vol 117/3 "Special Issue Journal of Materials Processing Technology" Ed T.Chandra, K. Higashi, C. Suranaroyona and C. Toma. Elsevier Science, UK (Oct 2001).

[84] Not Used

[85] Askeland. *The science and Engineering of Materials.* Pub Chapman and Hall (1995).

[86] T.Maki, T Nagamichi, N Abe, I Tamura *ISIJ* **71** (1985) p1367-1373

[87] A. Koethe Private Communication 1997

[88] R. Abushosha, O. Cominelli and B. Mintz *Mat Sci Tech* **15** March (1999) p278-286

[89] O. Cominelli, R. Abushosha and B. Mintz *Mat Sci Tech* Sept **15** (1999) p1058-1068

[90] N.E. Hannerz Trans *ISIJ* **25** (1985) p149

[91] RA Hubert and C Standert. *Proc. Thermec 97 Conf.* Ed T Chandra (1997) p 459-465

[92] Y.Maehara and T Nagamichi *Mat Sci Tech* **7** (1991) p 915-920

[93] B. Mintz R. Abushosha, O.G. Cominelli and M.A. Loyola de Oliveira *Proc. Thermec 97 Conf.* Ed T Chandra (1997) p 867

[94] B.Mintz and J.M. Arrowsmith *Met Technol* **6** (1979) p 24

[95] C. Oferman, C. A. Dacker, and C. Enstrom: *Scand. J. Metall.*, **10** (1981) p115

[96] E.T. Turkdogan *Proc. Conf on steelmaking* **70** (1987) p 399-416

[97] Private communication Alison Tuling South Africa 2001 (see Appendix A)

[98] David Crowther CORUS Swinden Laboratory Private Communication 2000

[99] *Annual Report Mega Project "Thin Slab Casting"* P3454 (1994), IFW

[100] G.I.S.L. Cardoso B. Mintz and S. Yue; *Ironmaking and Steelmaking* (1995), **32**, p 365-377

[101] S.V. Subrumanian Private communication (2001)

[102] R.Abushosha S. Ayyad B.Mintz. *Mat Sci Tech* **14** (1998), p-346-381

[103] O. Cominelli *PhD Thesis* City University 1998p 208-210.

APPENDIX A. REPORT BY ALISON TULING

1 TEM Investigation of Precipitation in Hot Ductility Tested Titanium Containing Steels.

21 Apr. 2001

2 Report for
Professor B. Mintz
Department of Mechanical Engineering and Aeronautics
City University, London

3 Author
Alison Tuling
Industrial metals and minerals research Institute
University of Pretoria

4 SUMMARY

The precipitation morphology of hot ductility test samples was investigated using extraction replica techniques and transmission electron microscopy (TEM). Large (>1000nm) composite sulphides and oxides were found in all three steels. In the case of the titanium bearing steels, titanium was also present in these large composite precipitates. No TiN was found in the melted areas of any of the titanium bearing steels.

In a check of the replica techniques it was found that large TiN (>800nm) were present in the base material of the highest titanium steel, while not present in the melted region when replicas were taken in the same extraction procedure. Additionally, fine crystalline precipitates (4nm) were seen in the base material, but were not present in the melted region, indicating the success of the replica technique in extracting fine particles.

The presence of copper containing sulphides seems to indicate that the melted regions are oxidised, which would also result in the loss of titanium and aluminium and lack of fine nitride precipitation.

5 INTRODUCTION

Longitudinally mounted hot ductility samples were received from City University London. These samples were part of a research project studying the interaction Al, Ti and Nb in of microalloyed steels during casting simulations, and the purpose of a TEM investigation at IMMRI was to characterise the TiN and AlN precipitate interaction.

For completeness hot ductility samples' composition, heat treatment and reduction in area results are documented in figure 1,2 and 3.

Figure 1 Table of steel compositions

Cast	C	Si	Mn	P	S	Al	N	Nb	Ti	Ti:N
P8H27	0.091	0.3	1.38	0.01	0.002	0.031	0.005	<0.005	<0.005	0
P8H29	0.100	0.3	1.40	0.01	0.002	0.027	0.005	<0.005	0.008	1.8
P8H33	0.100	0.3	1.40	0.01	0.002	0.028	0.005	<0.005	0.022	4.1

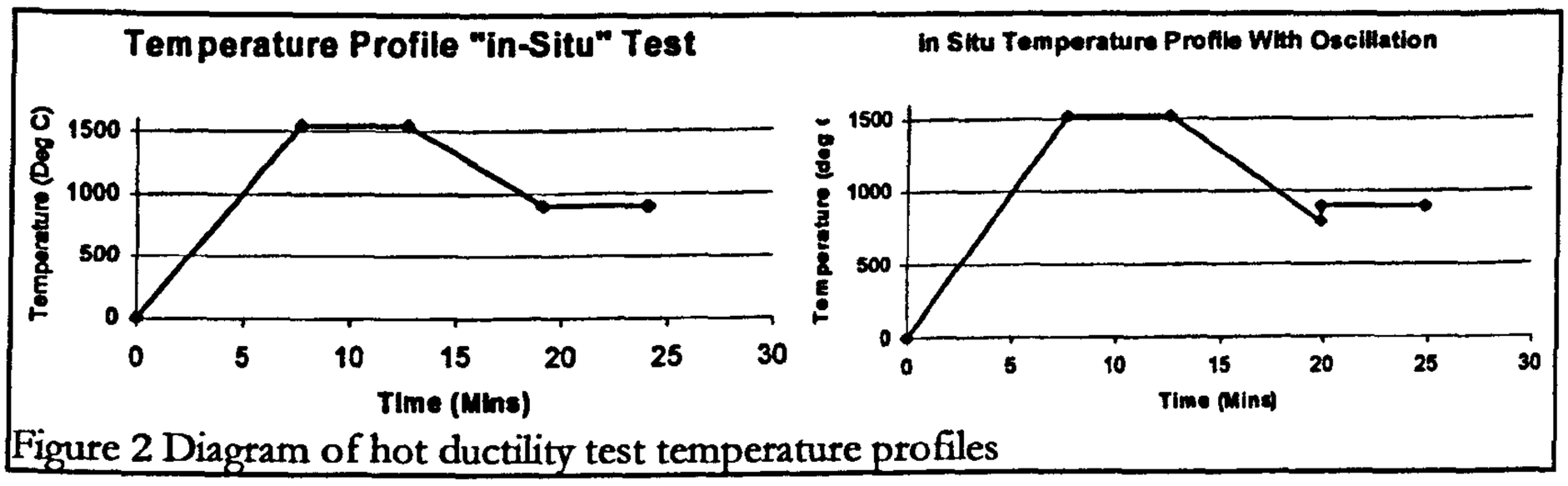

Figure 2 Diagram of hot ductility test temperature profiles

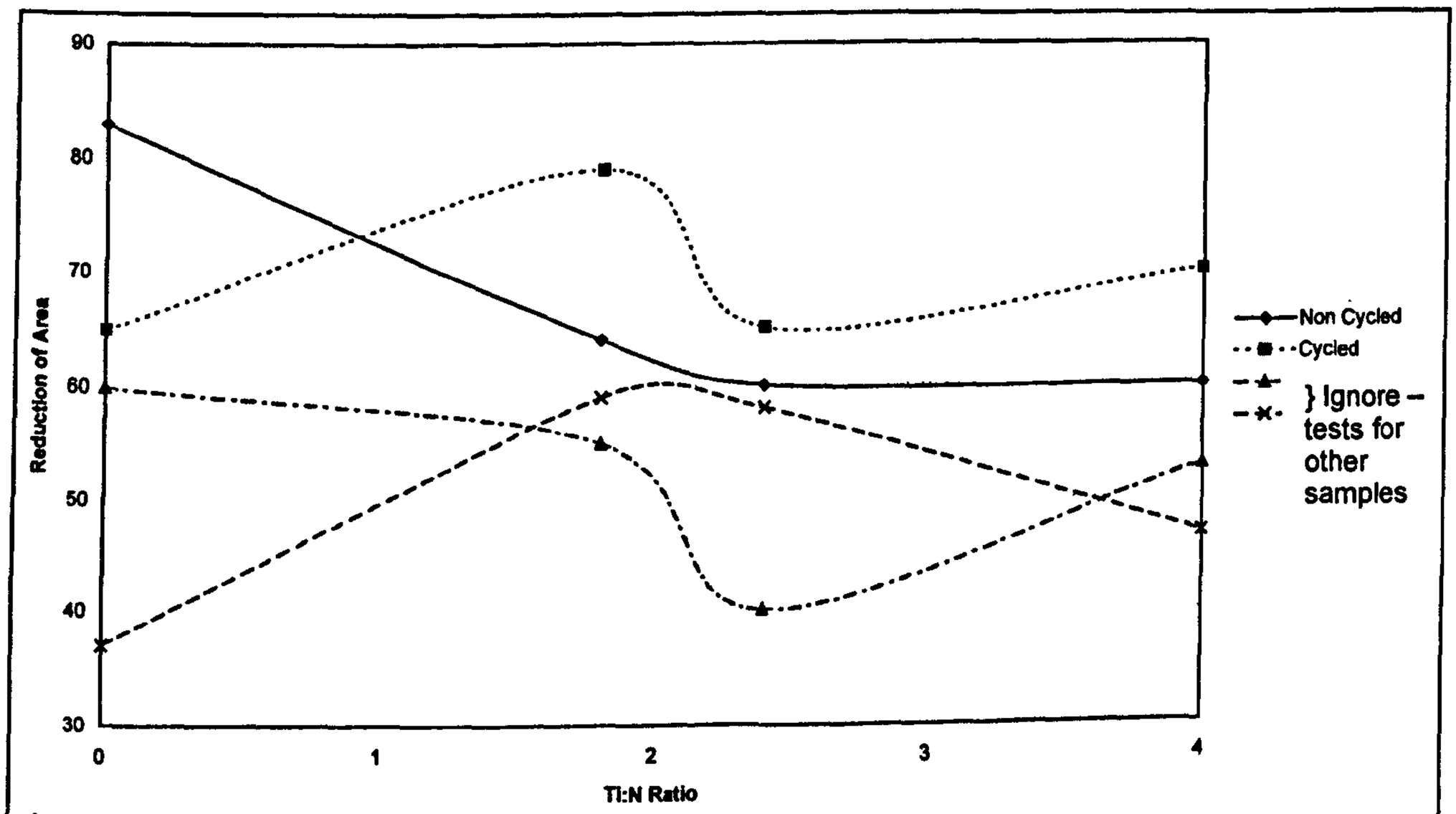

Figure 3 Diagram of reduction in area versus Ti:N ratio.

6 EXPERIMENTAL PROCEDURE.

Mechanically polished samples were etched with 2% nital, then ultrasonically cleaned in ethanol. The samples were then sputter coated with carbon. The area of interest (the area between the lines in figure 4) was scored into squares. The replicas were extracted with 10% nital, removed from the nital with a glass pipette and then floated on water. Subsequently they were caught on Cu grids and air-dried. Replicas were then studied in Philips CM200 TEM equipped with EDAX EDS (electron dispersive spectroscopy), at a voltage of 200 kV.

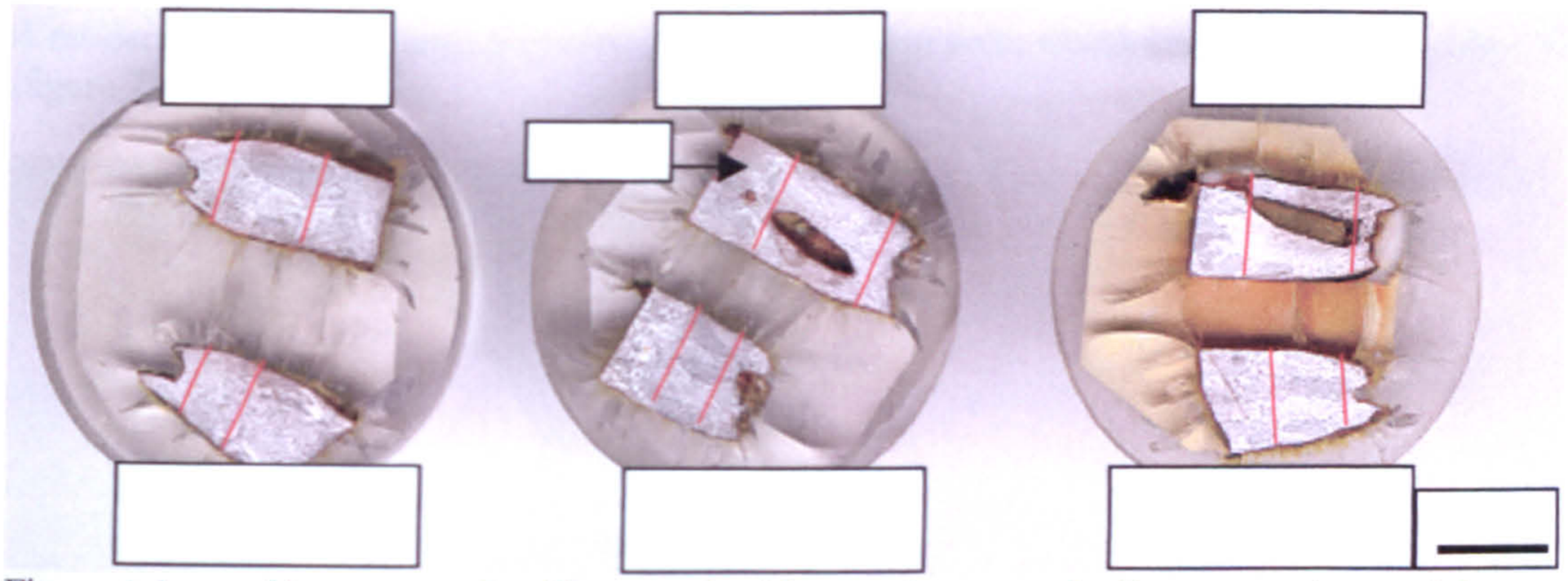

Figure 4 Area of interest on ductility samples (the area between the lines on each sample)

Since the results were not as expected, a further extraction was performed, using sample P8H33 direct (since it has the highest Ti and a relatively large area of non-melted base). The same extraction procedure as described above was used, save that replicas were taken from both the melted region of P8H33 as well as area 'a' as indicated in figure 4. The area 'a' will be referred to as the base material, and it has undergone some reheat cycle of unknown temperature and time. Thus a comparison of the two replicas that had been extracted under the same conditions could be performed

7 RESULTS

8 P8H27, Ti:N ratio 0

In both thermal cycles used, fine sulphides were found, figure 5 is a representative of these.

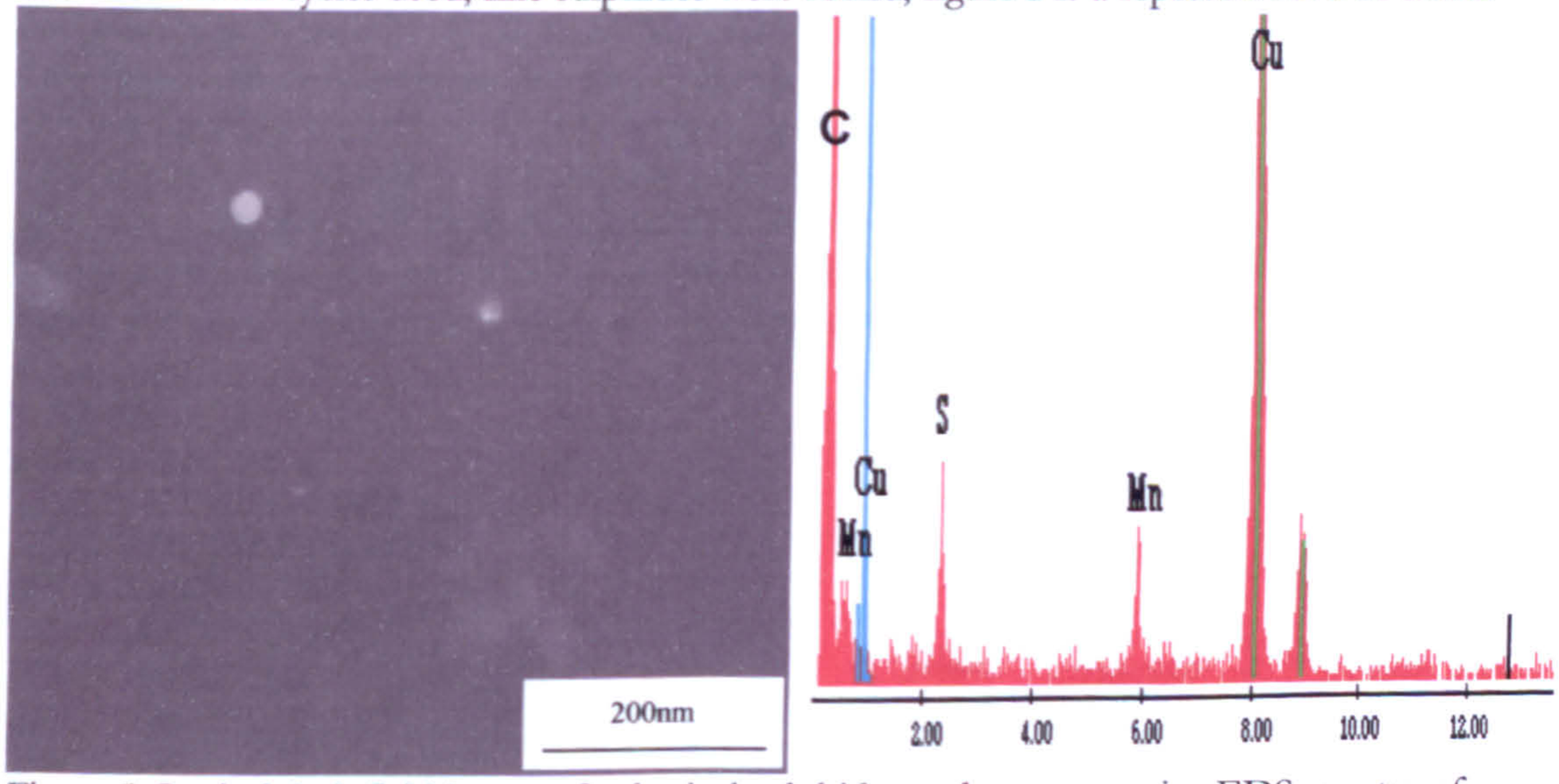

Figure 5 Conical dark field image of spherical sulphides and representative EDS spectra of sample . Sample P8H27 900 cycled at 1000.

In the EDS spectra, the presence of carbon can be attributed to the sputtered carbon, while some of the copper can be attributed to the copper grid that the replica was supported on. There was no significant difference in the size of these particles when comparing the cycled and direct thermal treatments.

Table 6 Details of precipitate statistics

Treatment	Sample size	Average (nm)	Minimum (nm)	Maximum (nm)	std dev (nm)
P8H27 direct	10	23	6	67	18
P8H27 cycled	15	29	12	65	15

A moderate amount of large particles (>2μm) were also seen, which consisted of *Al – Mg – O* (figure 7).

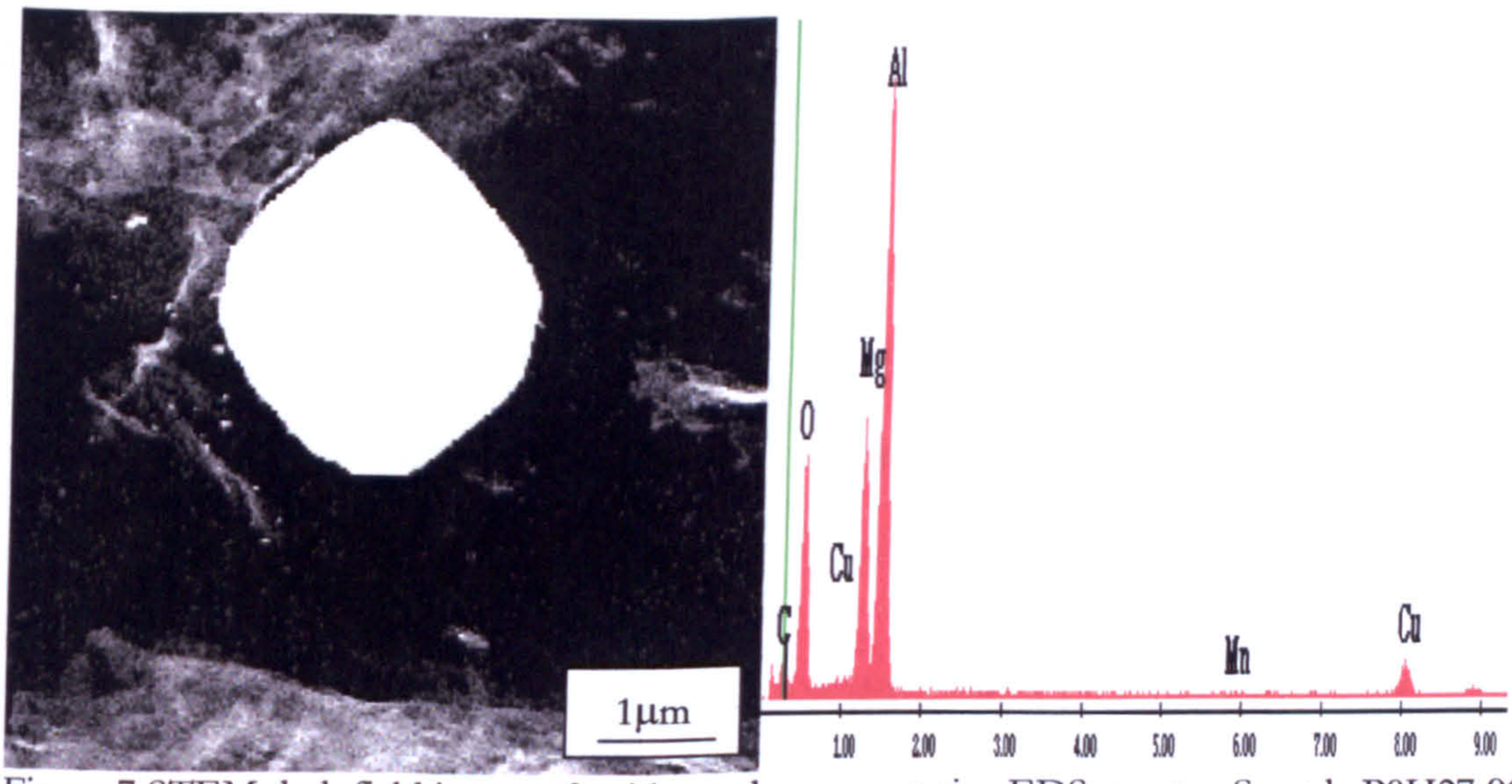

Figure 7 STEM dark field image of oxides and representative EDS spectra. Sample P8H27 900 direct.

9 P8H29 , Ti:N ratio 1.8

The finest precipitates in both the direct and cycled materials were of similar morphology and composition to that in P8H27 (MnS of ~30nm), they will not be discussed further. Titanium was only detected in large (>2μm) composite precipitates as seen in figure 8. The elements present in such precipitates were O, Al, Si, S, Ti, Mn, Cu (the carbon is likely to be from support film). Although some of the copper may be attributed to the grid, a comparison of EDS spectra (spot 1 and 7 in figure 8) shows that there is some copper associated with sulphur. If the copper peak in EDS spectrum from spot 7 is considered to be background then some of the copper from EDS spectrum of spot 1 must be due to copper in the particle. Note that both EDS spectra were acquired with the same spot and the same takeoff angle and for similar live time (51, 55sec). Figure 9 shows sulphide precipitates in a row (appears to be copper sulphide).

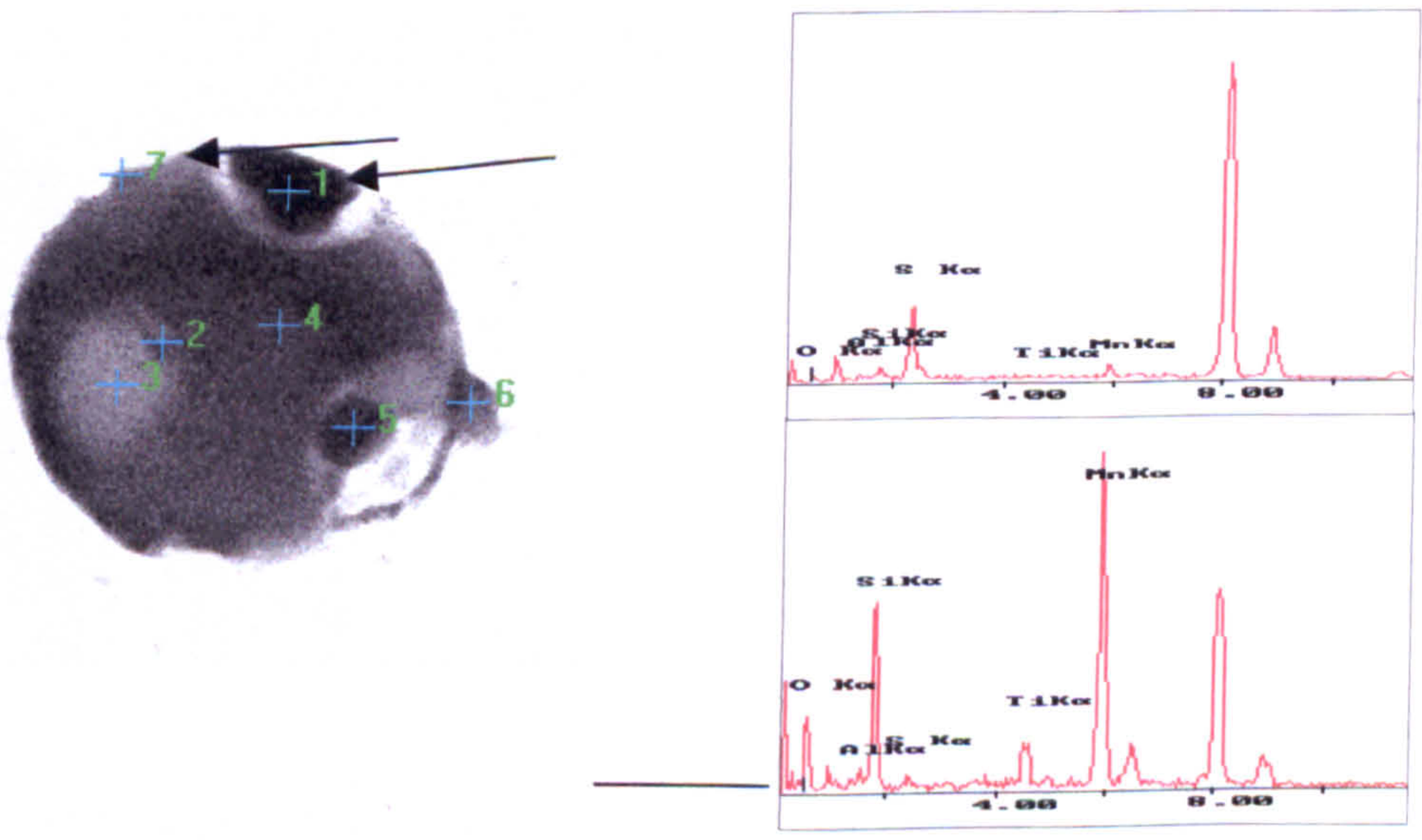

Figure 8 STEM bright field image of oxides and sulphides, with representative EDS spectra Sample P8H29 900 cycled.

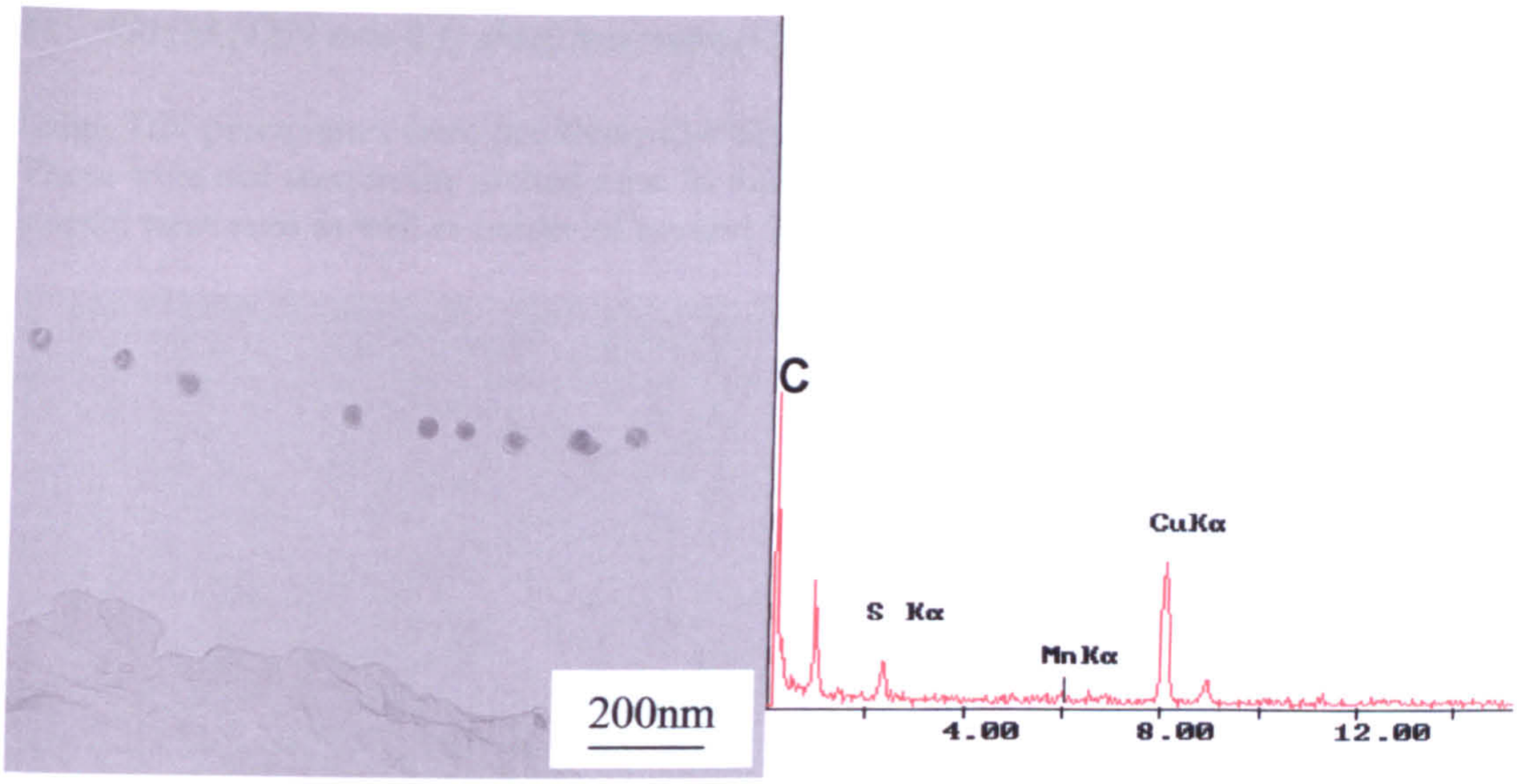

Figure 10 TEM bright field image of sulphides possibly along prior austenite grain boundary, with EDS of same. Sample P8H29 900 cycled at 1000.

10 P8H33, Ti:N ratio 4.1

No smaller precipitates (<100nm) were detected in either direct or cycled temperature treatments. The titanium was only found in large (>800nm) composite particles of oxides-sulphides as seen in figure 11. There is clear evidence of copper in these particles, apparently as sulphides (In figure 11 compare the 'background' copper in spot 2 with the copper peak in spot 1).

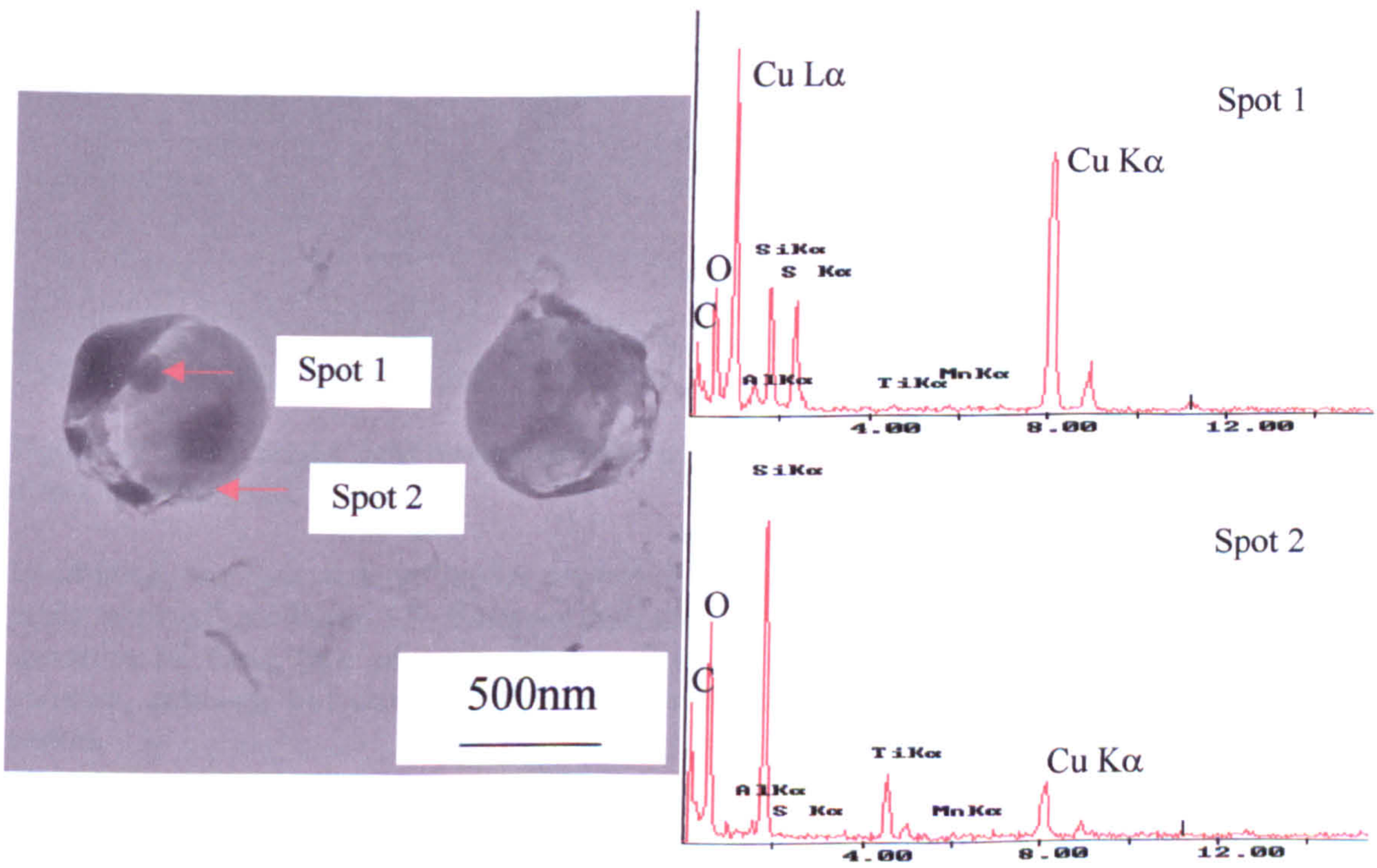

Figure 11 TEM bright field image of oxide-sulphide composite particles, with EDS of the same. EDS spectra collected at similar times. Sample P8H33 900 cycled at 1000.

11 *P8H33 (Ti:N ratio 4.1) direct, base material vs melted region*

Large TiN precipitates were positively identified in the base material, as can be seen in figure 12. These were not seen in the melted area. In the base material, filaments of Cu_2S, MnS (~400nm in length) were seen as well as oxides of around 200nm containing (O, Al, S, Ti, Mn, (Cu)).

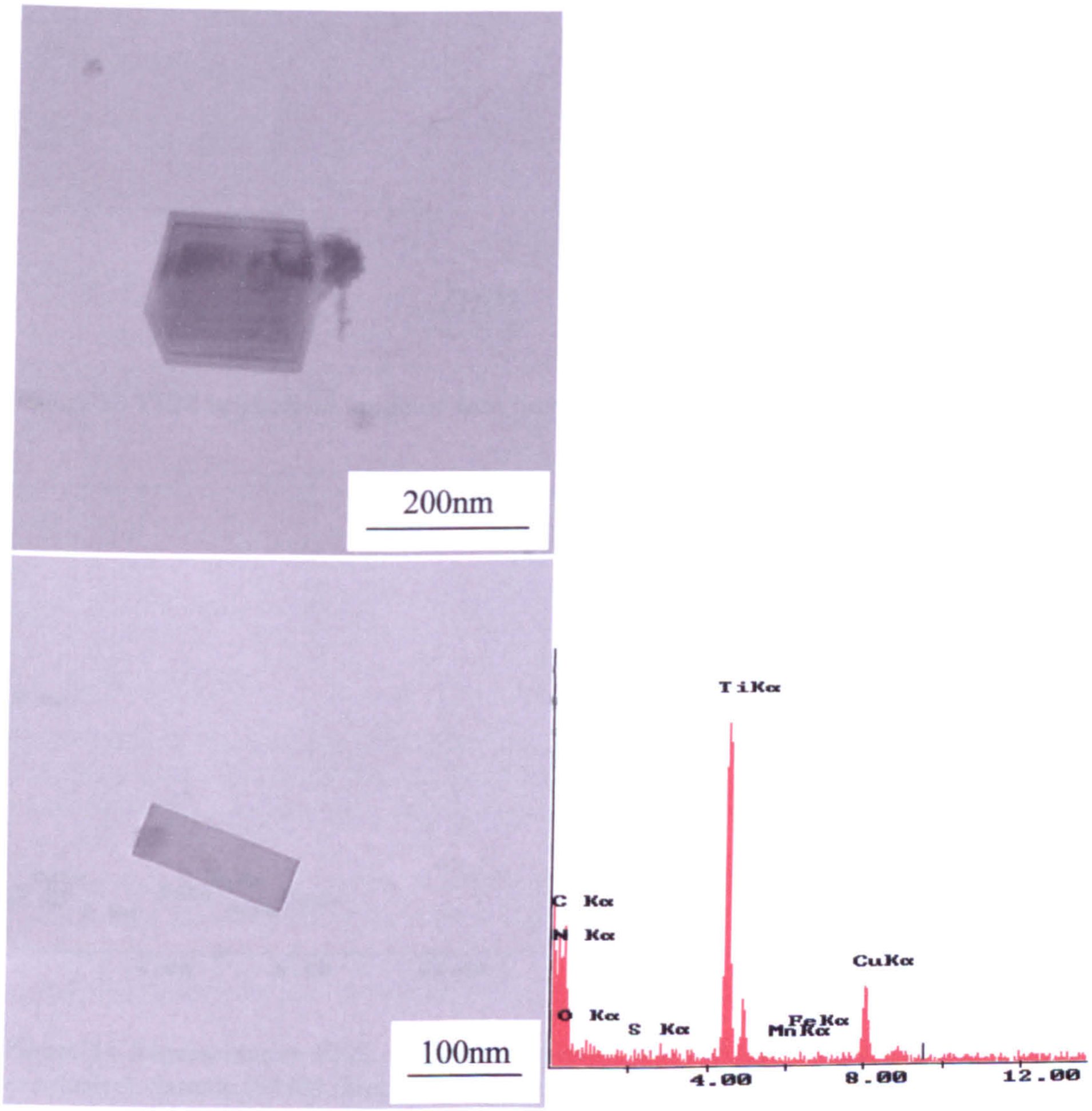

Figure 12 TEM bright field images of TiN and representative EDS spectrum. Sample P8H33 direct, base material.

In addition, the base material replica contained many crystalline precipitates of 4nm which were easily resolved (see figure 13), however their composition could not be confirmed, although the spectrum of these type of precipitates is furnished in figure 14, (indicates the presence of titanium, although not conclusively). These were not seen in the identically extracted melted region.

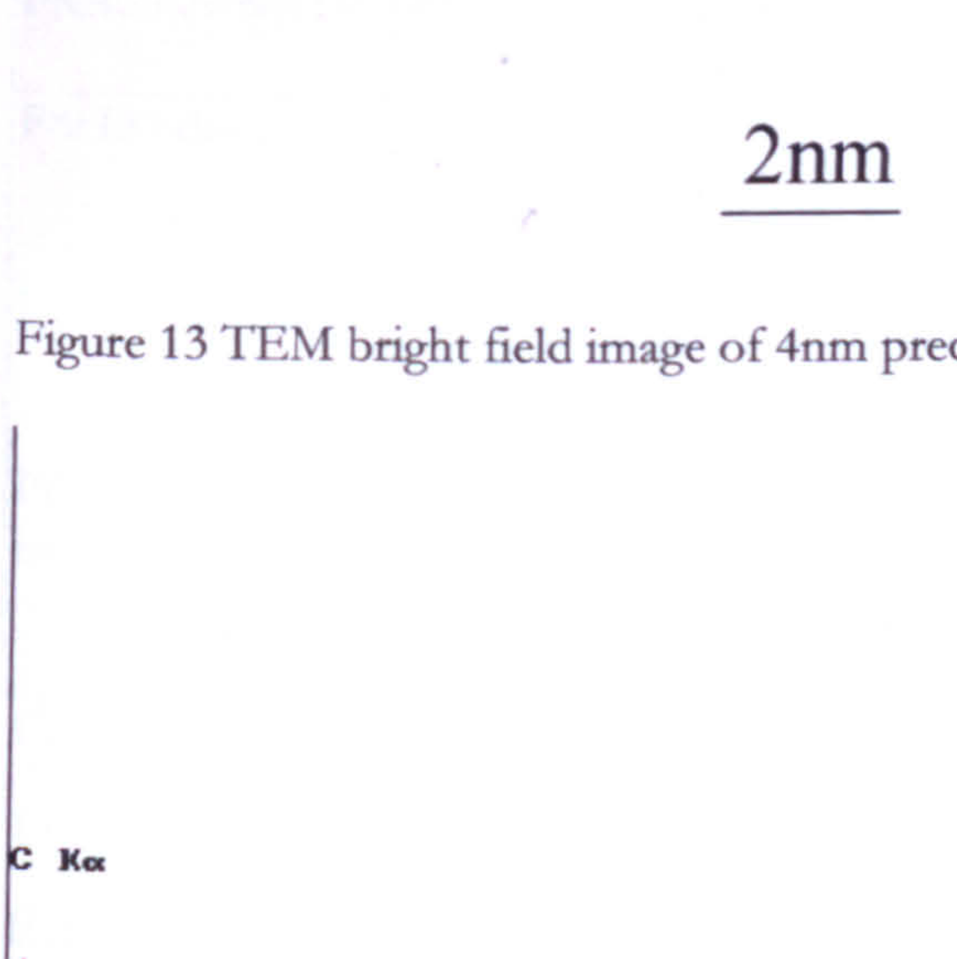

Figure 13 TEM bright field image of 4nm precipitates. Sample P8H33 direct, base material.

Figure 14 Representative EDS of 4nm precipitates, possibly indicating the presence of Ti (not conclusive). Sample P8H33 direct, base material.

Sample	size range	Average size	Comments
P8H27 direct	6-70nm	20nm	Sulphides (Mn-(Cu)-S)
	500nm		Oxides (Al-O)
	>2000nm		Oxides (Al-Mn-O)
P8H27 cycled	12-65nm	30nm	Sulphides (Mn-(Cu)-S)
	Large		Larger not catalogued
P8H29 direct	Small		Sulphides (Mn-(Cu)-S)
	>2000nm		Composite oxide/sulphides (Si-Al-Ti-Cu-Mn-S-O)
P8H29 cycled	30-35nm	30nm	Sulphides in row (Cu-S)
	>1000nm	2000nm	Composite oxides/sulphides (O-S-Mn-Cu; O-Si)
P8H33 direct	No small		
	>1000nm	2000nm	Oxides O, Al, Si, Ti, Mn
P8H33 cycled	No small		
	>800nm		Composite oxide, sulphides (O-Cu-S-Al; O-Cu-Si-S; O-Si-Ti)
P8H33 direct base	4-10nm		Crystalline
	100-800nm		TiN clearly rectangular or square, also others (O-S-Mn-Cu; O-Al-S-Ti-Mn-Cu)

13

14 DISCUSSION

Experimentally, the area that the replicas were taken from was not directly at the fracture surface. The area close to the fracture surface has had higher strain during final necking and possibly a localised heating, and thus the precipitates morphologies would be slightly different.

In the sample with no Ti, the fine precipitates (~30nm) are similar in both thermal cycles, this is borne out by the reduction of area curves (figure 3) which show that the ductilities are similar. The MnS has a solution temperature of 1340°C according to the equations* Gladman[1] uses. This indicates that the MnS would precipitate with similar morphology in the two thermal cycles.

The presence of copper in some of the spectra (figure 8, spot 1; figure 11, spot 1) cannot be attributed to just background copper radiation. The copper is also remarkably high for background in figures 5 and 10. Additionally, in figure 10 there is no manganese in the precipitates, and since pure sulphur would not be thermodynamically stable at such levels of sulphur (0.002%) these precipitates must be Cu_2S. Additionally, in the extraction procedure, great care was taken to ensure as little copper contamination as possible. A glass pipette was used to transfer the replicas from the nital to the water, rather than using a copper grid. This ensures that the only electrolyte that both copper grid and replica were simultaneously in contact with was distilled water.

It is also significant that in the large composite precipitates (figures 8,11) the Cu_2S is associated with oxides (O,Mn,Si,Ti). Unfortunately the Cu levels cannot be determined in these samples (they are too small for spark analysis and wet chemistry would destroy the sample), although it is of some merit to compare these with a study[2] where Cu has been deliberately added. It is concluded in that study, that the presence of copper and oxidising conditions lead to the formation of copper sulphides according to the following equation[3]:

---

* $\log K_\alpha[\%Mn][\%S] = -9020/T + 2.93$
where $K_\alpha = ([\%Mn][\%S]f_S^{Mn})/a_{MnS}$ and $\log f_S^{Mn} = (-215/T + 0.097)[\%Mn]$.

$$2MnS + 4Cu + O_2 = 2Cu_2S + 2MnO$$

It may be concluded that oxidising conditions existed in the melted region and can account for the lack of TiN or AlN as both Ti and Al are easily oxidised.

This fact combined with the ease at which TiN was detected in the high Ti steel (P8H33 900 direct sample) indicates that the replica procedure is extracting TiN successfully. Thus the lack of TiN in the melted region does seem to be a real material phenomenon.

The fine (4nm) precipitates in the base material also indicate that the replica technique is adequate. If these were present in the melted regions (where there was little grain boundary area and more intra grain regions where fine precipitation is expected) they would have been seen in the replica extracted at the same time as that of the base material.

The author is not convinced that the reduction in area results of P8H29 900 direct and P8H33 900 direct are representative of the material since there is a porosity in the centre of both of these samples, as may be seen in figure 4.

15 CONCLUSION

1. Large (>1000nm) composite sulphides and oxides were found in all three steels. In the case of the titanium bearing steels, titanium was also present in these large composite precipitates.
2. No TiN was found in the melted areas of any of the titanium bearing steels.
3. In a check of the replica techniques it was found that large TiN (>800nm) were present in the base material of the titanium steel, while not present in the melted region when replicas were taken in the same extraction procedure. Additionally fine crystalline precipitates (4nm) were seen in the base material which were not present in the melted region, indicating the success of the replica technique in extracting finer particles.
4. The presence of copper containing sulphides seems to indicate that the melted regions are oxidised, which would also account for the loss of titanium and aluminium and lack of fine nitride precipitation.

16 RECOMMENDATIONS

From the results and discussion, the author can only recommend that the ductility tests must be redone with greater care to the atmosphere around the samples.

17 REFERENCES

1. T. Gladman, 'The Physical Metallurgy of Microalloyed Steels', IOM, (1997), pp 81-135.

2. B. Mintz, R. Abushosha, D.N. Crowther, *Mat Sci. Tech.* 11 May (1995) pp474-481.

3. D.A Melford in 'Residuals, Additives and Material properties', ed A Kelly et al, The Royal Society, London, (1980),pp89-103; cited in B. Mintz, R. Abushosha, D.N. Crowther, *Mat Sci. Tech.* 11 May (1995) pp474-481.

4.

APPENDIX B. ORIGINAL RESULTS

1 Original Results

The results listed in the following section were not all considered suitable for inclusion in the main body of the thesis due to problems with the experimental arrangements. These problems are detailed in Chapter 4 of the thesis. The results are included within this appendix for information only.

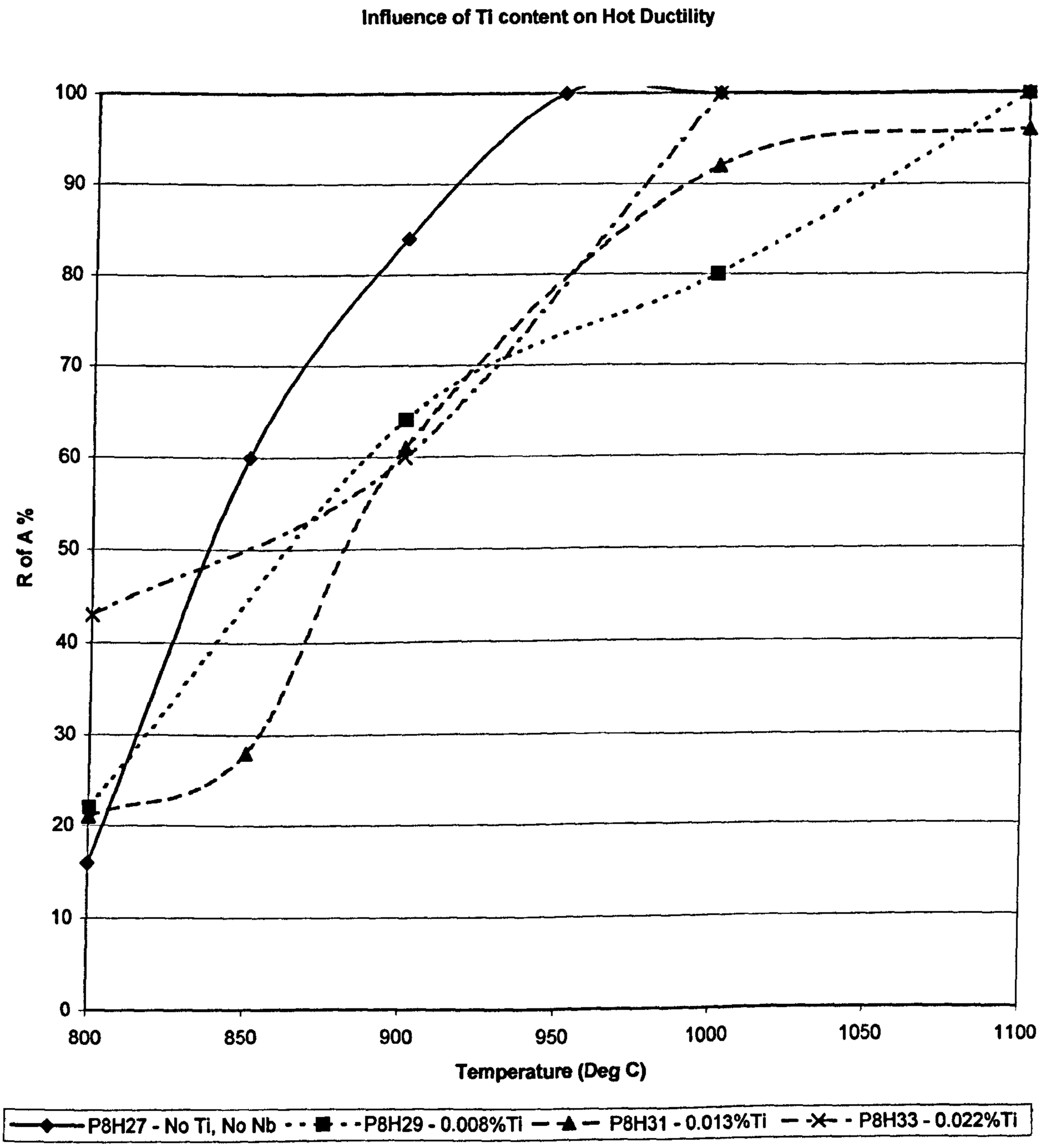

Figure 1 - The influence of Ti on Hot Ductility of Nb free steels having ~0.005%N

Figure 1 shows that the addition of Ti has an adverse affect on the hot ductility of the steel for temperatures in excess of 900°C although there is some indication that the highest Ti steel (0.022%) may be giving benefit to ductility at temperatures below 850°C.

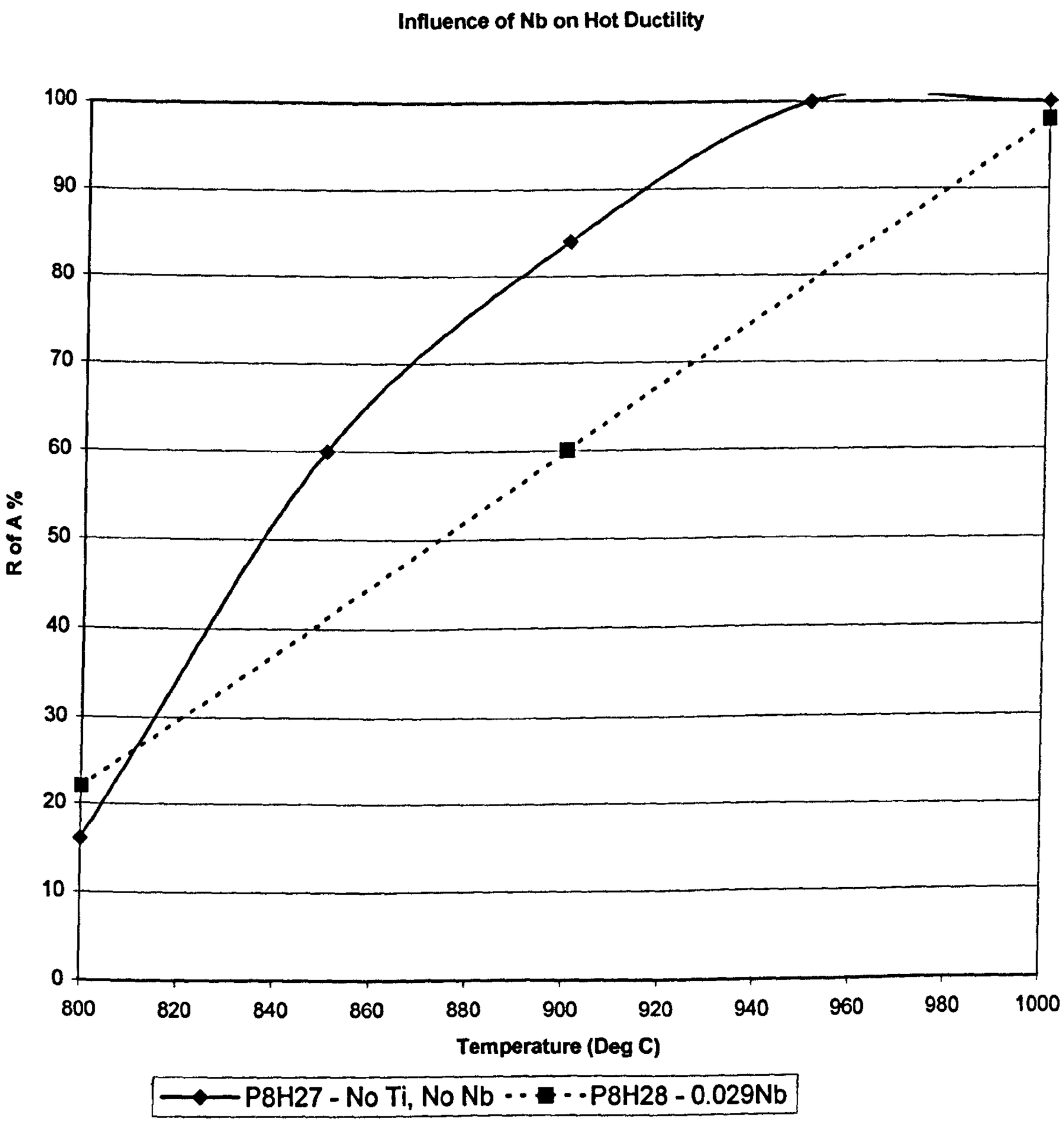

Figure 2 - The influence of Nb on hot ductility of steels with ~0.005% N

Similarly, Figure 2 shows that the addition of Nb to a plain steel causes a deterioration in the hot ductility. Both of the above are in line with expectations and previous work.

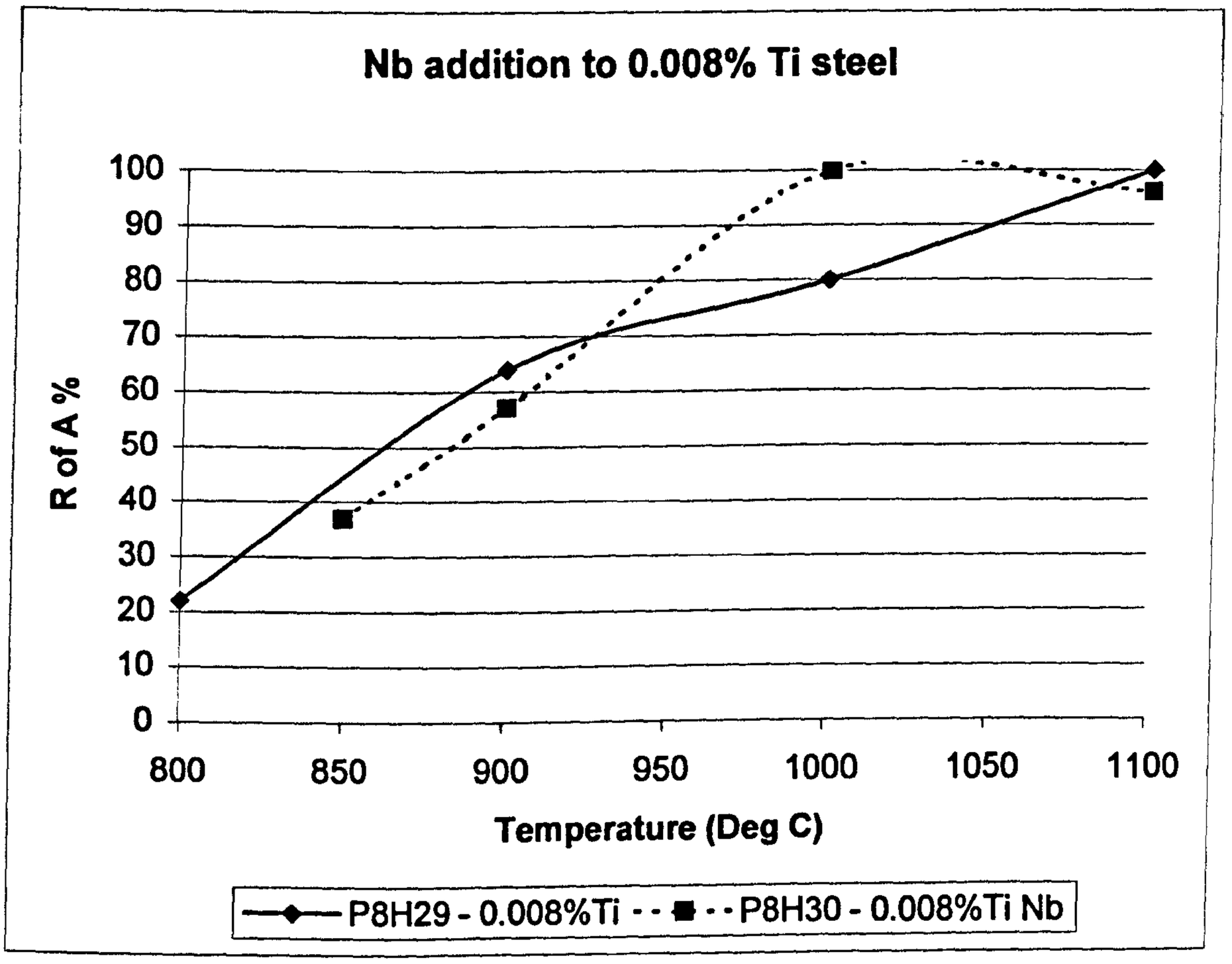

Figure 3 - Nb addition to 0.008% Ti steel

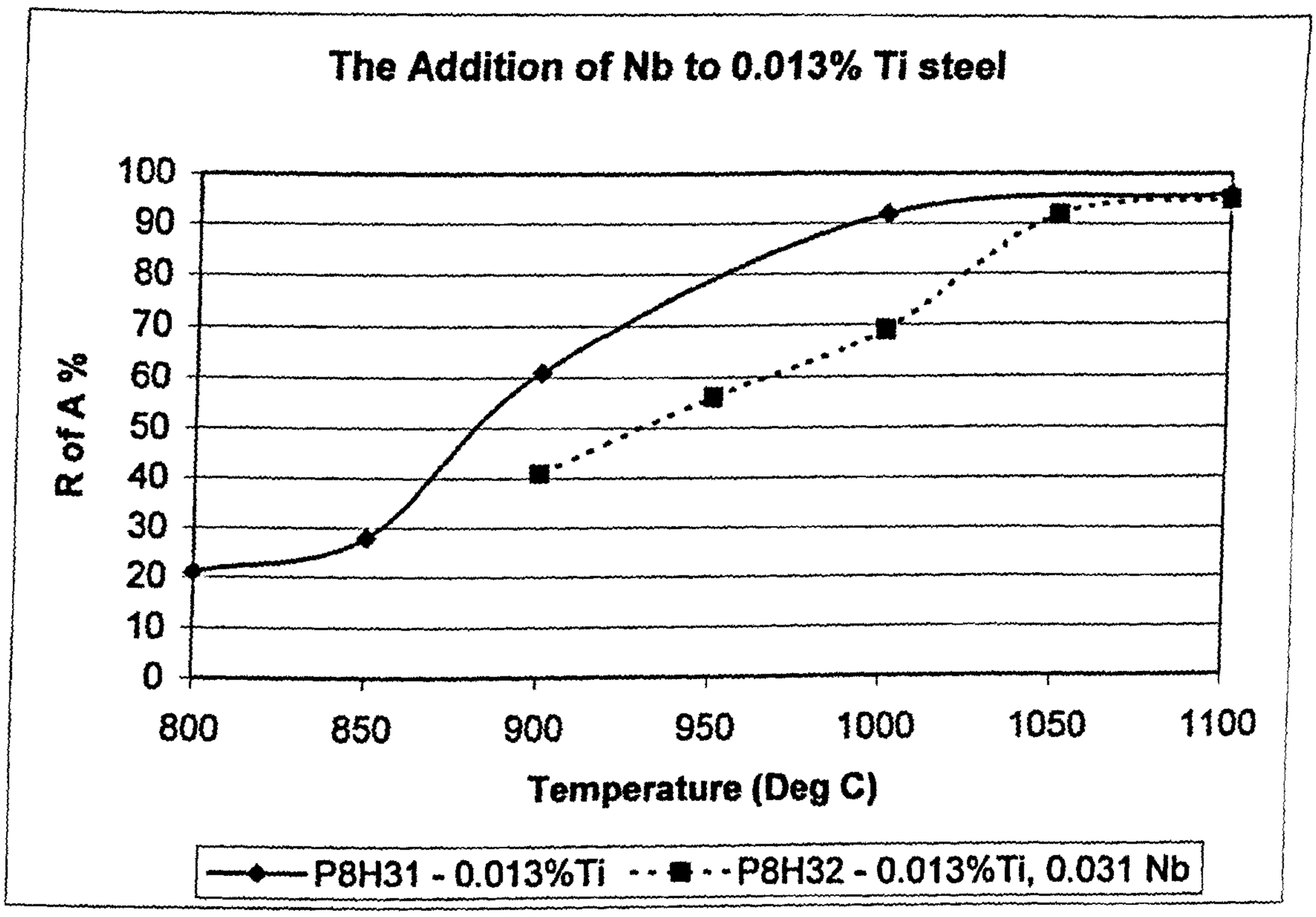

Figure 4 - The Addition of Nb to a 0.013% Ti Steel

PAGE

NUMBERING

AS ORIGINAL

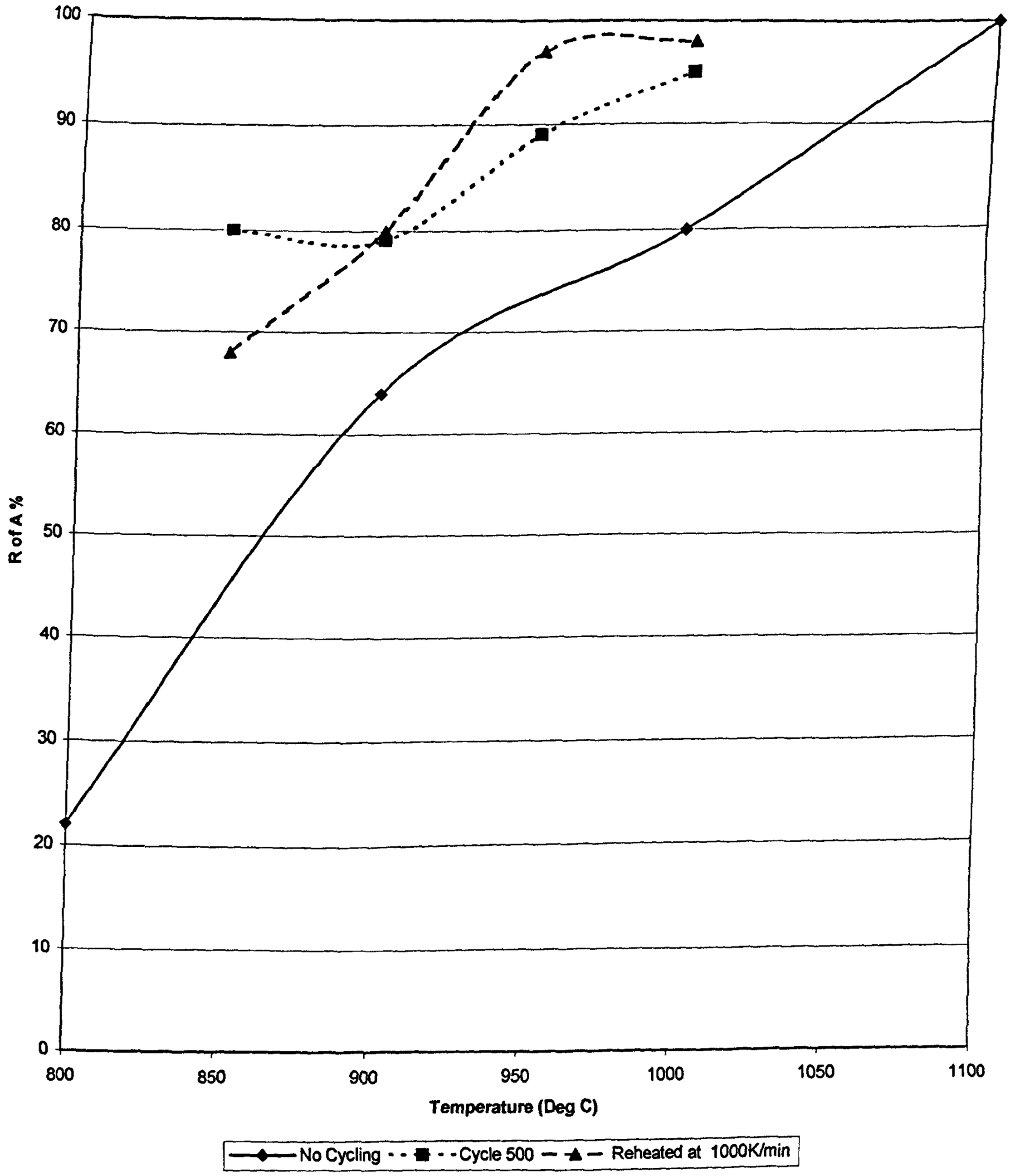

Figure 10 - The effect of undercooling on Nb free 0.008 Ti steel (Ti:N ~ 1.8)

Figure 10 shows that in this case the undercooling results in an improvement in ductility across the entire range in which it was tested. Again the influence of the heating rate is not obvious.

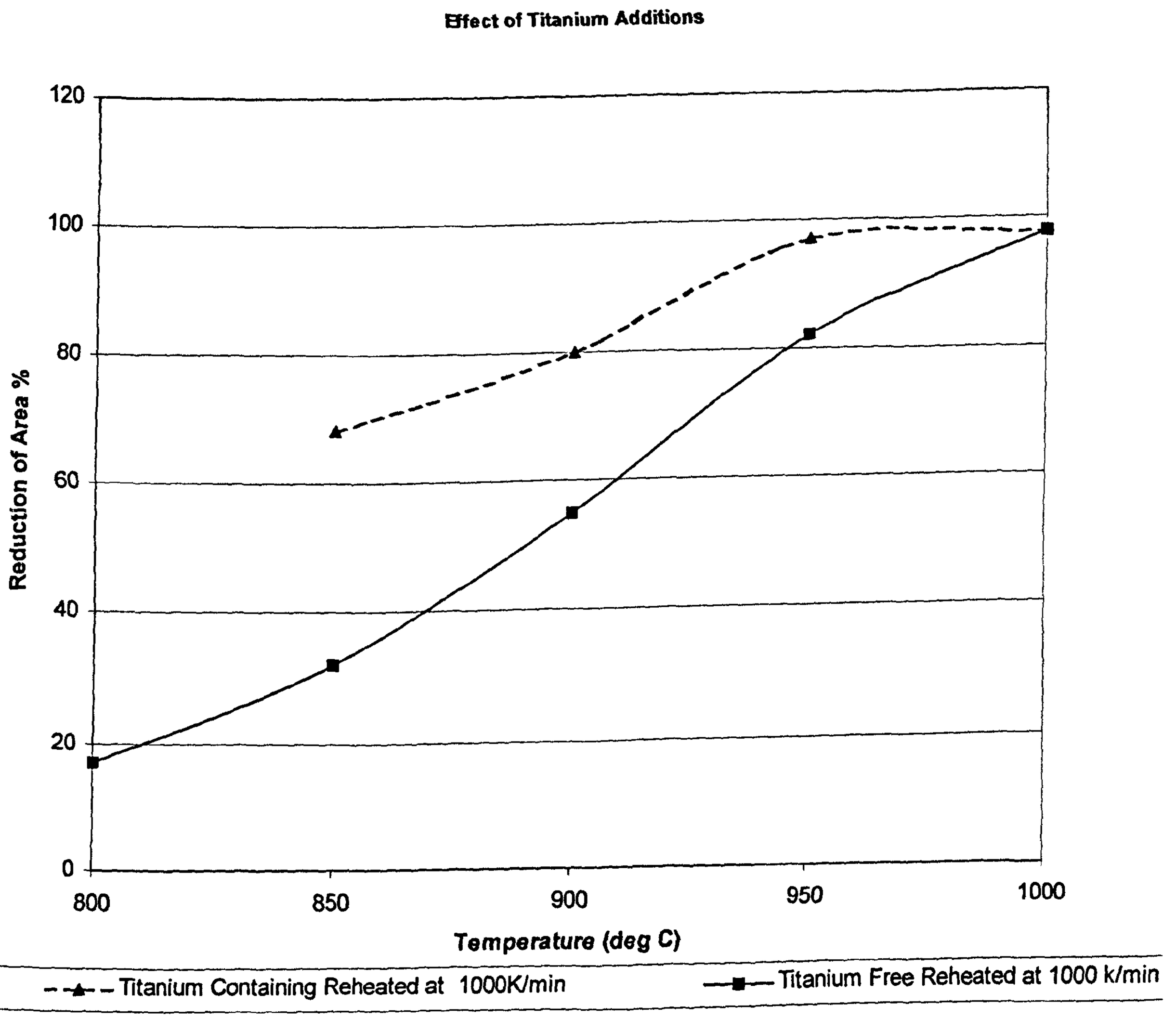

Figure 11 - The effect of undercooling on Ti additions

The above Figure shows the undercooled data from the Ti free steel (P8H27) plotted with the undercooled data from Figure 10 (0.008 Ti). This

curve clearly shows the benefit to ductility that can be achieved by adding Ti when undercooling is incorporated into the cooling cycle.

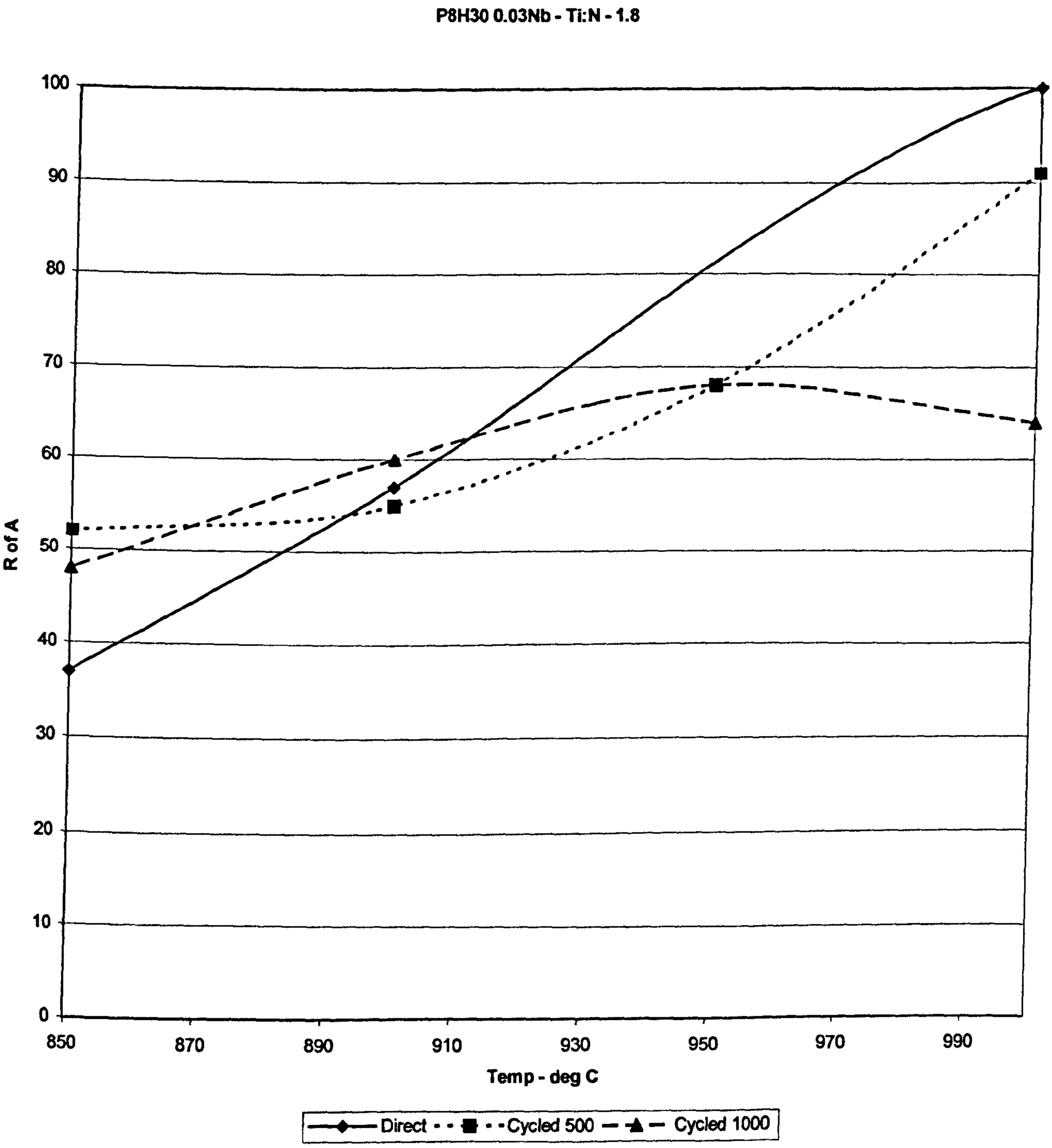

Figure 12 - The effect of undercooling on a Ti Nb steel

When both Ti and Nb are present it appears that the effect of undercooling on the samples is highly temperature dependant with slight

improvements being shown at the lower test temperatures but significant reductions in ductility at the higher temperatures.

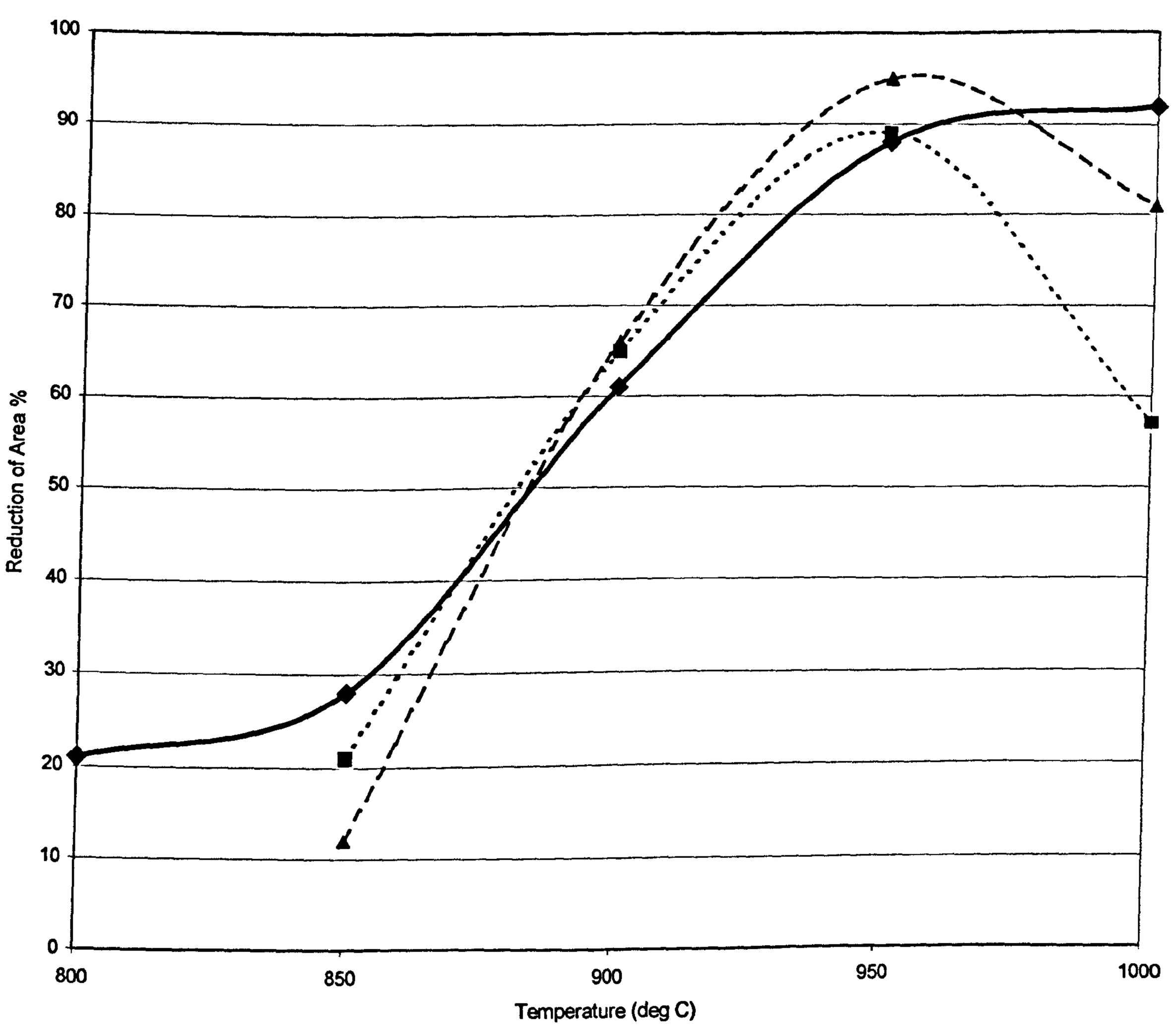

Figure 13 - The effect of undercooling on a Nb free steel with 0.013% Ti

In contrast to the improvements shown with the lower Ti (0.008%), Nb free steel, the above Figure shows that the effects of undercooling are limited on this steel (0.013% Ti) which has a Ti:N ratio of 2.3. A small improvement is shown at the upper temperature ranges.

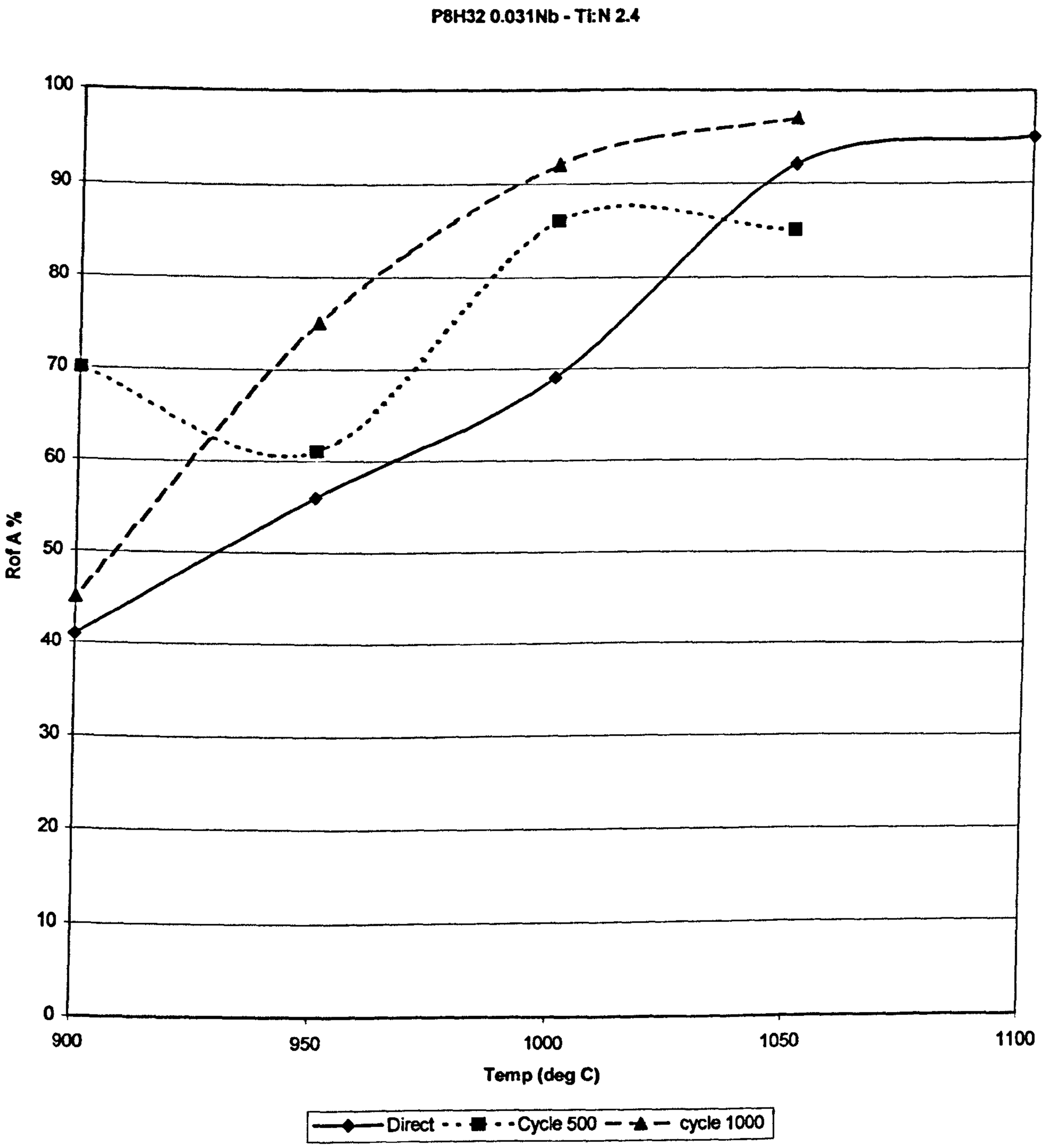

Figure 14 - Effect of undercooling on a Ti Nb steel

Figure 14 again shows the undercooling/reheating cycle producing an improvement in the hot ductility compared to the simply cooled set of samples.

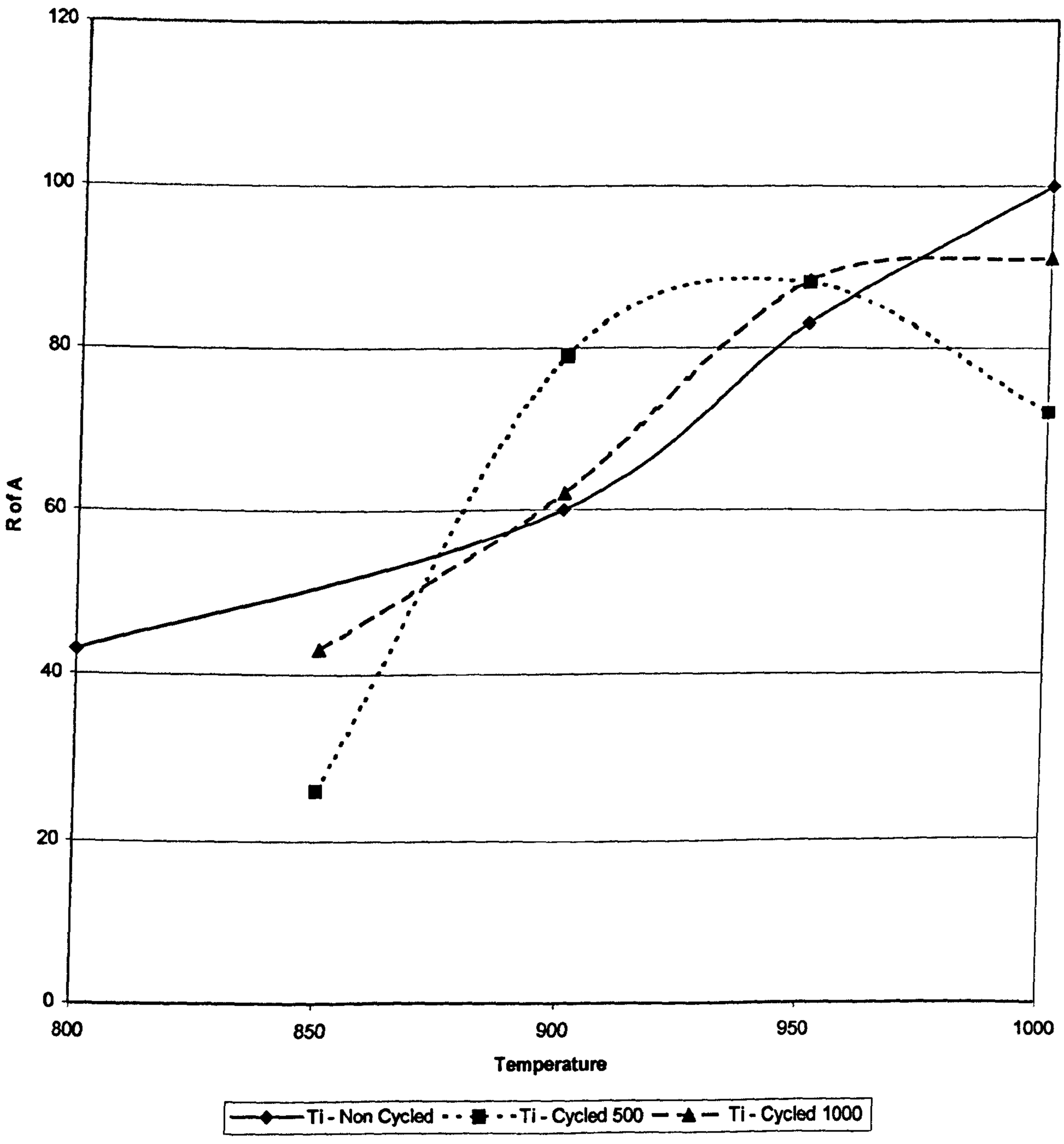

Figure 15 - Effect of undercooling on a steel with 0.022 % Ti

The above Figure shows the effect of undercooling on a steel with a Ti:N ratio of 4.2. This is greater than the stoichiometric ratio of 3.4. Again an

improvement is noted when undercooling is employed but this is less marked than with the lower Ti containing steel shown in Figure 9.

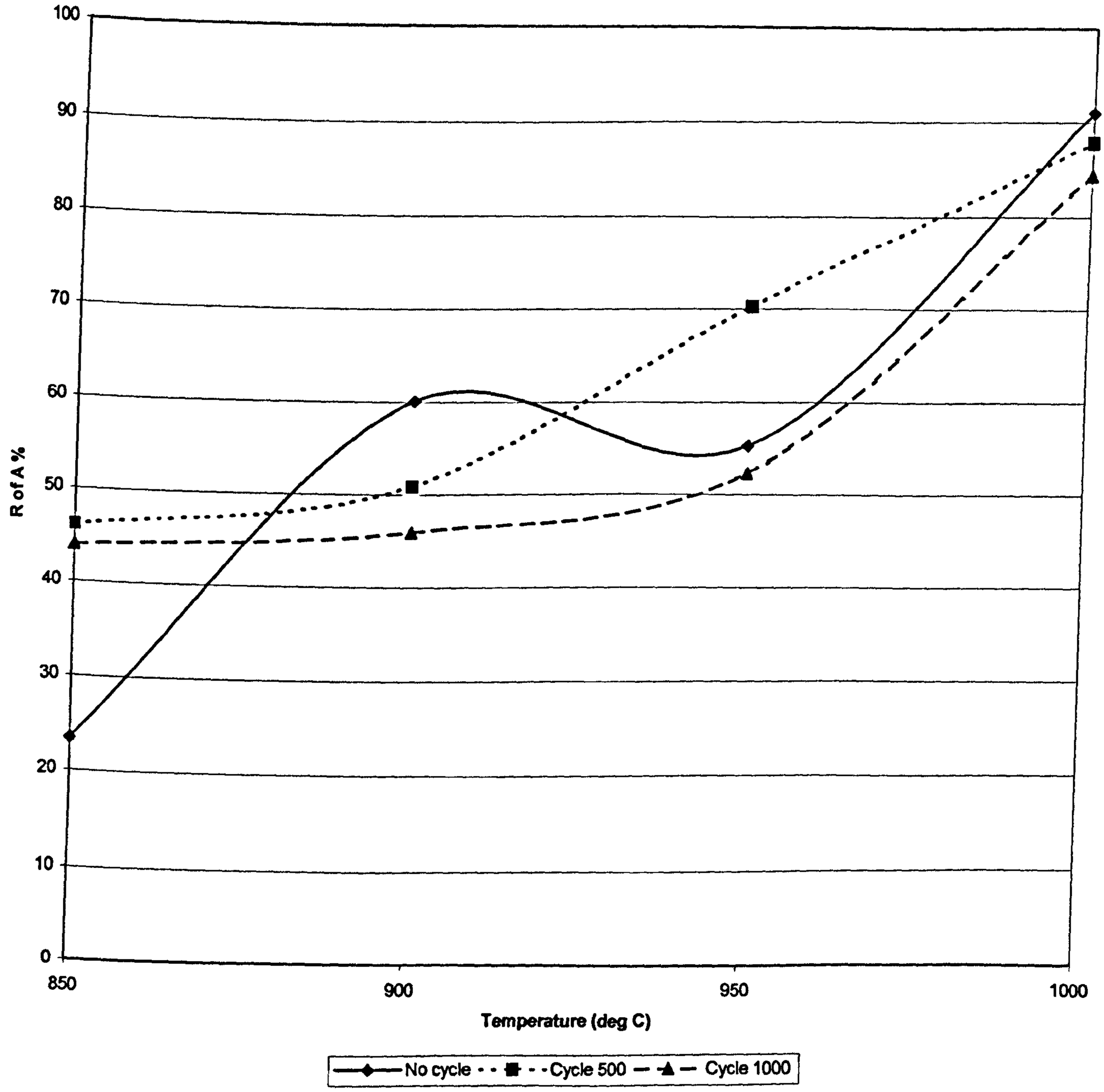

Figure 16 - The effect of undercooling on a Ti Nb steel with Ti:N ratio of 4.2

This Figure shows no clear pattern of results from the undercooling and reheating cycles.

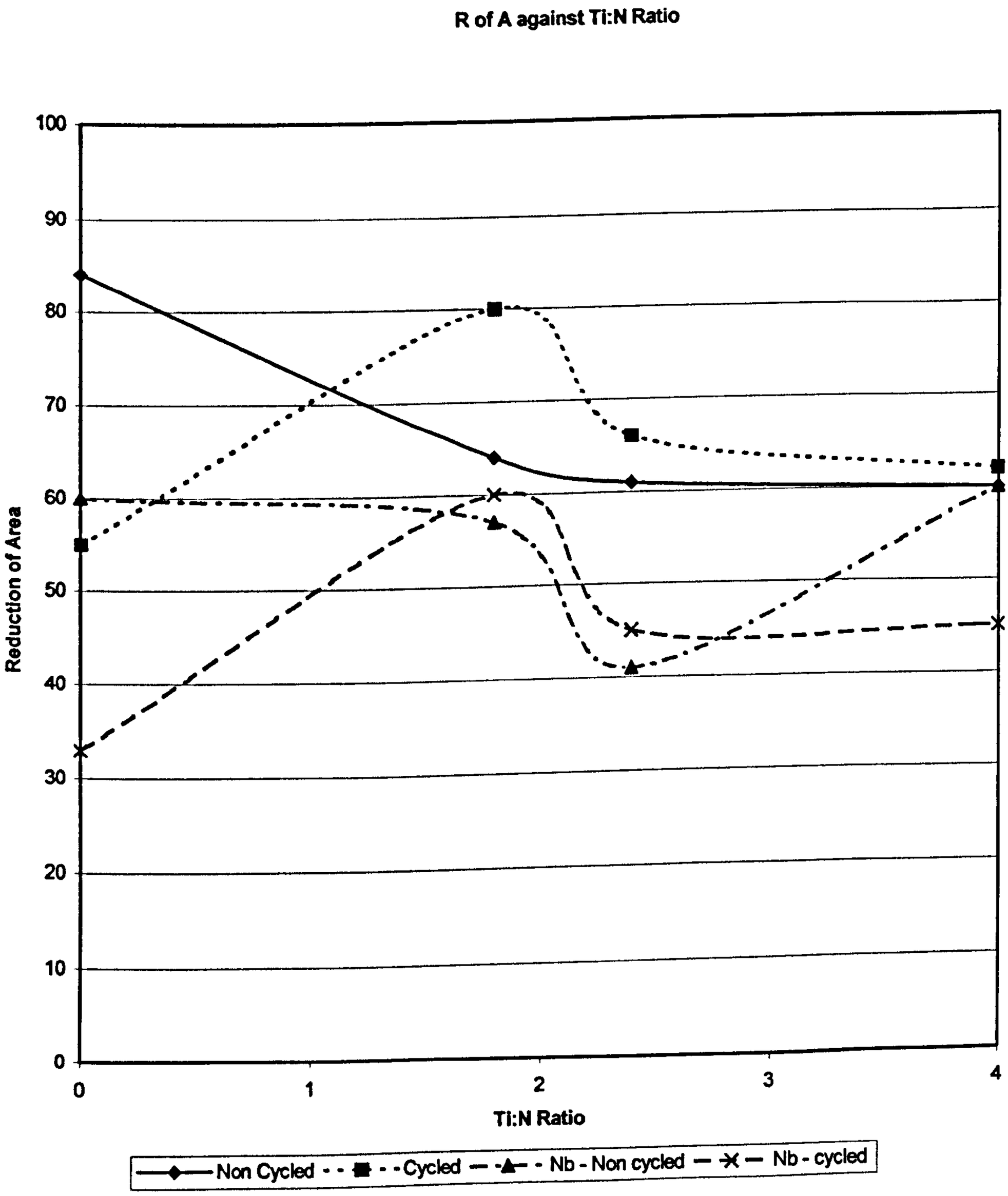

Figure 17 - Reduction of Area against Ti:N ratio at 900 Degrees C (reheat rate of 1000 deg C)

Figure 17 shows that there is a definite trend caused by the undercooling tests across the Ti:N range examined. The steels which were not

undercooled show a steady decline in ductility as the stoichiometric ratio (3.4) is approached. However, all the steels which have been undercooled and then reheated show a maximum ductility at a Ti:N ratio of 1.8. The Figure also shows that for a steel only containing Ti, once Ti:N > 1 the undercooling test produces better ductility than the straight cooling method.

The curves for the Ti, Nb steels show similar characteristics at the maximum ductility point of 1.8.

2 Solubility Products

The soluble Ti and N levels were calculated for the Nb free Ti containing steels using the following equation:

$$\text{Log Ks} = \frac{-8000}{T} + 0.322$$

Where Ks = [Ti][N]

The results are shown in the following set of Figures. All the steels contained 0.005% Total N.

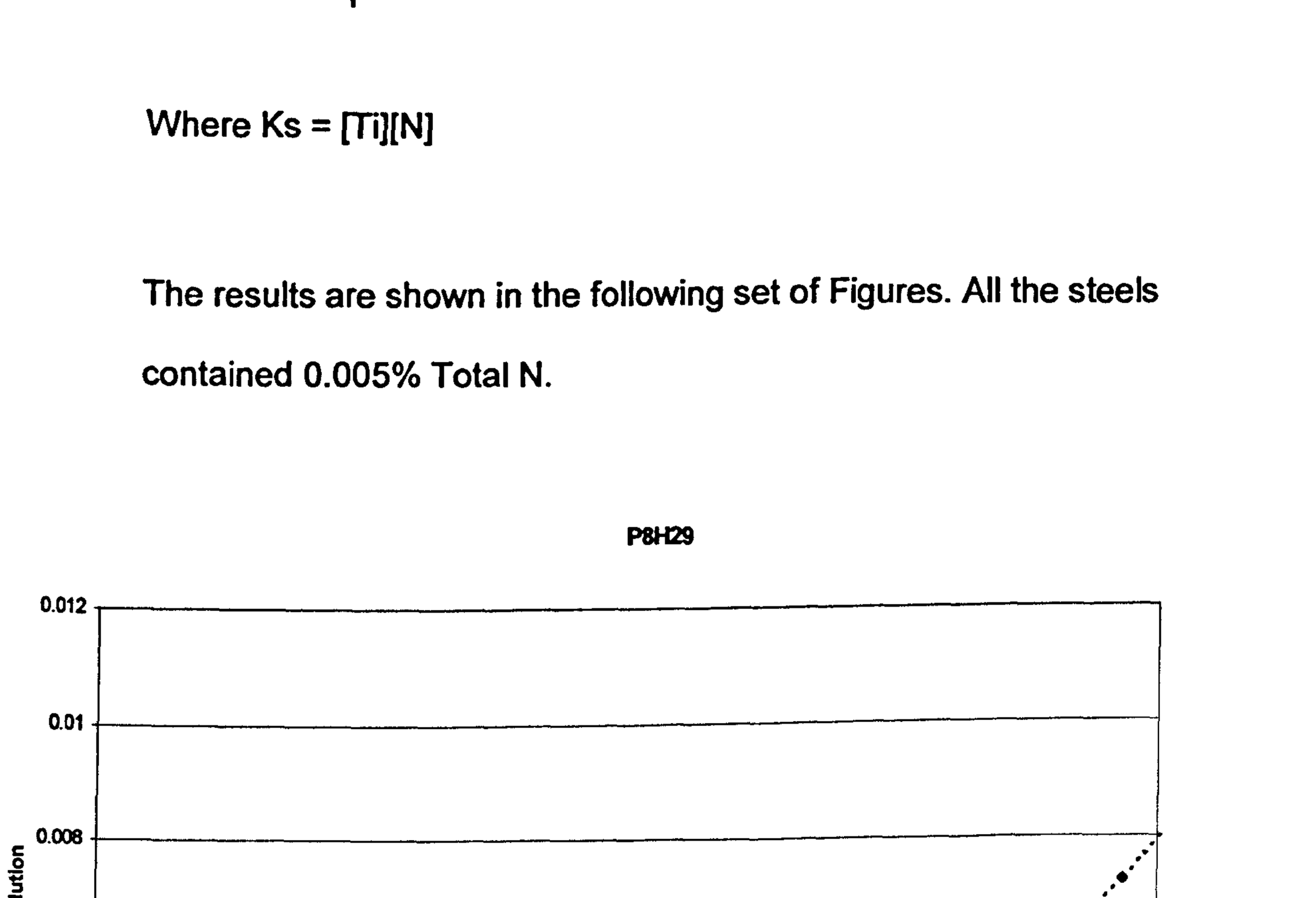

Figure 18 - Soluble Ti an N levels on a Nb free 0.008% Ti steel

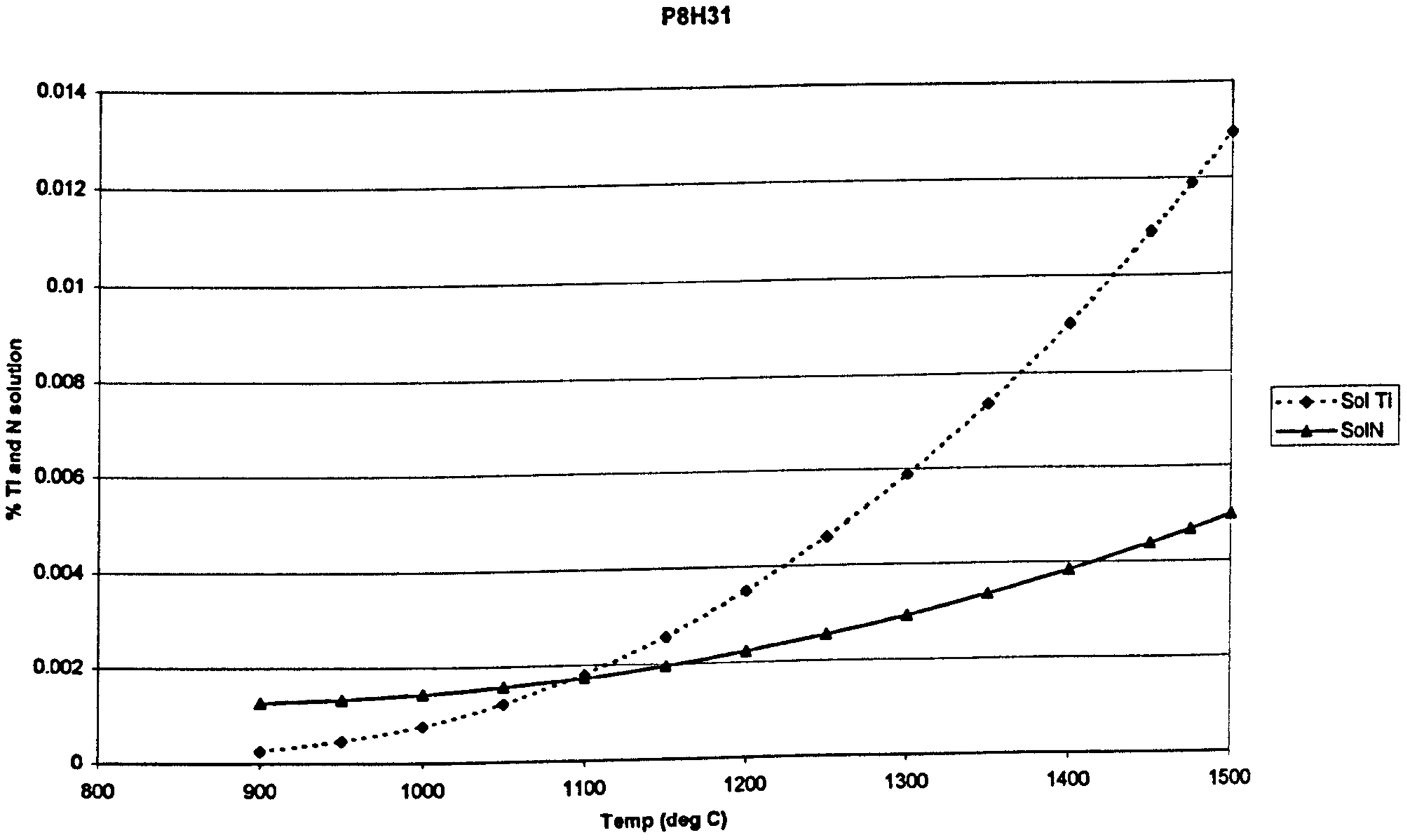

Figure 19 - Soluble Ti and N levels on a Nb free steel containing 0.013% Ti

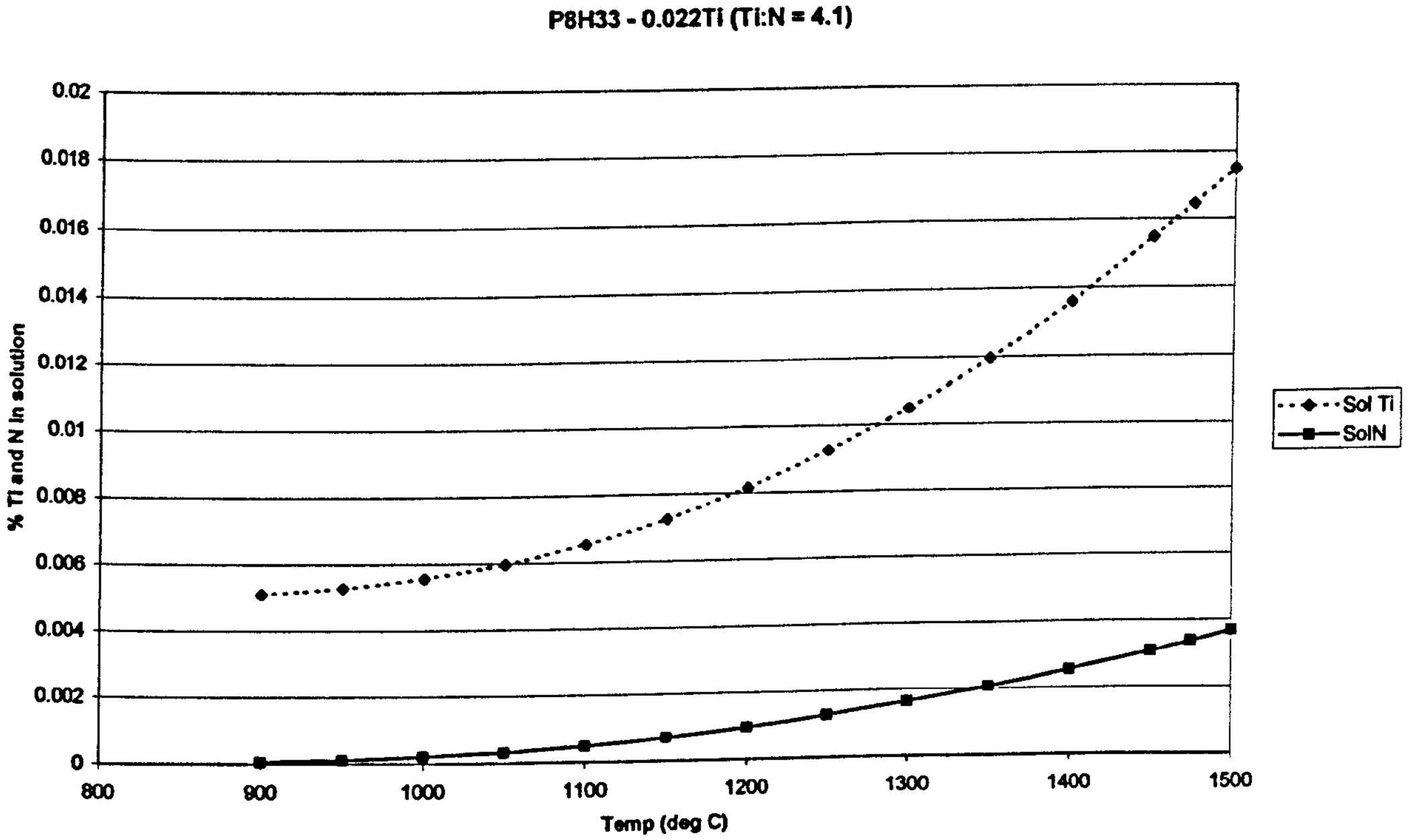

Figure 20 - Soluble Ti and N levels on Nb free steel with 0.022%Ti

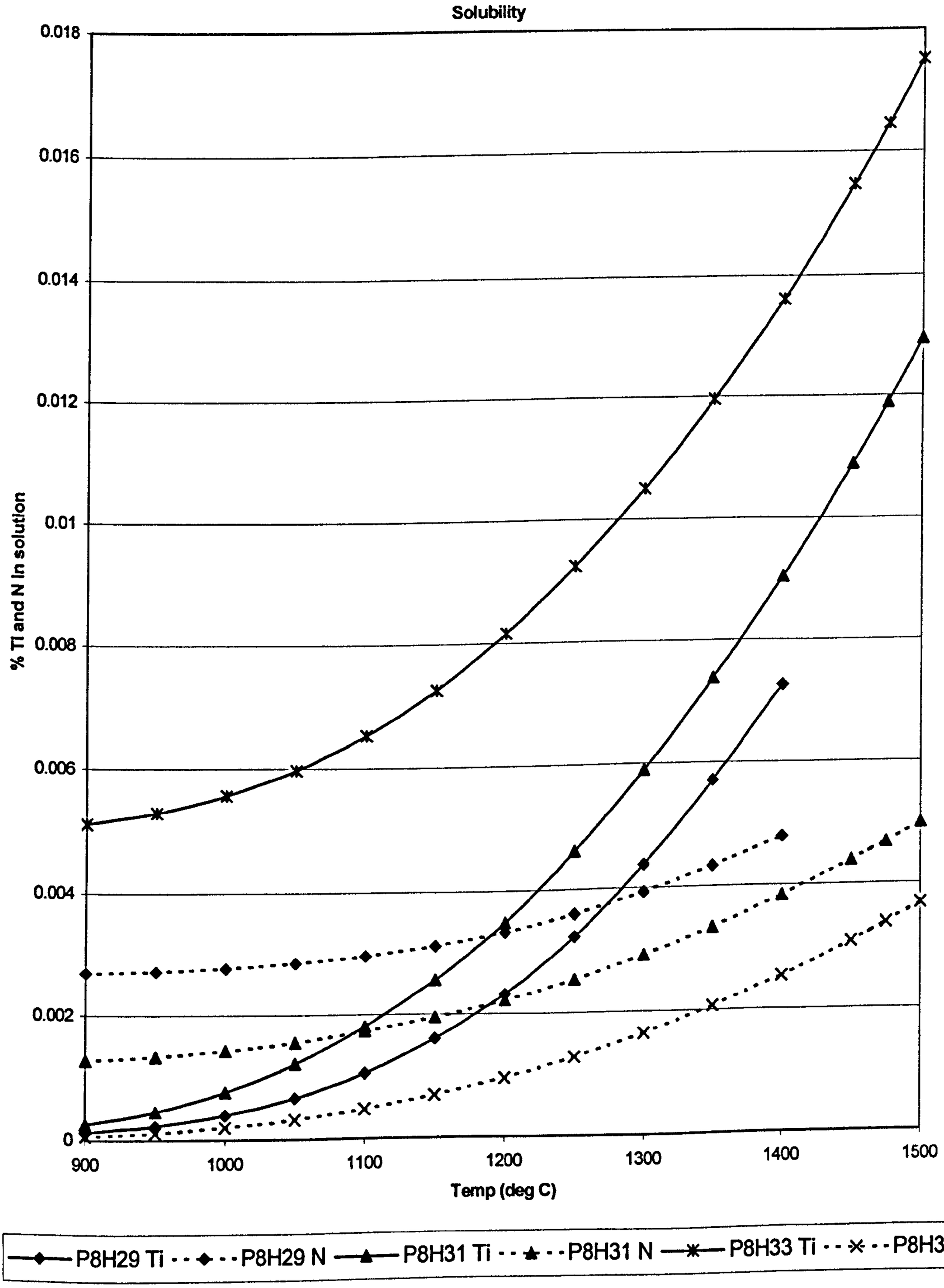

Figure 21 - Summary of solubility results

It can be seen from the curves shown in Figure 20 that for the Nb free steels, the temperature at which all the Ti is dissolved is 1420, 1500°C and the melting point of the steel for steels with 0.008, 0.013 and 0.022% Ti respectively. This indicates that very high temperatures are required to dissolve all the Ti and for Ti levels in excess of 0.015% it is necessary to melt the samples. "Solution Treating" at 1330°C as has been used by many research workers will result in the presence of TiN particles which will refine the grain size and give better hot ductility than in the as-cast coarse grained condition.

APPENDIX C. CORRESPONDANCE WITHALFRED KOETHE

Text cut off in original

Fri, 11 Jul 97 14:54:00 PDT
Alfred Koethe <A.Koethe@ifw-dresden.de>
Barrie Mintz' <B.Mintz@city.ac.uk>

Dear Barrie,

as I mentioned in Liege, we investigated (following a hint of the Thyssen people) the loss of alloying and microalloying elements when simulating the combined thin slab casting and direct hot rolling process in the torsion plastometer. The middle part of our sample (6 mm in diameter) is enclosed in a quartz glass tube, and a length of 15 ... 20 mm is inductively heated to the melting temperature. Through an outer quartz tube (diameter about 25 mm) argon is flowing to prevent oxidation from occuring. However, during the direct contact of liquid steel with the inner quartz tube SiO2 is reduced and Mn, Al, Ti are partially oxidized leading to the following changes in steel composition (in wt.-%):

Holding time in the liquid state /sec	Steel	Mn	Si	Al	Nb	Ti
0	Ti	1.31	0.37	0.022	-	0.014
10		1.33	0.33	0.019	-	0.013
60		1.04	0.45	<=.002	-	0.003
0	TiNb	1.31	0.33	0.02	0.021	0.013
10		1.18	0.39	0.007	0.021	0.009
60		0.95	0.46	0.003	0.020	0.004

Therefore we are now looking at a possibility to avoid direct contact between SiO2 and the molten steel. Since you are using a similar technique, maybe our results are of some interest for you, too.
As to our Ti-N ECSC project application: I'm just about revamping the application (main focus: hot ductility), and I suppose that I can send to you the new version in about one week.

Kind regards
Alfred

Date: Thu, 24 Jul 97 17:29:00 PDT
From: Alfred Koethe <A.Koethe@ifw-dresden.de>
To: 'Barrie Mintz' <B.Mintz@city.ac.uk>

Dear Barrie,

today I received a phone call from a leading manager of Thyssen Steel / Research Dpt. The main point was that they are shure that it would be impossible to get reliable results on hot ductility and microstructure development in hot direct rolling with simulation experiments in which the molten sample is surrounded by quartz, due to the oxydation of the microalloying elements. Our application would not pass the SERDEC commission if this problem will not be shown to be definitely solved (it might well be that this played a decisive role already in the unlucky fate of our last year's application). Unfortunately the analysis results of your samples will be available not earlier than about August 7 at the best. So it would be recommendable if you could consider a change in your experimental techniques, e. g. towards using aluminium oxide tubes, and to modify the text of the application accordingly.
Another point was that they are against steels with a carbon content of 0.1 % when thin slab casting shall be investigated. The cause is that today as well as in the foreseeable future nobody would be willing or able to produce these steels with peritectic composition via thin slab casting and direct rolling due to the immense problems of surface defects. They will send me a proposal for the steel compositions to be investigated from their point of view.

So much for the moment!

Kind regards
Alfred

Date: Wed, 30 Jul 97 17:42:00 PDT
From: Alfred Koethe <A.Koethe@ifw-dresden.de>
To: Mintz B <B.Mintz@city.ac.uk>
Subject: AW: your mail

Dear Barrie,
in fact we could limit the loss of Ti by keeping the melting time to . more than 10 s (even then there could be a Ti loss of about 30 %). I'm not shure whether or not the Thyssen people would accept that as sufficiently low. As to Nb and V: according to texbooks of metallurgy t. deoxydation potential increases in the order Cr - Mn - V - Nb - Si - Ti - Al - Zr - REM - Mg - Ca. Therefore, SiO2 will oxidize Ti and Al but should not remarkably oxidize Nb and V. This is in agreement with our findings on Ti, Al and Nb, but with V we have not yet carried out such experiments.
Probably Thyssen will propose two carbon levels: 0.1 % and 0.04 %, but combined with different nitrogen concentrations. Detailed proposals I have not yet received. On the other side, the spanish factory Esteban Orbegozo intends to study steels with 0.16% for cold forming applications, according to a today's information by Dr. Rodriguez from CEIT (they probably will take this material for their laboratory investigations too). So we will indeed have a broad range of carbon concentrations within the project.

Kind regards,
Alfred.

31 Jul 97 16:29:00 PDT
lfred Koethe <A.Koethe@ifw-dresden.de>
ltz B <B.Mintz@city.ac.uk>
ct: AW: AW: your mail

ar Barrie,

ll Loss of alloying elements: the small table I sent you recently was
bulk
analysis of total element concentration in the molten and re-solidified
part
of the sample (GD-ICP analysis on turning chips prepared from that part).
In addition we found at the surface of of molten and resolidified but undeformed samples by scanning electron microscopy small oxide pearls (size between a few and about 40 um) which were either single phase or multiphase particles containing Si, O, Ti, Al, and Mn.

2) Refusing letter of SERDEC of our last years application:
Th's is obviously a fault since the application has been withdrawn before

the last round of decisions as a result of a recommendation of the german SERDEC member Dr. Steffen. Dr. Steffen who I phoned on this question yesterday could not remember why it nevertheless remained "in the play". However, he assured me that this would not influence
negatively
our new application.I have not got any detailed information about the
cause
of the low ranking of the last years application.
What I heared inofficially was the following:
- high ranking by the Serdec member countries involved in the
application,
low ranking by the representatives of the countries not included (e.g. France), i. e. some form of politics.
- only a university and 2 research institutes, no steel producers
involved in
a project of that technical importance
- maybe inferior estimate of the appropriateness of the proposed experimental techniques of CUL, CEIT and IFW of melting the sam, es envelopped in quartz (somebody called it "a capital offence").
The missing forms I'm sending by letter.

With respect to the C content:
Thyssen propose that the steels of low N content of 0.005 % should have a carbon content of 0.04 % (industrial LD melts), whereas the high nitrogen steels could remain as proposed, with few crossing experiments.

Kind regards

Alfred

TEXT BOUND INTO THE SPINE

(1)

Date: Tue, 05 Aug 97 15:56:00 PDT
From: Alfred Koethe <A.Koethe@ifw-dresden.de>
To: 'Barrie Mintz' <B.Mintz@city.ac.uk>

Dear Barrie,
I just received the results of the analysis *of your samples.*
Unfortunately, two Si values cannot be used due a technical fault (*from a* broken part in the apparatus some foreign material had fallen into the crucible, and we had no material left to repeat this analysis).
However, the other results look quite well, i. e. with your experimental set-up you have indeed only small losses of Ti and Al, if any. The losses in Mn are probably not due to oxydation (regarding the low oxydation potential of Mn) but due to evaporation.
The following analytical methods were applied:
Ti, Nb, Mn: GD-ICP,
Al: AAS,
Si: Gravimetry.
The preparation of the turning chips from the molten part yielded not very much material for analysis, since the molten area was relatively small and disturbed by the fracture surfaces of both halfes. When repeating such analyses it would be better just do re-solidify the sample without fracturing it to alleviate the preparation of turning chips from the molten zone.
Results (in wt-%): 100

Sample	State	Mn	Si	Al	Ti	Nb	Ti
1	not molten	1.35	0.26	0.025	0.015	0.023	.015 — unmelted
1	molten	1.09	0.27	0.018	0.014	0.027	.014 — melted
2	not molten	1.26	0.24	0.022	0.014	0.023	.014 — unmelted
2	molten	1.20	fault	0.020	0.016	0.027	.016 — melted
3	not molten	1.28	0.26	0.020	0.015	0.025	.015 — unmelted
3	molten	1.09	fault	0.016	0.011	0.024	.011 — melted

The corrections to the text of the new proposal you mentioned in your recent e-mail I have not yet received.

Kind regards

Alfred

Osvaldo [illegible] [illegible] was purple

Mn	Si	Al	Ti	Nb
1.35	.26	.025	.015	.023
1.26	.24	.022	.014	.023
1.28	.26	.020	.015	.025

1.37	.29	.029	.020	.041 ✓	Gold
1.37	.30	.024	.019	.041	Purple
1.44	.35	.0008	.012	.042 ✓	Blue
1.44	.35	.009	.045	.043	Red

→ Gold

APPENDIX D. ELECTRON MICROSCOPY PROCEDURES

Appendix D – Detailed Experimental Procedure

Use of the Scanning Electron Microscope (SEM)

(1) Make sure that the SEM is switched on, and that there is a steady flow of water for cooling purposes.

(2) Using gloves to avoid contamination gently clean the sample with ethanol to remove any surface impurities.

(3) Using one of the provided allen keys, securely fit the sample to an empty, three slot holder.

(4) Place the holder (with the sample) into the primary holder (the one that attaches to the chamber floor), making sure that all 6 screws are secure.

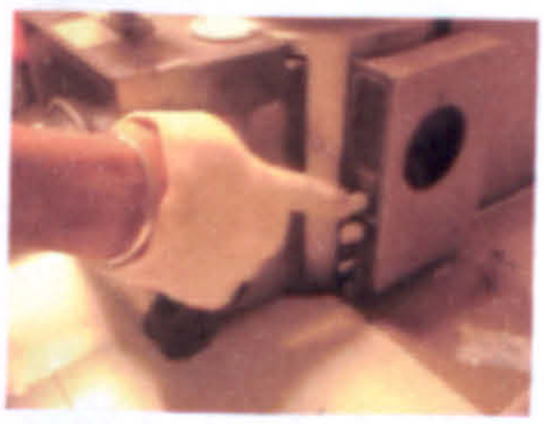

(5) Vent the chamber.

(6) Once the chamber has vented, indicated by a zero reading on the vacuum gauge, carefully slide it open, and remove any samples.

(7) Screw the primary holder to the chamber floor.

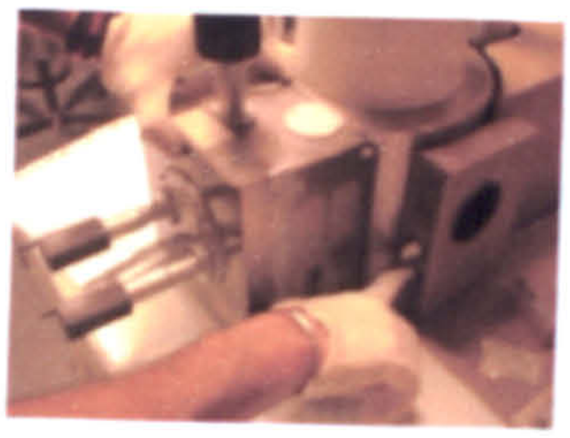

(8) Pump down the chamber.

(9) Wait for a magnification to appear. This usually happens when the vacuum gauge reads approximately 4½.

(10) Turn on the accelerating voltage and turn up the filament dial, making sure not to exceed the 3 o'clock position, in order to avoid damaging the SEM.

(11) Adjust the contrast and brightness until the image on the screen is clearly visible.

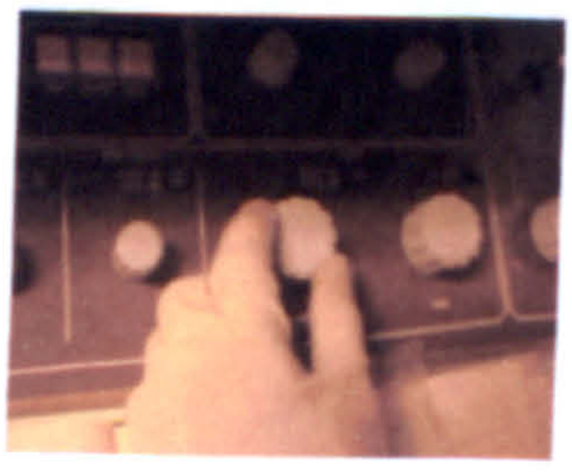

(12) Focus the image, using first the coarse adjustment dial (indicated in the picture), followed by the fine adjustment dial (located to the immediate right of the coarse adjustment dial).

(13) Once the image is in focus, use the indicated dials to move about the image, until an area of interest in discovered. Once ready, use the magnification dial at the far right of the platform to zoom in/out on the image.

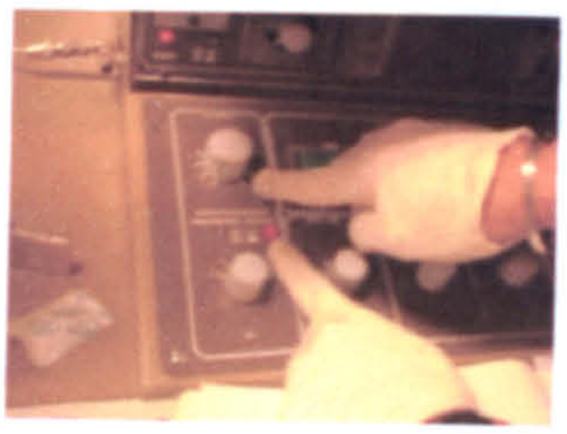

(14) When finished, turn down the filament, and turn off the accelerating voltage.

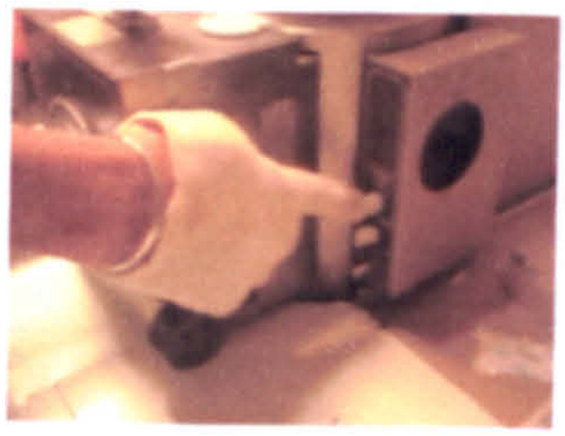

(15) Vent the chamber, as before.

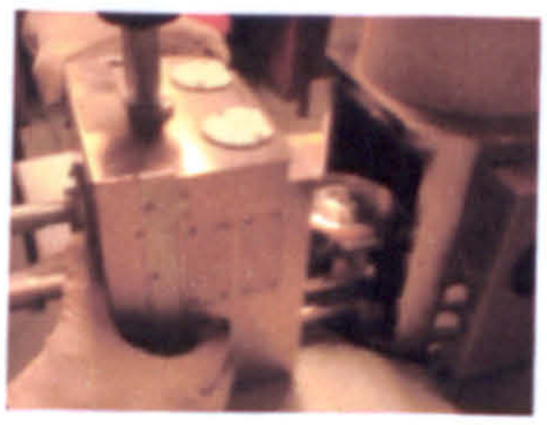

(16) Remove the sample from the chamber, and start again from step 1, with new samples. When finished totally, go to step 17.

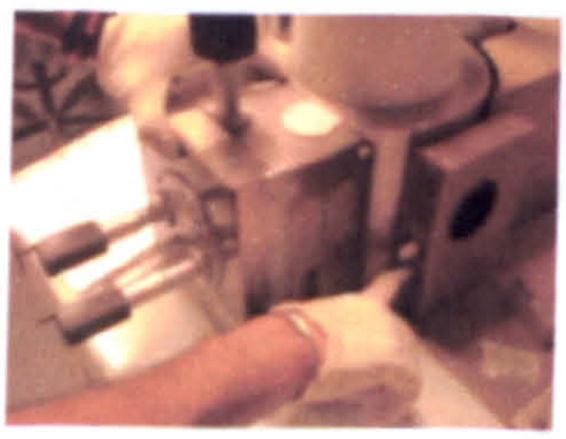

(17) Once the samples have all been removed from the chamber, pump down the chamber in order not to leave air pumping through the column.

Note: Do not adjust the spot size, or any other settings. If in doubt, seek assistance.

SEM photography

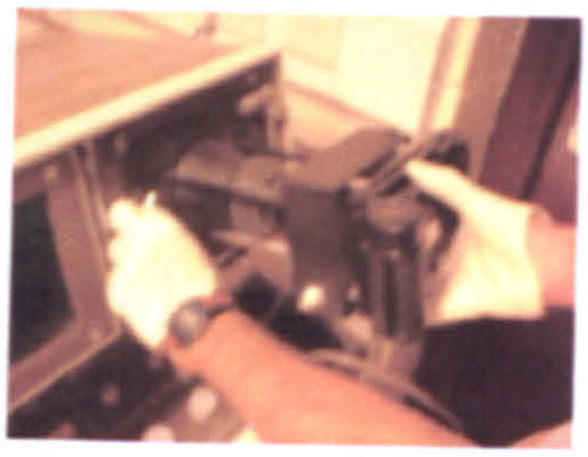

(1) Once the sample has been focused, and is ready to be photographed, attach the camera to the right hand screen of the SEM.

(2) Attach the camera data link cable to the SEM.

(3) Open the rear case of the camera, and move the film roller to the left hand side.

(4) Attach the film (Delta 100) to the right hand side, and wind it onto the roller. Close the camera back, and manually wind the film on until a 'click' is heard, and the film cannot be wound further.

(5) Press 'PIC TV' button followed by the 'EXP' button.

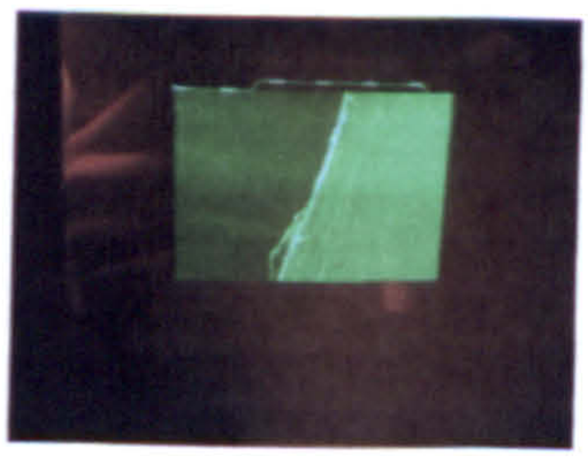

(6) The screen shown in the illustration will appear. Use the contrast and brightness dials, and adjust the image until 3½ bars appear above the image as shown.

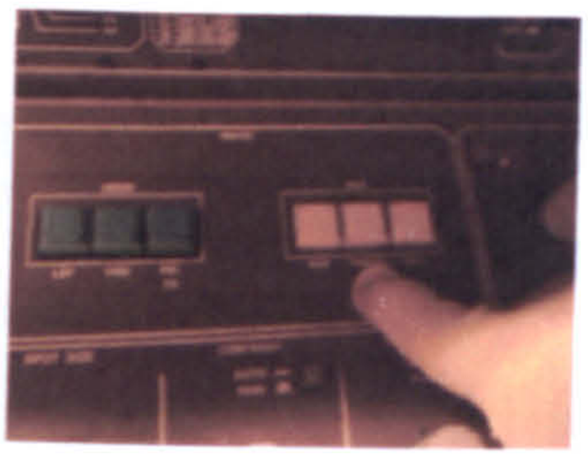

(7) Press the 'PHOTO' button.

(8) Press the shutter release button on the camera.

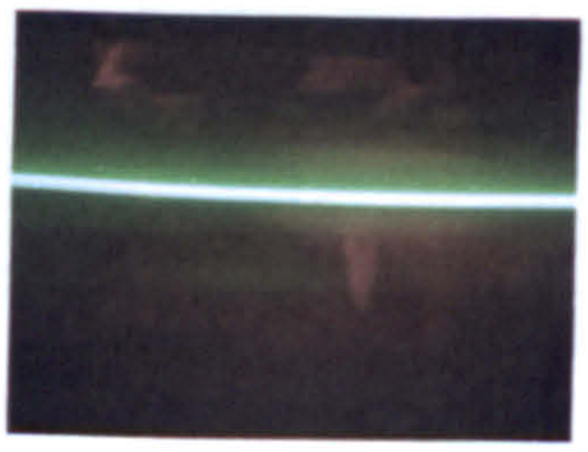

(9) A line will raster down the screen. Once the line reaches the bottom, a 'click' will be heard. Push the catch next to the shutter release button to the right, and wind on the film, ready for the next photo. Repeat the process until the film is completely exposed. When finished, make sure the film is fully wound on, and then remove from the camera, making sure not to expose the film to any light.

Developing the camera film

(1) <u>All lights must be switched off</u> (the illustrations have been shown with the light for explanation purposes only). Separate the film from the paper.

(2) Feed the front edge of the film onto the spool, past the ball bearings on the inside edge of the spool. Give the film a gentle tug to ensure that it has located properly on the spool. Use the ratchet mechanism to wind the rest of the film onto the spool, making sure the film remains attached at all times.

(3) Place the spool into the developing tank, making sure that the protruding end is on top. Attach and secure the funnel section of the tank. The lights can now be switched back on.

(4) Thoroughly mix 540mls of water at a temperature of 68.8 – 70°F with 60mls of developer.

(5) Pour the water/developer mixture into the tank, fix the lid securely in place, and let it soak into the film for 6½mins. The tank should be agitated periodically to keep the developer active.

(6) After giving the correct timing for the developer, pour the solution down the sink. Add 600mls of stopbath, and agitate for ½ min.

(7) Pour the stopbath back into its bottle, and add 600mls of fixer. Leave the fixer for 5mins, with periodic stirring, and then pour back into the bottle.

(8) Use the hose to flush out the tank with water for ~5mins.

(9) Add wetting solution to the tank, and carefully agitate for ~1min.

(10) Carefully remove the film from the spool, handling it at the edges only, and squeegee it dry (making sure the squeegee is wet). Place the film in the drying cabinet, and leave to dry at 20°C for 30mins. The negative can now be printed from.

APPENDIX E. PAPERS PUBLISHED DURING THE WORK PROGRAM

THE INFLUENCE OF Ti ON THE HOT DUCTILITY OF STEELS AND TO THE PROBLEM OF TRANSVERSE CRACKING

By

B.Mintz And C.Spradbery

Dept. Mechanical Engineering And Aeronautics

City University, London

ABSTRACT

A Ti free and Ti containing steel have been examined in an attempt to reconcile the poor hot ductility behaviour normally found in as-cast Ti containing steels with the established commercial improvement in surface quality which occurs on adding small Ti additions to continuously cast steel.

Tensile samples were cast in situ and cooled to test temperatures in the range 1000-800 °C, strained at $3 \times 10^{-3}s^{-1}$ to failure and the reduction of area (R of A) obtained. The cooling rate from solidification to the test temperature was 100 $Kmin^{-1}$. As in previous work, the Ti addition caused the ductility to deteriorate particularly in the higher temperature range. Fine Ti containing particles were found to be the cause of this poor ductility.

In addition to establishing the normal hot ductility behaviour of these steels, tests were also carried out in which a temperature cycle was introduced, the temperature being taken 100°C below the test temperature before straining to failure. This was carried out to more accurately simulate the cooling conditions that the strand undergoes before straightening. Whereas the undercooling caused the ductility to deteriorate for the Ti free steel, ductility of the Ti containing steel was relatively unaffected. Of more importance, whereas without temperature cycling the Ti containing steel gave the worse ductility, introducing the temperature cycle could reverse this trend. It is suggested that the undercooling encourages precipitation and produces an additional finer precipitation of AlN for the Ti free steel which remains when the temperature is raised to the tensile test temperature. For the Ti containing steel, precipitation of TiN once formed is very stable and not affected by undercooling or cycling.

It is concluded that in order to assess the potency of Ti additions in reducing the susceptibility to transverse cracking from laboratory hot tensile tests not only is it necessary to cast the tensile samples but the cooling conditions must be chosen to simulate more closely those that occur during the actual continuous casting operation.

INTRODUCTION

The influence of small Ti additions on the hot ductility of steels has been studied recently in two papers [1,2]. It was shown that in order to obtain the optimum ductility, the particle volume fraction should be as low as possible and particles should be coarse. For low N steels (0.005%N), a high Ti:N ratio was recommended 4-5:1. The excess Ti then favoured growth

of the particles and a higher product of Ti and N favoured precipitation at higher temperatures encouraging coarser particles. If higher N steels (0.01%N) were produced, then a low Ti addition was recommended to limit the volume fraction of Ti containing particles and a low Al level to prevent precipitation of AlN.

A major problem with this laboratory work was the failure to show that Ti additions were beneficial to ductility[1,2] .Ti additions invariably gave worse ductility than similar Ti free steels. In contrast to the laboratory work, commercially, small Ti additions have been found to reduce the incidence of transverse cracking[3-8]. A possible cause of this difference in behaviour between laboratory testing and commercial experience may be related to the difference in the cooling patterns. In the laboratory test, an average cooling rate of 25-100°C/min is chosen to represent the cooling close to the surface during the continuous casting process. However, commercial conditions are far more complex. Typically, the strand surface cools very rapidly at first, often reaches a minimum and the temperature then rises again, followed by a large number of cycles in which the temperature falls as the water sprays impinge on the strand' followed by a rise in temperature as the strand enters the guide rolls, Fig.l.

Where some attempt has been made to simulate the commercial conditions more accurately, the introduction of temperature cycling in Ti free steels has always resulted in a deterioration in ductility[3,9-12]. This has been found to be the case for C-Mn-Al and C-Mn-Nb-Al steels. It is believed that the undercooling that takes place during the cycling encourages precipitation which remains on raising the temperature resulting in more overall precipitation. In contrast to this behaviour, the introduction of temperature cycling to Ti containing steels during cooling has been found to have little effect on hot ductility[12]. There is evidence to show that[1,2] the Ti always combines with all the available N and it is suggested that the TiN particles once formed are very stable and resist coarsening when the temperature is raised again during cycling.

Nevertheless, in this earlier work[12], even after temperature cycling, the ductility of the Ti containing steel was always worse than the Ti free. It was suggested that this could be due to the Ti:N ratio for this steel being at the stoichiometric composition for TiN (3.4:1) and this would both give rise to the maximum volume fraction of TiN particles and also the finest precipitation. A further possibility that might also have contributed to the poor ductility was the relatively low soluble Al level for the Ti containing steel. Strid and Easterling have reported that Al increases the coarsening rate of TiN[13].

The present work is aimed at exploring whether a Ti addition outside the stoichiometric level for TiN can be used to improve ductility when an undercooling temperature step is included in the cooling pattern.

To this end a Ti containing and a Ti free steel of otherwise similar composition have been chosen for examination but in this case the Ti:N ratio is 2.6:1, reducing the volume fraction of TiN particles and the steels had higher soluble Al and lower N levels.

EXPERIMENTAL

The composition of the steels examined wt.per.cent were as follows:

C	Si	Mn	P	S	Sol.Al	N	Ti	Ti:N Ratio
0.091	0.30	1.38	0.010	0.002	0.031	0.005	<0.005	-
0.110	0.30	1.41	0.009	0.002	0.028	0.005	0.013	2.6
0.087*	0.31	1.40	0.011	0.004	0.013	0.0068	<0.005	-
0.097*	0.33	1.41	0.012	0.004	0.020	0.0069	0.024	3.48

The steels were laboratory 50kg vacuum melts rolled to 15mm thick plate.
Also included in this table are the Ti and Ti free steels from the previous investigation[12], marked with asterisks.

An actual continuously cast temperature profile close to the surface is shown in Fig.1 and can be seen, to be very complex. The amplitude of the temperature cycles is of the order of ±70°C. Although the laboratory cooling cycles were computer controlled allowing a temperature accuracy of ±5°C, it was not possible to follow precisely the commercial cooling cycle at the surface as given in Fig.l. The cooling cycle was therefore very much simplified such that an undercooling step of 100°C was added to the normally used laboratory cooling pattern, Fig.2. One of the features of the commercial operation is that the heating and cooling parts of the temperature cycle take place very rapidly somewhere in the region of 300°C a minute depending on the particular plant in operation. In order to simulate this more closely two heating rates to the test temperature were used after undercooling, 500 and 1000°C/min.

Tensile samples of length 70mm and diameter 7.94 mm were machined from the plates with their axis parallel to the rolling direction. The samples were placed inside silica tubes having an 0.2mm diametrical clearance. A hole of 2mm diameter was drilled from one end of each sample to the mid-length so that a thermocouple could be inserted. The samples were heated by an induction unit, so that approximately 22mm of the length at the mid-length position could be melted. The molten region was contained in the silica sheath, which in turn was enclosed by a silica tube through which argon could be circulated to prevent oxidation from occurring. Samples were melted at 1540 °C for 5 min, resolidified and cooled to the required test temperature in the range 700-1100°C.

Three cooling patterns were chosen for examination. Cooling pattern 1 involved cooling at a constant rate of 100°C/min to the test temperature, holding for 5 min and then straining to failure using a strain rate of 3×10^{-3}/sec, Fig. 2a. Cooling pattern 2 used the same cooling rate but the temperature was taken to 100°C below the test temperature and then heated back up to this temperature at a rate of 500°C/min, held for 5 min and then tested as in cooling pattern 1, Fig.2b. Cooling pattern 3 was the same as 2 but the heating rate to the test temperature after the undercooling was faster at 1000°C/min. After fracture, the samples were gas quenched to room temperature in approximately 2 min.

RESULTS

The hot ductility curves are shown in Figs. 3 and 4 for the Ti free and Ti containing steels, respectively. It can be seen for the Ti free steel, the introduction of this undercooling causes

the trough to widen and this is most marked when the higher heating rate to the test temperature is used. In contrast, the introduction of the temperature oscillation in the Ti containing steel can be seen to have little influence on hot ductility, Fig 4. When all the results from Figs 3 and 4 are plotted together Fig. 5, it can be seen that without undercooling the Ti containing steel gives the worse ductility, in accordance with previous observations.[1,2] A fine precipitation of TiN can be seen to be responsible for the poor ductility Fig 6. Of greatest interest however, is the finding that at the higher heating rate, the Ti containing steel actually gives better ductility than the Ti free steel, Fig.5.

DISCUSSION

The results from the present and previous investigation are given in Fig.7a and b, respectively for Ti free and Ti containing steels. It can be seen that the hot ductility curve for the Ti free steel given no undercooling is very similar to that obtained in the earlier examination[12], Fig.7a. This is not too surprising as the AlN precipitation is controlled by the product of the soluble Al and N and they are reasonably similar[10,14]. The effects of cycling and undercooling are also seen to be similar. Increasing amplitude of the cycles in the first investigation causes the ductility to deteriorate in a similar manner to introducing undercooling and raising the heating rate.

Previous work [9] on Ti free, Nb containing steels had noted that introducing a temperature oscillation of ±100°C led to a finer more concentrated precipitation and this was more effective in delaying dynamic recrystallisation to higher temperatures so that the trough extended to 1050°C. This could be related to the nose of the PTT diagram (i.e. Precipitation-Temperature-Time curves, the nose corresponding to the maximum rate of precipitation) for Nb(CN) precipitation being at 950°C[15] so that the undercooling would allow time at this temperature resulting in more and finer precipitation than obtained on direct cooling to 950°C.

Similar reasoning has been applied to account for the worse ductility shown by C-Mn-Al steels[10] when cycled except in this case the maximum rate of precipitation occurs at a lower temperature (815°C).[16]

Thus, in the case of C-Mn-Al steels, undercooling into this temperature range, i.e. 850°C will ensure that when the temperature is raised 100°C to the test temperature~950°C precipitation will be greater than if the cooling had been directly to the test temperature. Not only will there be more precipitation present but the precipitation is also likely to be finer and both of these will give rise to worse ductility[14].

In the present instance it is clear that undercooling by 100°C will create a similar response in allowing more and finer AlN precipitation to occur, but it is less clear as to why the heating rate after undercooling should influence ductility. One possibility is that increasing the heating rate leaves less opportunity for growth of the precipitates to take place, but the shorter times involved would be unlikely to make much difference as a 5min hold is given prior to testing. It is possible that the higher thermal stresses involved in rapid heating may encourage more precipitation. Detailed examination of particle distribution is required to clarify these possibilities. In the case of the Ti containing steels, it can be seen that the hot ductility without undercooling is better than obtained previously but is still worse than for the Ti free. Fig. 5. The better ductility is due to the lower Ti:N ratio.

The previous work[12] was carried out on a Ti-N steel having the stoichiometric Ti:N ratio of 3.4:1. Such a composition would give rise to the maximum amount of TiN as well as the finest particle size.

The PTT curves for TiN have not been established but the nose of these curves are likely to be at significantly higher temperatures and precipitation is likely to be much more rapid making it less susceptible to changes in temperature. On cycling both investigations show little change in ductility suggesting that once TiN forms it is very stable. Both examinations also suggest that the form of the TiN is not much influenced by the temperature in this lower temperature range 900-800°C; i.e. the undercooling in this case does not lead to increased and finer precipitation.

However, although the Ti probably combines with all the available N, the size of the TiN particles has been shown from previous examinations[1,2] to refine as the temperature decreases. This should result in some deterioration in ductility on undercooling and indeed some steel compositions containing small Ti additions have given reduced ductility when cycled[17]. Reduced ductility might also be expected when there is insufficient Ti available to combine with all the N and a significant amount of N is available for further AlN precipitation. These compositions are presently being examined to define more precisely the acceptable Ti:N ratios for better ductility.

COMMERCIAL IMPLICATIONS

The present work has shown that it is necessary to introduce some form of undercooling to the laboratory test conditions when examining Ti containing steels and comparing them with Ti free steels. Only then is it possible to show up the true potential benefit of Ti additions to hot ductility in relation to the problem of transverse cracking during continuous casting.

It would be expected from this work that provided the levels of Ti and N are outside that for the stoichiometric composition of TiN (i.e.> or < 3.4:1), it is likely Ti will be a beneficial element to add to reduce cracking. However, the situation with Ti containing steels is complex and further work is necessary to confirm these findings.

ACKNOWLEDGEMENTS

The authors would like to thank Corus, Swinden Laboratories for the supply of steel. One of the authors, (C.S) would like to thank Corus for supporting a CASE award and EPSRC for financial support. (Grant No.98590041)

REFERENCES

1. R.Abushosha, O.Comineli & B.Mintz: Mater.Sci. and Technol;1999,15,pp278-286.
2. O.Comineli, R.Abushosha & B.Mintz: Mater.Sci. and Technol;1999,15,ppl058-1068.
3. T.H.Coleman and J.R.Wilcox:Mater.Sci and Technol.;1985,1,80.
4. E.T.Turkdogan:AIME Steelmaking Conf. Proc.;1987,70,399.
5. M.Hater,R.Klages,B.Redenz and K.Taffner:Open Hearth Proc. AIME, 1973,56,pp202-217.
6. B.Patrick and V.Ludlow:Rev.Metall., Cah.Inf.Tech.,1994,pp1081- 1089.

7. G.Woollen;personal communication, British Steel,Scunthorpe Works,1994.
8. J.G.Willams HSLA steels technology and applications, 261; 1984, Philadelphia, PA,ASM.
9. B.Mintz,J.M.Stewart and D.N.Crowther; Trans.Iron Steel Inst. Jpn;1987,27,pp959-964.
10. G.I.S.L Cardoso, B.Mintz & S.Yue; Ironmaking and Steelmaking, 1995, 22,No.5,pp365-377.
11. C. Offerman, C.A.Dacker and C. Enstrom:Scan.J.Metall., 1981,,10,115.
12.B.Mintz, R.Abushosha, S.Ayyad &G.I.S.L.Cardoso; HSLA Steels '95 Proc. Ed. Liu Guoxun ,H.Stuart, Zhang Hongtao, Li Chengji. Published by China Sci and Technol. Press. Proc. of 3rd Int.Conf. an HSLA steels,Oct.,1995,Beijing, China, pp342-345.
13. J.Strid and K.L.Easterling:Acta Metall.1985,33,pp2057-2074.
14.B.Mintz: ISIJ Int.,1999,39 No.9,pp 833-855.
15. I.Weiss and J.J. Jonas;Metall. Trans.A, 1975,10A,831
16.W.C. Leslie, R.L. Rickett, C.L. Dotson and C.S.Walton: Trans.ASM. 1954,46,1470
17. C.Spradbery...private communication 1999 City University.

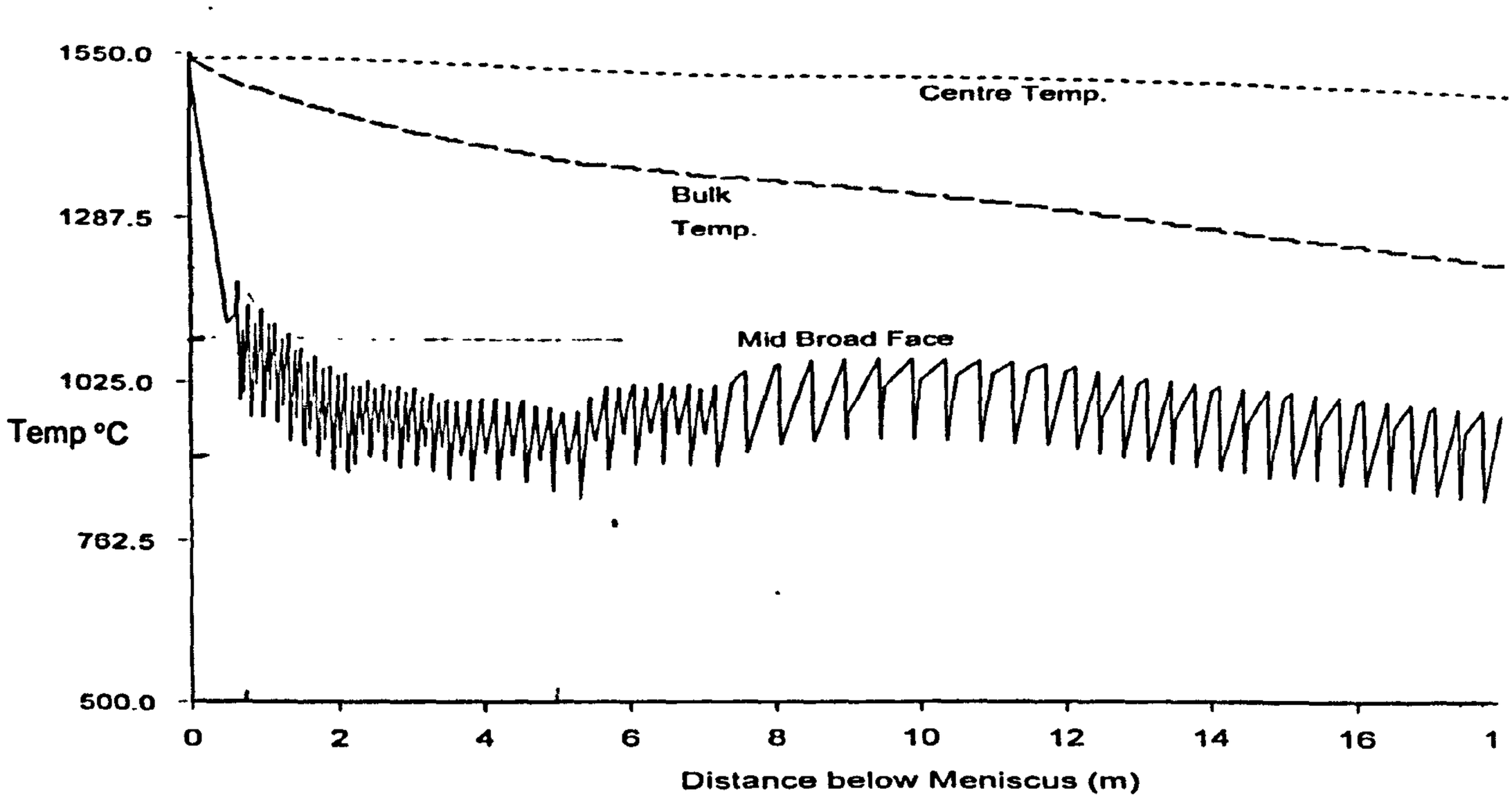

Figure 1 Temperature Profile for a Continuously Cast Strand

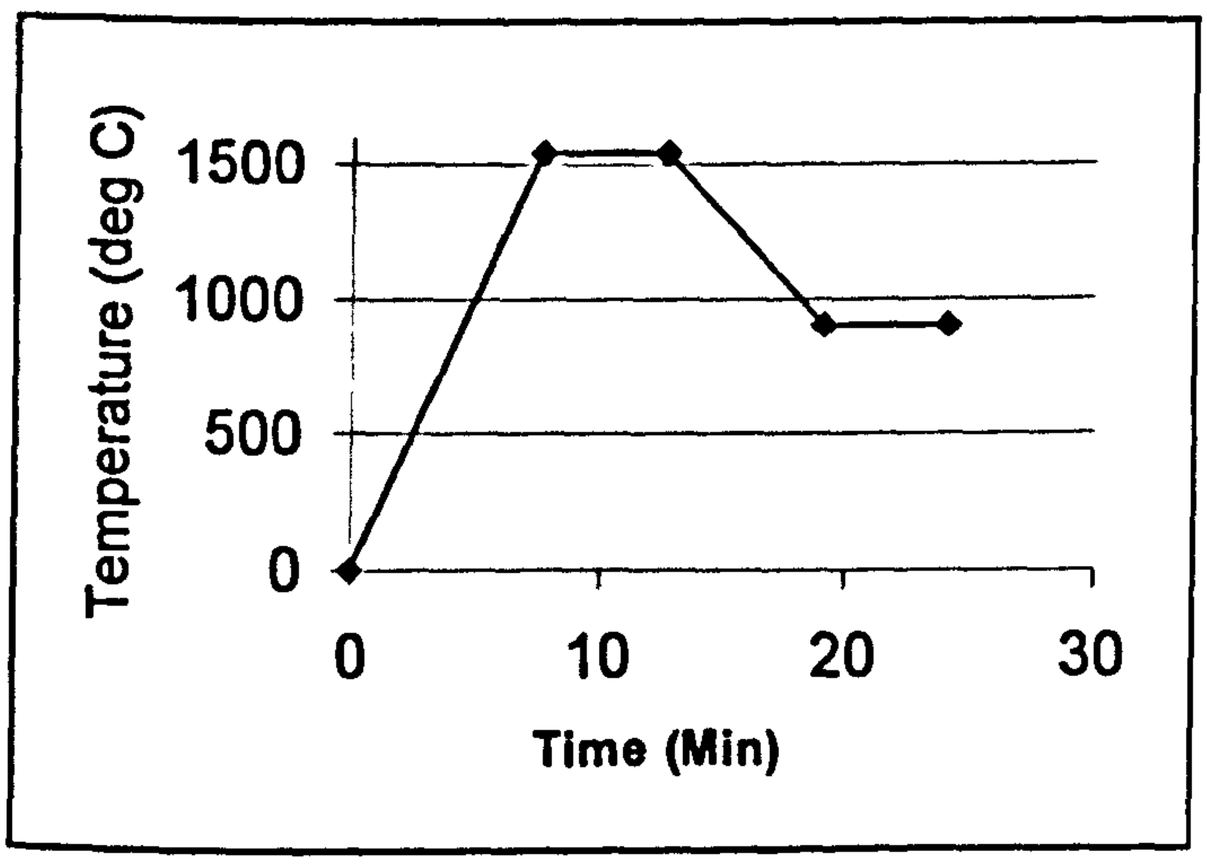

Figure 2a In Situ Temperature Profile

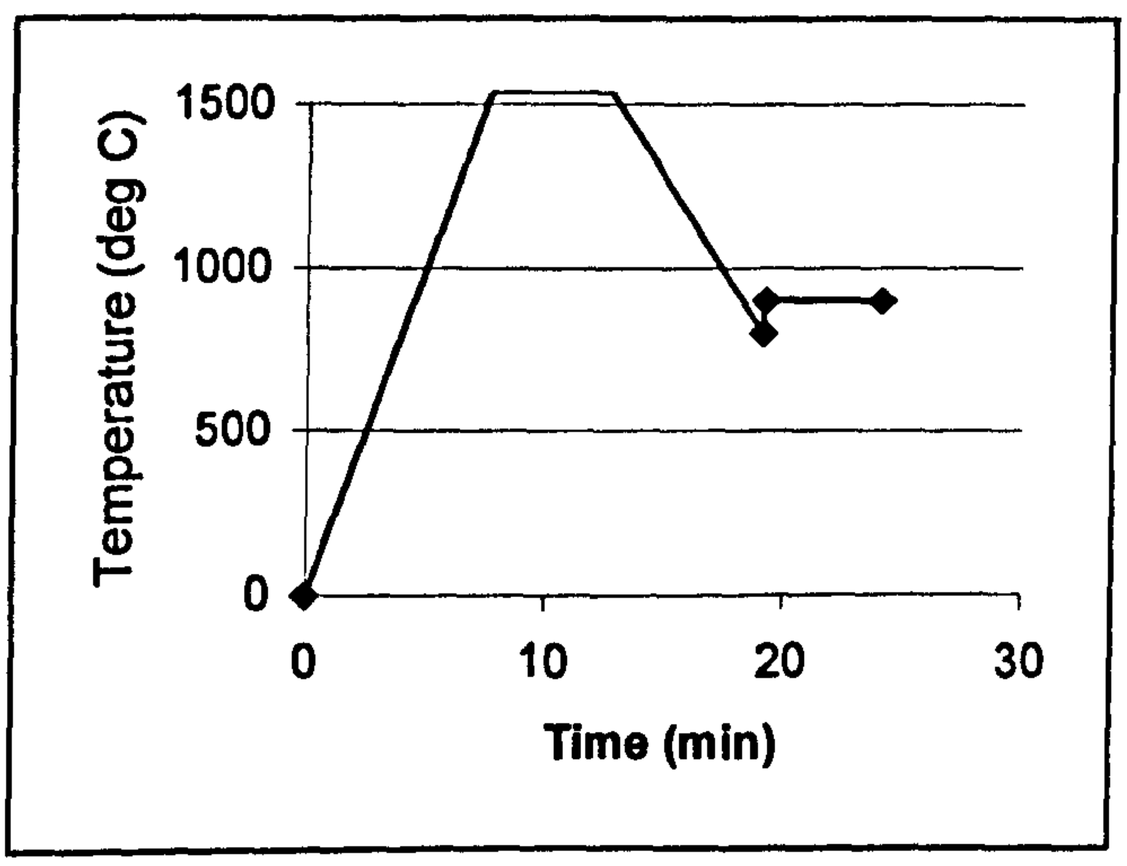

Fig 2b Temp. Profile with 100 K Step

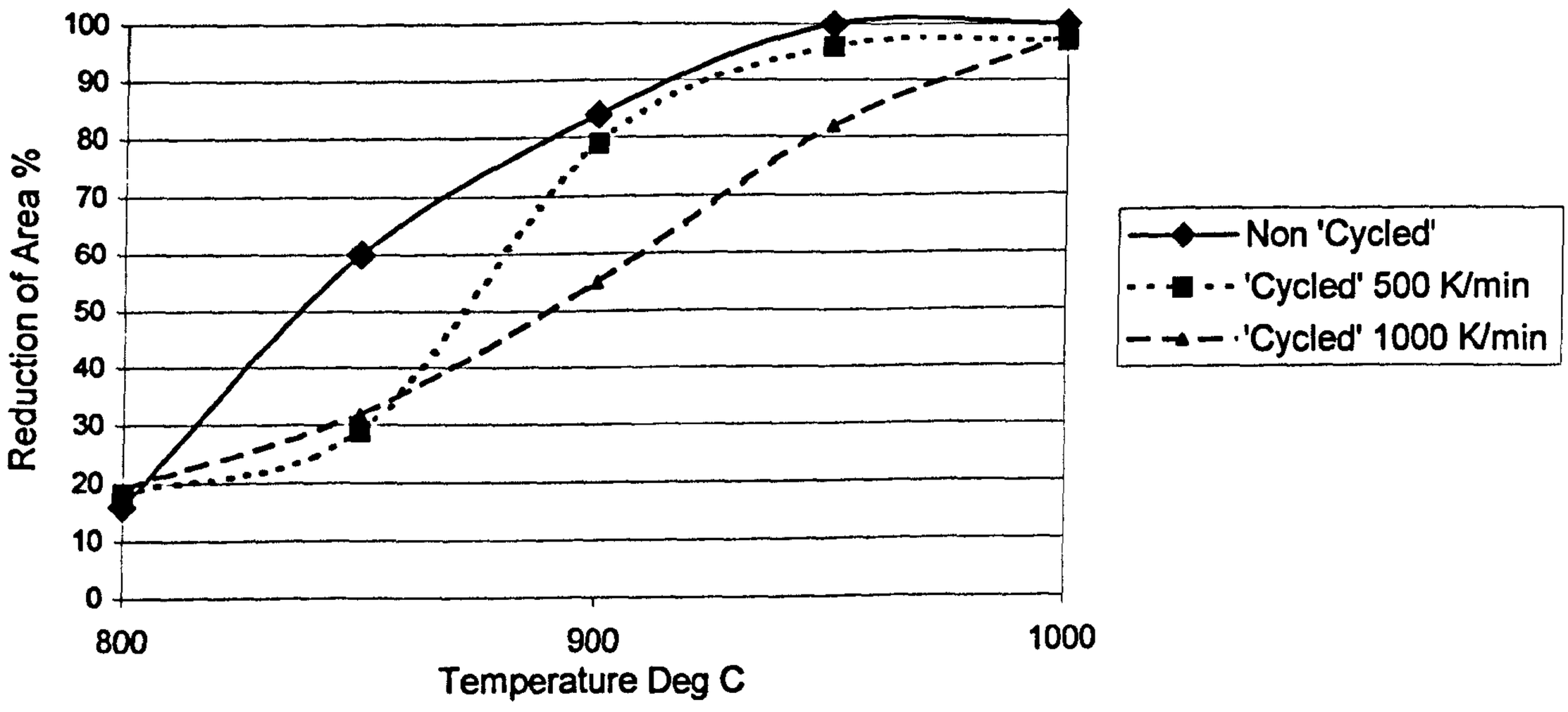

Figure 3 Influence of introducing an undercooling step for the Ti free steel on the hot ductility curves

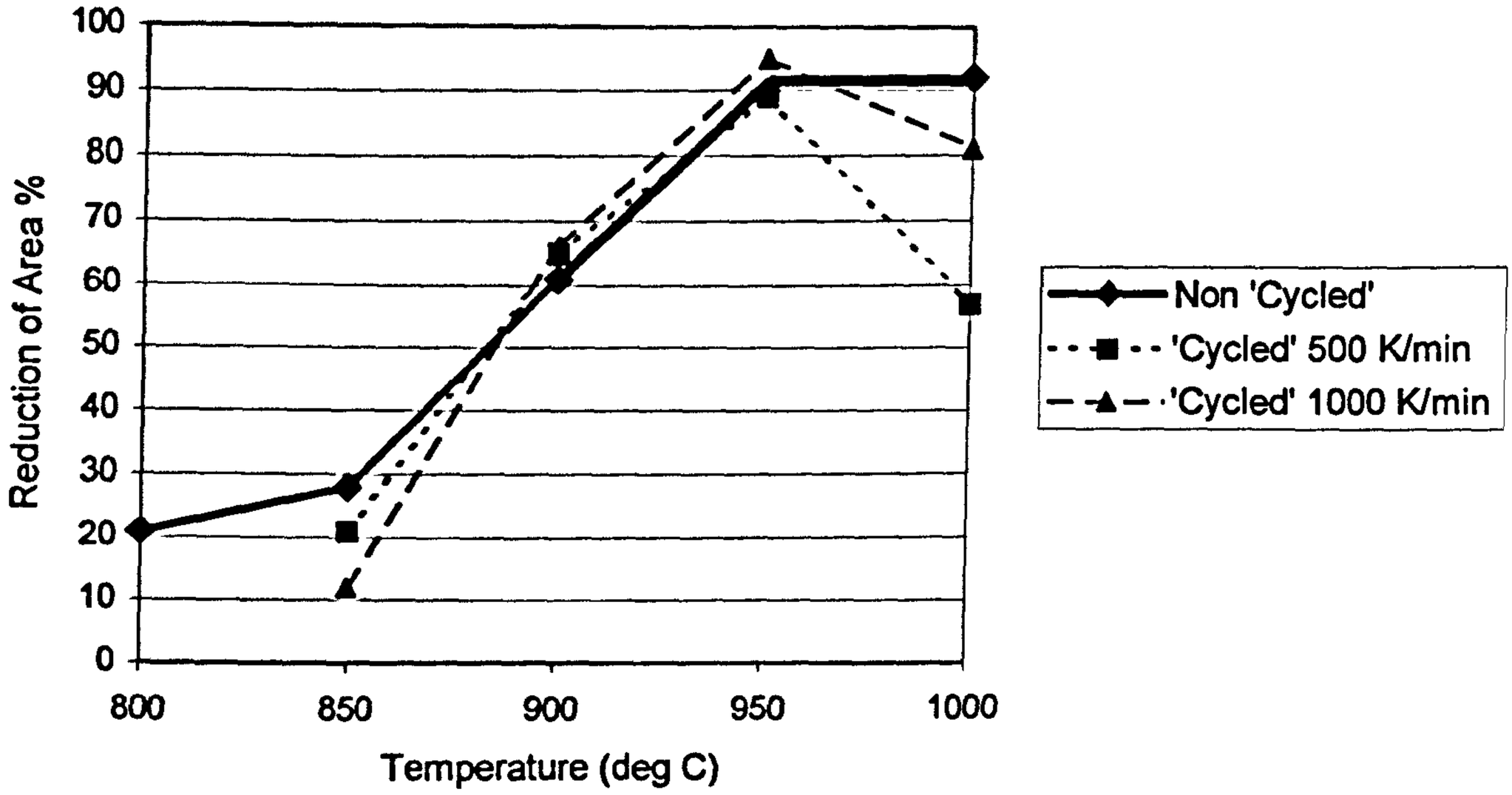

Figure 4 Influence of the undercooling on the hot ductility of the Ti containing steel

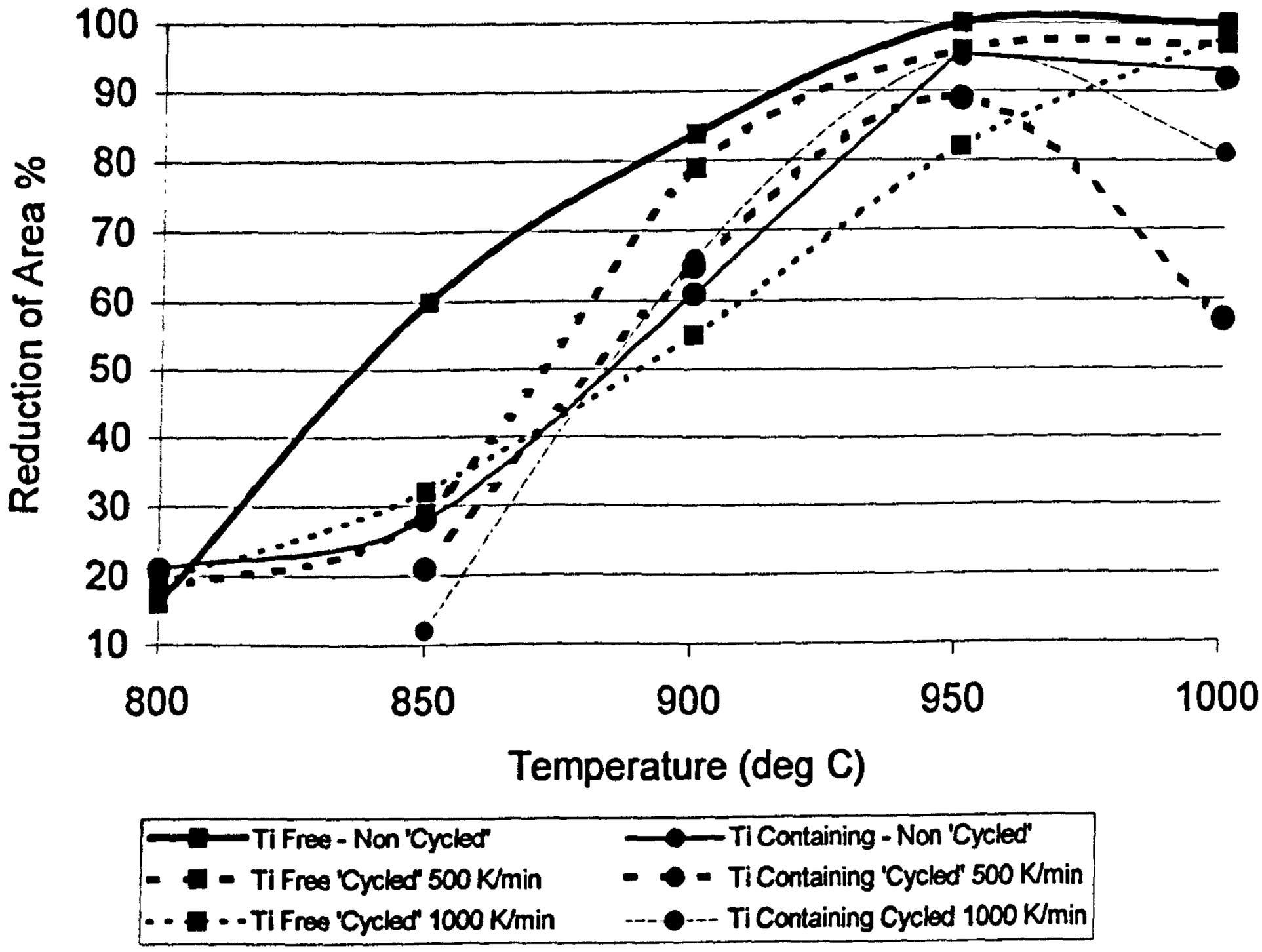

Figure 5 Influence of undercooling on Ti containing and Ti free steels

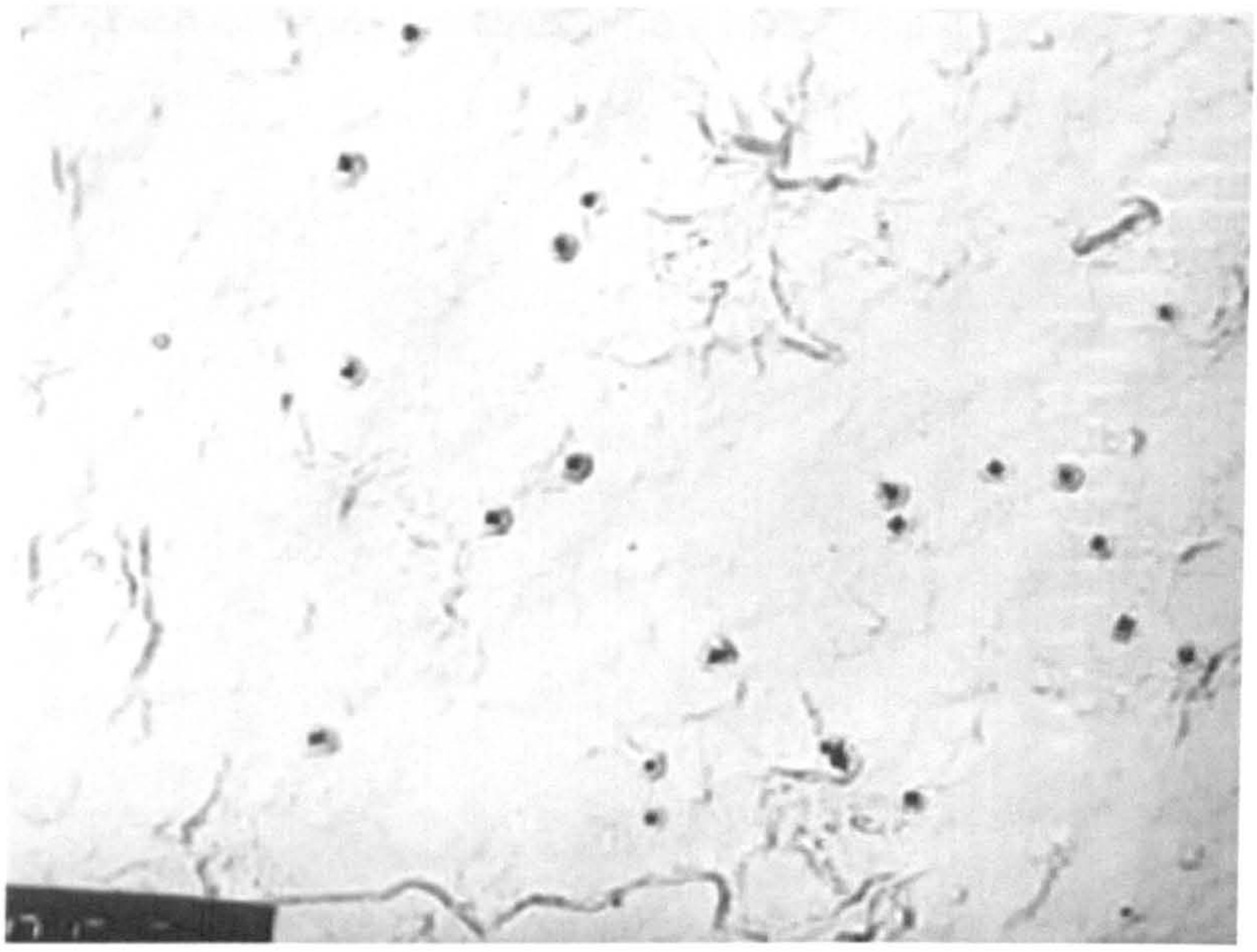

Figure 6 Fine TiN precipitates in steel with Ti:N ratio of 2.3:1 tested at 950°C and cooled at 100 K/min (X50,000)

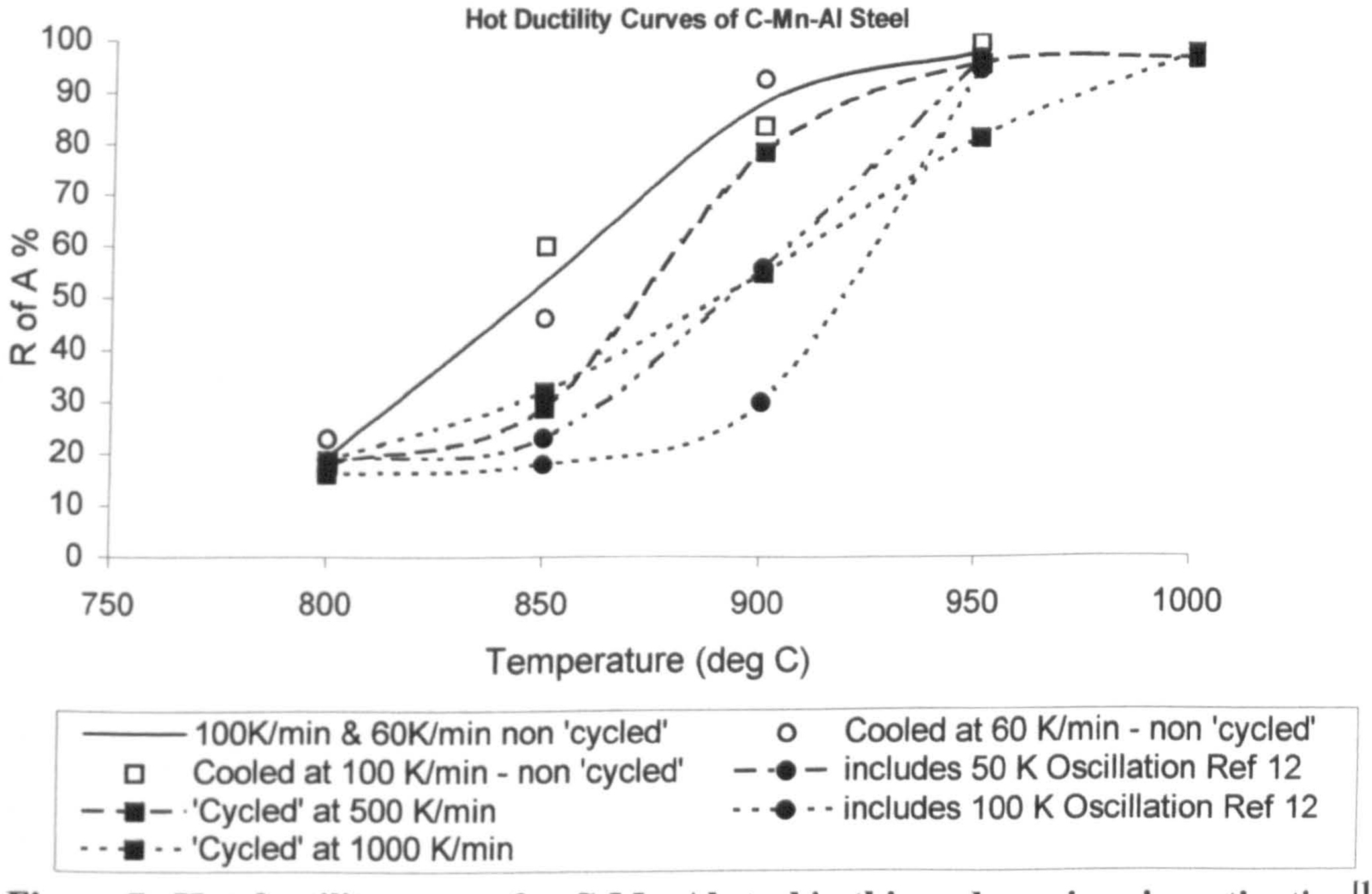

Figure 7a Hot ductility curves for C-Mn-Al steel in this and previous investigation[12]

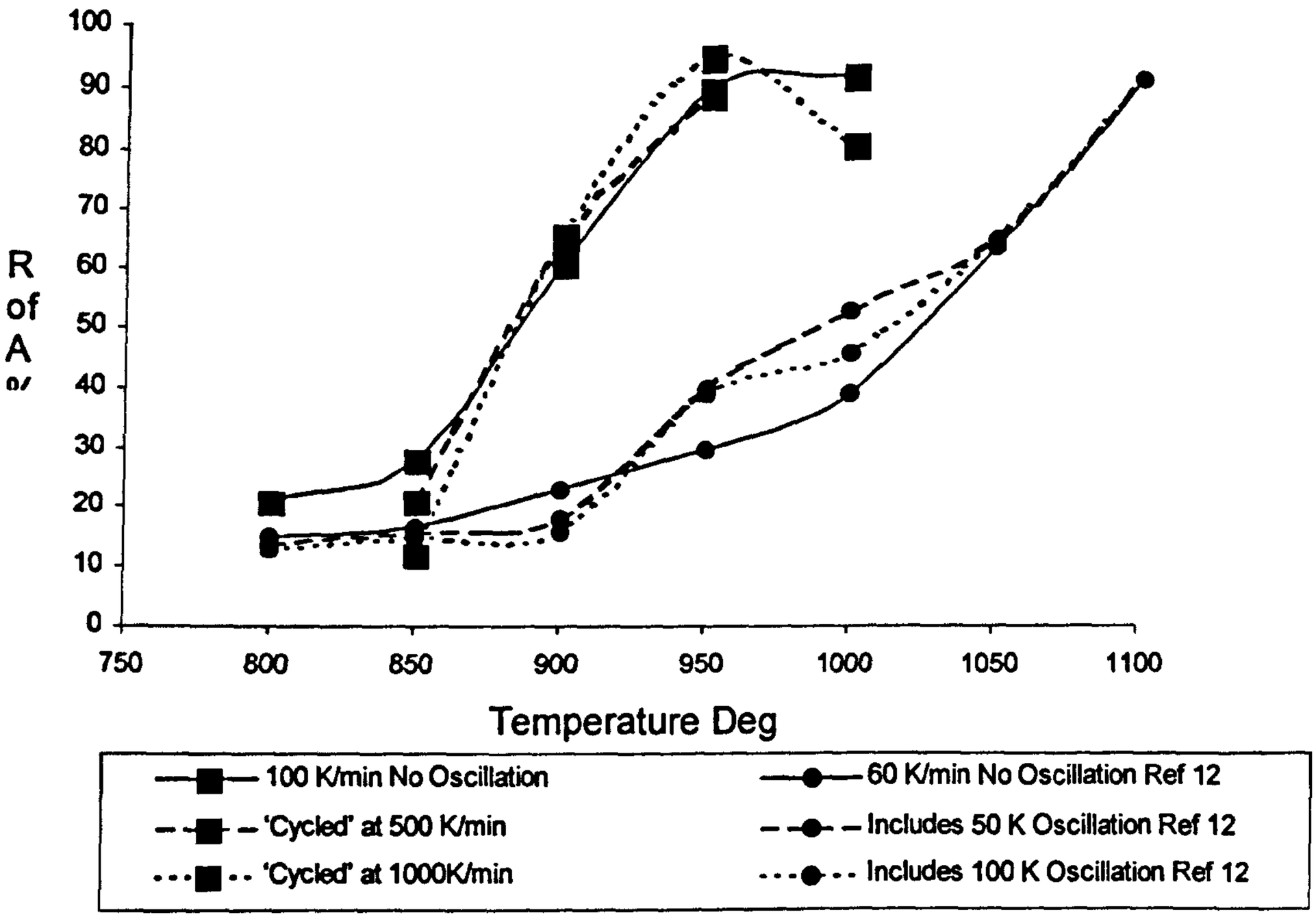

Figure 7b Hot ductilty curves for Ti containing steels in this and previous investigation[12]

Hot Ductility and its Relationship to the Problem of Transverse cracking - Recent Advances

B.Mintz,[+] O.Comineli,[*] G.I.S.L.Cardoso[0] and C.Spradbery[+]

+ Dept, Mech. Eng. and Aeronautics, City University, London, England
** Dept.Mech.Eng., UFES, Brazil*
o CST Vitoria, Brazil.

Abstract

Some of the more recent advances in improving the hot ductility of steels and avoiding transverse cracking during continuous casting are reviewed.

The width of the ductility trough can be very much reduced if large amounts of deformation induced ferrite can be formed just below the Ae_3 temperature, ferrite having excellent ductility. Reducing the C or Mn to low levels can encourage ferrite formation leading to very narrow troughs which make it much easier to avoid the problem of transverse cracking.

A small Ti addition can also be of benefit to hot ductility and prevent cracking. In order to show up these improvements in laboratory testing, it is necessary not only to cast the tensile specimens and cool directly to the test temperature but some undercooling is also required to more accurately simulate the commercial process. Provided the Ti level is below the level required for the stoichiometric for TiN better hot ductility will probably be realised.

Finally, the presence of columnar grains on the slab surface have been shown to be largely responsible for this cracking and methods to prevent their formation are discussed.

Keywords; Transverse cracking, steel, hot ductility

Introduction

Considerable research work has been carried out in the last 20 years into the problem of transverse cracking during the continuous casting of steel[1,2]. When a steel is continuously cast, it is generally cast in a curved mould so that the strand can be transferred from the vertical to the horizontal plane and so enable long lengths to be cast. Since the steel is cast in a curved mould, at some stage the strand has to be straightened and this puts the top surface and edges into tension and this may lead to cracks forming along the oscillation markings, transversely to the casting direction. Steels that contain Nb are particularly susceptible. The cracks are intergranular, and the presence both of inclusions and precipitates has been found responsible for the weakness at the austenite grain boundaries.

Nb is particularly detrimental as a fine dynamically produced precipitation of Nb(CN) is formed within the γ grains increasing the strength of the γ and this is often accompanied by a fine but coarser precipitation of Nb(CN) at the boundaries which is associated with a soft precipitate free zone. The closely spaced precipitation of Nb(CN) at the boundaries makes it easier for cracks

formed on grain boundary sliding to interlink and the soft precipitate free zone encourages the strain to be concentrated in the boundary regions.

A simple hot ductility test is often enough to give some indication as to how well a steel will behave during the straightening operation[2]. The tensile testing conditions are chosen to simulate the casting conditions as closely as is possible with a simple test. The tensile specimen is heated to ~1330 °C to dissolve all the microalloying precipitates and AlN and produce a coarse grain size reminiscent of the as-cast gain size. The specimen is then cooled at 60K/min, the average cooling rate close to the surface of conventionally continuously cast steel,(240mm thick slab) and tensile tested in the temperature range 1000-700°C; this covering the temperature range in which the straightening operation is carried out. The strain rate for testing is chosen to be that used during straightening, $3 \times 10^{-3} s^{-1}$. The reduction of area at failure, (R of A) is taken as the measure of the ductility of the steel.

A typical hot ductility curve is shown in Fig. 1. It can be seen to he composed of 3 regions; a low and high temperature range over which the ductility is excellent and a trough in which the ductility can be very poor and spans the temperature range over which the straightening operation is performed.

Considerable progress has been made in understanding this trough and preventing cracking from occurring. Thus steel producers either straighten at high or low temperatures to avoid the trough and closely control the microalloying and Al additions to the bare minimum to give the required properties in the final product. S levels are also kept as low as possible and modification is resorted to frequently. Nevertheless, even with all these precautions, transverse cracking can still at times be a very serious problem and even threaten steel production. In some cases the problem is tolerated rather than completely resolved. For example, with Nb containing steels, even when all the precautions are taken, it is common to roll wide and trim off the edges leading to a considerable scrap loss. This is because although cracks no longer form on the broad face, they are still present on the edges.

The following paper discusses some of the more recent work which should help to reduce the incidence of cracking

1. Reducing the carbon level

One possible method of avoiding transverse cracking may be to lower the carbon content of the steel to the 0.06-0.08%C range and this is presently being studied. There is no doubt that the peritectic C range (0. l-0.16%C) is normally associated with transverse cracking[3]. One possible reason is that this range of carbon favours a coarse dendritic structure. The growth of such austenite grains can he impeded by the presence of second phase particles either to the left (the delta phase) or right (the liquid phase) of the peritectic. Another explanation is that in the peritectic range, the change from bcc δ to the compact fcc γ structure causes a shrinkage of the shell away from the mould walls reducing the heat extraction resulting in a thinner shell which is more susceptible to cracking[3].

However, more recent work by the authors have suggested yet a third possibility, that reducing the carbon or manganese levels narrows the trough so that there is a much bigger window available for straightening at temperatures which will not give rise to cracks[4,5]. Suzuki et al [6] have shown that with Mn free steels, reducing the C level both results in a narrower and shallower trough and at the 0.05%C level the trough has almost vanished, Fig.2. However, when a higher Mn level of 1.4% was used by Crowther and Mintz [7], the depth of the trough was not influenced by the C content and wide troughs were always present. More recently, Cowley et al[4.5] have found that narrow troughs can again be obtained provided the Mn level is low, (0.6%Mn) at the 0.1%C level. Fig.3.

This latest work has shown that deformation induced ferrite can form in large amounts just below the Ae_3 provided the C and Mn levels are sufficiently low.

Generally, for high Mn steels having C levels in the peritectic range, deformation induced ferrite forms readily just below the Ae_3 but only as a thin soft layer at the boundary surrounding the stronger austenite grains. Strain concentrates in this soft band by causing voiding around the MnS inclusions situated at the boundary leading to intergranular failure. Ductility can only improve when a high volume fraction of ferrite is present and this requires going to temperatures just below the Ar_3 undeformed when large amounts of ferrite can form without deformation. The trough can often extend by well over 100°C when this happens making it very difficult commercially to avoid bending in the low ductility temperature regime.

However, if the ferrite film at the boundary can be strengthened, the γ band immediately adjacent to it will deform and transform to ferrite. In this way, the whole γ grain will be able to progressively transform to ferrite from the periphery to the centre, and large amounts of ferrite can be produced just below the Ae_3 resulting in narrow troughs. It is not entirely clear how this occurs but strengthening of the band by recrystallisation of the ferrite to a fine grain size may be needed. Presumably the higher the Ae_3 temperature, the more readily deformation induced ferrite can form.

2. Adding small Ti additions

It is generally accepted that adding a small Ti addition will help to reduce the transverse cracking problem and improve surface quality[1,8]. However, this is not always the case[9] and there is insufficient information concerning the optimum Ti/N ratio required to improve the ductility. Much of the laboratory work has failed to show the benefits of adding Ti as fine Ti rich particles are generally produced which reduce the ductility [10,11].

More recently, however, the laboratory technique has been improved to simulate the commercial casting conditions more closely and better agreement between commercial and laboratory experience is now possible[12]. In this revised simulation, not only are the tensile samples cast and cooled directly to the straightening temperature range but an undercooling step of 100°C is introduced prior to testing. The cooling programme undergone by the strand is complex. The surface after solidification is cooled very rapidly at first, reaches quite often a minimum temperature and then rises again close to the straightening temperature. The temperature then cycles, the temperature rising as the strand enters the guide rolls and decreases as the sprays

impinge on the cast on exit. In the laboratory work to date, improvements in ductility for Ti containing steels over Ti free steels have only been found with this undercooling step in the cooling programme, when the Ti/N ratio is less than the stoichiometric for TiN, (i.e. <3.4:1)[12].

The hot ductility curves for a Ti free and a Ti containing steel with a Ti/N ratio of 1.8:1 are given in Fig4[13]. It is believed that the Ti takes most of the N out of solution preventing the precipitation at the boundaries of the more detrimental AlN. However, for the Ti to be effective it must produce sufficiently coarse precipitates of low volume fraction to be a benefit to ductility.

3. Prevention of columnar grains

There is no doubt that the grain size at the surface of the slab can be very important in controlling ductility. Coarser grain sizes encourage intergranular failure because they encourage crack propagation [1,2]. The coarser the grain size, the longer are the cracks at the boundaries and the greater is the stress concentration acting at their tips. Furthermore, the crack can progress much more readily through the grain structure as it has fewer triple points to surmount where its direction would need to change. Finally, with microalloyed steels, for a given volume fraction of particles precipitated at the boundaries, the particles will be more closely packed at the boundaries in a coarse than in a fine grained material.

The influence of the grain size for equiaxed grain structures on ductility is shown in Fig 5. It can be seen that the reduction of area values increase as the grain size becomes finer. It is also noticeable that above a certain grain size ~400μm, further coarsening of the grain size only has a very small effect on the ductility. However, all this previous work has been carried out on equiaxed grain structures. One of the authors has noted that severe transverse cracking in commercially produced slabs is always associated with coarse columnar grains progressing inwards from the surface[9]. These grains can often have dimensions in their long direction in excess of 8mm. Some recent work, Fig. 6 has examined the effect of the direction of testing on the hot ductility of large columnar gains and shown that ductility is adversely affected when the direction of stressing is perpendicular to the long direction so that the normal stress is able to open up the cracks along the boundaries as shown in Figs.6 and 7.[14]. Revaux et al have also found that coarse columnar grains when stressed perpendicularly to the long direction of the grain give worse ductility than similar coarse grained equiaxed structures [15].

A possible solution to the transverse cracking problem might be therefore to break up these columnar grains when they are forming by controlled magnetic stirring. Another possibility is that the ISP thin slab casting route in which some predeformation is given to the strand while it is still pasty may he able to break up the as cast dendritic structure. It should however be noted that, thin slab casting without deformation, produces a columnar structure and there is no significant refinement of the grain structure compared to that obtained by conventional casting, even though the surface cooling is enhanced [16]

References

1. B.Mintz, ISIJ Int.39 (1999) 833-855.
2. Bmintz, S. Yue, J.Jonas Int Mater Rev 36 (1991) 187.
3. Y.Maehara,KYasumuto,V.Sugitani and K.Gunji,Trans.ISIJ 25, (1985), 1045.
4. A.Cowley. R.Abushosha, B.Mintz. Mater.Sci.Technol.14 (1998) 1145-1 153.
5. R. Abushosha, S.Ayyad, B.Mintz, Mater.Sci. Technol 14(1998) 227-235.
6. H.G. Suzuki S. Nishimura, J .Imamura,Y .Nakamura,Trans.lSIJ 24 (1984) 169.
7. D.N.Crowther,B.Mintz,.,Mater.Sci.Technol.2, (1986) 671.
8. D.N.Crowther,B.Mintz in Ti technology in microalloyed steels, Ed. T.N. Baker, IOM, London,(1997),98-l 14.
9. B.Mintz, unpublished work on commercial data
10. O..Comineli,R.Abushosha,B.Mintz,Mater.Sci. Technol. 15 (1999)1058-1068.
11. R.Abushosha,O.Comineli,B.Mintz,Mater.Sci.Technol.15 (1999) 278-286.
12. B..Mintz, C.Spradbery in Thermomechanical Processing of Steels IOM,London, 2000,p.143-152.
13.C.Spradbery City University London, unpublished work (1999)
14. B.Mintz,A.Cowley,R.Abushosha, Mater.Sci.Technol. 16 (2000) 1-6
15. T.Revaux,J.P.Bricaut and J.Oudin, J.Mater.Eng.Perform, 5 (1996) 260
16. R.Abushosha, S.Ayyad,B.Mintz, Mater. Sci. Technol. 14 (1998) 346-354

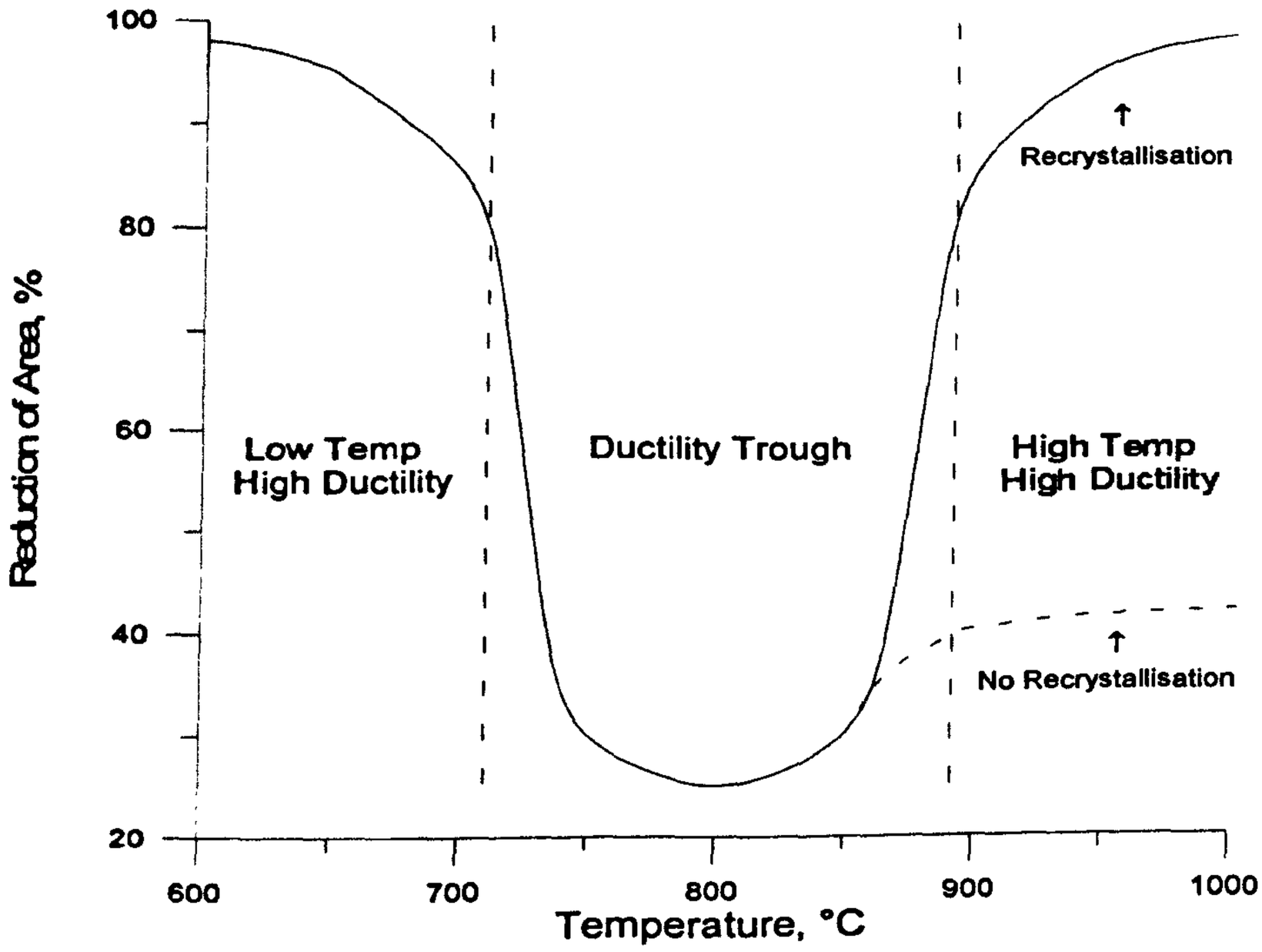

Figure 1. Typical hot ductility curve for steels (Ref 1)

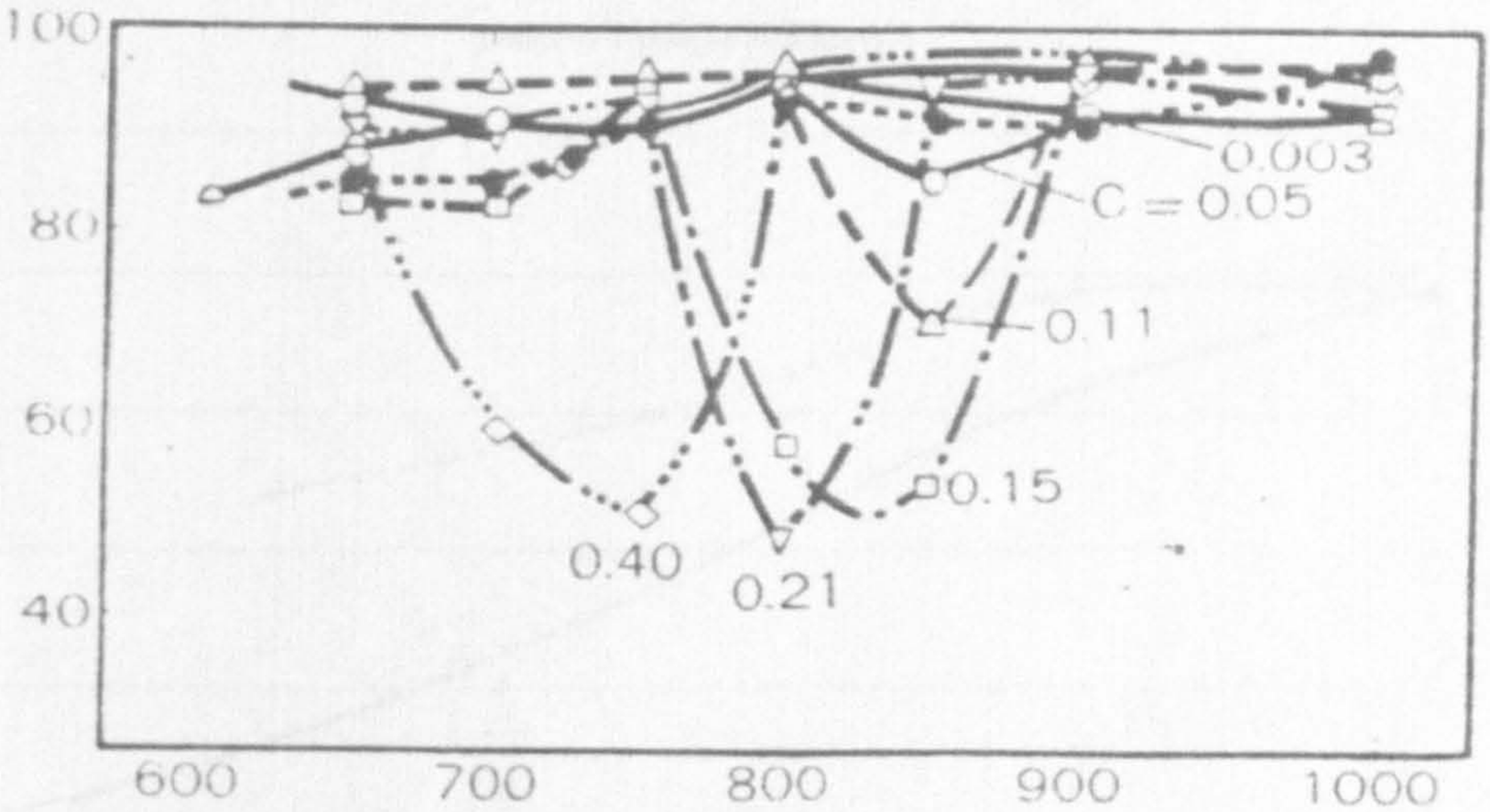

Figure 2. Influence of carbon on Mn free steels on the hot ductility curves. (Ref 6)

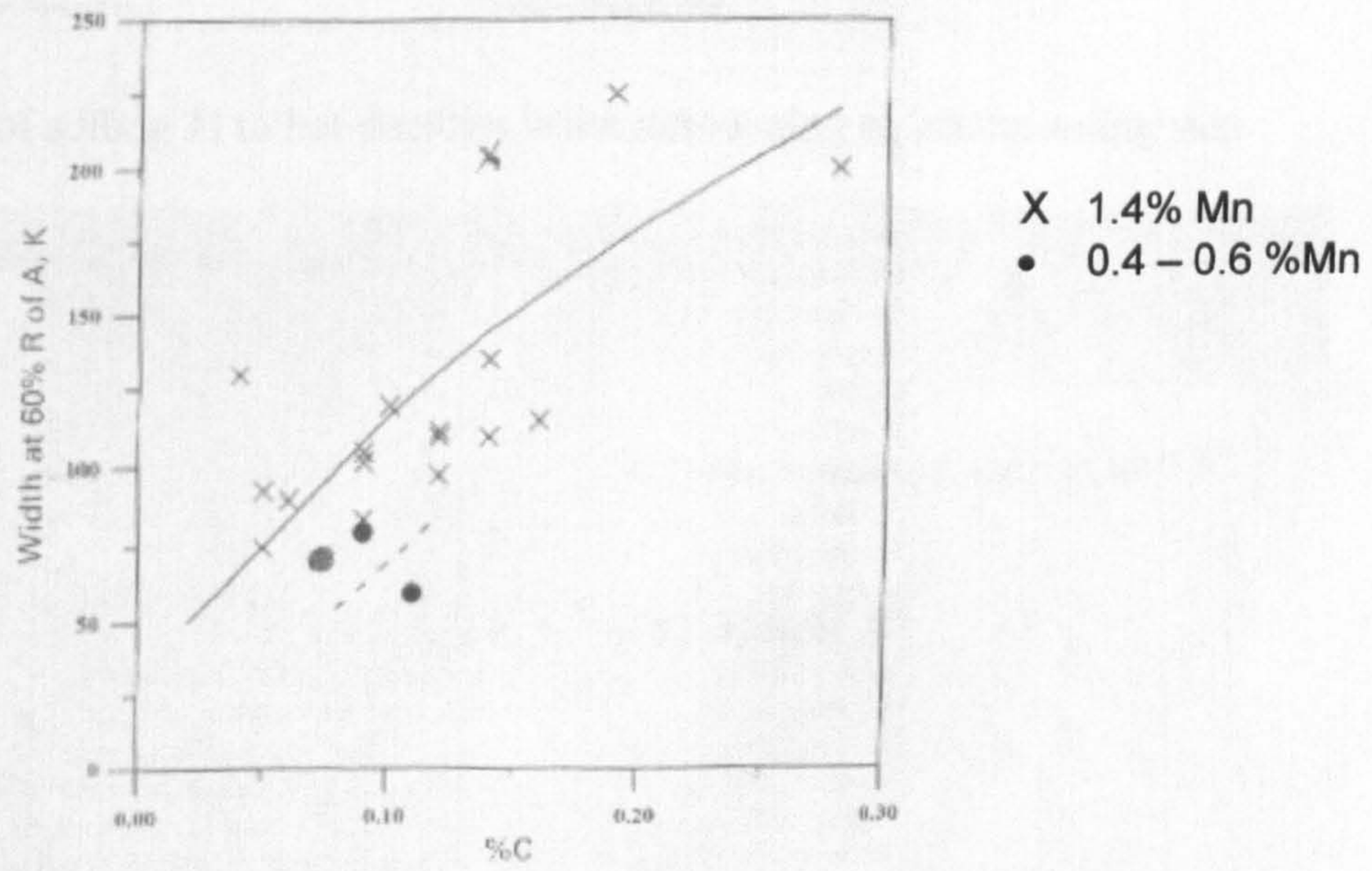

Figure 3. Influence of Mn and C on the width of the ductility trough (Ref 5)

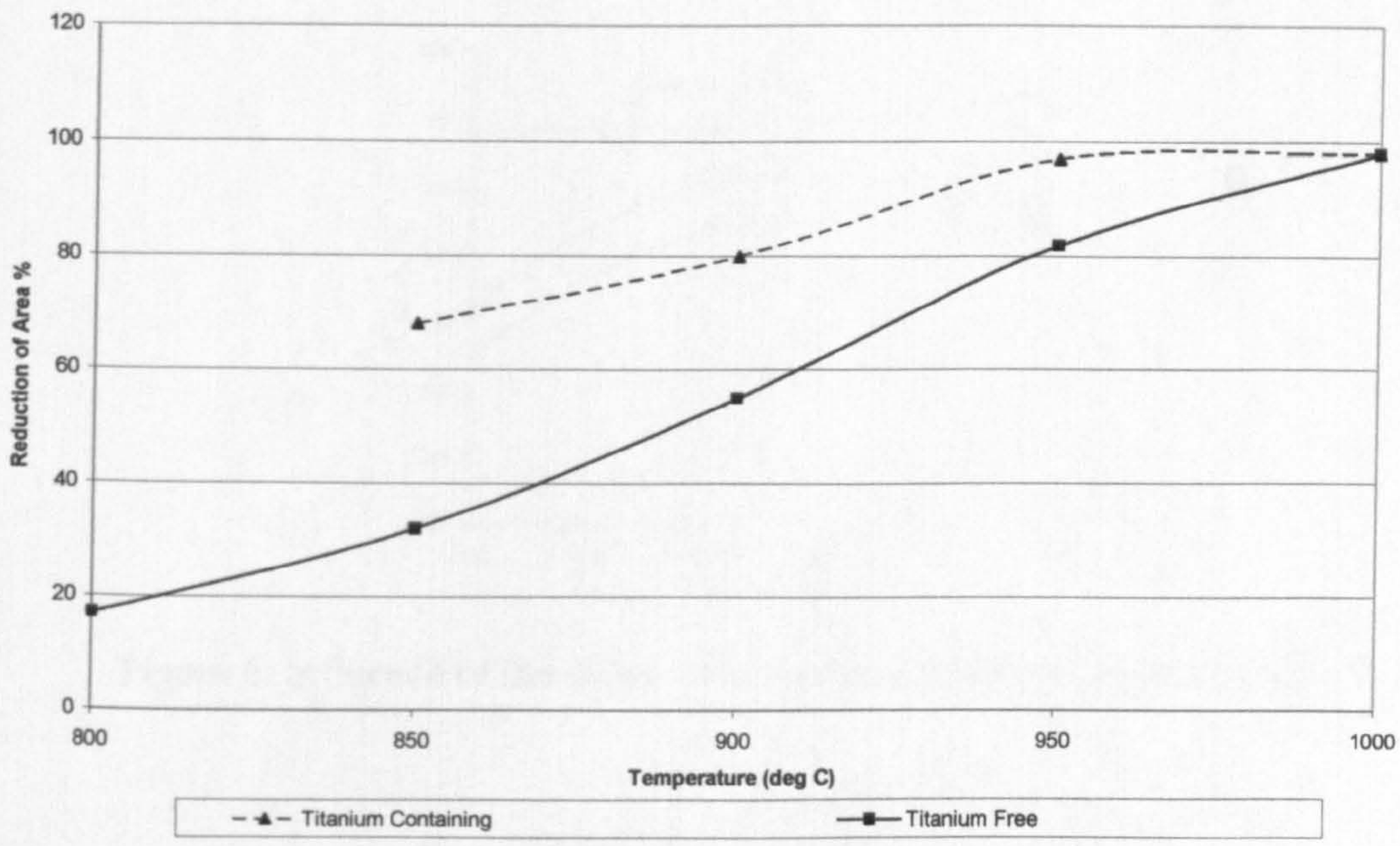

Figure 4. Benefit of adding Ti to hot ductility when introducing an undercooling step

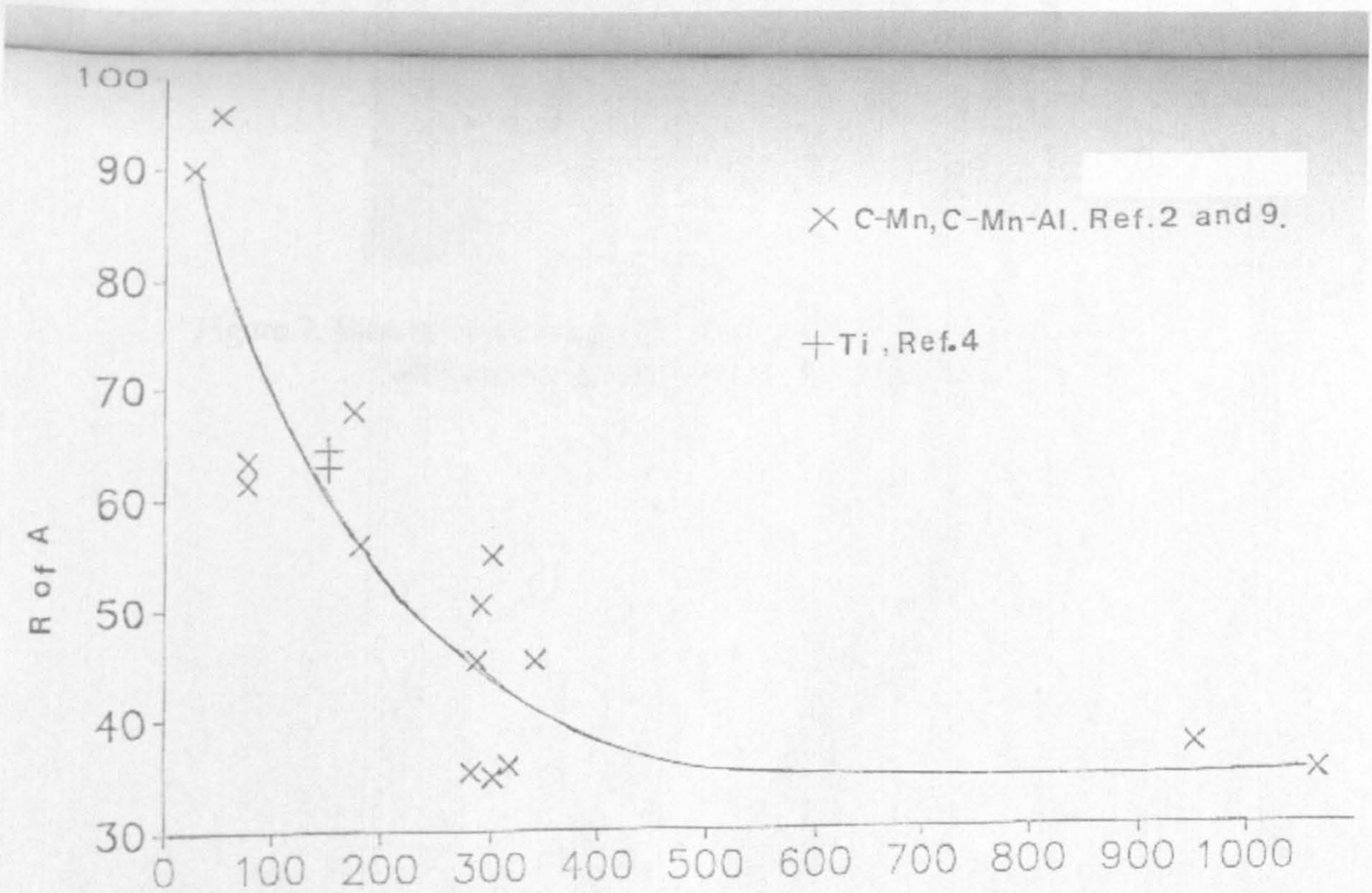

Figure 5. Influence of grain size on R of A values (Ref 8)

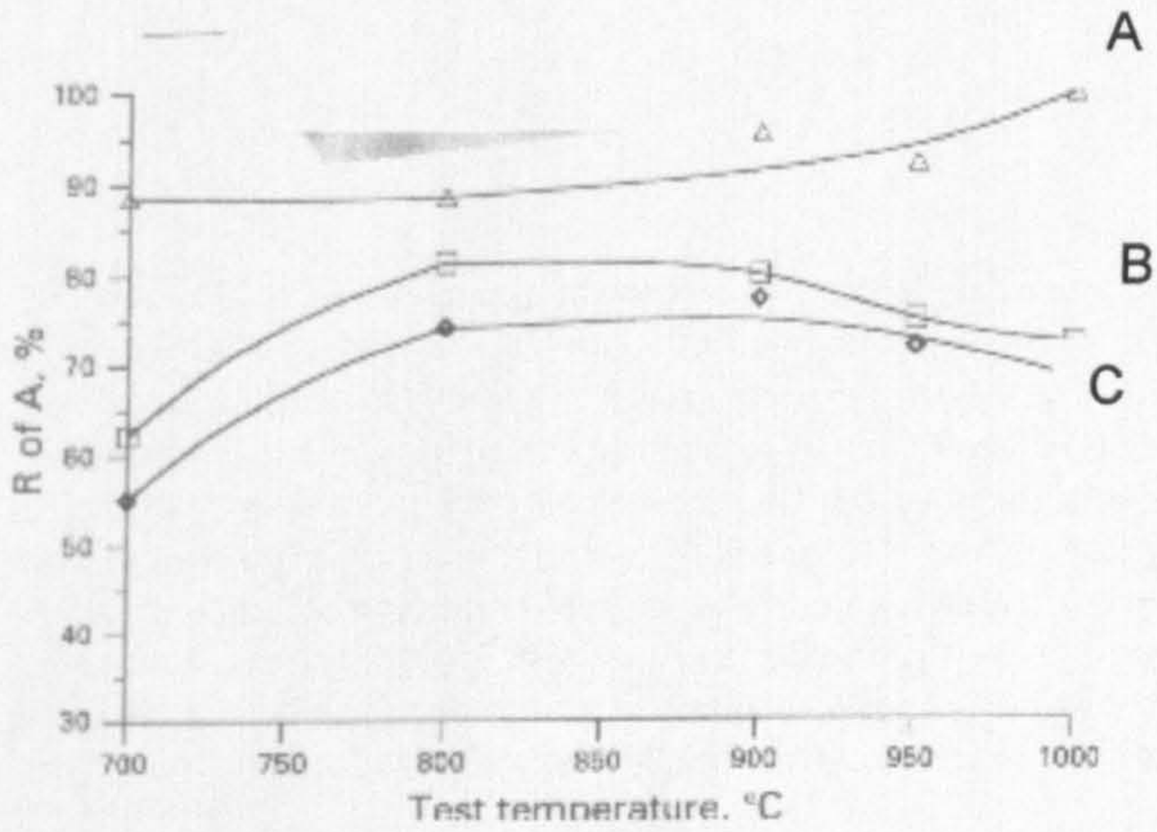

Figure 6. Influence of the shape of the columnar grains on hot ductility (Ref 14)

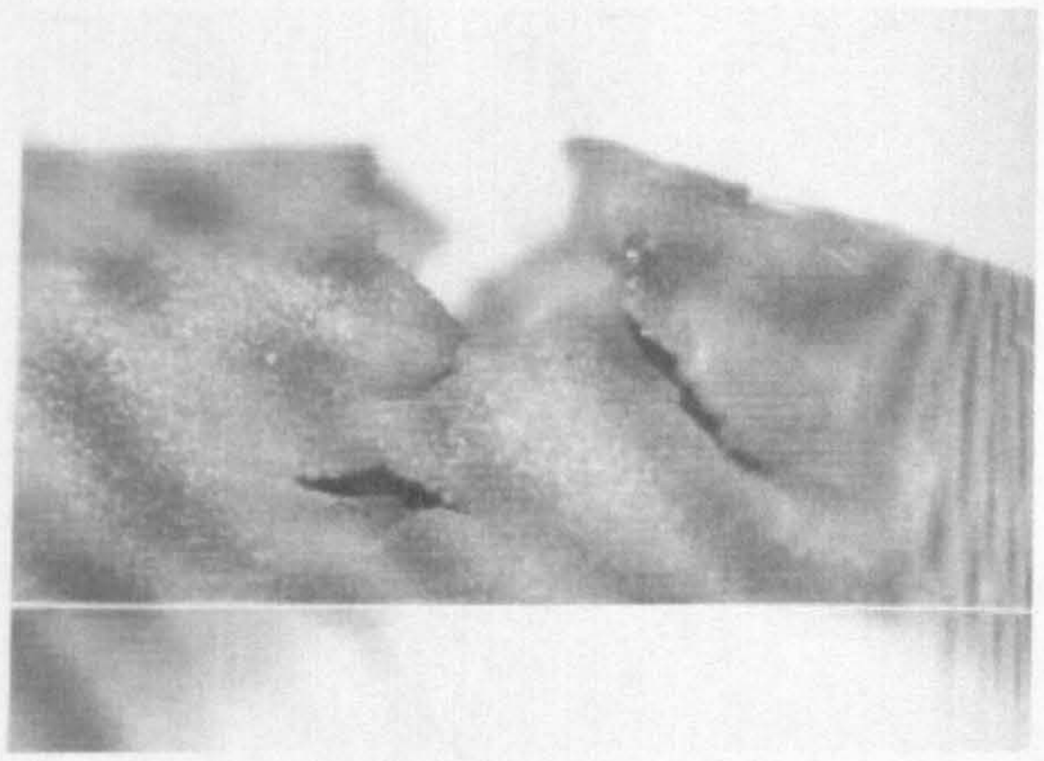

Figure 7. Ease of crack propagation along columnar grains (Ref. 14)
Tensile samples taken in casting direction A